ADHESIVELY BONDED LAP JOINTS OF PULTRUDED GFRP SHAPES

THÈSE N° 2964 (2004)

PRÉSENTÉE À LA FACULTÉ ENVIRONEMENT NATUREL, ARCHITECTURAL ET CONSTRUIT

Institut de structures

SECTION D'ARCHITECTURE

ÉCOLE POLYTECHNIQUE FÉDÉRALE DE LAUSANNE

POUR L'OBTENTION DU GRADE DE DOCTEUR ÈS SCIENCES

PAR

Till VALLÉE

Diplom-Ingenieur, Technische Hochschule Darmstadt, Allemagne
et de nationalité allemande

acceptée sur proposition du jury:

Prof. Th. Keller, directeur de thèse
Prof. M.A. Hirt, rapporteur
Prof. U. Meier, rapporteur
Prof. J.-D. Wörner, rapporteur
Dr A. Zhou, rapporteur

Lausanne, EPFL
2004

THÈSE PRÉSENTÉE À LA FACULTÉ ENVIRONNEMENT NATUREL, ARCHITECTURAL ET CONSTRUIT – INSTITUT DE STRUCTURES – SECTION D'ARCHITECTURE POUR L'OBTENTION DU GRADE DE DOCTEUR ÈS SCIENCES

Adhesively Bonded Lap Joints of Pultruded GFRP Shapes

Till Vallée

DIPL.-ING. TECHNISCHE HOCHSCHULE DARMSTADT

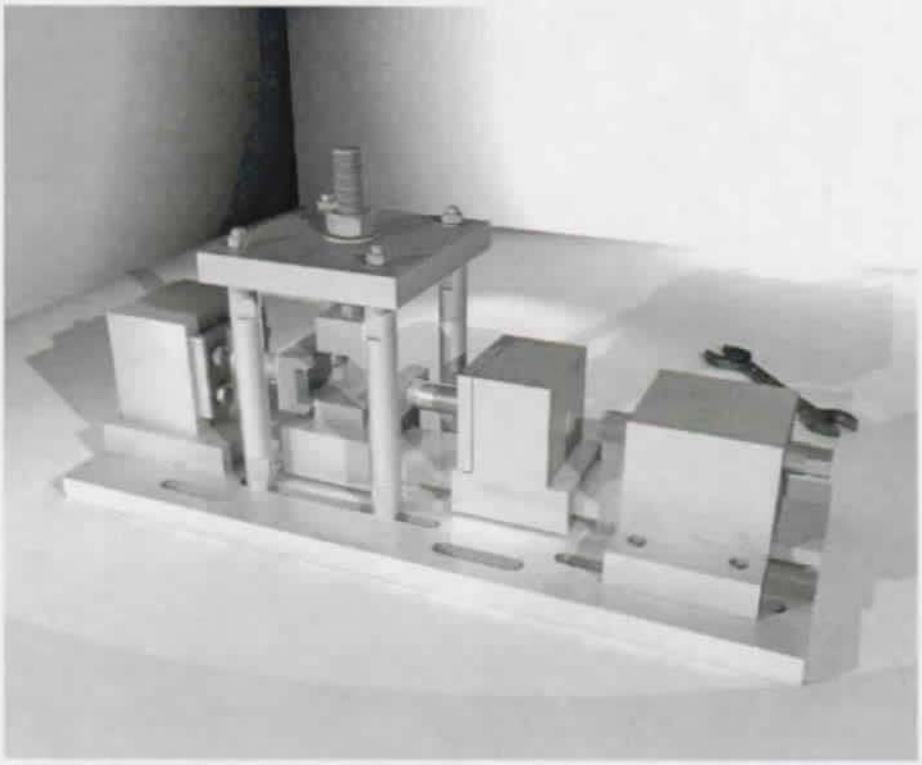

COMPOSITION DU JURY DE THÈSE

Prof. Ines LAMUNIÈRE – *Présidente*
Prof. Thomas KELLER – *Directeur de thèse*
Prof. Manfred HIRT – *Rapporteur*
Prof. Urs MEIER – *Rapporteur*
Prof. Johann-Dietrich WÖRNER – *Rapporteur*
Dr. Aixi ZHOU – *Rapporteur*

Contents

List of Figures

List of Tables

VERSION ABREGÉE

RESUMÉ

L'importance des matériaux composites à fibre de verre n'a cessé de croître ces dernières années. Ils sont de plus en plus utilisés en tant que matériau de construction en génie civil. C'est surtout l'introduction de la pultrusion comme moyen de fabrication industriel qui a permis de produire de grandes quantités de matériaux composites à fibre de verre, offrant ainsi les avantages liés à ce dernier — comme le bon rapport résistance-poids ou l'insensibilité à la corrosion — à des prix compétitifs.

Les problèmes liés à la conception avec les matériaux composites pultrudés (MCP) sont les assemblages. Jusqu'à présent, on se servait des connections traditionnellement héritées de la construction métallique pour joindre entre eux des éléments en MCP. Mais à cause des caractéristiques propres du matériau — fibreux, anisotropique et a rupture fragile — les assemblages collés seraient beaucoup plus adaptées. Toutefois, pratiquement rien n'a été fait dans le domaine de la recherche sur ce sujet.

La présente recherche se veut une contribution pour combler ce déficit en offrant à l'ingénieur un moyen de dimensionner de manière sûre et économique des assemblages collés de profilés en MCP sous des charges statiques. Cette thèse présente les étapes qui ont mené à cette méthode. Après une courte introduction aux objectifs de la recherche et aux méthodes utilisées, l'état actuel de la recherche est documenté. La majorité des publications se borne actuellement à décrire les contraintes dans les joints collés à simple ou double recouvrement, se limitant à des systèmes idéalisés aux adhérents isotropes. De même il n'existe pratiquement pas de critère de rupture adapté aux MCP.

Pour remédier à cette situation, des essais ont été conduits sur le matériau composite pultrudé pour en déterminer l'architecture — par pyrolyse — et la résistance — a l'aide d'un appareil spécifiquement développé par l'auteur à cet effet : le CCLAB SHEAR-TENSILE DEVICE. Cet appareil permet de déterminer expérimentalement la résistance mécanique d'échantillons de MCP à l'action combinée de contraintes dans le sens de l'épaisseur et de cisaillement. Cet appareil a aussi permis de déterminer le module d'élasticité dans le sens de l'épaisseur permettant ainsi de formuler l'orthotropie du matériau en éléments finis.

D'autres essais ont été conduits sur des joints à simple et à double recouvrement pour évaluer l'influence de paramètres tels que la longueur du recouvrement, l'épaisseur de la couche de colle ou de mesures de réduction de contraintes — comme les chanfreins — sur la charge ultime. Tous ces essais ont été effectués sur des spécimens de taille relativement grande pour éviter toute influence relative à la taille des spécimens. Les résultats obtenus ont montré que l'effet de l'épaisseur de la couche de colle ou celle des chanfreins sur la charge ultime de joints collés est de loin moins grande que ce qui avait été prédit dans les publications antérieures. Certains spécimens ont été pourvus de jauges d'extensiométrie pour étudier plus en détail le cheminement des contraintes axiales le long du recouvrement. Des calculs comparatifs — aux éléments finis — ont démontré qu'il était possible de déterminer numériquement les contraintes dans des joints collés, en prenant soin de formuler les propriétés orthotropes du matériau. La rupture de certains joints collés a aussi été filmée à haute vitesse (à 2 000 images par seconde) permettant ainsi de mieux comprendre le processus de ruine. Ce processus est intimement lié à l'architecture des MCP, la rupture étant initiée à l'intérieur du matériau.

Tous les spécimens testés on été modélisés en éléments finis en utilisant des éléments orthotropes. En combinant les numériques avec la détermination expérimentale de la résistance du matériau, il a été possible de formuler une méthode pour prédire la charge ultime de joints collés qui a pu être validée sur un grand nombre de configurations géométriques différentes de joints à simple et à double recouvrement.

Une version simplifiée de cette méthode a aussi été formulée. Basée sur des formules analytiques pour la détermination des contraintes, elle permettra aux ingénieurs de rapidement dimensionner les joints collés de matériaux en composite pultrudés à simple et à double recouvrement.

ZUSAMMENFASSUNG

Die Bedeutung von Glasfaserverstärkten Kunstoffen (GFK) im Bauwesen hat im letzten Jahrzehnt stetig zugenommen. Die Einführung der Pultrusion als Herstellungsverfahren hat es ermöglicht, die Vorteile von GFK-Profilen — u.A. hohes Festigkeits-Gewicht-Verhältnis, Korrosionsbeständigkeit — wirtschaftlich attraktiv anzubieten.

Eine wichtige offene Frage beim Entwurf mit GFK ist immer noch die Thematik der Anschlüsse. Bis heute werden die Anschlüsse im Bereich GFK immer noch wie im Stahlbau ausgeführt: GFK-Profile werden hauptsächlich zusammengeschraubt. Wegen dem anisotropen und spröden Charakter des Werkstoffes ist dies allerdings nicht materialgerecht. Geklebte Anschlüsse wären die bessere Alternative, allerdings ist das Thema in Bezug auf GFK noch kaum erforscht worden.

Die hier beschriebene Forschungsarbeit soll diese Lücke schließen, indem sie Ingenieuren einen Leitfaden zum Entwurf von geklebten Anschlüssen von pultrudierten GFK Profilen unter statischen Lasten anbietet. Das vorliegende Schriftstück erläutert die Schritte, die zum Bemessungsverfaren geführt haben. Nach einer kurzen Einführung, Zielsetzung und Beschreibung der verwendeten Methodik wird der Stand der Technik erläutert. Die Durchsicht der aktuellen Literatur zum Thema zeigt, dass das Gebiet der geklebten Anschlüsse von pultrudierten GFK wenig Beachtung genossen hat, sowohl experimentell als auch theoretisch. Einige Veröffentlichungen haben sich der Thematik der geklebten Laschenanschlüsse gewidmet, unterstellen aber idealisierte Systeme mit meistens isotropischen und linear-elastischen Materialien. Desgleichen gibt es kein experimentell ermitteltes und bestätigtes Versagenskriterium für pultrudierte GFK.

Um diese Lücken zu schließen, wurden Versuche auf verschiedenen Ebenen durchgeführt: Ermittlung eines Bruchkriteriums für GFK unter Verwendung eines selbst entworfenen Gerätes — dem CCLAB SHEAR-TENSILE DEVICE, welches die Ermittlung des Materialwiderstandes gegenüber Schubspannungen und Spannungen rechtwinklig zur GFK-Ebene unter beliebiger Kombination zueinander ermöglicht. Das CCLAB SHEAR-TENSILE DEVICE wurde auch dazu benutzt, den Elastizitätsmodul rechtwinklig zur GFK-Ebene zu ermitteln. Dieser wurde später zur numerischen Formulierung der Orthotropie verwendet.

Neben den experimentellen Untersuchungen am Grundmaterial wurden Versuche an geklebten Einfach- und Doppellaschenanschlüssen durchgeführt. Dabei wurde der Einfluss der Überlappungslänge, der Dicke der Lamellen sowie von Abfasungen auf die Bruchlast von geklebten Anschlüssen von GFK-Lamellen untersucht. Um Maßstabseffekte zu vermeiden, wurden großmaßstäbliche Versuche durchgeführt. Eines der Ergebnisse war die Tatsache, dass der Einfluss der Klebschichtdicke sowie von Abfasungen bei weitem viel geringer ausfiel als es vorhergegangene Veröffentlichungen beschrieben haben. Des weiteren wurde, bei ausgesuchten Doppellaschenanschlüssen, die Entwicklung der Axialdehnungen entlang der geklebten Fuge experimentell mit Hilfe von Dehnmessstreifen ermittelt. Auch wurde das Versagen der geklebten Anschlüsse mit Hilfe einer Hochgeschwindigkeitskamera — bis zu 2000 Bilder pro Sekunde — gefilmt um den Versagenmechanismus zu ermitteln. All diese Versuche haben gezeigt, dass das Versagen immer im Grundmaterial GFK stattfindet, und nicht in der Klebschicht.

Alle experimentell untersuchten Versuchskörper wurden mit Hilfe der FEM modelliert, dabei wurde orthotropes Materialverhalten unterstellt. Unter Zuhilfenahme des experimentell ermittelten Versagenskriteriums wurde ein Verfahren entwickelt, welches die Bruchlast von geklebten Laschenanschlüssen vorhersagt. Das Verfahren wurde an einer großen Anzahl von experimentellen Ergebnissen verifiziert.

Eine vereinfachte Fassung dieses Verfahrens, basierend auf bestehenden analytischen Formeln, wurde daraufhin entwickelt, welches es dem entwerfenden Bauingenieur erlauben wird, schnell und sicher geklebte Anschlüsse von pultrudierten GFK Profilen zu bemessen.

SUMMARY

The importance of Fibre Reinforced Polymers (FRPs) as a material used for civil engineering purposes has grown in the last decade. Especially the introduction of pultrusion at an industrial level as a way to produce big batches of FRP made it possible to offer the advantages — like the high strength-to-weight ratio or the good corrosion resistance — at a reasonable cost.

One issue when designing with pultruded FRPs are the connections. Up to now, connections between pultruded FRPs have been designed in the same way as structural steel connections, mainly through bolts. Because of the fibrous and layered character and the anisotropy of pultruded FRPs, bolting is not a material-adapted way to connect. Adhesive bonding is by far better suited, but has not yet been investigated for the special case of pultruded FRPs.

This research is intended to fill the gap by offering designing engineers a method allowing them to dimension safe and economic adhesively bonded joints of pultruded FRPs under static loads. The present Thesis is aimed to show the steps leading to this method. After a short introduction, where the objectives and methods used are listed, the actual state of the art is presented. The review of actual literature shows that not much has been done on the special field of adhesively bonded connections of pultruded FRPs, neither experimentally nor theoretically. Some publications treat the global aspect of bonded connections for special cases like the single and double lap joints, but all on idealized mechanical systems with isotropic adherents. Also, there are no detailed reports of a mechanical failure criterion for both describing and quantifying the failure of pultruded FRPs.

To overcome this, experimental investigations were carried out at different levels: the basic FRP material has been investigated in both senses of revealing the fibre architecture — with the help of burn-off tests — and the material strength — using a device the Author especially developed for this purpose: the CCLAB SHEAR-TENSILE DEVICE. This device allows the determination of the material strength subjected to combinations of out-of-plane and shear stresses. The device was also used to determine an important basic material property necessary to numerically formulate the anisotropy: the out-of-plane E-Modulus.

Besides the investigations on the basic material, experiments on bonded single and double lap joints were carried out where the influence of parameters like the length of the bonded overlap, the thickness of the adherents and stress reduction methods (like chamfers of fillets) on the ultimate load was investigated. All of these experimental investigations were carried out on relatively big specimens to avoid the influence of any size effects. The experimental results showed that the adhesive layer thickness and stress reduction measures like chamfers are by far less influential that former publications expected them. For selected geometric configurations, the axial strain development along the bonded splice was experimentally gathered using strain gauges. Comparisons with FEA showed that by using the right mechanical input parameters in regard to the anisotropy, it is possible to model, with sufficient accuracy the stresses inside adhesively bonded joints of pultruded FRPs. Some single and double lap joints were filmed using a high-speed camera (up to 2 000 fps) to investigate the failure process. This failure process is closely linked to the fibre architecture in the sense that it has been shown that the failure is triggered inside the laminate.

The entire group of experimentally investigated specimens were then modeled with the Finite Element Method using orthotropic elements. In combination with the experimentally gathered material failure criterion, it was possible to formulate a method based on the comparison of stresses in the joint and the material resistance to predict the ultimate load of single and double lap joints, which was validated for a wide range of geometrical configurations.

A simplified version of this method, based on existing analytical formulæ, was then developed to make the strength prediction of adhesively bonded joints of pultruded FRP shapes available for civil engineering purposes.

ACKNOWLEDGMENT

I would like to first express my deep thanks to Prof. Thomas KELLER to have granted me his full confidence, trust and liberty in carrying out this research.

My genuine thanks goes to the people who accepted to act as jury members this this Thesis: Prof. Thomas KELLER from the CCLab [committee chair], Prof. Inès LAMUNIÈRE [President], Prof. Manfred HIRT from the ICOM, Prof. Urs MEIER from the EMPA, Prof. Johann-Dietrich WÖRNER from the TECHNISCHE UNIVERSITÄT DARMSTADT and last but not least to Aixi ZHOU, PhD, from the CCLab.

I want to express my gratitude to the partners of the industry — SIKA, FIBERLINE, SCOBALIT and the KTI/CTI[1] — who partly founded the project as well as to the excellent SWISS INTITUTE OF TECHNOLOGY (EPFL) who allowed me to spend three exciting years on this interesting project.

I would like then to thank all my — present and former — colleagues at the CCLab: Julia DE CASTRO, Tommaso TIRELLI, Martin SCHOLLMAYER, Herbert GÜRTLER, Craig TRACY, Florian RIEBEL, Sean DOOLEY and Lucienne DI BIASE. Some helped *manually* in the lab and all *intellectually* in the frame of discussions.
Special thanks are due to Herbert GÜRTLER. Without his help, it would probably not have been possible to develop the CCLAB TENSILE SHEAR DEVICE, a keystone of this work.

A profound thank you also to my colleagues from the LCC1: Dan BOLOMEY, Cristina BOO, Pierre ZURBRUEGG and David GUZMAN to have given me the energy to go on in times of lower motivation. They have a bigger part in the fulfillment of this work than they might think.

Not to forget *Madame* SOMMER, as she backed me in the majority of the administrative parts I will always be grateful for her help.

Thank you to the colleagues from the *Institut de Structures*, the IS: Sylvain DEMIERRE — the man who solves every problem, all the technicians: Gérard OREILLER, Roland GYSLER, François PERRIN, Gilbert PIDOUX and Hans-Jakob REIST. The collaboration was sometimes not easy, but always successful. All did a great job!

A bottomless thanks to the guys from the *Atelier des maquettes*, Bernard BORBOËN, Antoine GAGLIARDI and the others. They helped me very much in the elaboration and optimization in manufacturing the test specimens.

Without the help of my friends from the IT3 — Paulo DE JESUS, Nicolas CHEVALLEY, Catherine CORNAZ and Michel HERZEN — who helped so many times to solve technical problems related to the management of the network, it would have probably taken much more time to finish the job — to not mention the liters of coffee I owe them.

A special thanks to the three students I had the honor to supervise their masters theses: Ralf GUMMERSBACH, Jan SIEBRECHT and Zhang JIE. Their valuable work has been largely used for my Thesis.
I do not want to forget the help of Juan-David VILLEGAS, a former student who helped me very much in manufacturing some specimens.

Last, but not least, I want also to thank the ALGERIAN MINISTRY OF PUBLIC EDUCATION for the excellent education received. I express the same gratitude towards my former university, the TECHNISCHE UNIVERSITÄT DARMSTADT.

I must acknowledge that any errors of fact or interpretation, anything misleading or incomprehensible remaining in this work come from my oversight, ignorance or refusal to hear excellent advice.

[1] The Swiss Innovation Agency.

Part I.

Introduction and Objectives

Repetita non placent...

1. Composites and Civil Engineering

1.1. Composites in construction

The history of civil engineering is characterized by several big developmental steps mainly triggered by the introduction of new materials.
First Men used wood and stones, later, probably in *Mesopotamia*[1], he started using his first composite material: the adobe — a composite of clay and organic fibers: straw.
Some 8 000 years later we did the same by inventing Fiber Reinforced Polymers (FRP).
The principle is easy to understand: combining the advantages of two — or more — materials to create a new system having advantages of its constituents.

After having been introduced for applications like aviation (see Fig. 1.1-a), boat construction (Fig. 1.1-b), automobile industry and aerospace, FRP's entered the world of civil engineering application where they reached a first peak in term of building material for experimental housing projects in the 1950's and 1960's.

The use of FRP as a building material declined in the 1970's for different reasons [2]. The revival of FRP's came with the 1990's with the introduction of Pultrusion at an industrial level[2] as a new way of manufacturing FRP-laminates. At present the pultrusion industry grows steadily in the US as well as in Europe.

FRP might well be the material of the 21st Century as claimed by M. V. Karbhari & L. Zhao in [3]. A good introduction to some of the current and future application fields for FRP's is given by [3].

1.2. Joints

As civil engineers are traditionally not very agile in switching from one technology to another, they used — up to now — the connection techniques inherited from structural steel to connect their profiles made of pultruded FRP.

Obviously bolting and riveting is not adapted to the very anisotropic, fibrous and brittle material. One material-adapted way to connect Fiber Reinforced Polymer laminates is adhesive bonding.
But even if adhesive bonding would be better suited, leading even to higher bearing loads[3], no building has ever been erected using this technique.
The reasons for that lie on different levels:

① Adhesive bonding for load bearing elements has not been used outside some experimental or demonstration studies;

② There is no Standard or Code ruling any connections adhesively bonded for load bearing elements;

③ The manufacturers of pultruded laminates do not offer much technical help or guidance for joining other than by bolts.

[1] Çatal Hüyük, 6 000 BC. See [1].
[2] Even if pultrusion was already known as a manufacturing process since the 1950's in very basic forms.
[3] As shown in Chapter 13 of this Thesis.

(a) A composite plane

(b) A composite sail boat

Figure 1.1.: Composite applications

2. OBJECTIVES

The global objective of this Thesis is to contribute to the development of a viable and safe Structural Design Method for axially loaded Adhesively Bonded Joints of Pultruded GFRP Shapes to be used by civil engineers.

To be compatible with usual civil engineering practice, predicting the lap joint strength should be based on comparing an actual stress level to a system given resistance. To formulate such a dimensioning method, it will be necessary to carry out investigations at different levels of the adhesively bonded lap joints made of pultruded FRPs.

One of the main tasks to perform is to **determine the stress-strain state inside adhesively bonded joints**. For this, it will be necessary to **build-up numerical models** of the mechanical systems considered using a Finite Element program. To provide accurate mechanical input data to the FEA, it will be necessary to **carry out experimental investigations on the materials involved**: the adhesive and the FRP.

The validity and accuracy of such numerical models have to be checked on real physical experiments. It is crucial that the FEA is able to model both the global load deformation behaviour and the local strain state, especially in the overlap zone. For this purpose one of the objectives will be to **experimentally determine the axial strain profile along the bonded overlap** of several geometrical configurations using strain gauges.

Experimental and numerical investigations have to investigate in greater depth the influence of chamfers on both the ultimate load and the stress-strain state.

The next objective is then the **mechanical description of the stress state leading to failure. A device allowing to simultaneously measure the material strength towards both out-of-plane and shear stresses** has to be developed.

Having reached these objectives, it should then be a relatively easy task to **combine the gathered knowledge to formulate a Structural Design Method for Adhesively Bonded Joints of Pultruded GFRP Shapes**. The accuracy of this prediction method will be checked on the experimental results.

As for every **modern dimensioning method**, the aspect of safety is expressed by a corresponding **partial safety factor**. These factors can be deduced from the experimental data collected throughout the achievement of the other objectives.

Part II.

State of the Art

Quot capita tot census!

3. Description of the Stress State in the Joint

In order that adhesive bonding may be fully utilized by civil engineers, it is necessary to be able to predict the behaviour and strength of bonded joints having known material properties, geometries and loads.

This ability is thus an important step towards predicting the behaviour and strength of whole structures. It is obvious that such a prediction would reduce considerably the amount of extensive and expensive experimental series and can therefore be considered as the *conditio sine qua non* for a safe and economic design.

A prerequisite for successfully dimensioning joint strengths is the understanding of the stress-strain state in the joint and a reliable failure criterion of the joint.

There are basically two different approaches to solve such issues:

- The first one is the **analytical** approach based on solving the differential equations describing the mechanical and kinematic characteristics of the joints;
- The second one, **numerical**, consists in solving the problem using Finite Element programs.

3.1. Analytical Descriptions

To use the analytical method, several simplifications and idealizations of all the components and the geometry have to be made. Any deviation from idealized geometries (chamfers, spews and fillets) or strict linear isotropic mechanical behaviour (of the adherents and the adhesive) is almost impossible to include.

3.1.1. Linear-elastic considerations

The first to analytically describe adhesively bonded lap joints was O. Volkersen in [4]. This very basic description — originally intended to describe the load transfer in riveted connections — accounted only for longitudinal tensile deformations of the adherents and a pure shear stress state in the adhesive layer.

The next major step was then taken by Goland & Reissner in [5] by taking into account both shear deformations in the adherents and eccentricities in a single-lap joint. Despite the lack in the mechanical description, the results given by their equations show the main characteristics of adhesively bonded joints: the stress concentration towards the ends of the overlap.

Further investigations carried out by O. Volkersen in [6], Renton & Vinson in [7] and Allman in [8] led to an enhanced description of peeling[1] stresses in the adhesive-adherend interface and bending, shearing and stretching of the adherents. There investigations can be considered near to the maximum reachable by closed linear-analytical description.

A good summary for the state of the art related to analytical formulæ for double lap joints is given in [9], for single lap joints see [10].

A simplified two-stage analytical model for predicting the distribution of shear and axial stresses in a variety of adhesive joints has been described by Roberts in [11]. Comparison of results obtained by this method – based on linear-elastic material properties — with results obtained using the Finite Element Method have confirmed a good approximation for idealized boundary conditions, but highlighted the fact that a number of details such as **rounding of sharp corners, spews, tapering and fillets considerably reduces the stress concentrations.**

It must be highlighted that no publication offers hints on how to analytically deduce the out-of-plane stresses. Only simplified formulæ are given.

[1] Peeling stresses are those stresses acting at the adhesive-adherend interface in the out-of-plane direction. They have not to be confounded with the out-of-plane stresses acting in both the adhesive and the adherents.

3.1.2. ELASTO-PLASTIC CONSIDERATIONS

All analyses mentioned above considered a perfectly linear-elastic behaviour of both the adherents and the adhesive. Since very basic considerations lead to the fact that the easiest way to reduce the sharp stress peaks at the ends of the joint would be the use of a mechanically plastic adhesive, different authors attempted to introduce this feature in an analytical description. The first one to publish such results was HART-SMITH in [12] and [13].
HART-SMITH used a bi-linear model elastic-perfectly-plastic approximation. As a concession to the difficulty to solve the equations in a closed form, he omitted to introduce a similar constitutive law for the out-of-plane stresses.

A very concise and interesting non-linear adhesively bonded joint design analysis is given by D. A. BIGWOOD & A. D. CROCOMBE in [16] showing different degrees of non-linearity. The authors claim that their analysis produces good results compared with results obtained by Finite Element Analysis.

This section will be concluded by giving a reference summarizing the state of the art concerning the analytical aspect of the mechanics of single lap joints worth being considered: [17] by R. D. ADAMS.

3.2. NUMERICAL DESCRIPTIONS

The second approach is based on the Finite Element Method (FEM). It's not worth spending many words on the principles[2] of this now widely spread method that must be considered as being part of the usual tools for engineers.

The range of joint geometries and material non-linearities or orthotropy that can be investigated by FEA is virtually unlimited. The only limitation seems to be the time needed to process a calculation, a parameter that should be taken in account when considering studies involving various parameters.

Besides these advantages, some dangers should not be concealed. The FEM needs a careful check of both the input and the output to avoid GIGO[3]-effects. The risk is big for users to start believing in the FEM as being a substitution for experimental work, while it's only a representation of what has been modeled. Another aspect worth being mentioned is the fact that the FEM is not a tool intended for preliminary investigations.

J. DE CASTRO demonstrated in [31] the good correlation between experimentally and numerically gathered axial strains on the adhesively bonded splice of bonded joints of pultruded adherents.
Besides this, it has been shown in [31] that the experimentally gathered displacement — using a video-extensometer, see Fig. 3.1 — agree well with numerical ones, demonstrating by this the suitability of numerical modelization of bonded lap joints of pultruded profiles.

As demontrated in [19] and [20], it is possible to derivate 3d micromodels for the non-linear analysis of pultruded FRP composite materials that can predict the nonlinear response under different multi-axial stress states. These elements can explicitly *recognize* the response of the roving and CFM[4] composite systems.

Instead of showing the historical development of the FEM related to adhesively bonded joints analysis — a development mainly dictated by the increase in computer power – selected publications related to the work currently underway will be briefly summarized.

3.2.1. MODELING THE ADHESIVE LAYER

One important issue when modeling adhesively bonded joints is the fact that the adhesive layer is usually very thin. The thickness of this layer directly defines the size of the corresponding finite element size leading to huge numbers of elements. This effect is also related to the number of elements selected to model the adhesive layer.
F. RIEBEL investigated in [15] the stresses in the adhesive layer with increasing refinement. The investigation came to the conclusion that for more than 3 stacked elements in the thickness direction, the stresses converge.

3.2.2. 2D- VS. 3D-FE ANALYSIS

FE investigations can be conducted as 2d- or 3d-Analyses. Obviously 2d-models are easier to generate and do not need the huge calculation times needed for 3d-Analyses. Thus, it is of great importance to check if 2d-Analysis results coincide with those obtained from 3d-Analyses.

G. RICHARDSON, A. D. CROCOMBE & P. A. SMITH have checked this issue in [18] with the result

[2] A good introduction to the FEM is given in [14]
[3] Garbage In - Garbage Out.
[4] See under section 9.2.2 the meaning of the technical terms used to describe the architecture of a pultruded profile.

that a 2d-Analysis reproduces the conditions at various positions across the width of a 3d-modeled joint. Their **3d-Analysis showed also that the adhesive remains in a state of plane stress over 80 % of the width of the joints studied.**

J. de Castro showed in [31] that the strain profile over the width of the adherents near to the end of the overlap — where they reach their maximum — were slightly lower than inside the joint, so that failure could be expected to be initiated inside — and not at the border of — the overlapped zone.

R.C. Andruet made — amongst others — in his PhD thesis [26] a 3d calculations of a single lap joint represented in Fig 3.2. The results, displayed in Fig. 3.3, clearly show that the stresses are relatively equal over the whole width of the specimen with a reduction towards the free edges.

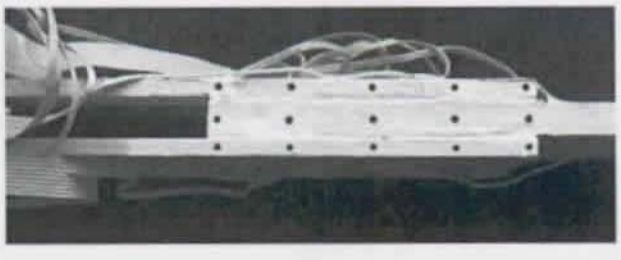

Figure 3.1.: A double lap joint investigated in [31] using the video-extesometer

3.2.3. Plain Stress state vs. Triaxial Stress state

The adhesive layer in bonded joints is subjected not only to a out-of-plane stress σ_z[5] and a shear stress τ_{xz}, but also to two axial stresses, σ_x parallel and σ_y perpendicular to the joint axis due to the constraint imparted by the adherents[6].

Investigations on analytical and numerical basis carried out by C. H. Wang & L. R. F. Rose and described in [22] lead to the following conclusions:

① The axial stress σ_x and transverse stress σ_y in the adhesive layer seem to have a magnitude comparable to that of the out-of-plane stress σ_z;

② The onset of plastic yielding in the adhesive layer and failure are strongly affected by the triaxial stress state;

③ The plastic yielding shear level in the adhesive layer is dependent of the level of peeling stress.

Those facts should be taken into account when carrying out experiments with high levels of plasticity in the adhesive layer.

3.2.4. FEA of bonded joints

Several papers deal with the Finite Element Analysis of adhesively bonded joints. It is not possible in the frame of this work to cite all of them. Some of those directly related to the work presented here will be briefly cited.

A relatively general technical note has been published by G. Wu & A. D. Crocombe describing the simplified finite element modeling of structural adhesive joints [21]. The authors have modeled the following typically used structural joints:

① Single lap joints;

② Double lap joints;

③ T-type joints;

④ Stiffeners.

The authors came to the following conclusions:

① Adhesive stresses from a relatively coarsly meshed model can be used for design purposes;

② Simplified models provide reliable results for single and double lap joints;

③ For more complex systems, hybrid FE formulations can lead to a reduction of computational time.

G. Li & P. Lee-Sullivan investigated and documented in [23] balanced single-lap joints[7] in tension (see Fig. 3.4) and compared the FEA with their own experimental results.
The paper is one of the few comparing experimentally gathered values to FEA results, the agreement was found to be good.

In the work of G. Li, P. Lee-Sullivan & R. W. Thring in [24] — a nonlinear Finite Element Analysis — the stress and strain distributions across the adhesive thickness in composite single-lap joints was investigated.
In this investigation, it has been shown that the maximum out-of-plane and shear stresses do not act in the centerline of the adhesive layer, but are closer to the adherents. This is clear evidence that **deeper investigations concerning failure cannot only**

[5] Axis designation according to Fig. 3.3.
[6] This problem is directly bound to the question of carrying out a 2d- or 3d-Analysis.
[7] Having two equal adherents, in geometry and material.

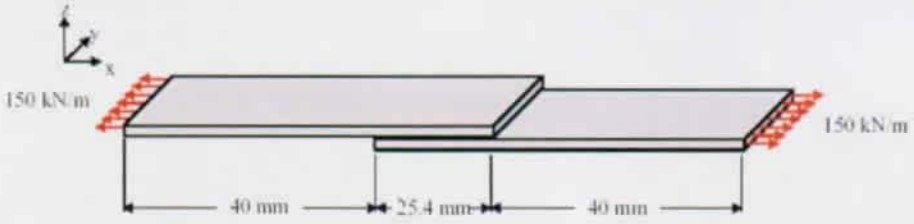

Figure 3.2.: The single lap joint investigated in [26]

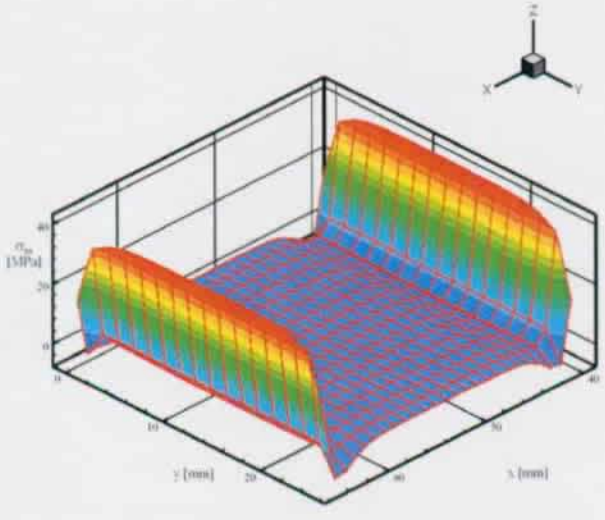

(a) Axial stresses

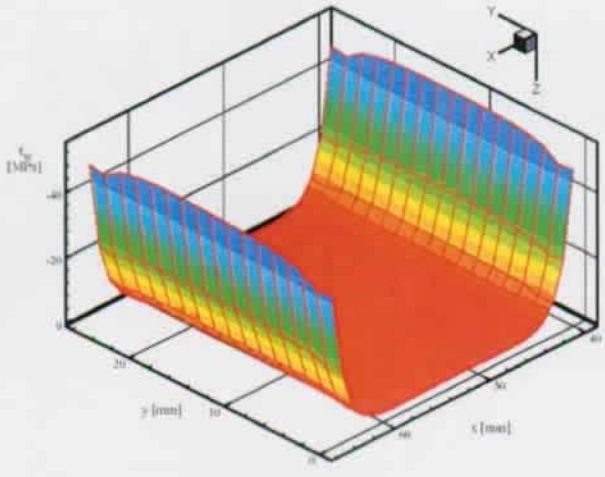

(b) Shear stresses

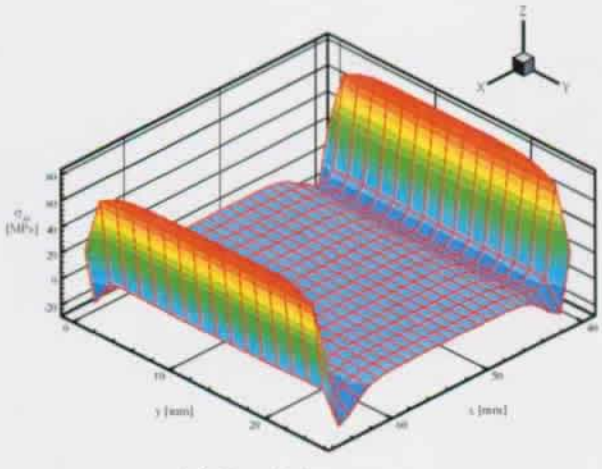

(c) Out-of-plane stresses

Figure 3.3.: The results of the single lap joint investigation in [26]

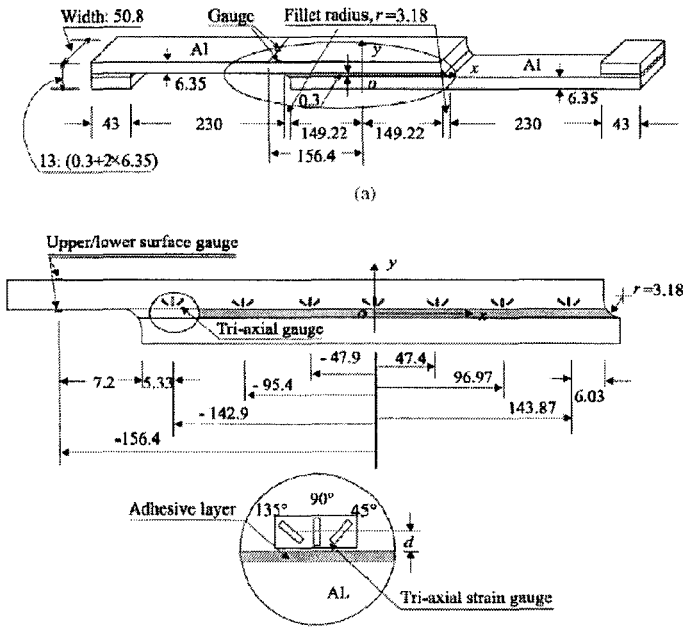

Figure 3.4.: The single lap joint investigated in [23]

rely on overly general expressions like those given by the closed-form analytical solutions.
Two main results of the research are:

① The maximum tensile out-of-plane[8] stresses and strains within the adhesive bond occur near the adhesive-adherend interface at the corner ends of the joint overlap;

② The peak shear stresses and strains lie between the centerline and the adhesive-adherend interface.

It is proposed that **the crack leading to failure** will propagate within the adhesive layer near the interface before joining diagonally across the adhesive thickness **due to the combination of mixed-mode peel[9] and shear stresses.**

A. E. BOGDANOVICH & I. KIZHAKKETHARA published in [25] a work on a 3d finite element analysis[10] of double-lap composite adhesively bonded joints.
This very well documented work highlighted one important fact that will be of importance in the frame of this Thesis: the effect of the spew fillet on the stress distribution near the end of the overlap[11], see Fig. 3.5 .
These investigations confirm those that were carried out before concerning the effect of spews on both the shear and out-of-plane stresses.
Consequently **it is of great importance to take these stress-reduction measures into account when predicting failure initiation in the joint.**

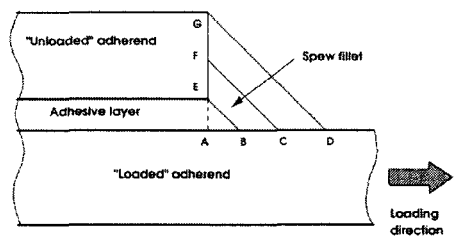

(a) Principle

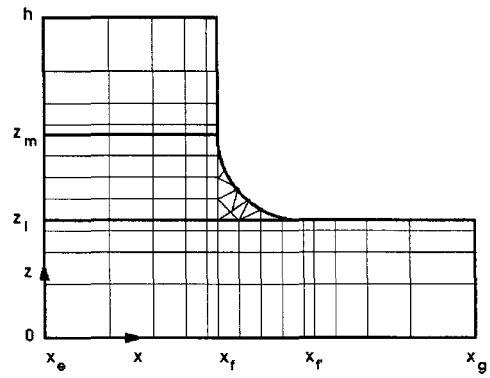

(b) Meshed

Figure 3.5.: The modeling of the spew in [25]

[8] Peel in the original paper.
[9] In the terminology of this Thesis it would be out-of-plane stress.
[10] Using ABAQUS.
[11] More on this topic in Sections 5.2.1 and 27.2.3

A totally different approach has been selected by R.C. ANDRUET in his Ph.D.-Thesis [26] which was summarized in [27]. Instead of using commercial — or academic — FEA software, unique 2d and 3d adhesive elements were formulated for stress and displacement analysis in adhesively bonded joints. The fact that the FEA was programmed by the author and that it is available as *analytical open source* — allows to include some interesting features, among them a failure criteria[12].
It is also possible — even if it was not described in both [26] and [27] — to include chamfers in the geometrical model. It would be interesting to know if it would also be possible to include spews and/or their effects, because this could be the starting point of a tailor-made software package for dimensioning purposes replacing the resource consuming commercial FEA programs.

[12] This is basically also possible in commercial programs, but in a not so *transparent* way like in a open source one.

4. Failure Criteria

4.1. General statements

The prediction of both the failure load and the failure mode of adhesively bonded composite joints — see Fig. 4.1 for an example of failed adhesively bonded joint — is a task made very complex by many factors. Adhesive joints are generally not well behaved from an analytical point of view. The reasons for that lie in the strong anisotropy of the composite adherents, the very complex multi-axial stress distribution in the adhesive and the not well investigated delamination strength. Because of this complexity and the lack of deeper investigations, most joints are designed using rules of thumb and general guidelines.

The most valuable resource concerning viable failure criteria for fibrous composite materials is certainly L. J. Hart-Smith.
L. J. Hart-Smith developed several failure models valid for layered-up composites, among them the *the original and truncated maximum-strain failure model* [28], the *Ten-Percent Rule* [29] and the *generalized maximum-shear-stress failure criterion* [30].
Unfortunately these **failure models have not yet been validated for pultruded composites.** It might be interesting to investigate the fact if pultruded composites behaved mechanically like layered-up composites.

4.2. Generalities

There are basically two ways to formulate a failure criterion:

① **Based on a realistic failure hypothesis:** if the complexity of the system is not too high, a realistic hypothesis of failure can be deduced and used to describe a failure criterion through analytical or numerical methods. This method fails for complex systems like those treated in the framework of this research. Such a formulation has the obvious advantage to build on a solid mechanical base and would be valid for a large range of geometrical configurations;

② **Based on material experiments:** if the complexity of the systems prohibits the formulation of a usable failure hypothesis, experiments have to be carried out varying the whole set of free parameters and trying to fit the results in a simple mathematical expression. Because of the mathematical approximation results from just limited geometrical configurations, the failure criterion can only be valid for some of these configurations.

4.2.1. Additional remarks

① In a complex system — like the adhesively bonded joint of pultruded shapes — several different failure modes and therefore failure criteria can be involved and should be investigated;

② Dimensioning is defined as keeping the stress-state of the system within the limits defined by the failure criteria. Mathematically this is done by keeping $\mathfrak{F}(\sigma_i, \tau_i, \sigma_{i,u}, \tau_{ij,u}, ..) \leq 1$.

4.2.2. Classical material strength vs. fracture mechanics

Two different approaches are possible for investigating the question of ultimate strength and associated failure mechanism:

① A first one based on **classical material strength**, which consists on comparing the existing stress-level to a predetermined ultimate stress-level;

② An second approach based on **fracture mechanics**, a tool intensively used by mechanical Engineers dealing with composites.

4.2.3. Mathematical formulation

A failure criteria is defined as a mathematical function $\mathfrak{F}$ depending of the following parameters:

① **The variables stresses[1] acting in the joint.** Depending of the complexity of the system, several stress components can be included: σ_i and τ_{ij};

[1] The definition given here was made on the level of stresses. Besides this failure model, there are also models based on maximum strain. Basically the same remarks stated above are then valid if the word *stress* is replaced by *strain*.
A good overview of the state of the art in regard to the topic of predicting failure models of certain fibrous composite composites laminates by the maximum strain is given by the publication of L. J. Hart-Smith [28].

② **The material strengths** that are ideally only material dependent. Among those parameters describing the stiffness (like E_i, G_{ij}-Modulus and the associated POISSON-ratios ν_{ij}) and others describing the ultimate strength ($\sigma_{i,u}$ and $\tau_{ij,u}$).

The failure criteria can be geometrically represented by a curve. The *dimension* of this curve is given by the number of *free* parameters.
Failure criteria are usually represented as curves, see [28], [29], [30] and [38] among others.

4.2.4. FAILURE MECHANISM OF A BONDED JOINT

Basically several elements in an adhesively bonded joint (see Fig. 4.1 for an example) could fail, leading to different formulation of a failure criteria.

① **Failure of one of the pultruded elements:** Simple tension/compression, shear and bending experiments — ideally carried out by the manufacturer — should quickly make it possible to describe failure for any load combination;

② **Failure of the Adhesive layer:** The failure of the adhesive layer is the mechanism mostly described in design manuals (see [66]). The basic failure mode for adhesives is of course related to the main stress-state encountered: the shear. The associated failure criteria is simply described by $\tau_{xz} \leq \tau_{xz,u}$. If the peeling stresses become significantly greater, interaction formulæ for shear τ_{xz} and out-of-plane stresses σ_z might better describe the failure. Such interaction formulæ are not directly accessible and have to — experimentally — be deduced;

③ **Delamination of the pultruded elements:** Bonded joints might also fail in the joint region by delamination. To better understand this failure process — see Fig. 4.1 — it is necessary to keep in mind that pultrusion leads to a typical architecture with the layering described in Section 9.2.2.

Typical failure modes of adhesively bonded single lap joints of brittle and ductile adherents are presented and discussed by K. LIECHTI, W. S. JOHNSON & D. A. DILLARD in [71]. For *filamentary composite adherents*[2] (FRPs) the following has been stated: *The failure usually occurs in the composite and not in the adhesive bondline.* This is due to the fact that FRPs are extremely weak in the out-of-plane direction for both the tensile σ_z and the τ_{xz} shear stresses. This weakness leads to the fact that thicker adherents would not lead to increased ultimate loads.

A classification of failure modes of FRP joints was made by the ASTM, it has been represented in Fig. 4.2.

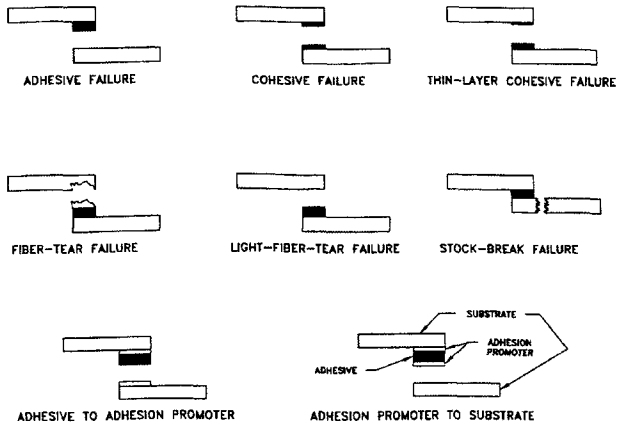

Figure 4.2.: *Classification of failure modes in FRP Joints according to ASTM D 5573-99*

4.3. FAILURE CRITERIA BASED ON CLASSICAL MATERIAL STRENGTH

The basic idea behind the use of failure criteria based on classical material strength is the natural reflex of engineers to reuse the knowledge and principles they are used to dealing with.

The very basic formulation of such a criteria could be described by the following set of equations:

$$\tau_{ij,max} \leq \tau_{ij,u} \tag{4.1}$$

and/or

$$\sigma_{i,max} \leq \sigma_{i,u} \tag{4.2}$$

where τ are shear stresses, σ are out-of-plane stresses, the index $\ldots_u$ stands for ultimate and the indexes $\ldots_i$ stand for each of the components involved in the joint.
This criterion may be used with a certain accuracy for systems close to some idealization. But when it comes to systems civil engineers are used to dealing with, things are not that easy.

[2] As denoted in [71].

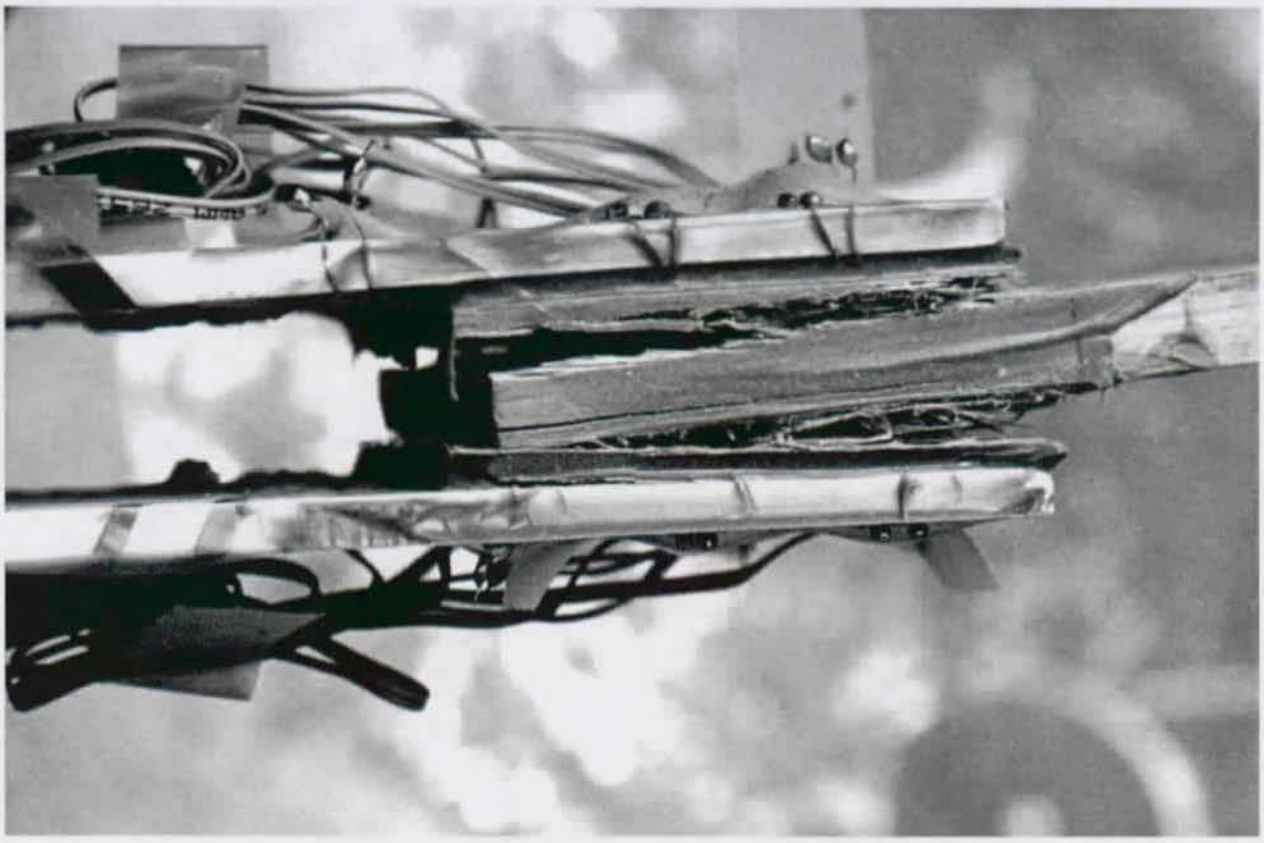

Figure 4.1.: Failure of an adhesively bonded joint [78]

4.3.1. Static strength of Adhesively Bonded Arall-Joints

R. S. Long described in [32] a experimental series where Arall[3]-Joints — Single-Lap and Double-Lap — were driven up to failure.
Fig. 4.3 shows the layering of the material.

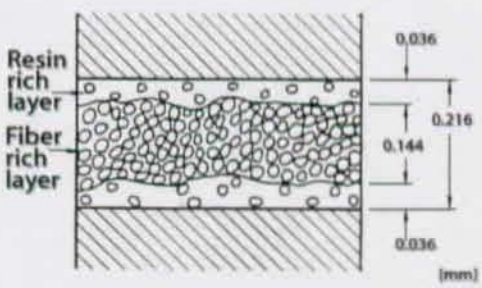

Figure 4.3.: Layering of the ARALL-1 composite according to [32]

Failure values for the ultimate out-of-plane[4] stress $\sigma_{z,u}$ were obtained using a simple apparatus — a Flatwise Tensile Experimental Device, see Fig. 4.4. The corresponding ultimate shear stresses $\tau_{xz,u}$ were obtained using 0°-Iosipescu-tests on prepeg samples.
It is a little unfortunate that the material resistance values had to be gathered using two totally different mechanical devices.

Using the FEA for modeling the single and double lap joints and assuming that failure was triggered mainly by exceeding the out-of-plane ultimate stress, it was possible for the authors to derive a kind of *ARALL-1 interlaminar failure criterion* represented in Fig. 4.5.

[3] Aramid-Aluminum-Composites
[4] Denoted peeling stresses in [32]. See also Fig. 4.5 where *Peel stresses* on the ordinate have to be understood as *out-of-plane stresses*.

Two relatively simple failure criteria were stated and compared to the experimental results. The authors tested the following simple mathematical interaction for a possible failure criterion:

$$\frac{\sigma_z}{\sigma_{z,u}} + \left(\frac{\tau_{xz}}{\tau_{xz,u}}\right)^2 \leq 1 \tag{4.3}$$

$$\left(\frac{\sigma_z}{\sigma_{z,u}}\right)^2 + \left(\frac{\tau_{xz}}{\tau_{xz,u}}\right)^2 \leq 1 \tag{4.4}$$

where σ_z are the out-of-plane stresses, τ_{xz} the shear stress and $\ldots_u$ represents the failure-value.

Equation 4.3 was found to best fit the experimentally gathered material strength. As it can be recognized, the data set is very small. Obviously the authors relied on their mathematical regression formulæ to fill the gap, especially towards higher shear stresses.

With the help of a high-speed camera (up to 200 fps) it was possible to have a closer look at the mechanism leading to failure. R. S. LONG describes the failure sequence — represented in Fig. 4.6 for a single lap joint — as the following:

(a) First the adhesive fillet separated from the adherend;

(b) Then the crack progressed along the bondline;

(c) Then the crack propagates into one of the adherents;

(d) Up to the end, no failure of the adhesive bondline could be observed.

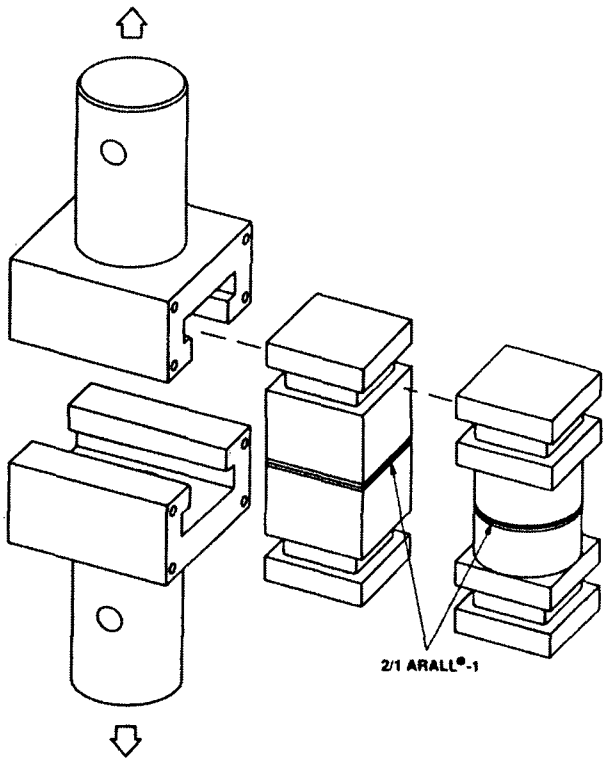

Figure 4.4.: The Flatwise Tensile Test Device according to [32]

4.3.2. THE CONCEPT OF ULTIMATE TENSILE STRESS OVER A ZONE

A different approach to the problem of predicting the static strength of adhesively-bonded joints was reported by J.D. CLARK & I. J. MCGREGOR in [33].

The summarized idea behind this concept is the fact that — according to the authors — failure occurs when the ultimate tensile out-of-plane stress of the adhesive material is exceeded over a zone of finite size, and not — as implicitly stated in quite all former publications — in a single spot.
The authors checked their assumption with several experimental investigations and FEA on 3 different joint types — simple-lap, double-lap and T-peel — using epoxies as adhesives and aluminum for the adherents. They claimed a good correlation between the results obtained using their concept and their experiments.

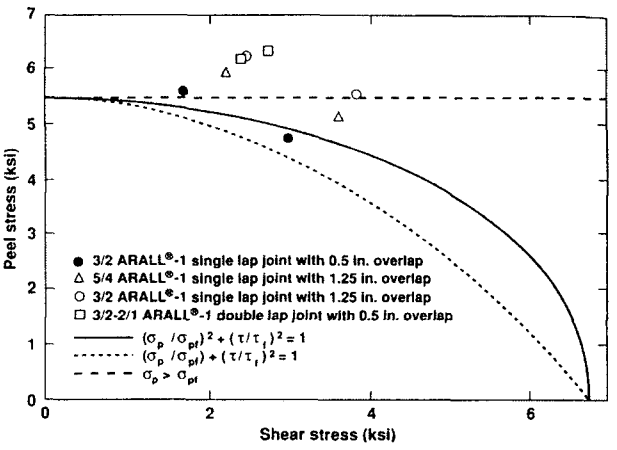

Figure 4.5.: The ARALL-1 interlaminar failure criterion according to [32] — *Peel stresses* in the ordinates stands for out-of-plane stresses in the terminology of this Thesis

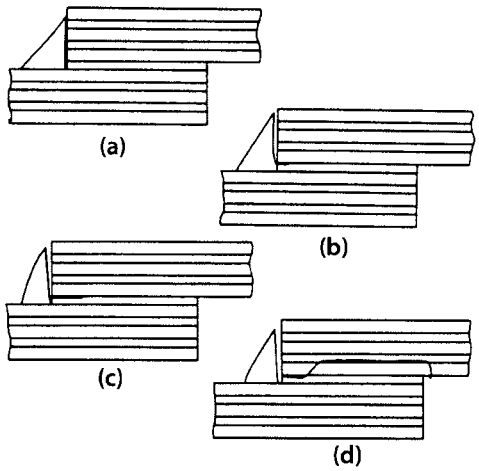

Figure 4.6.: The failure sequence observed according to [32]

Unfortunately no indications are given how to determine the size of the finite area — which is considered to be *a property of the adhesive.* More, no mechanical interpretation is given, so that the concept is to be considered as just a phenomenological description.

4.3.3. INFLUENCE OF AXIAL STRESSES

When considering bonded joints, axial strains also act inside the adherents. The effect of axial stress on the strength parameters was cited in [32] and described in [38] for layered-up laminates. It was suggested that these effects can be described by a reduction of all the ultimate strengths involved by a constant *weakening factor* $f_w(\sigma_x)$:

$$f_w(\sigma_x) = 1 - \left(\frac{\sigma_x}{\sigma_{xD}}\right)^n \tag{4.5}$$

The exponent n is to be determined experimentally. Former investigations led to a factor between 4 and 6, σ_{xD} is another experimentally determined factor. Because of the relatively high value of the exponent n, strength losses should be negligible if the stresses are significantly below the ultimate limit strength.

4.4. FAILURE CRITERIA BASED ON FRACTURE MECHANICS

The first one to give a formalized strength theory of anisotropic materials was S. W. TSAI in [36].

A good global introduction to the failure mechanism is given by F. ERDOGAN in [37], while the issue of composites — dedicated to engineers — is given by A. PUCK in [38].

Reviewing these references shows that the special aspect of pultruded materials has not yet been treated separately.

It might be interesting at this point to reproduce the statement of A. PUCK — taken from [38] and related to the strength of layered up FRPs: *Es besteht eine gewisse Gleichwertigkeit der bruchmechanischen Formulierungen und der klassischen Ansätze der Bruchbedingungen mit Spannungen und Festigkeiten. Von dort aus gesehen gibt es somit keine schwerwiegenden Bedenken dagegen, die in der Ingenieurpraxis geläufige klassische Form der Bruchbedingung beizubehalten.*[5]

Because of the complexity of the subject and the fact that this Research will focus more on fracture criteria based on the **classical material strength theory**, only a short introduction to selected publications dealing with bonded lap joints of FRPs will be made.

An introduction is given by G. FERNLUND & J. K. SPELT in [34]. The first part of this publication describes an analytical method for calculating the energy strain release rate of structural adhesive joints. The equations derived make it easy to apply the principles of fracture mechanics failure criteria to loaded joints for design purposes. The second part describes some experimental investigations to verify the assumptions made in part one.
Without going in the details of both experimentally investigating and interpretation of the results, the procedure developed claims to give *a reliable, conservative* estimate of the failure load.

In another publication, G. FERNLUND, J. K. SPELT & AL. [35] summarized, formalized and widened the concept described in [34] to both single and double lap joints for engineering applications.
The authors conclude by pointing out the good correlation between experimental and analytical results obtained by the method described and emphasize the *closed form nature* of the approach.

[5] The Authors translation:
There is a certain equivalence of the fracture-mechanics formulation and the classical material strength formulation dealing with tensions and strengths. From this point of view there are thus no serious objections to maintain the classical material strength for common engineering practice.

4.5. ADHESIVES

The adhesive manufacturers are able to give basic values (mainly ultimate stresses σ_u, τ_u, $\sigma - \varepsilon$- or $\tau - \gamma$-relations) needed by designing engineers, but *higher Fracture Theories*[6] of adhesives are rare.

The easiest way to determine a failure criterion for adhesives — valid over a range of stresses and stress combinations — is to formulate the mechanical properties for clearly given separated stress states like pure shear or axial compression and tension.

B. DUNCAN & G. DEAN have published in [91] methods to measure properties of modern adhesives. The article gives precious indications on formulæ to predict the contribution from the yield mechanism as well as on experimental methods on how to gather the required parameters. The authors conclude with the remark that for an accurate modeling of adhesively bonded joints, the knowledge of the adhesive behaviour close to failure initiation is important.

4.5.1. BULK PROPERTIES OF ADHESIVES

Two clearly different possibilities are offered: gathering the material properties of the bulk adhesive or In-Situ[7].

The determination on bulk adhesive material is the way selected by the most standards, recommendations or codes (like ISO 527[8] and ASTM D-695-96[9]).

4.5.2. IN-SITU PROPERTIES OF ADHESIVES

besides this, it is possible to carry out experimental investigations putting the adhesive in mechanical situations close to the concern of a given system, leading to *in-situ* material properties.
R. BREDAMO & P. A. GRADIN have performed a testing of *in-situ* properties of adhesives on an experimental and numerical level and documented the results in [41]. It was found that analytical or numerical expressions for determining the in-situ properties of adhesives correlate — within few percent — with experimental ones. It is therefore possible to design own experimental setups and to determine specific material properties in correlation with numerical models.

Similar investigations based on a purely analytical basis were performed by W. J. RENTON in [42] with recommendations concerning the shape — in terms of specimen aspect ratios — leading to uniform stresses.

[6] One example of such a criterion for an epoxy is given by C. K. LIM & AL. in [40].
[7] In-Situ property means here the property of the adhesive as it is inside it mechanical system — for example as an adhesive layer.
[8] For adhesive axial tensile ultimate stress.
[9] For adhesive axial compressive ultimate stress.

5. JOINTS

To date investigations on adhesively bonded joints for composites have only been formulated at a highly academic level in both senses of being confined to some theoretical systems (very small specimens, materials not used in Civil Engineering etc.) and formulated in a encrypted language (systems of differential equations, fracture mechanics) that prohibits a wider use[1]. An important fact is also that the major part of research carried out up to now was not made on pultruded profiles, but on layered-up composites.

In his *Analysis and Design of Advanced Composite Bonded Joints* — [12] — L. J. HART-SMITH addressed the majority of issues related to adhesively bonded joints, offering solutions if available. The basic statements are still valid nowadays and are to be found found as entries in regulations, such as the EUROCOMP design manual [66].
L. J. HART-SMITH adressed — among other — the following topics: analytical formulations, practical design considerations, scaling effects, surface preparation, adhesive plasticity, stress reduction techniques etc. Of course, the publication being more than 30 years old, cannot be considered as up to date. Nevertheless, it is a precious resource for those interested in adhesively bonded joints of composite materials.

The following section highlights some important aspects concerning adhesively bonded connections and the issues of importance for this research.

5.1. RELATIVE STIFFNESS ADHERAND/ADHESIVE

The effect of the relative stiffness of the adherents and the adhesive on the stresses in idealized adhesively bonded joints has been investigated by W. J. RENTON & J. R. VINSON in [43].

The analysis is based on LAMINATE PLATE THEORY leading to an 8^{th}-Order differential equation.

The authors have investigated different parameters on the stress distribution:

① The ratio of the primary shear moduli $\frac{G_{xz,A}}{G_{xz,a}}$[2];

② The overlap length;

③ The ratio of the in-plane stiffness of the effective shear $\frac{E_{x,A}}{G_{xz,a}}$;

The main results are the following:

① With increasing $\frac{G_{xz,A}}{G_{xz,a}}$, the adhesive shear and out-of-plane stress profile tends to be flatter[3];

② With increasing overlap lengths, the shear and out-of-plane stress peaks at the end of the overlaps tend to be more sharp;

③ With increasing $\frac{E_{x,A}}{G_{xz,a}}$-ratio, the shear and out-of-plane stress profiles tend to flatten;

besides these parameters, the influence of the adhesive layer was also investigated.

Based on the results presented, the following conclusions to increase the static and fatigue load were formulated, among them the following:

① Joining identical adherents (in material and geometry);

② Choosing an adhesive as soft as possible;

③ Taking an adherend thickness at least 10 times the adhesive thickness.

The conclusion is that reducing the stiffness of the adhesive relative to the adherents tends to flatten the corresponding σ_z and τ_{xz} stresses along the bonded overlap.

5.2. STRESS REDUCTION METHODS

In the following section some selected papers related to these topics are presented. Without claiming to give a complete overview, they nevertheless cover the main aspects of the issues discussed above.

5.2.1. CHAMFERS, SCARFS AND STEPS

The topic of scarfed and stepped adhesively bonded lap joints has been investigated by F. MORTENSEN & O. TH. THOMSEN in [44]. The paper illustrates a unified approach for the analysis of adhesively bonded scarfed and stepped joints. The authors base their

[1] [39] is a typical representative of such publications.
[2] **A** for Adherend and **a** for adhesive.
[3] This tendency is not as clear as for the shear stress profile.

approach on a mathematical-mechanical basis including a KIRCHHOFF formulation for the orthotropic adherents including non-linear material properties for the adhesives.
The same authors extended the filed on investigable joint configurations in [45] and [46] by widening the mathematical-mechanical formulation of the problem. The results were validated by comparative FEA calculations. Fig. 5.3 show typical configurations investigated.
These publications clearly shows the dilemma of the analysis of such complex systems by starting with relatively simple general formulations and ending up in FEA. When it comes to practical use, the method cannot be used unless formulated as a program.
In [44], [45] and [46] the authors state some general recommendations, very similar to those stated before in [43]:

① Use identical or nearly identical adherents;

② Use an overlap length of minimum ten times the *minimum adherend thickness*;

③ Use an adhesive with relatively low values of the elastic shear and tensile moduli;

④ Use advanced joint configurations[4] instead of standard joint configurations.

A direct linear-elastic analysis of double symmetric bonded joints have been formulated by A. M. ALBAT & D. P. ROMILLY in [47]. The approach, a derivation of generally accepted linear-elastic principles, has been — amongst others — applied to the case of tapered double lap joints, as shown in Fig. 5.4. The method presented has the immense advantage of being easily codable in mathematical interpreters like MATLAB, a tool more and more used by designing engineers. *While being a very useful tool for understanding the stress distributions in these joints and reinforcements, it is recognized that more elaborate analysis methods will generally be required when investigating failure modes...* conclude the authors.

5.2.2. FILLETS AND ROUNDING

The effect of a spew fillet on the stress reduction in adhesively bonded composite single-lap joints has been investigated by M. Y. TSAI & J. MORTON in [48]. By directly comparing two single-lap joints, one with and one without a spew[5] fillet, using experimental[6] and and numerical[7] means, the authors came to the following conclusions:

① The global deformation of the test specimen is verified by comparing the experimental and numerical results;

② The experimentally and numerically gathered longitudinal strains as determined by numerical and experimental means concord;

③ The adhesive shear and peeling[8] stresses are significantly reduced by the spew fillet.

A similar topic was investigated by T. P. LANG & P. K. MALLICK in [49]. The authors numerically investigated several types of single lap joint spew geometries — from square ones to arc-fillets[9]. The effect of these spews was investigated on the axial, shear and out-of-plane stress concentrations at the end of the overlap. The authors drew some conclusions, among them:

① Spews have a significant impact on the reduction of all stresses at the end of the overlap;

② This effect should not be neglected in the stress analysis;

③ The stress reduction is increased by larger triangular spews;

④ For arc spews the reduction effect is independent of the arc spew radius.

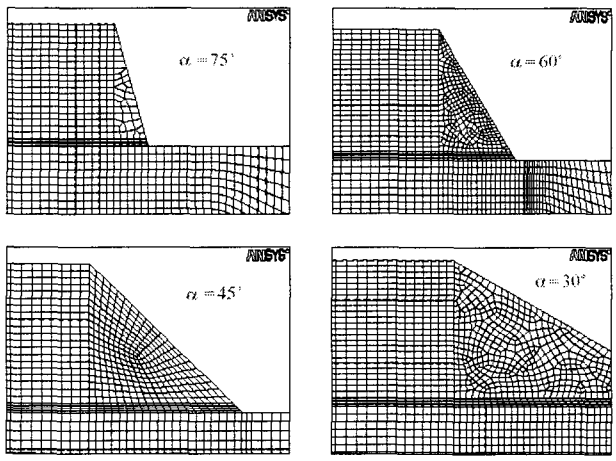

Figure 5.1.: The spew angle as defined in [50]

[4] Like scarfed or stepped ones.
[5] A spew is defined as ther portion of the adhesive that is squeezed out from the lap area and forming a bead at the end of the overlap.
[6] Using the MOIRÉ-technique to obtain the surface deformations and strain gauges to determine axial strains.
[7] Using the FEA-package ABAQUS.
[8] Or out-of-plane.
[9] As those investigated — and simply called fillets — in the frame of this Thesis, see Part III.

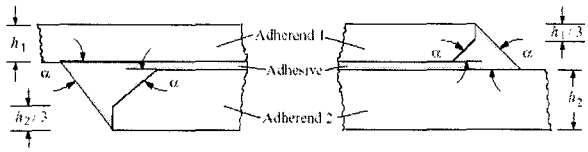

Figure 5.2.: The chamfer angle as defined in [50]

G. BELINGARDI, L. GOGLIO & A. TARDITI made a 2d FEA[10] comparative investigation on the effect of spew and chamfer size on stresses in adhesive joints and documented the results in [50]. In a first step they investigated the effect of the spew angle (as defined in Fig. 5.1) on the stress distribution close to the overlap end. In a second step they investigated the effect of the angle of a chamfer (see Fig. 5.2) on the stresses. As a main conclusion they outlined that these — feasible and geometrically simple to achieve — measures offer an advantage in terms of stress reduction of a magnitude for the out-of-plane stresses and half an order for the shear stresses. They also outline the fact that these results were obtained considering a pure linear-elastic material description.

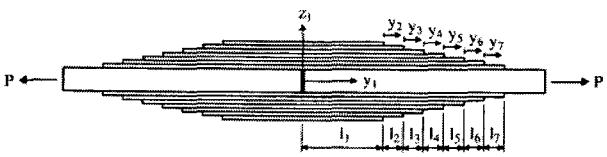

Figure 5.4.: The tapered double lap joint investigated in [47]

Another way to formulate the stress concentration at the corner singularities was selected by C. H. WANG & L. R. F. ROSE in [51]. Stress intensity factors were determined for — the limiting case of rigid substrates for — the corner singularity at the adhesive/adherend interface in bonded single and double lap joints (see Fig. 5.5).
The authors developed a theory to derive non-dimensional stress concentration factors (see Fig. 5.6) for peel and shear. Using these factors it is possible to estimate the stress intensity factor for different corner singularities. Combining these results with former analytical formulæ the authors claim to get a good agreement with FEA results.

5.3. EFFECT OF BOND THICKNESS

S. MALL & G. RAMAMURTHY in [52] have carried out a study about the effect of bond thickness on fracture and fatigue strength of adhesively bonded composite joints.

[10]Using ANSYS.

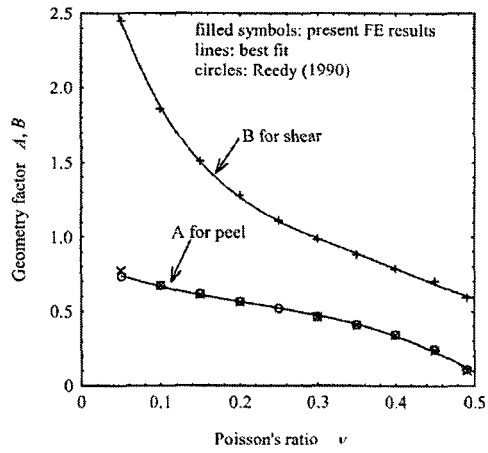

Figure 5.6.: Non-dimensional stress intensity factors for peel and shear, [51]

While the systems considered — neither the adherend material, the adhesive, geometry, loading nor failure pattern were comparable — have not the slightest relation to those investigated in the frame of this Thesis, it might be interesting to reproduce their conclusions here. For the specific composite bonded system investigated in [52]:

① The energy release rate increased at higher adhesive thicknesses with the adhesive thickness;

② The fatigue resistance increased at higher adhesive thicknesses with the adhesive thickness.

5.4. TENON AND MORTISE JOINTS AND SINGLE LAP JOINTS

Among the few publications related to the comparison of experimental and analytical investigations, [57] is presented at this point.
B. FARGETTE, Y. GILIBERT & L. RIMLINGER have experimentally investigated the axial strain development along the bonded overlap for joints tenon and mortise joints and single lap joints of $10 \times 10\,mm^2$ steel and aluminum bars.
The authors came to the conclusion that within the elastic range the analytical formulaæ can be used for an accurate strain prediction, differences appear only at such loads inducing plastic behavior.

5.5. CONCLUDING WORDS

R. D. ADAMS reviewed in [53] the main issues concerning the strength prediction for lap joints, especially with composite adherents.

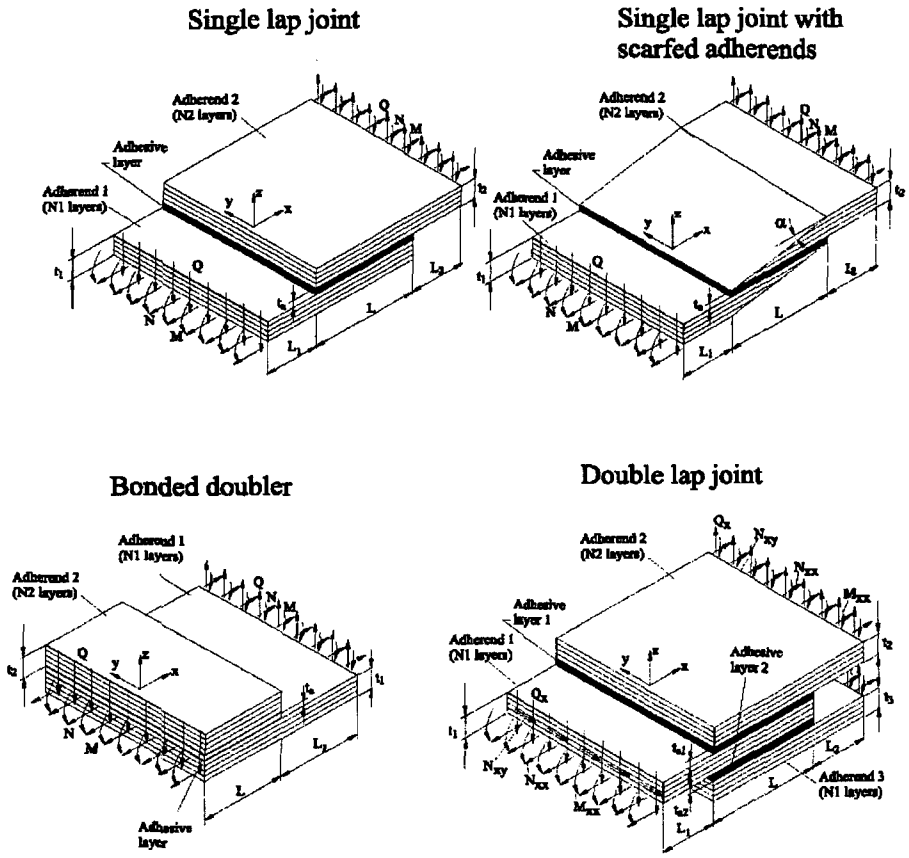

Figure 5.3.: Some systems investigated in [45]

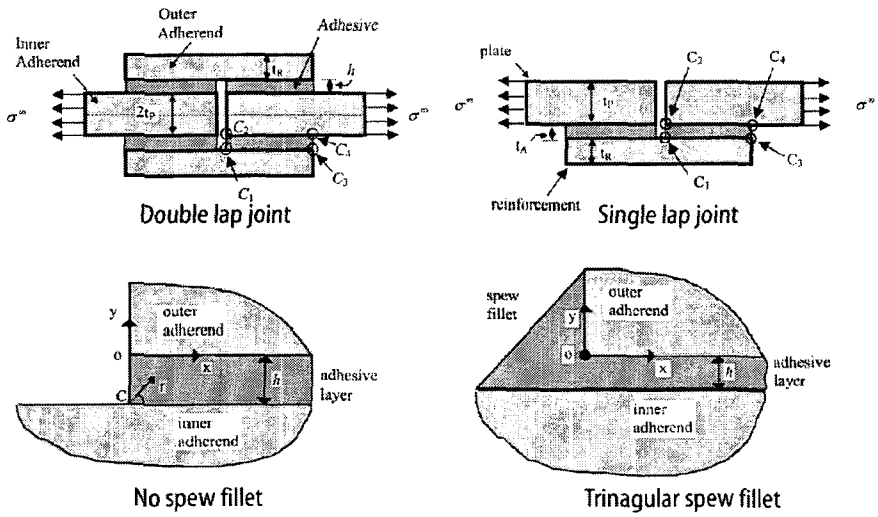

Figure 5.5.: The systems investigated by C. H. WANG & L. R. F. ROSE in [51]

The main conclusions were already discussed in the sections above, but it might be interesting to list some of them:

① Analytical techniques — such as those discussed in Section 3.1 — cannot be used for lap joint strength;

② Finite Element approaches can model lap joints with more accuracy — from the mechanical and geometrical point of view;

③ Among the failure modes, two are of particular interest: the interlaminar failure of the FRP and the cohesive failure of the adhesive layer;

④ Applying a failure criteria to FEA results, the failure load could be determined.

The paper represents something like the state of the art of the late 1980's.

5.5.1. CONCLUSIONS

L. J. HART-SMITH published in [54] the progress to date[11] and the remaining challenges in adhesive bonding of composite materials.
The paper includes a historic overview about the application of bonded joints in aviation. This is not the right place to discuss all the issues, but some of HART-SMITHs conclusion can be directly used as conclusions for this section:

① *In well-designed bonded joints [...] the adherend will fail first, at such a high load that the fibers are being fully used and not wasted by poor design*;

② *One [should] always design bonded joints with tapered ends to the exterior adherents to preclude the generation of intolerable peel stresses, without any loss of shear strength.*

[11] *To date* related to July 2002.

6. Developments at the CCLab

Figure 6.1.: The Pontresina Bridge

Besides the small scale experiments mainly carried out on non-pultruded material described in previous sections, some full-scale experiments have been conducted in the last three years by the Composite Construction Laboratory (CCLab) at the EPFL.
The CCLab was also involved in the planning and erection of some structures.

A very concise state of the art of the *Use of Fiber Reinforced Polymers in Bridge Construction* has been published in July 2001 by the CCLab [65].

6.1. The Pontresina Bridge

The pedestrian Bridge in *Pontresina/Switzerland*, was a first step towards material adapted joining technique for pultruded FRP. One of the two 12 500 mm long truss-spans was *traditionally* bolted while the other one was adhesively bond[1], see Fig. 6.1. Experiments carried out showed that, as expected, the glued span is stiffer that the bolted one. More details can be found in [56].

6.2. EyeCatcher

Another step towards material adapted techniques was made by erecting the 15 m tall 5-storey EyeCatcher at the Swiss Building Fair 99, see Fig. 6.3.

[1] Even if bolts were added in the second span, the loading mechanism does not activate them.

Pultruded GFRP were used. Adhesives were used to bond available pultruded cross-section together to form larger profiles. Bolting was used to connect larger parts of the buildings with the aim to dismantle and relocate it after the fair. The EyeCatcher is actually the tallest all-composite building in the World.
More details can be found in [55] and [56].

6.2.1. Bonded girder experiments

The primary load-carrying structure of this EyeCatcher had to be adhesively assembled from smaller available pultruded profiles. These composite beams, represented in Fig. 6.2, were then bolted to build up the whole structure. Bolting was selected to make it possible to dismantle the building in order to move it.

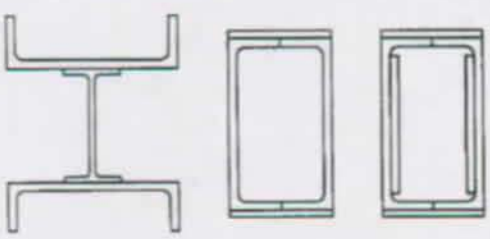

Figure 6.2.: The bonded girders of Sec. 6.2.1

To check the structural safety and ultimate load of such built-up profiles, four-point bending experiments were carried out in 1999 — a description can be found in [55].
A two-components epoxy adhesive was used. The main results were that the system stayed almost linear up to failure. Failure occurred **in the FRP base-material** and **not in the adhesive joint**. These results demonstrated clearly the suitability of adhesion as a joining method for even larger structures.

6.2.2. Adhesively bonded Sandwich Girder Experiments

The next step towards further integrations of both architectural and structural functions led to the investigation of a girder with a web made of translucent sandwich elements while the flanges consisted of pultruded profiles bonded together.
Experiments were carried out at the CCLab (Fig. 6.4) to further investigate the load bearing capacities and failure mechanisms of such systems —

Figure 6.3.: The EyeCatcher

see also [55] for more details. The positive experimental results showed that such Meta-Composite profiles may be a serious option for future applications.

M. Schollmayer studied this girder in the frame of his master thesis [58].
The thesis mainly deals with the experimental description of the components and the behavior of this girder under load. The failure mechanisms is discussed and an analytical model to describe the stiffness and determine an estimation of the ultimate load are offered.

6.3. Double-lap joint experiments

Experiments on double-lap joints using pultruded flat profiles bonded together with SikaDur 330 (an epoxy) and SikaForce 7851 (a polyurethane) were carried out during summer 2001. A description is given in [59], [78] and [79]. FEA showed a good concordance with the experimental gathered results.

The most surprising result was the fact that the strengths and measured axial strain profiles along the bonded overlap were quite identical for the epoxy bonded and the polyurethane bonded specimen. This is despite the fact that the epoxy behaves much more stiffer than the polyurethane.

6.4. FRP-deck on Steel-Girders

H. Gürtler investigated the behaviour of adhesively bonded FRP-made DuraSpan and Asset-profiles on steel girders, see Fig. 6.5.
His investigations showed that it is possible to increase both the ultimate load and the stiffness of the DuraSpan and Asset-Steel system by bonding.
The experimental results showed clearly that bonding is a serious option and that full composite action can be assumed using the right adhesive.
Papers concerning this topic were already submitted and are in press: [61] and [62].

6.5. Fatigue of adhesively bonded joints

T. Tirelli made experimental investigations — reported in [63] and published in [64]— on the fatigue behaviour of simple FRP-flat-profiles and double-lap joints.
Fatigue experiments on adhesively connected pultruded profiles were performed in a laboratory environment. The first objective was to determine if fatigue limits exist and if so, how their magnitude is compared to real shear stress amplitudes in GFRP bridge structures subjected to fatigue loads. The investigations showed that a fatigue limit could be found.

A further objective was to evaluate measurement methods with respect to a possible detection of damage initiation and progression. During the experiments, damage initiation and progression were not detected with the selected set-up. Failures always occurred in a very brittle manner without warning in the adherents.

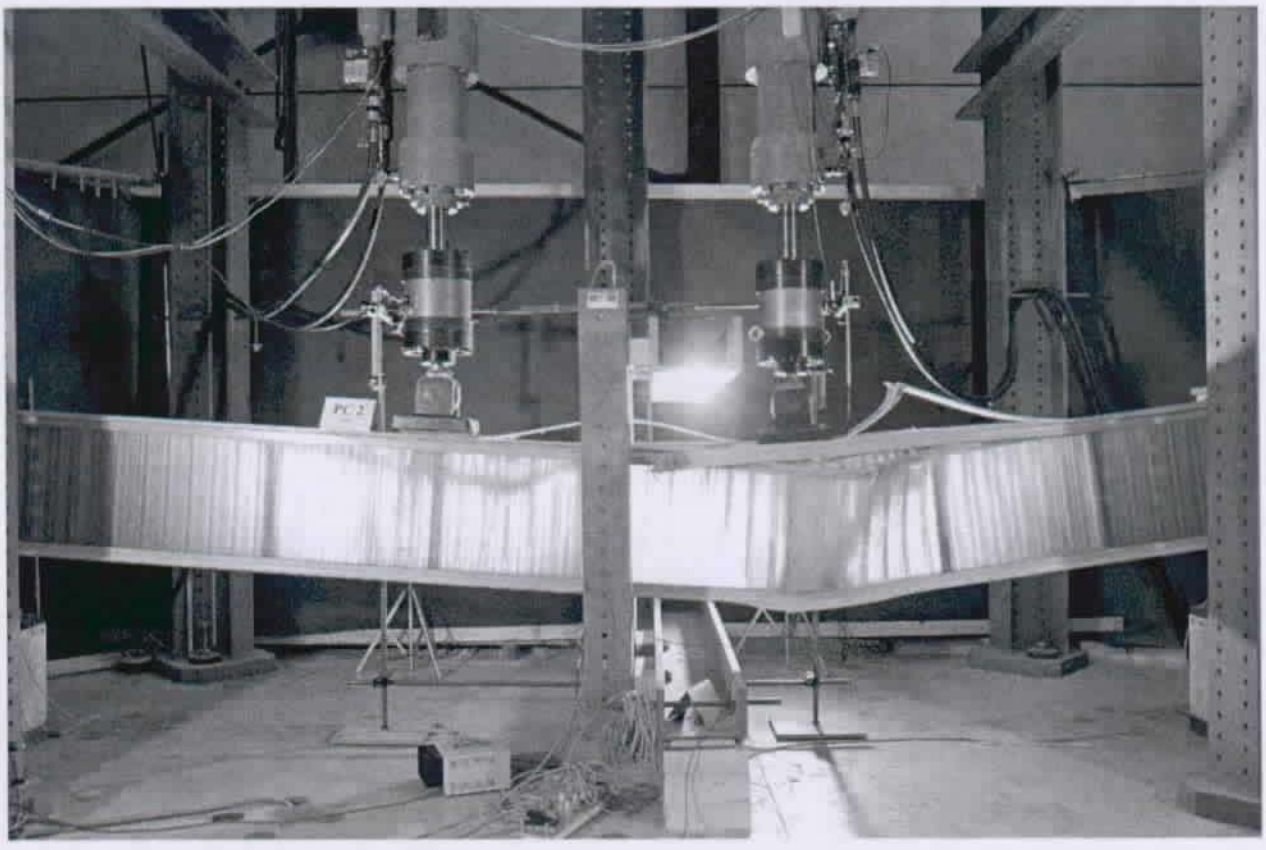

Figure 6.4.: Experiments on sandwich girders according to [55]

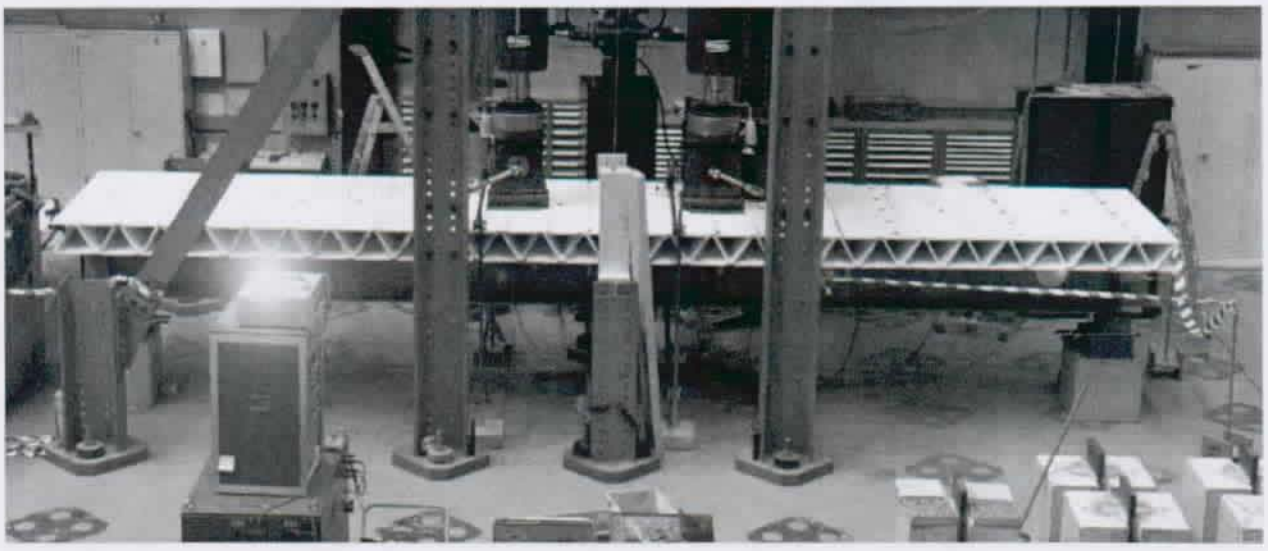

(a) The Asset-deck

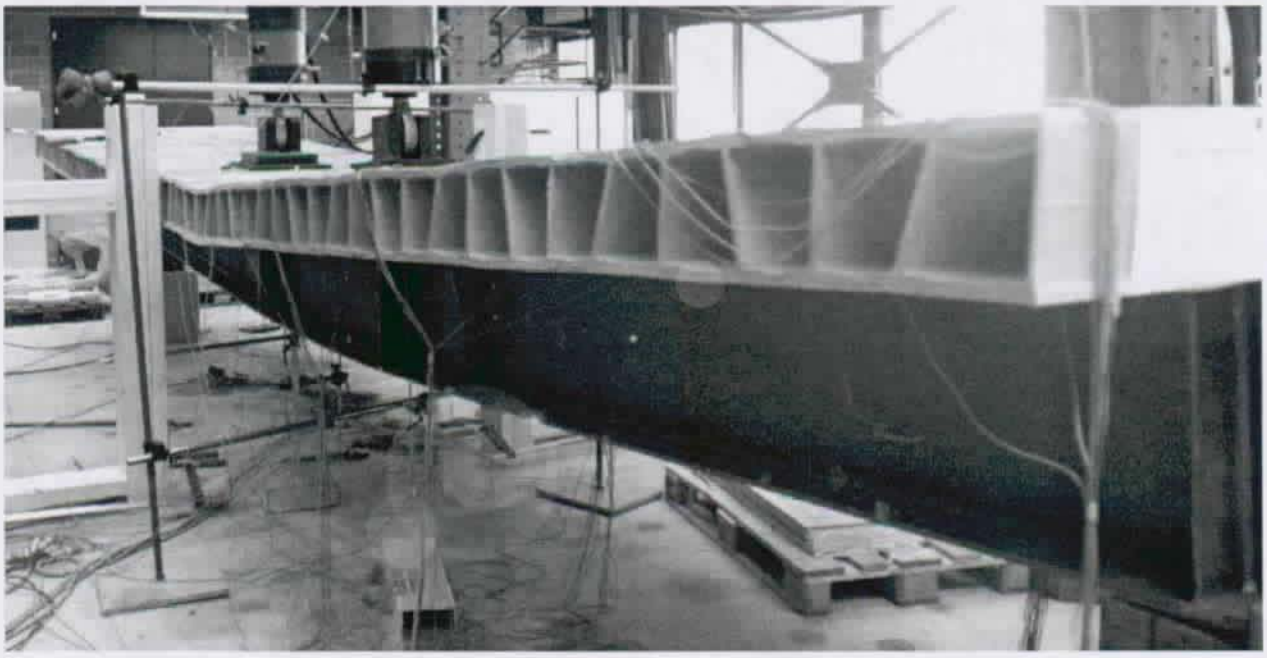

(b) The DuraSpan-deck

Figure 6.5.: Bridge-deck experiments carried out by H. Gürtler

7. Available Design Aids

As stated before, there is no code currently available to help civil engineers dimensioning either bolted or adhesively bonded Fiber Reinforced Polymer Structures.

Available Design Aids are supplied by the manufacturers of the pultruded profiles[1], by Organizations or Associations like the EuroComp, the German Arbeitskreis Tragende Kunststoffbauteile im Bauwesen or the Task Committee on Design of the Structural Plastics Research Council of the Technical Council on Research of the American Society of Civil Engineers.
The following is intended to quickly introduce some of the available publications.

7.1. The Eurocomp Design Code and Handbook

This book provides a very complete overview of design guidance [66]. The section related to bonding (pp. 183-236) offers different levels of complexity for dimensioning adhesively bonded joints based on simple classic material strength theories with no interaction formulæ . There are also some practical advice to reduce stress peaks by constructive means (chamfers, roundings etc.).
The approach is, at least, not fully adapted to be used for usual adhesively bonded joints of pultruded profiles, mainly because this publication assumes failure to occur in the adhesive layer or the material under one individual stress component, rather than under a combination of them. Besides this, some mathematical formulations are not adapted for civil engineering application, probably because they were drawn from some small size samples.

7.2. The Fiberline Design Manual

This reference is the most comprehensive European manual within the field of structural GFRP profiles [67]. The manual covers the following subjects: Assembling methods and dimensioning **for bolted connections**, Chemical resistance, Fire-technical properties and Environment and recycling.

[1]For example Fiberline in Denmark or Creative Pultrusions in the USA

While the manual is very useful for dimensioning profiles and bolted connections, no indication related to bonding is given.

7.3. The Creative Pultrusions Pultex Pultrusion Global Design Manual

The manual [68] is distributed on CD-ROM as a collection of *pdf.*-files. The year 2000 issue gives a basic introduction to the fabrication process, to the profile palette and to some methods of joining pultruded shapes. All that is, however, on a very low technical or scientific level.
The part related to adhesive bonding (in chapter 9) is very short and introduces potential users to aspects of surface preparation, adhesive choice and the different stresses acting in a bonded joint. No serious technical help is given.

7.4. Tragende Kunststoffbauteile im Bauwesen

This document [69], formulated as a Guideline, is intended to collect regulations, design rules and other generally recognized procedures in dimensioning FRP structures. The circle of people addressed is formed by active Designing Civil Engineers. The general form of the text is very code-like. No topic has been omitted, but are treated in a very general way.

7.5. ASTM Standards

The American Society for Testing and Materials issues every year the updated collections of Standard Test Practices [70], among them various experiments can be used to gather basic data for dimensioning purposes.
Unfortunately, no Standards are available for experimentally gather mechanical properties of pultruded material.

8. Concluding remarks concerning the state of the art

The review of the state of the art concerning the Structural Design Method for Adhesively Bonded Joints of Pultruded GFRP Shapes has been intentionally split into different parts. In a first conclusion, selected topics will be evaluated and then a general conclusion will be drawn.

8.1. Analytical formulæ

The state of the art concerning the analytical formulation of the single and double lap joint problems can be considered as being pushed to its limits. Viable **analytical formulæ exist** and might be used. It must be highlighted that these formulæ are **only valid for idealized geometries**, so that their use is probably limited to a very narrow class of problems.

Attempts to **broaden the strict limitations to geometrical or mechanical idealization** were made by several authors, but did generally **lead to a deviation of the closed-form solution**, losing by this their main argument for being used by designing engineers. Especially the attempts to include the material orthotropy lead either to high-order differential equation or to formulations close to FEA only having numerical solutions.

8.2. Finite Element Analysis

Using the FEA, it is possible to overcome the majority of the limitations stated in the previous section. Since its generalization and democratization in the 1970's and especially 1980's, a great number of investigations have been carried out, outlining important aspects like the influence of the orthotropy of the adherents, the influence of adhesive plasticity and — probably much more important — the influence of geometrical changes like spews, fillets and chamfers.

The influence of spews, fillets and chamfers is by far the most important one when it comes to the reduction of all involved stresses.

8.3. Failure criteria

The great missing link between the determination of the stress state inside adhesively bonded joints and the prediction of its ultimate loads is obviously the failure criteria.
While some general theories for predicting the failure loads and mechanism of layered-up composites have been formulated, **the specific topic of pultruded composites has not yet been treated.**

Some very few algebraic fitting functions based on experimental investigations have been suggested, but no systematic work has yet been done to characterize the failure of pultruded composites.

8.4. Experimental investigations and completed projects

Former experimental investigations and completed projects show **the suitability of adhesive bonding as a way to connect pultruded elements much more effectively** .

It has been shown that adhesively bonded joints of pultruded shapes have a specific failure mechanism. Failure is triggered inside one of the adherents by interlaminar failure. Adhesive failure was not observed, even for relatively soft and weak adhesives.

8.5. Conclusion

The state of the art was partly reviewed with the aim of identifying already existing parts of a structural verification method based on comparing the actual stress level — the *load side* — inside an adhesively bonded joint with a previously gathered material resistance — the *resistance side.*

Because of the orthotropic material and the big influence of geometrically difficult to handle aspects like spews and chamfers, analytical solutions alone will probably not be very helpful for describing the stress state inside adhesively bonded joints. With the help of the FEA, it might be possible to formulate

certain effects — like spews or chamfers — through stress intensity factors. This would allow one to ascertain the *load side* of the structural verification.

Ascertaining the *resistance side* on a theoretical basis seems out of range of current material knowledge, so that experimental investigations on pultruded FRP have to be carried out to improve the material resistance to combined loading: most likely shear and out-of-plane stress (the two dominating stresses acting in the adhesively bonded lap joints).

Joining the load side with the resistance side leads then to a STRUCTURAL DESIGN METHOD FOR ADHESIVELY BONDED JOINTS OF PULTRUDED GFRP SHAPES. The only step left is then the formulation of safety in the structural verification method.

Part III.

Experimental Investigations

Quis quid, ubi, quibus auxiliis, cur, quomodo, quando?

9. The pultruded material

The Author judged it useful to include a **first chapter** — of this part — **for describing the basic material the entire research deals with: the pultruded fiber reinforced polymers**. The main characteristics, fabrication process, fiber architecture and advantages/disatvantages are shortly presented in the following sections.

9.1. Manufacturing process

Pultrusion[1] is a manufacturing process for producing continuous lengths of FRP structural shapes.
Basically the fabrication process — described in Fig. 9.1 — is the following:

① The glass fiber — in form of rovings — is continuously pulled trough a shape-giving guide to be placed accurately in the desired cross-section;

② The fibers are then impregnated in a processing equipment where they are *wetted* by the resin

③ The *wet* mixture of resin and fibers is then pulled through the heated equipment where it is cured in its final geometry.

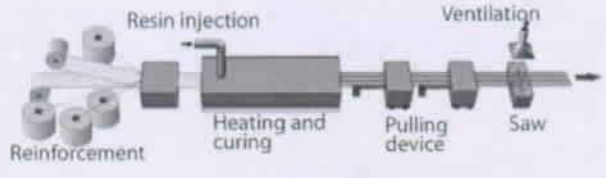

(a) Scheme

(b) At Fiberline

Figure 9.1.: Pultrusion machine

The aforementioned *pulled glass fibers* includes also a certain number of complex weaves and mats.

[1] A good introduction is given by [73].

9.2. Material architecture

Pultrusion leads to a typical kind of inner architecture as shown in Figs. 9.7 to 9.8:

① An outer surface veil made of randomly oriented relatively loose polyester fibers
↪ *Protection of the profile against mechanical and chemical aggression*;

② One or more combined mats and fabrics made of orthogonal and relatively tight held fibers
↪ *Shear strength of the profile*;

③ The inner core of axial high strength fibers
↪ *Axial strength of the profile.*

The basic difference between rovings and mats is that the rovings consist only of axially pulled fibers, see Fig. 9.2.

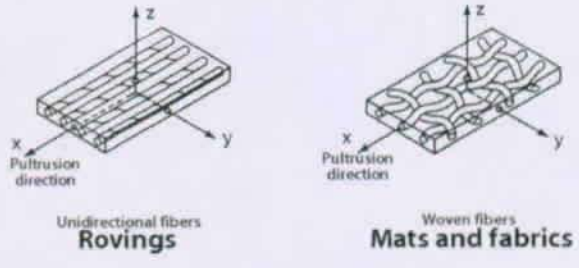

Figure 9.2.: The basic difference between rovings and mats

Currently, several Pultruders — like Fiberline — deliver a large palette of profiles, mainly in form of shapes inherited from the older Structural Steel construction, see Fig. 9.3.

Because of the nature of the product, the material is orthotropic; pultruded profiles have different mechanical properties in the three main axes x, y and z.

9.2.1. Analytical formulation of the behavior of pultruded FRP sections

It is possible to compute the global mechanical behaviour of pultruded FRP sectiona using the

Mechanics of Laminated Beams (MLB). J. F. DAVALORS, E. J. BARBERO ET AL. have shown in [74] that the material architecture of pultruded FRP can be efficiently modeled — based on the information delivered by the producers — as a layered system.
The authors have checked this issue and compared the computed values of given pultruded sections with experimental results and came to the conclusion that the MLB can be used as an efficient tool for engineering design.

J. F. DAVALOS, Y. KIM & E. J. BARBERO showed in [75] how to formulate a layerwise beam element — based on the generalized laminate plat etheory (GLPT) forulated by J. N. REDDY in [76] — for the analysis of frames with laminated sections.

An analysis of the mechanical behaviour and characterization of pultruded glass fiber-resin matrix composites was carried out by S. PACIORNIK, F. M. MARTINHO, M. H. P. DE MAURICIO & J. R. M. D'ALMEIDA in [77]. According to the publication, many of the mechanical and environmental properties of pultruded shapes can be tracked back knowing the composition of the resin, glass fiber and filler as well as their weight/volume-fractions and spatial distribution.

Without entering into the details of these publications, it must be retained that analytical methods exist to predict the mechanical response of systems made of pultruded shapes.

9.2.2. FIBERLINE'S PULTRUDED SHAPES

The experimental investigations carried out in the frame of this Thesis (see Chapters 10, 11, 12 and 13) were done with pultruded shapes manufactured by FIBERLINE.

FIBERLINE structural profiles are in accordance with the EN13 706[2], a European standard valid for pultruded profiles for construction purposes.

At FIBERLINE, the resin is injected, though former pultrusion processes worked on a basis of a resin bath. FIBERLINE claims that the injection of the resin leads to a better quality of the final product.

It is worth spending some words on the fiber architecture of this material because this knowledge is important for the interpretation of all experimental results.
Like all pultruded material, the shapes supplied by FIBERLINE have the basic architecture described in Section 9.2.2 which can be revealed by burning-off the resin — in a furnace at 450°C — (see Fig. 9.5) or by having a closer look using a microscope (Figs. 9.6, 9.7 and 9.8).
The layering, represented in Fig. 9.4, is the following:

① **Surface Veil**
↪ very thin, no strength, protection function.

② **Mat(s)**
↪ much thicker than the Veil and either a combination of a Chopped Strand Mat and a $0°\pm90°$ weave or just a CSM.

③ Inner Core called **Rovings**
↪ only rovings are used in the inner core in mainly two types: an ordinary smooth yarn and a blown yarn called *Mock*.

To see the effective architecture of the material and to analyze the void content of the matrix, the cross section of some specimens was observed using the microscopy (Fig. 9.6). Small pieces were cut from the middle of the profiles, machined at high speed to polish the surface using successively finer grades of carbide grit paper and ultrasonically cleaned at each step.

The rovings cannot be considered as a homogeneous layer: there are packages of axial fibers having

[2] EN13 706 is a European standard valid for pultruded profiles for construction purposes.
Minimum requirements for the quality and tolerances are defined by this code, as well as the strength and stiffness ratios of structural profiles.
Pultruded structural profiles are classified into two classes: E23 and E17. The E23 class defines higher quality shapes.

a uniform distribution of fairly constant diameter, and neighbouring fibers of differing diameter (Figs. 9.6-c to -f).

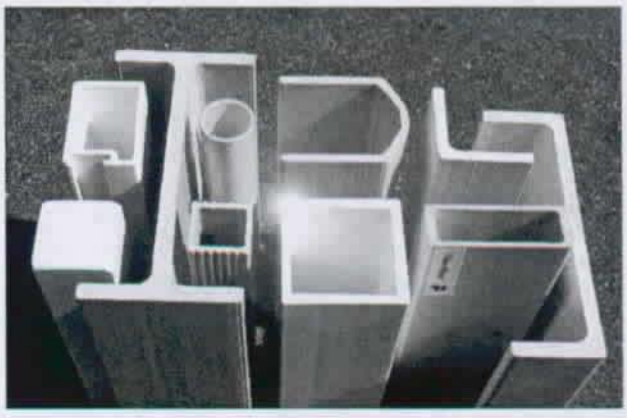

Figure 9.3.: Pultruded profiles supplied in traditional steel-structure shapes

Figure 9.5.: Fiber architecture of a flat profile revealed by a burn-off tests

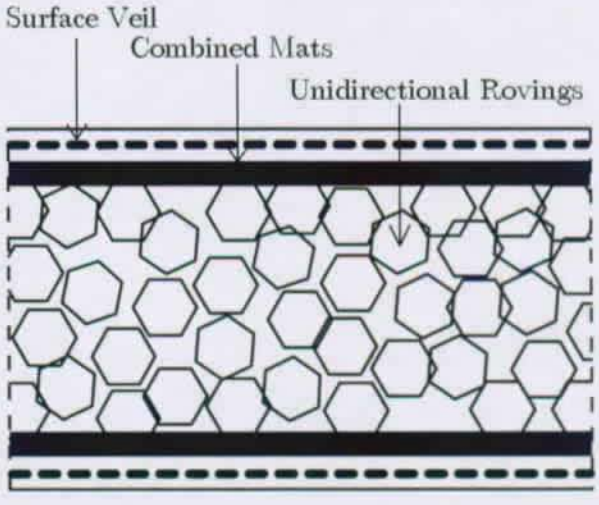

Figure 9.4.: Schematic drawing of a profile (size not proportional).

Fig. 9.8 shows also clearly that this layering varies in terms of thickness: the layer of mats is not a straight line, but is *oscillating* around an average distance from the free surface. Finally, the fiber fractions of the profiles are listed in Table 9.1 and were determined by weighing specimens before and after a resin burn-off. The volume fractions were calculated using an E-glass density of $2.56 \frac{g}{cm^3}$.

Each different material thickness features a different fiber architecture, this has to be kept in mind.

The mechanical values of these profiles can be found in Appendix B.

Profiles 10 mm thick		
Reinforcement	**Fiber content**	
	volume frac.	weight frac.
Rovings (UD)	**0.32**	0.47
4 Combined Mats	0.14	0.20
Total	**0.46**	**0.67**

Profiles 5 mm thick		
Reinforcement	**Fiber content**	
	volume frac.	weight frac.
Rovings (UD)	**0.37**	0.53
2 Combined Mats	0.10	0.14
Total	**0.47**	**0.67**

Table 9.1.: Fiber fractions by volume and weight of the pultruded profiles used (data experimentally determined).

(a) Pieces cut from profiles in a epoxy carrier before polish

(b) Polishing machine.

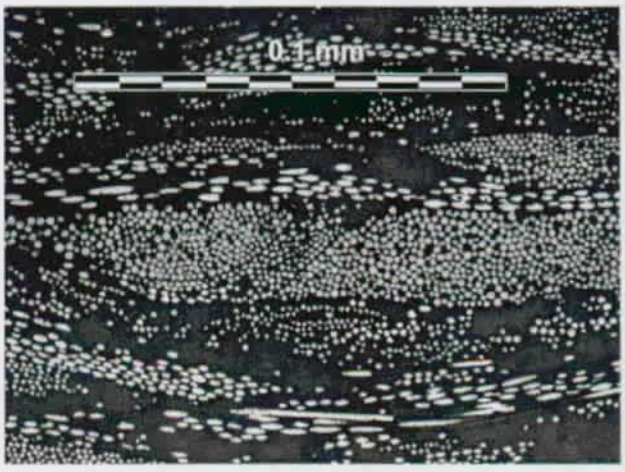

(c) Detail of the mats (50x) .

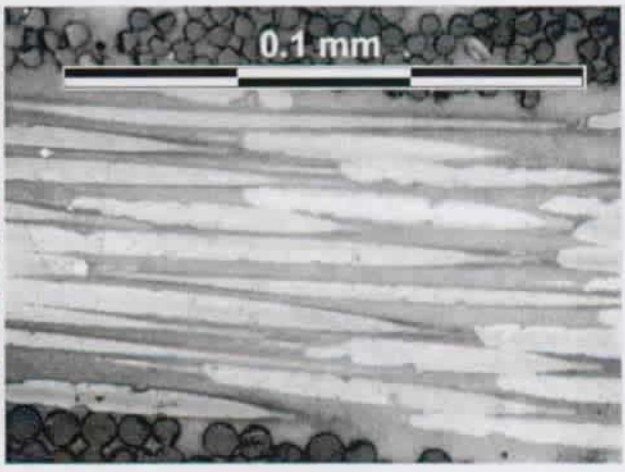

(d) Detail of the mats (200x) .

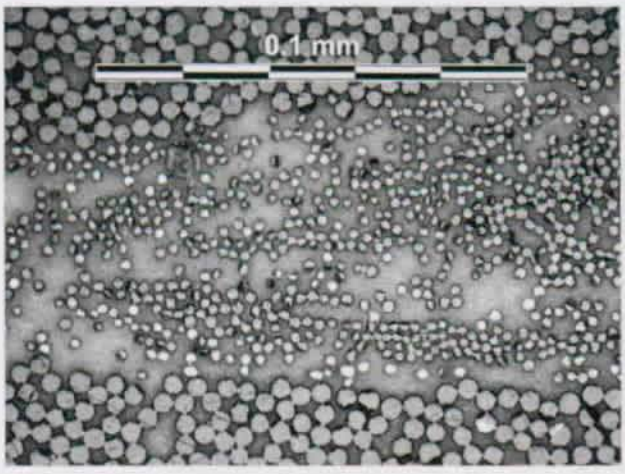

(e) Detail of the rovings (100x). It is possible to recognize fibers of different diameters.

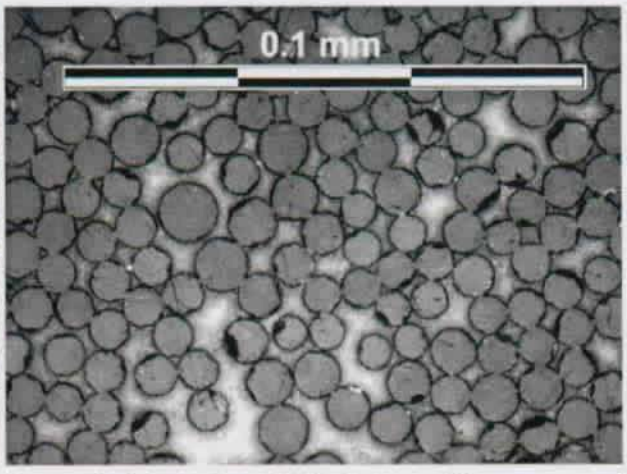

(f) Detail of the rovings (200x). It is possible to see a good embedment of the fibers and the absence of voids in the matrix.

Figure 9.6.: Microscopy

9.3. ADVANTAGES

Using Pultrusion, it is possible to produce big batches of profiles at an affordable cost.

Because of obvious advantages like:

① **High Strength**: Pultruded shapes are stronger than structural steel in terms of weight;

② **Lightweight**: Pultruded shapes are are 20-25 % the weight of steel and 70 % the weight of aluminum allowing them to be easily transported, handled and lifted into place.

③ **Corrosion/Rot Resistant**: Pultruded shapes are very resistant to chemical and environmental aggressions;

④ **Non-Conductive**: Glass reinforced Pultrusion have low thermal conductivity and are electrically non-conductive;

⑤ **Electro-Magnetic Transparency**: Pultruded products are transparent to radio waves, microwaves and other electromagnetic frequencies;

⑥ **Dimensional Stability**: The coefficient of thermal expansion of pultruded products is slightly less than steel and significantly less than aluminum;

⑦ **Aesthetics**: Pultruded profiles are pigmented throughout the thickness of the part and can be made to virtually any desired custom color.

they know a increased interest and success.

Among the few disadvantages, the following may be cited:

① **Low stiffness**: Pultruded composites are penalized by showing a low material stiffness, the E-Modulus typically lies around 10-20% of the corresponding steel value;

② **Undefined fire resistance**: Though many additives, fillers, and coatings are available to increase the fire retardence of these inherently flammable resins, little can be done to improve their structural endurance when exposed to an outside heat source;

③ The resistance related to environmental aggressions;

④ The ecological aspect.

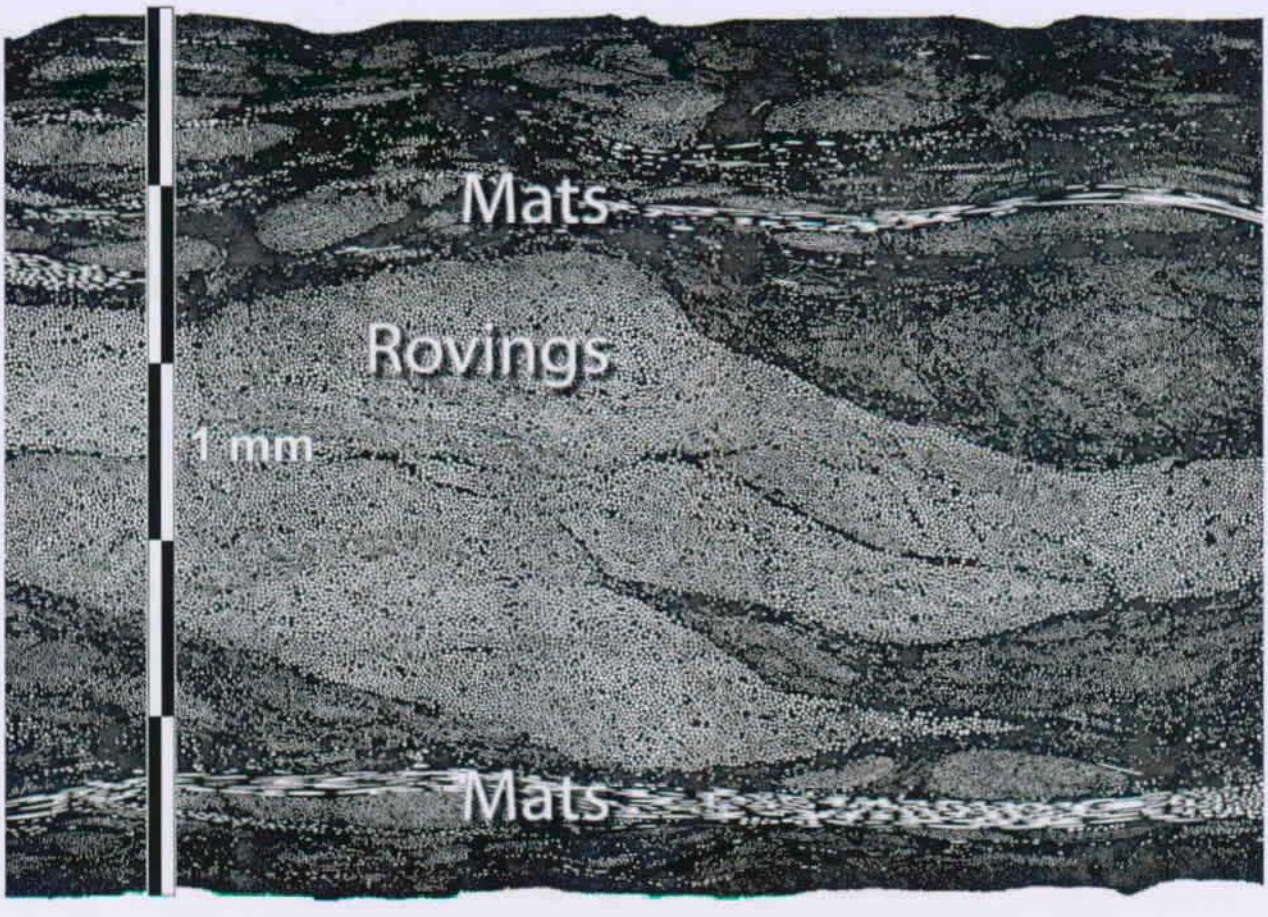

Figure 9.7.: Cross Section of a typical FIBERLINE structural 5 mm flat profile

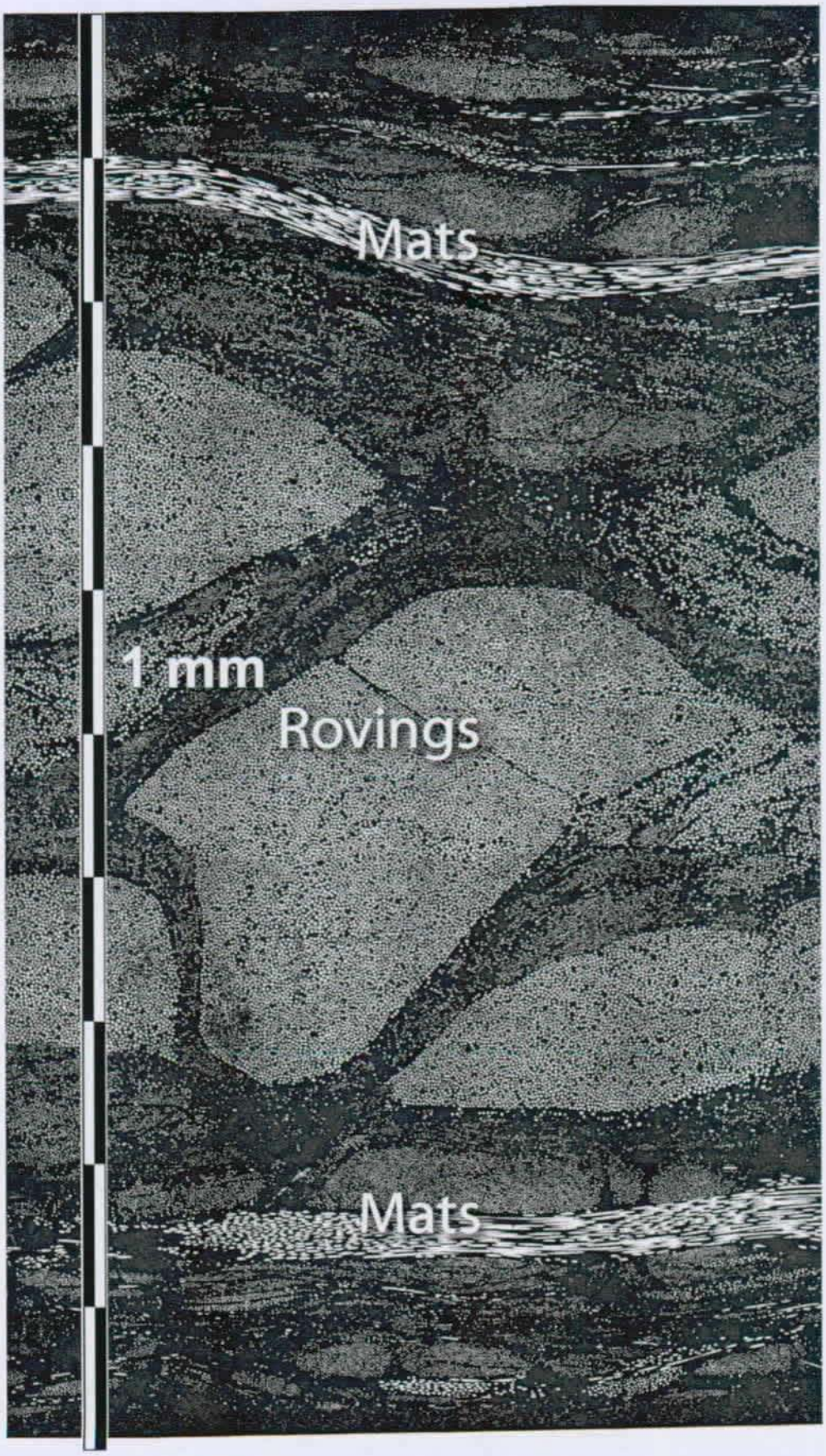

Figure 9.8.: Cross Section of a typical FIBERLINE structural 10 mm flat profile

10. Experimental Investigations on unchamfered Double Lap Joints

10.1. Objectives

The main objectives of this experimental series are:

❶ **The experimental determination of ultimate loads of typical bonded pultruded FRP-joint;**

❷ **The experimental description of the strain-state inside typical bonded pultruded FRP-joint;**

❸ **Checking the influence of major design parameters** — the length of the bonded overlap and the thickness of the adherents — **on the ultimate load and the strain distribution;**

❹ **Checking the suitability of numerical formulations and analytical approximations.**

To reach these objectives, the following was initiated:

① Design of a simple experimental specimen;
↪ Easy to manufacture and to reproduce.

② Featuring full experimental series[1];
↪ Influence of single parameters easier to identify.

10.2. Experimental setup

10.2.1. Specimen description

Geometric specifications

To investigate the mechanical behaviour of bonded joints using FRP profiles, a typical kind of joint had to be chosen.

For the purpose of this experimental investigation, the double lap joint offered a lot of advantages, among them:

① Easy to manufacture;

② Only few parameters that can be varied;

③ 3 axes of symmetry;

④ Reduction of eccentricities to a minimum.

[1] In the sense of a *rectangular grid* of series in which two parameters are varied independently of each other.

The specimens were manufactured from a batch of 500 mm by 100 mm flat profiles, see Fig. 10.1. The inner flat profiles were always twice as thick as the outer flat profiles, so that the cumulative cross-section was kept constant.
The flat profiles were bonded together by a 3 mm thick layer of adhesive[2].
Figs. 10.2 and Fig. 10.3 sketch the shape of a typical specimen.

The large scale of the specimen was chosen to avoid any ambiguity concerning scale effects.

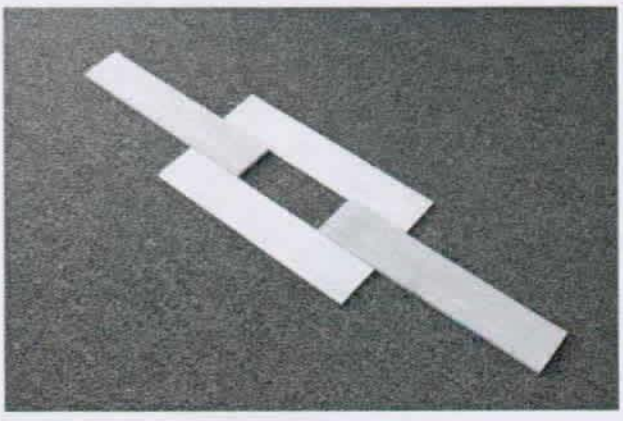

Figure 10.1.: A specimen before being bond

10.2.2. Experimental series

All specimens were built using the flat shapes described before. The following geometrical parameters were varied:

① The length of the overlap or bonded splice:
↪ 50 mm overlap, 75 mm and 100 mm overlap

② The combination of thicknesses for the inner and outer flat profiles:
↪ 3 mm and 6 mm, 4 mm and 8 mm and 6 mm and 12 mm

[2] This relatively thick adhesive layer thickness was chosen because it was planned to cross-analyze them later using FEA. The Author was aware that 3 mm thick adhesive layers were beyond typical civil engineering application values. But in regard to the remarks stated in Section 3.2, it was decided to not increase the number of necessary elements by reducing too much the adhesive layer thickness.

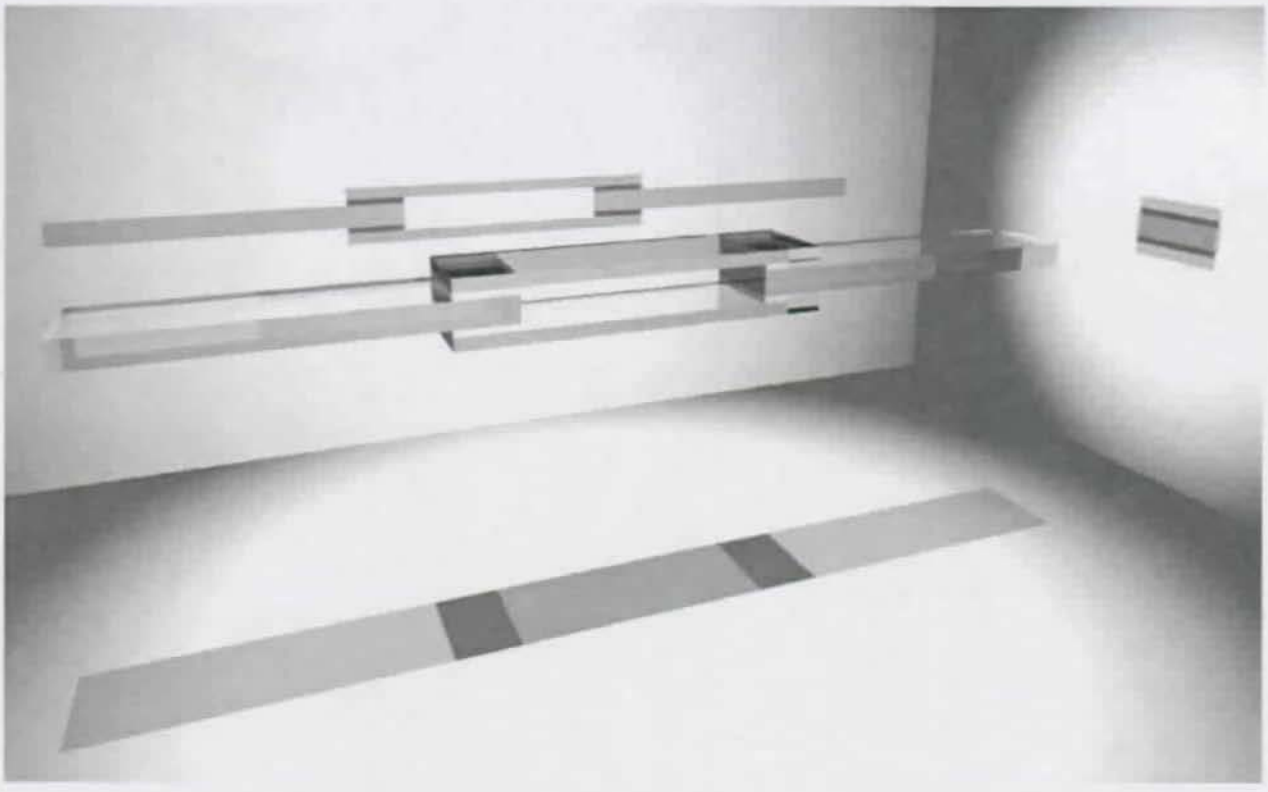

Figure 10.2.: Layout of the experimental specimen

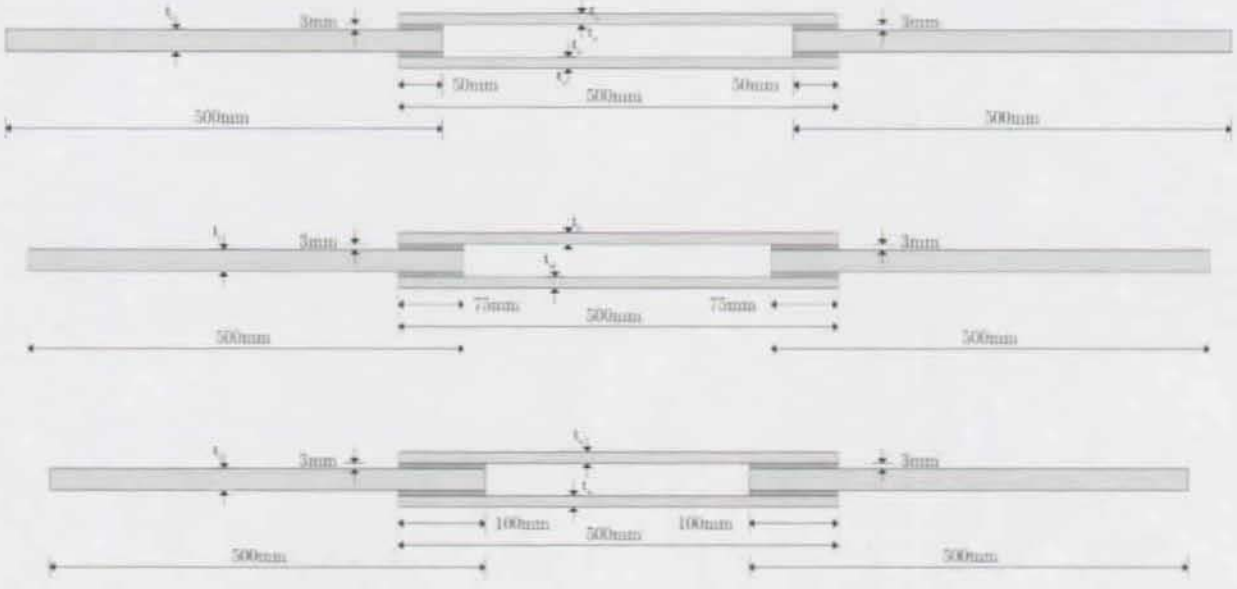

Figure 10.3.: Specimen geometry

All specimens were 100 mm wide; all were instrumented with the 40 strain gauges in the way described above. Combining both varied parameters leads to 9 different specimen. Table 10.3 lists all investigated specimen. The nomenclature described in Appendix A was used.

SURFACE TREATMENT

The surface treatment of composite materials prior to bonding is very important in order to obtain an optimal joint strength. M. DAVIS & D. BOND have outlined in [80] that the *surface preparation is the most significant factor in determining the [...] performance of a bonded joint, and the only method for producing a durable bond is to ensure that the surface is prepared [...]*..

To avoid contaminating the bonded connections with greases, the surfaces subjected to bonding were treated in the following manner (see Figs. 10.4):

① Cleaning and degreasing using acetone a first time;

② Mechanically abrading the surface veil using a handy grinding machine up to the first visible fibers of the mat;

③ Re-cleaning and re-degreasing the surface using acetone a second time.

All operations involving potentially greasy materials or tools were avoided. During all the time the experimental specimen were manufactured, the persons had to wear Latex gloves.

ADHESIVE

To ensure a constant thickness of the adhesive (3 mm for this experimental series) high precision glass beads (see Fig. 10.7) were placed into the epoxy. These very precisely manufactured beads acted as spacers between the flat profiles and were left inside the splice. Care had to be taken that the beads were not placed directly on a strain gauge and not too close to the edge to avoid washing them out with the excess adhesive.

Care was also taken to ensure an adhesive fillet of $r_f = 1$ mm for all manufactured specimen.

10.2.3. DATA GATHERING

The following was measured during this experimental series:

① The axial strain development along the inner side of the outer flat profile — using strain gauges, and

② The load-displacement of the specimen — by the experimental device, up to failure.

STRAIN GAUGES

To experimentally measure the axial strain development along the bonded splice, strain gauges were sticked on the 4 inner sides of the 2 outer flat profiles.

Basic formulæ and general FE Analysis show that the axial stress gradient concentrates towards the ends of the bonded splice, whereas the center part of it shows a rather flat gradient.
In order to reduce the number of necessary strain gauges they were positioned within approximately the outer thirds of the overlap.
Care had to be taken to investigate the issue of possible eccentricity: two gauges of each set were used to measure any moments of eccentricity due to an eventual misalignment of the flat profiles. Eight gauges collected strain data in the true areas of interest further towards the ends of the overlap (see Figs. 10.5 and 10.6).

Strain gauges[3] were used. These gauges are 5×6 mm^2 small (including the carrier). This small size was chosen to get clear readings on very distinct points of measurement on the specimens. This small size had also the advantage to reduce considerably the degradation of the bonded surface.

Because the strain gauges were not directly aligned in the splice, the question of the axial strain distribution perpendicular to the axial direction is of importance. This issue has been discussed in Section 3.2.2 with the conclusion that **the axial strain distribution can be considered as constant over the width of the flat profile**.

THE EXPERIMENTAL DEVICE

The experimental machine was a SCHENCK HYDROPULS-ZYLINDER TYP PL (see Fig. 10.8), which can be operated for tension and compression at a maximum load of 1 000 kN with a displacement of up to 450 mm. The load can be applied in static

[3] Of the type *1,5/120LY18* manufactured by HOTTINGER BALDWIN MESSTECHNIK GMBH.

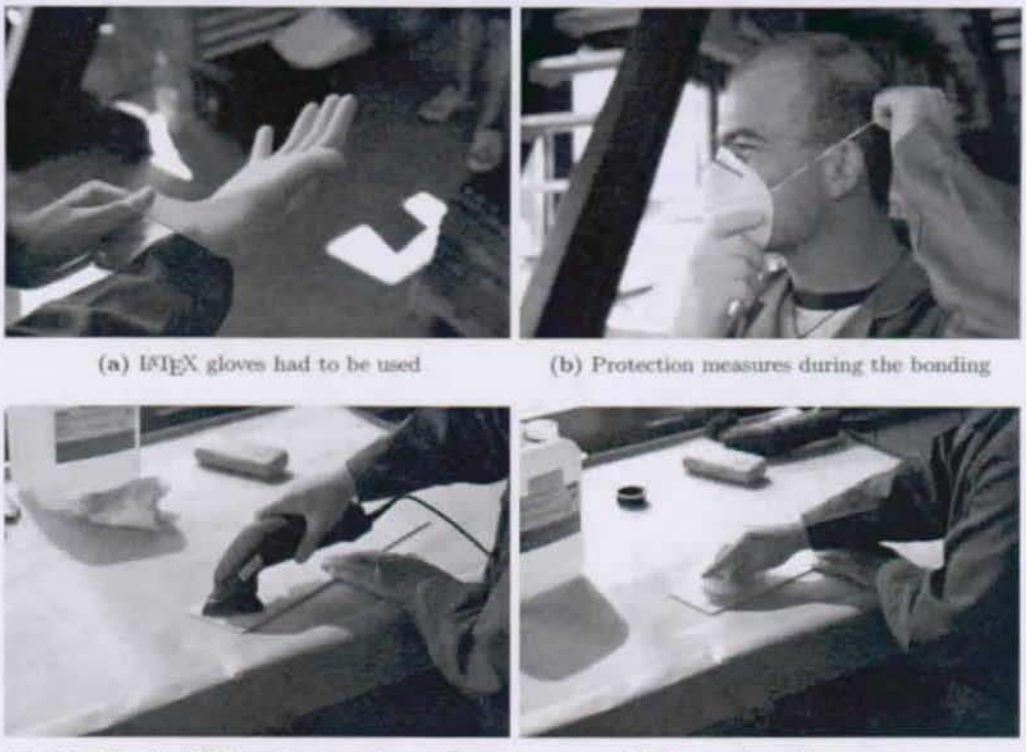

(a) LaTeX gloves had to be used

(b) Protection measures during the bonding

(c) Grinding the FRP surface to enhance the adhesion

(d) Degreasing using acetone

Figure 10.4.: Surface preparation

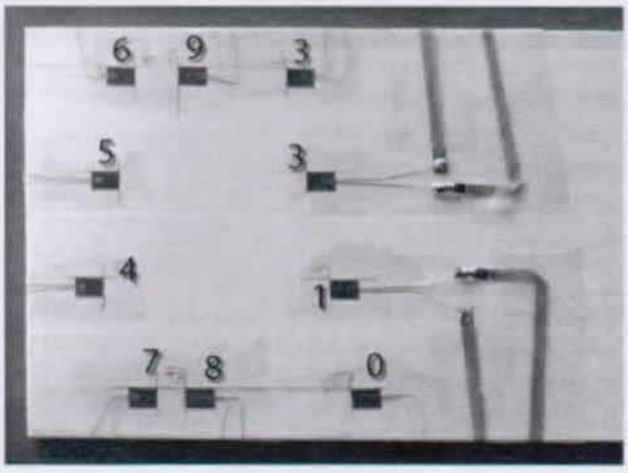

Figure 10.5.: Strain gauges sticked on the specimen

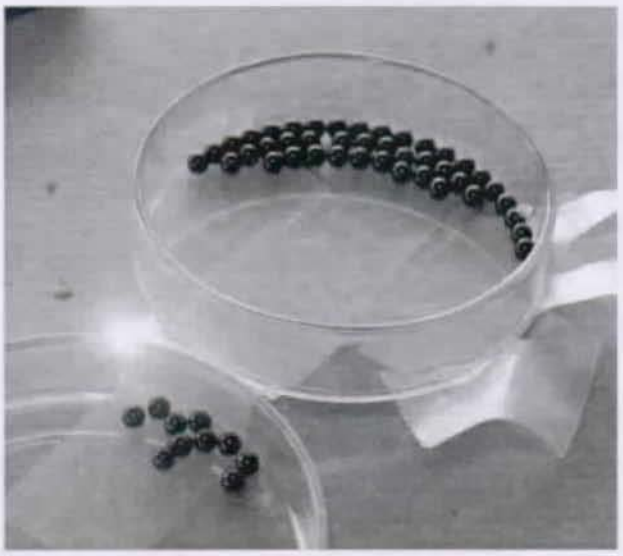

Figure 10.7.: 3 mm high-precision glass beads used to guarantee the adhesive layer thickness

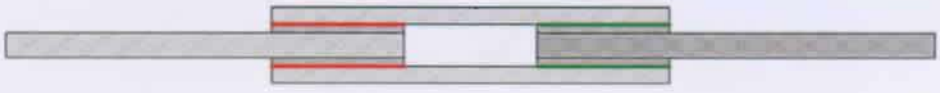

(a) Location of the splices

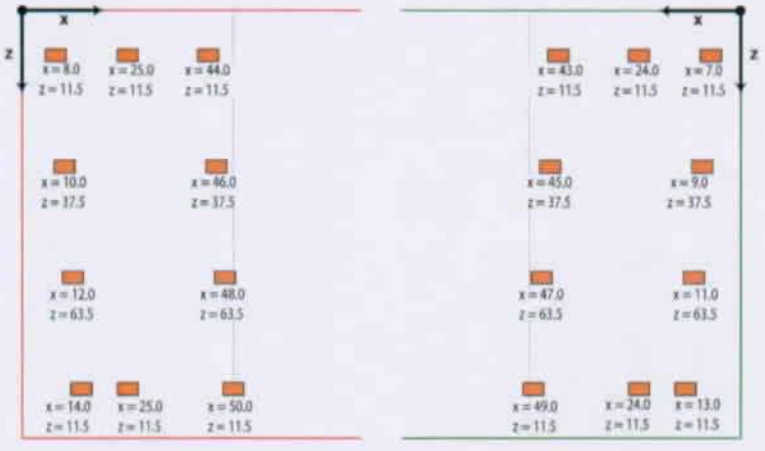

(b) 50 mm overlap

(c) 75 mm overlap

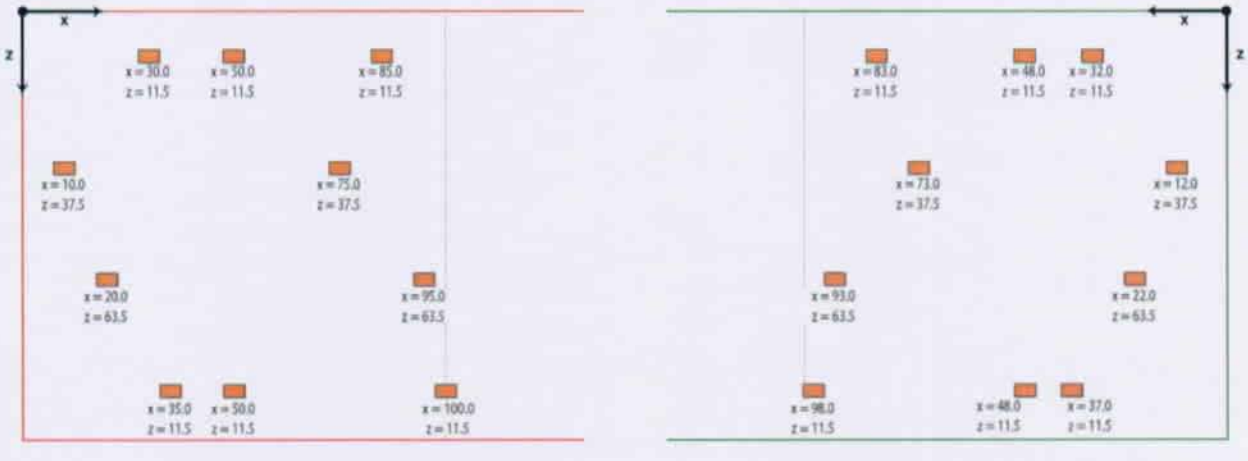

(d) 100 mm overlap

Figure 10.6.: Location of the strain gauges

or dynamic way and controlled by either force or displacement.

The experimental investigations documented here were performed displacement controlled. The axial displacement, the corresponding force and the strain gauge data were gathered.

The load rate was kept for all specimen to $0.5\,\frac{\text{mm}}{\text{min}}$.

A UPM60 unit collected the data coming through 40 channels.

Figure 10.8.: The Schenck 1000 kN experimental device

10.2.4. Material properties

FRP material

The delivered flat profiles came already cut in thicknesses of 3 mm, 4 mm, 6 mm, 8 mm and 12 mm.
It is very important to notice that every different thickness featured a different type of material (see also Section 9.2.2).

Fiberline's related data-sheet gives only ranges of values for the delivered material. For the further interpretation and comparison of the experimental results, it was crucial to have reliable and accurate results concerning, at least the basic mechanical characteristics, like the axial Modulus of Elasticity E_x and ultimate limit stress $\sigma_{x,u}$.

Experiments[4] were carried out by the Author to determine Young's Modulus of the different flat profiles. A look at the load-deformation diagrams of those experiments demonstrated clearly that the relation between load and deformation was linear until the ultimate limit. The results of those experiments — average of a series of 3 experiments for each flat profile thickness — are shown below in Table 10.1.

Adhesives

The SikaDur 330 epoxy from Sika was used to bond the flat profiles together.

All specimens were manufactured with an adhesive fillet showing a radius of $r_f = 1$ mm .

Compression experiments according to ASTM 695 and tension experiments according to ISO 527 were carried out on the adhesive. The main results are given in Table C.2[5].

The adhesive had approximatively 2 weeks to cure at room temperature. The temperature in the laboratory lied around 22 ± 2 °C.

10.3. Experimental results

In the following only the main raw experiment results are presented. An extended discussion and interpretation of this experiment series will follow in part VI of this Thesis.

It should be emphasized that each geometrical configuration was experimented only once, so no statistical confidence can be given.

10.3.1. Load-displacement plots

All specimens were driven up to failure, the associated load-deformation plots[6] are displayed in Fig. 10.11. As it can be seen, the load-displacement plots are almost linear up to failure.
It can also be clearly recognized that the overlap length has no real influence on the stiffness of adhesively bonded joints. The different stiffnesses — expressed by the slope of the curves — depend only on the material thickness combination.

[4] Refer to Appendix B for further details concerning these experimental investigations.
[5] More details concerning this adhesive can be found in Appendix C.
[6] As gathered by the Schenck-Device.

Lamella Thickness	E_x	$\sigma_{x,u}$ in MPa
3 mm	34 657 ± 334	334 ± 4
4 mm	28 921 ± 222	222 ± 9
6 mm	34 417 ± 453	453 ± 8
8 mm	32 820 ± 336	336 ± 5
12 mm	29 792 ± 338	338 ± 6

Table 10.1.: Mechanical properties of the FIBERLINE FRP-Lamellas investigated

Property	E in MPa	ε_u in %	σ_u in MPa
SIKADUR 330 under tension	4 550	0.97	≈ 39
SIKADUR 330 under compression	≈ 3000	9.65	80.7

Table 10.2.: The main mechanical properties of SIKADUR 330

Geometry	Chamfering[a]	$\frac{Overlap}{t_{adh.}}$	$\frac{t_o}{t_i}$	#	F_u in kN	Failure[b]	Picture(s)	Alias[c]	Remark(s)
D	N	$\frac{50}{3}$	$\frac{3}{6}$	1[e]	81.92	①	Appendix D	A1	-
D	N	$\frac{50}{3}$	$\frac{4}{8}$	1[e]	77.76	①	Appendix D	A2	-
D	N	$\frac{50}{3}$	$\frac{6}{12}$	1[e]	86.02	①	-	A1	-
D	N	$\frac{75}{3}$	$\frac{3}{6}$	1[e]	89.97	②	Appendix D	B1	-
D	N	$\frac{75}{3}$	$\frac{4}{8}$	1[e]	71.37	①	Appendix D	B2	-
D	N	$\frac{75}{3}$	$\frac{6}{12}$	1[e]	120.00	①	Appendix D	B3	-
D	N	$\frac{100}{3}$	$\frac{3}{6}$	1[e]	110.10	②	Appendix D	C1	-
D	N	$\frac{100}{3}$	$\frac{4}{8}$	1[e]	86.84	①	Appendix D	C2	-
D	N	$\frac{100}{3}$	$\frac{6}{12}$	1[e]	131.90	①	Appendix D	C3	-

[a]N:No chamfering, S: slight chamfering, F: full chamfering.
[b]①: Outer fleece fiber tear failure of the **inner** flat profile, ②: Outer fleece fiber tear failure of the **outer** flat profile.
[c]The alias is the denomination used during the experimental handling and in the experimental reports.

Table 10.3.: Listing of all *unchamfered* specimen with an adhesive layer thickness of 3 mm

10.3.2. ULTIMATE LOADS AND FAILURE MODE DESCRIPTION

The ultimate loads reached and the associated failure modes observed are listed in Tab. 10.3 and displayed in Fig. 10.9.

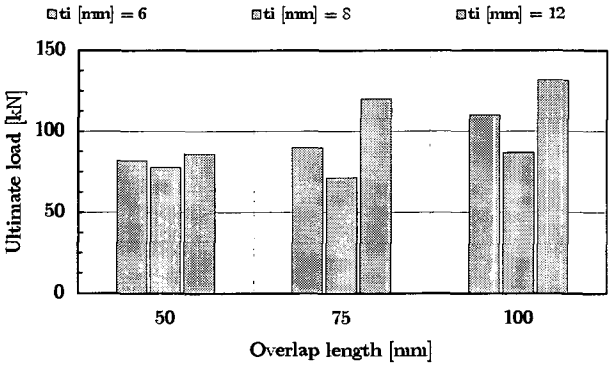

Figure 10.9.: Ultimate loads vs. overlap lengths

Failure never occurred by shear failure in the adhesive layer, but by *delamination* of the pultruded shapes. This *delamination* occurred on the level between the outer surface veil and the mats (refer to Section 9.2.2 for more details concerning the material architecture).

As stated before, each material thickness features a different pultruded material, so that the lower failure loads in the series with the 4 mm-8 mm-combination is not due to the thickness of the element, but to a different (and in this case weaker) laminate architecture.

10.3.3. STRAIN DISTRIBUTION

The collected data is represented in Figs. 10.12 to 10.20 and shows the axial strain distribution plotted along the bonded splice as measured, by each strain gauge[7]. Due to the geometrical symmetry of the bonded splices in the specimen, it was decided to overlay the gathered strains of all 4 splices on just one diagram. Fig. 10.10 shows on which path the results were plotted.

The values correspond to a purely arbitrary reference force of 50 kN so that the influence of the geometry on the axial strain development is easier to distinguish, independent of the joint strength.
Because of the purely linear behaviour of all the mechanical components making the joints, strain profiles for other load steps can be linearly deduced.

[7]Refer to Table 10.3 for the designation of the specimen.

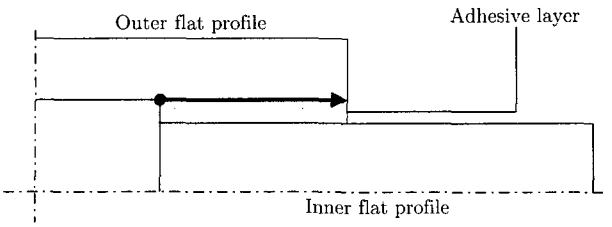

Figure 10.10.: The path investigated

The experimental results are compared to those obtained by FEA. The FE results are related to the analysis carried out in Chapter V.

As it can be seen, the experimental and numerical results show a relatively good agreement. Both show that the axial strain are built up on the extremities of the overlap, letting a flat part in the middle. For longer overlaps this middle part becomes larger.

10.4. CONCLUSIONS

Experiments on adhesively bonded joints were carried out. Ultimate loads for different combinations of flat profile thicknesses were investigated. All specimen were fully instrumented, which allowed the determination of the strain development along the bonded joint.

The following first conclusions can be made:

- **Failure occurs in a very sudden and brittle manner, without warning signs[8];**
- **Ultimate loads increase underproportionally with the overlap length;**
- **Ultimate loads depend very much of the pultruded material used;**
- **The strain development along the splice was investigated and found to correlate good with FEA results[9].**

Deeper interpretations will follow in part VI.

[8]Exception made of some audible cracks at around $\frac{2}{3}$ of the failure load.
[9]The FE results are related to the analysis carried out in Chapter V.

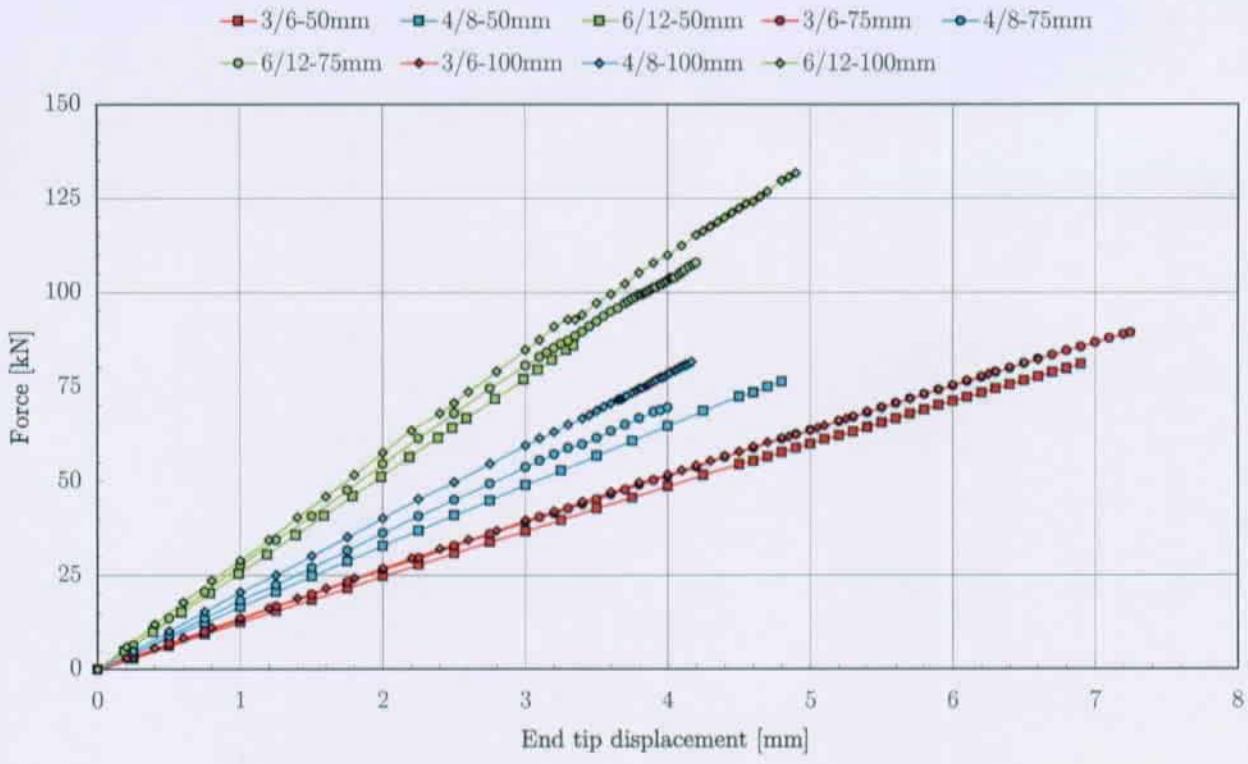

Figure 10.11.: Load-deformation graphs of all specimens investigated

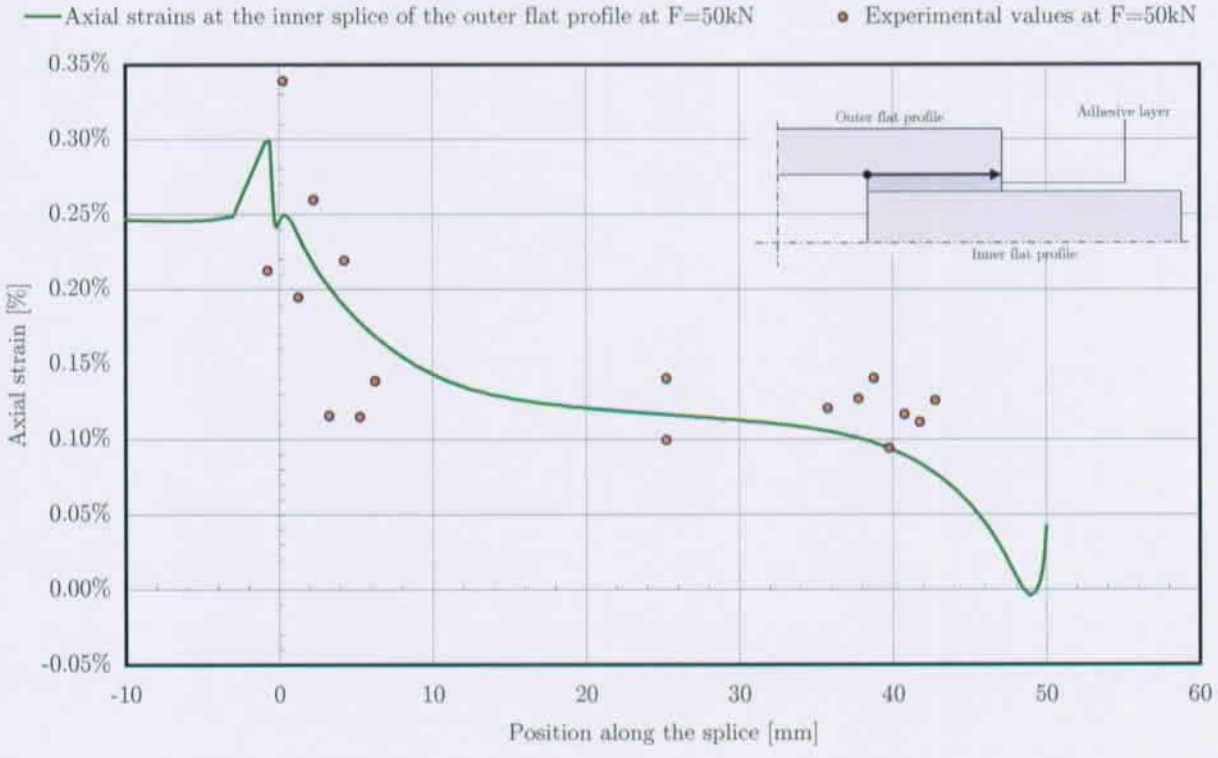

Figure 10.12.: Strain distribution for DN$\frac{50}{3}\frac{3}{6}1^e$ - Line= FEA, dots = experimental

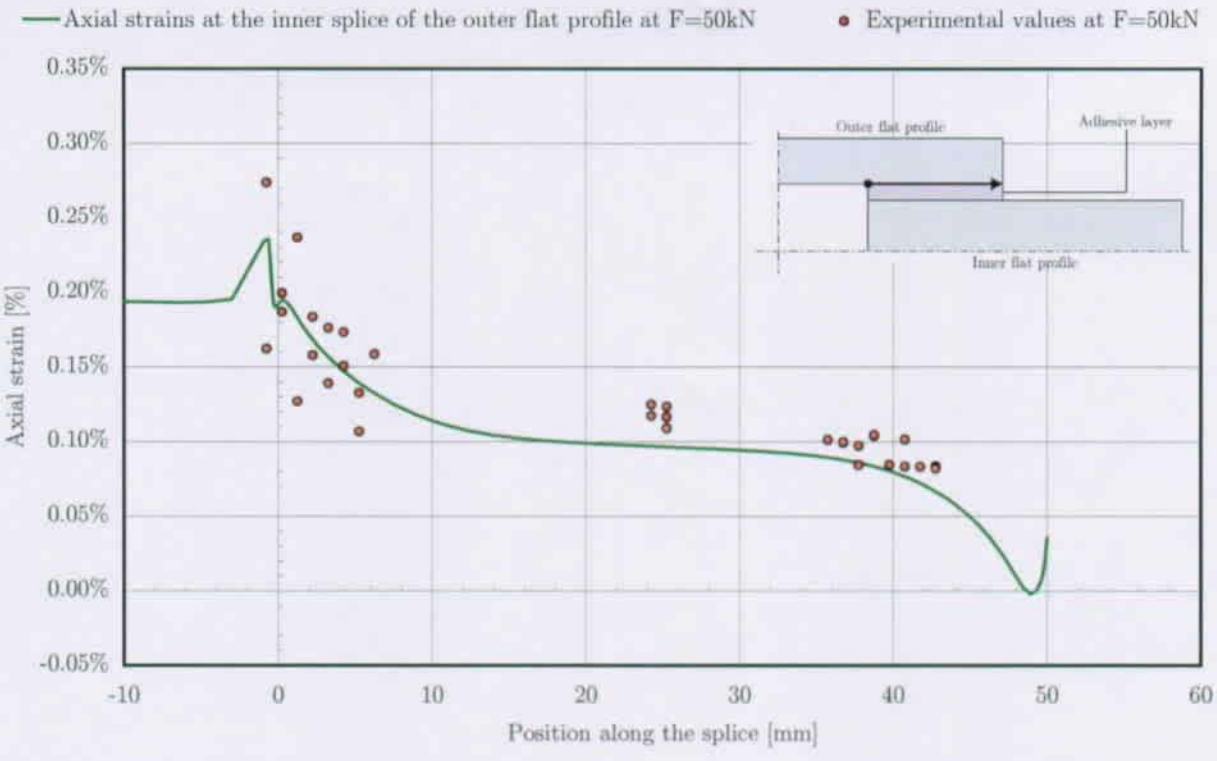

Figure 10.13.: Strain distribution for DN$\frac{50}{3}\frac{4}{8}1^e$ - Line= FEA, dots = experimental

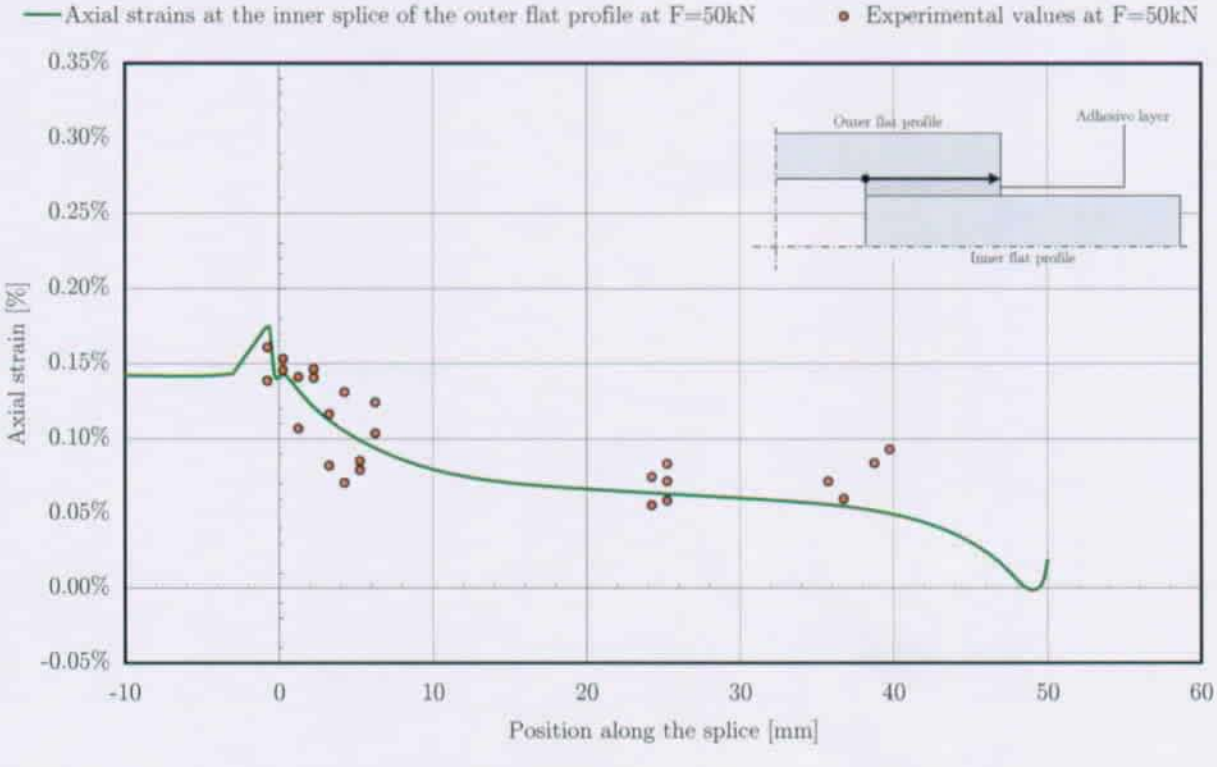

Figure 10.14.: Strain distribution for DN$\frac{50}{3}\frac{6}{12}1^e$ - Line= FEA, dots = experimental

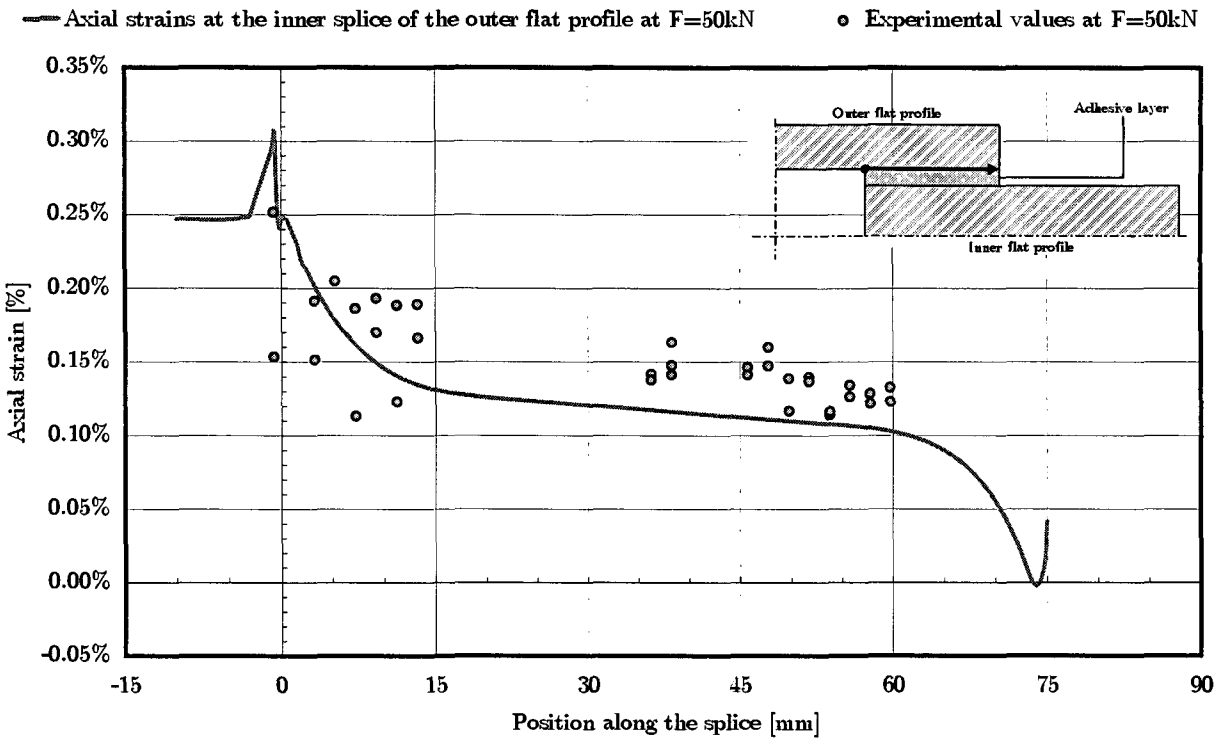

Figure 10.15.: Strain distribution for DN$\frac{75}{3}\frac{3}{6}1^e$ - Line= FEA, dots = experimental

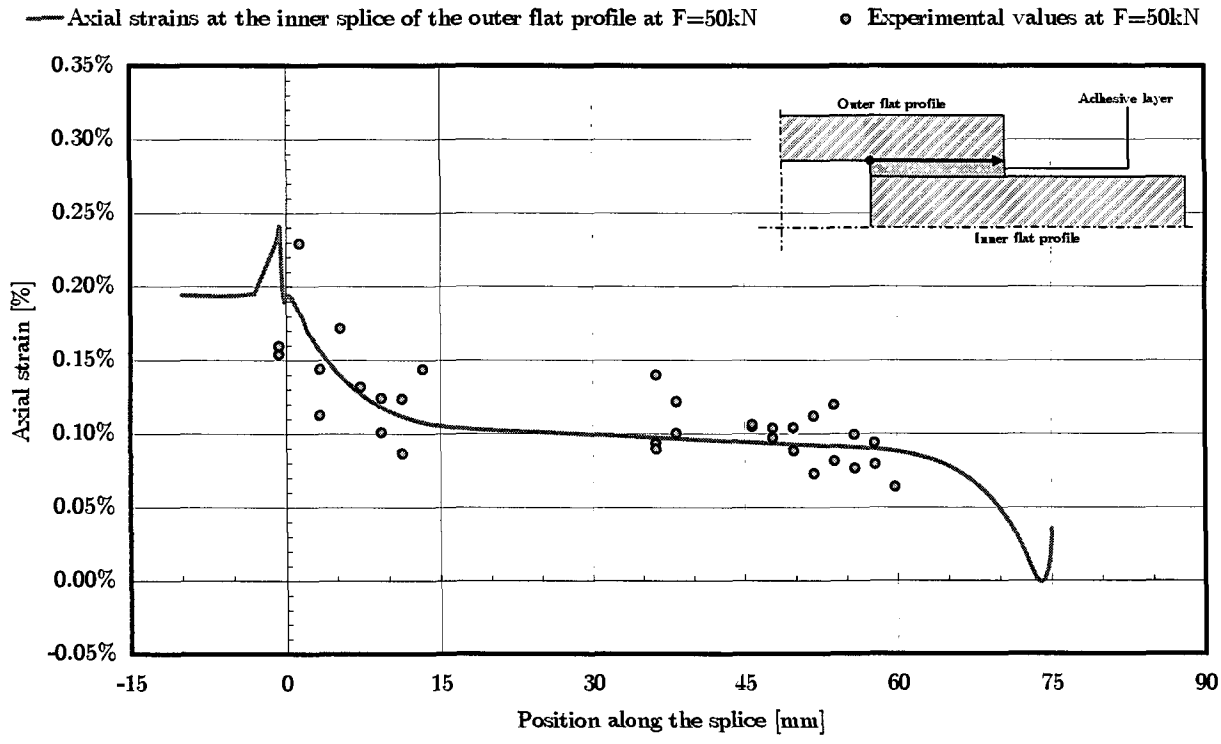

Figure 10.16.: Strain distribution for DN$\frac{75}{3}\frac{4}{8}1^e$ - Line= FEA, dots = experimental

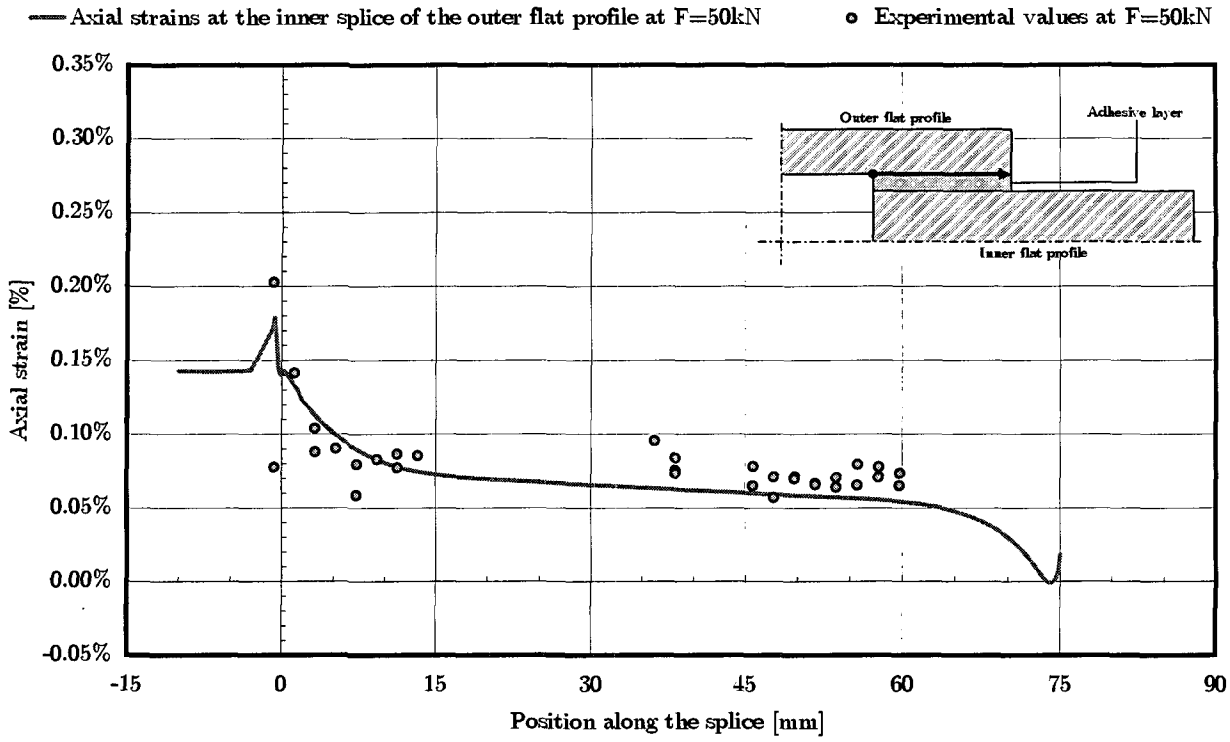

Figure 10.17.: Strain distribution for DN$\frac{75}{3}\frac{6}{12}1^e$ - Line= FEA, dots = experimental

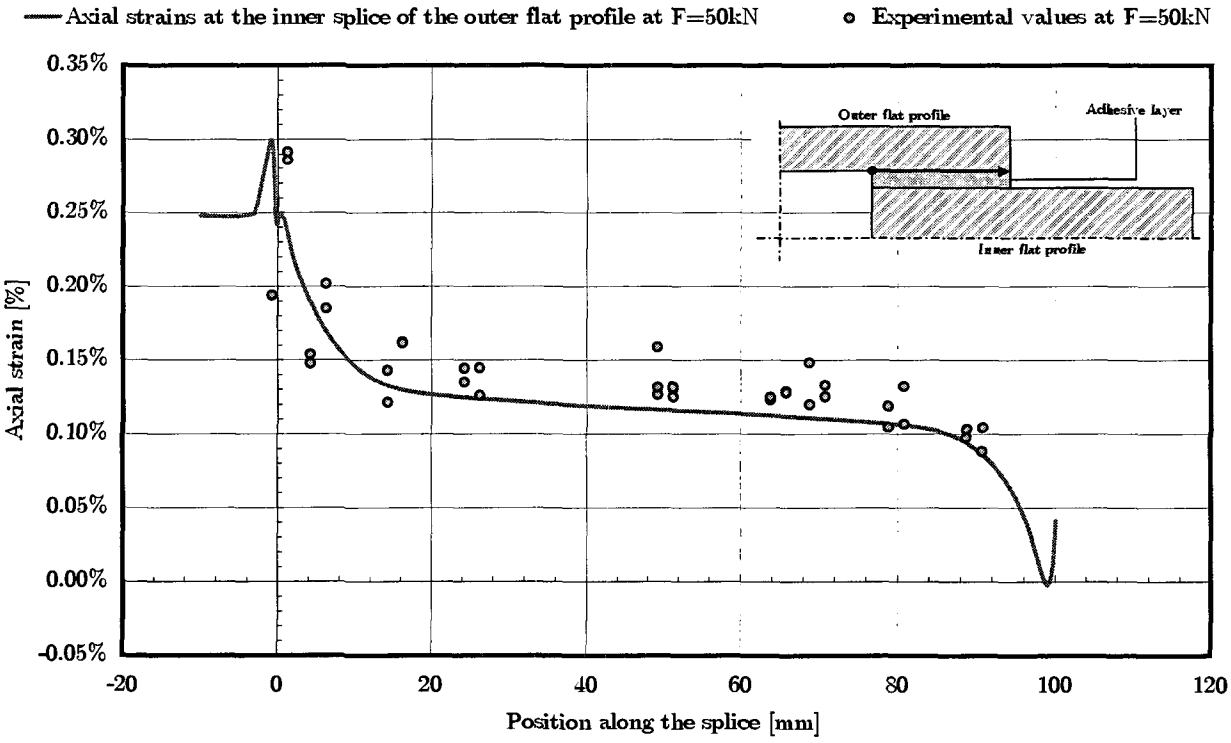

Figure 10.18.: Strain distribution for DN$\frac{100}{3}\frac{3}{6}1^e$ - Line= FEA, dots = experimental

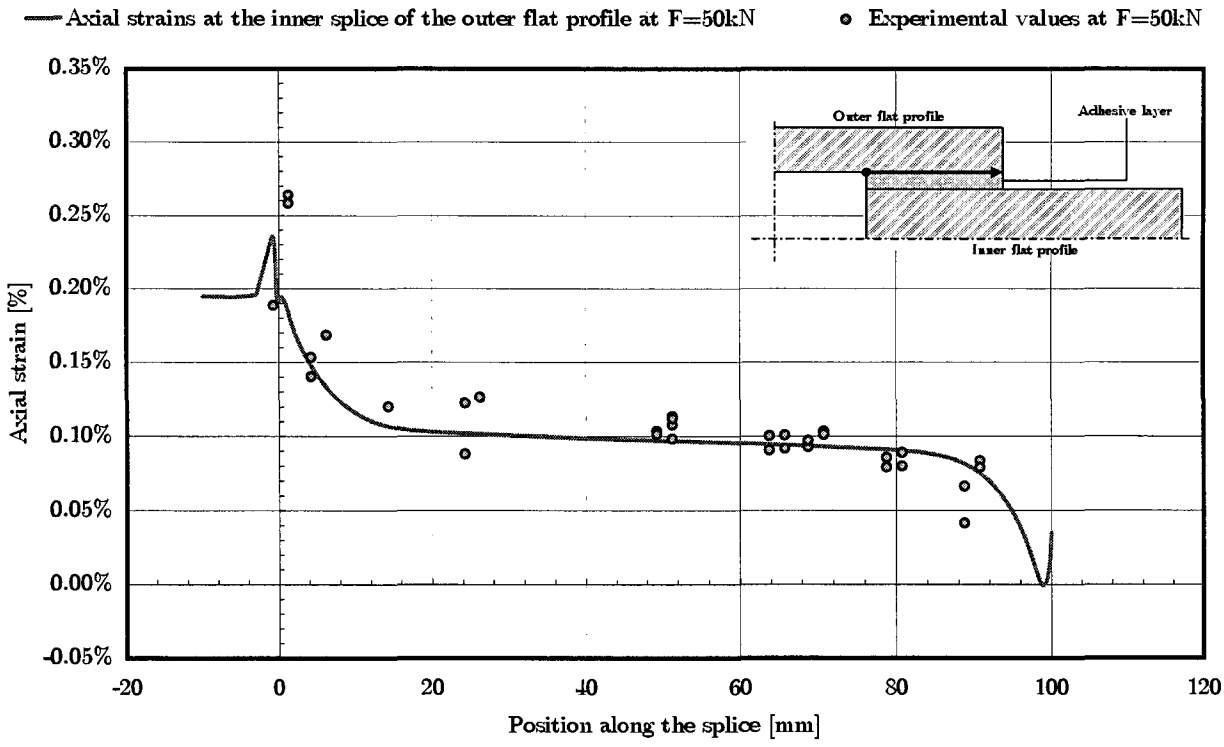

Figure 10.19.: Strain distribution for DN$\frac{100}{3}\frac{4}{8}1^e$ - Line= FEA, dots = experimental

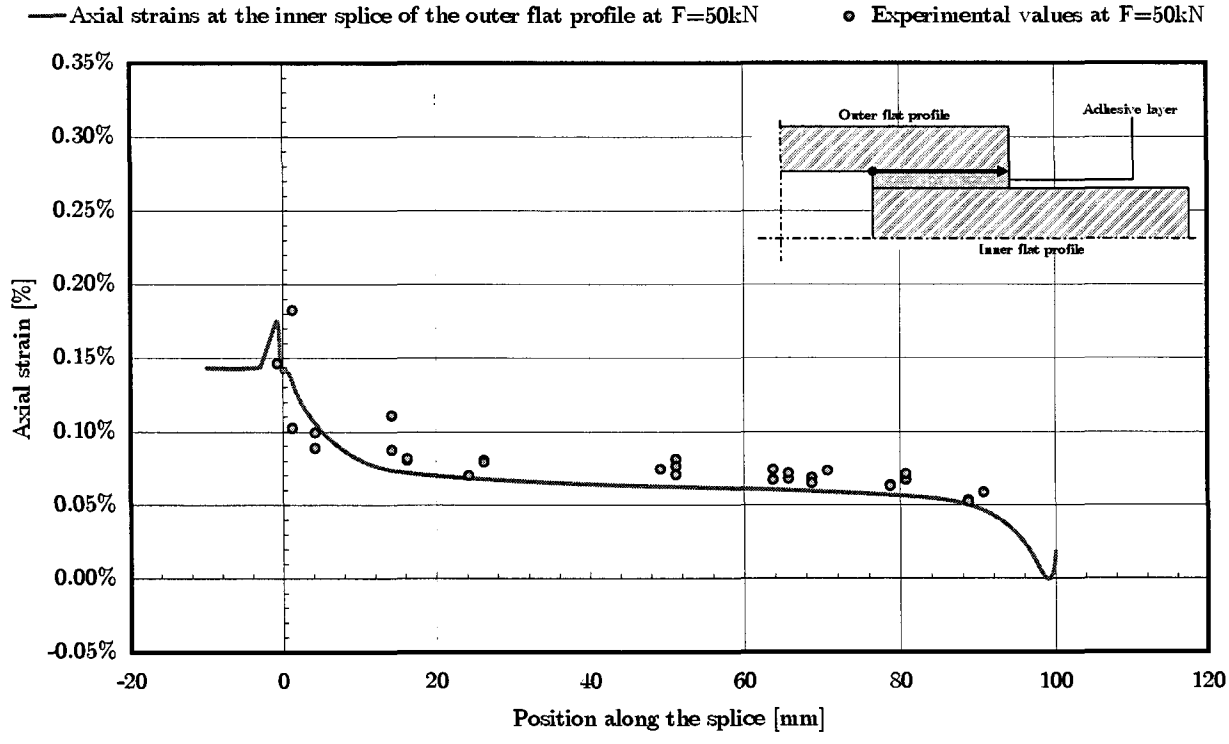

Figure 10.20.: Strain distribution for DN$\frac{100}{3}\frac{6}{12}1^e$ - Line= FEA, dots = experimental

11. Experimental Investigations on chamfered Double-Lap Joints

11.1. Objectives

This experimental series featured double-lap joint experiments similar to those investigated in the experimenal series described in Chapter 10.
The full experimental report is available at the CCLab [81].

The experimental series featured two main objectives:

❶ **The determination of the ultimate loads for a series of specimens featuring different levels of chamfering.**
↪ The aim is to evaluate the influence of these stress-reduction measures on the ultimate limit strength;

❷ **The determination of the strain-stress state inside the adhesively bonded joint.**
↪ The aim is to crosscheck with the FEA. Further details concerning the carried out FEA can be found in Part V.

The experimental program consists of a series of specimen differing in the following aspects:

① Chamfering:
three different levels of chamfering;

② Overlap length:
three different values.

③ Adhesive layer thickness:
two different values.

The specimen specifications were selected to obtain series of specimen with only one parameter varied to easier identify their influence.

Some of the specimen[1] were fully instrumented with 40 strain gauges distributed over the 4 bonded splices.

[1] Denoted by an *e* in Tabs. 11.2 and 11.3.

11.2. Experimental setup

11.2.1. Specimen description

Geometric specifications

All double lap joints specimens were manufactured using a set of four 100 mm × 500 mm flat profiles, two outer flat profiles of 5 mm thickness and two inner flat profiles of 10 mm thickness. **The material is not identical to the flat profiles described in Chapter 10.**

Three different overlaps were investigated:

① 50 mm

② 75 mm

③ 100 mm

Two different adhesive thicknesses were investigated:

① 1 mm

② 3 mm

The three different levels of chamfering are described in Fig. 11.1:

① No chamfering

② Slight chamfering:
↪ a chamfer over half the overlap and ending at half the outer flat profile thickness.

③ Full chamfering:
↪ a chamfer over the full overlap and ending at a final thickness of close to zero.

All these parameters lead to the specimens listed in Tabs. 11.2 and 11.3.

Adhesive layer

All specimens were manufactured with an adhesive fillet showing a radius of $r_f = 1$ mm .
To ensure the thickness, calibrated glass beads were put into the adhesive layer, see Section 10.2.3.

Surface treatment

The surface treatment was the same as for the experimental investigations described in Chapter 10.

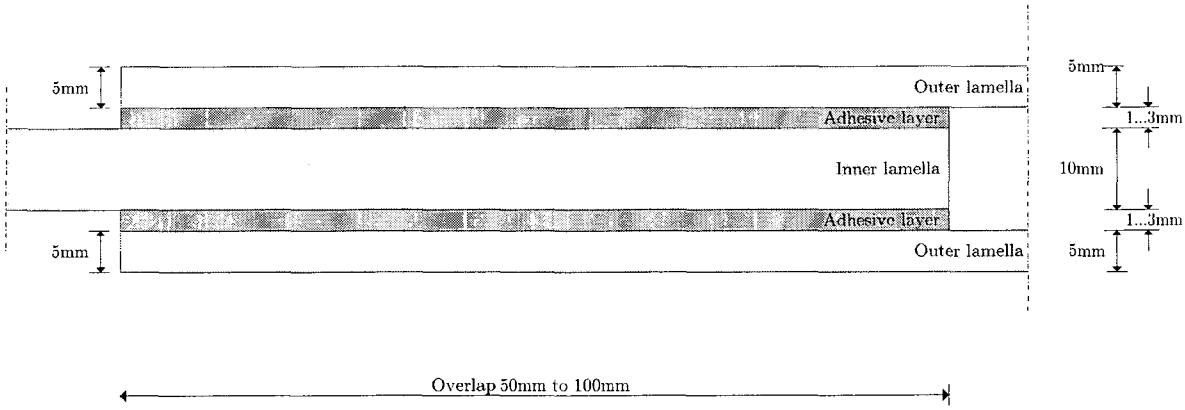

(a) No chamfering

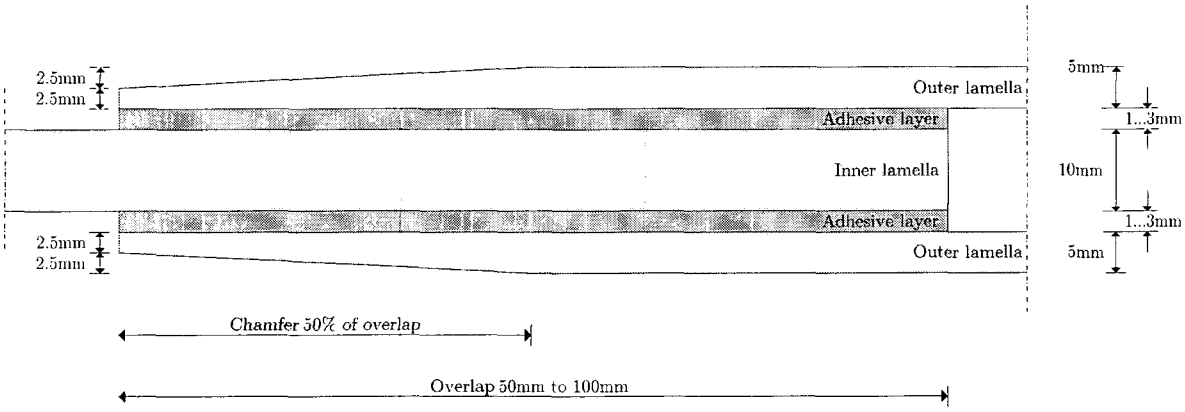

(b) Slight chamfering

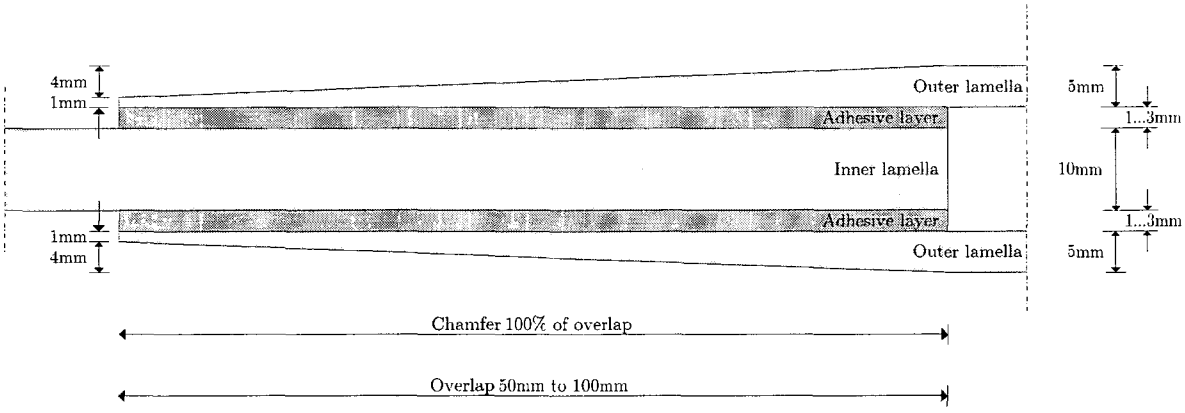

(c) Full chamfering

Figure 11.1.: Definition of chamfering levels

11.2.2. DATA GATHERING

The following was measured during this experimental series:

① The axial strain development along the inner side of the outer flat profile (using strain gauges) of chosen geometrical configurations and

② The load-displacement of the specimen (using the SCHENCK), up to failure.

STRAIN GAUGES

Refer to Section 10.2.3 to have an overview of the strain gauge type and their positioning inside the joints.

THE EXPERIMENTAL DEVICE AND DATA GATHERING UNIT

The same SCHENCK HYDROPULS-ZYLINDER TYP PL as described in Section 10.2.3 was used. The same loading rate of approximatively $0.5\,\frac{mm}{min}$ as chosen for the previous experimental investigation on unchamfered double lap joints (chapter 10) was taken.
A UPM60 unit collected the data coming through 40 channels.

11.2.3. MATERIAL PROPERTIES

FRP-MATERIAL

The FRP-Profiles were supplied by the Danish pultruder FIBERLINE. Tension experiments to gather ultimate strengths and elastic Moduli E_x were carried out at the CCLAB. The gathered values are given by Tab. 11.1, see also Appendix B.

ADHESIVE

The adhesive used was the SIKADUR 330 supplied by our research partner SIKA, the material was investigated for previous experimental series. See Tab. C.2 for further details.

The adhesive had approximatively 2 months to cure at room temperature. The temperature in the experimental laboratory lied around 22 ± 2 °C.

11.2.4. EXPERIMENTAL SERIES

Tabs. 11.2 and 11.3 list all the manufactured and experimentally investigated specimens during this experimental investigation.

11.3. EXPERIMENTAL RESULTS

All experiments showed he following in common:

① All load-deformations curves were almost linear up to the failure;

② The failure occurred suddenly without warning sings[2];

③ The failure always occurred in the material of one of the FRP-flat profiles.

11.3.1. LOAD-DISPLACEMENT PLOTS

All specimens were driven up to failure, the associated load-deformation plots are displayed in Fig. 11.2. As it can be seen, the load-displacement plots are close to linear up to failure.

Similarly to Fig. 10.11, it can also be clearly recognized that neither the chamfer level nor the adhesive layer thickness had an influence of the stiffness of adhesively bonded joints.

11.3.2. ULTIMATE LOADS

Tabs. 11.2 and 11.3 list the ultimate loads reached during the experimental investigations.

As it can be seen, the influence of the chamfering on the lap joint strength is not very important, see Fig.11.3.

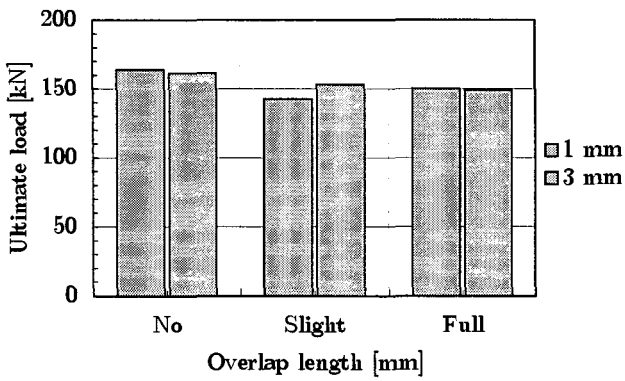

Figure 11.3.: Ultimate loads vs. chamfer level for an overlap of 100 mm

11.3.3. FAILURE MODES

The failure always occurred inside the flat profiles. Figs. 11.5 shows an example.

[2]Exception made of audible cracks at approximatively $\frac{2}{3}$ of the failure load F_u for quite all specimen.

Lamella Thickness	E_x [a] in MPa	$\sigma_{x,u}$ [b] in MPa	Fiber architecture
5 mm	34 348 ± 620	332 ± 18	F[c]-M[d]-R[e]-M-F
10 mm	32 525 ± 1 330	332 ± 14	F-M-M-R-M-M-F

[a] Axial E-Modulus
[b] Axial strength
[c] Fleece.
[d] Mat.
[e] Rovings.

Table 11.1.: Mechanical properties of the Fiberline FRP-Lamellas experimentally investigated

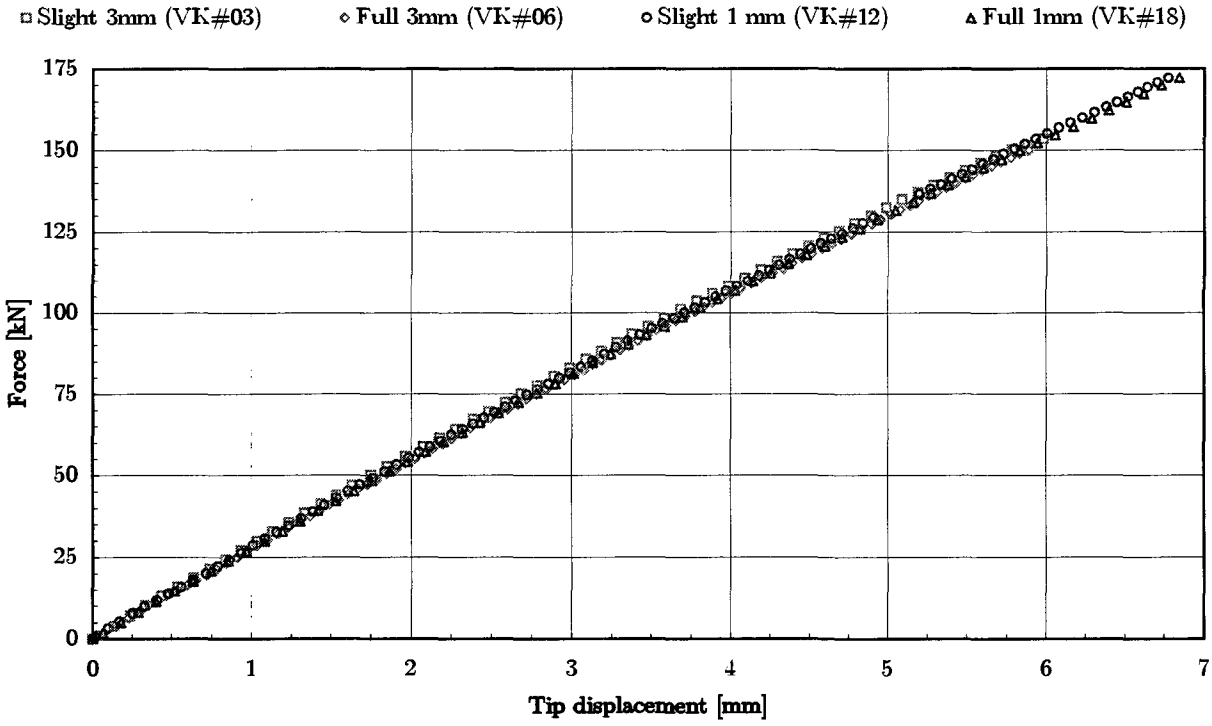

Figure 11.2.: Load-deformation graphs of specimen with 100 mm overlap

Geometry	Chamfering[a]	$\frac{Overlap}{t_{adh.}}$	$\frac{t_2}{t_1}$	#	F_u in kN	Failure[b]	Picture(s)	Alias[c]	Remark(s)
D	N	50	5	1	102	①	Appendix D	VK10	-
D	N	50	5	2	100.0	①	-	50N-1	-
D	N	50	5	3	107.6	①	-	50N-2	-
D	N	50	5	4	94.2	①	-	50N-3	-
D	S	50	5	1	100	①	-	VK11	-
D	S	50	5	2	95.4	①	Appendix D	50S-1	-
D	S	50	5	3	96.4	①	-	50S-2	-
D	S	50	5	4	83.9	①	-	50S-3	-
D	F	50	5	1	103.8	①	-	N1a	-
D	F	50	5	2	111.9	①	-	N1b	-
D	F	50	5	3	99.0	①	-	50F-1	-
D	F	50	5	4	126.8	①	-	50F-2	-
D	F	50	5	5	100.1	①	-	50F-3	-
D	N	75	5	1	???	①	Appendix D	VK13	Test failed
D	N	75	5	2	116.1	①	Appendix D	75N-1	-
D	N	75	5	3	123.8	①	-	75N-2	-
D	N	75	5	4	128.7	①	-	75N-3	-
D	S	75	5	1	149	①	Appendix D	VK14	-
D	S	75	5	2	119.9	①	Appendix D	75S-1	-
D	S	75	5	3	126.7	①	-	75S-2	-
D	S	75	5	4	128.7	①	-	75S-3	-
D	F	75	5	2	90.2	①	-	N2a	Badly bonded
D	F	75	5	3	151.2	①	-	N2b	-
D	F	75	5	4	137.7	①	-	75F-1	-
D	F	75	5	5	141.6	①	-	75F-2	-
D	F	75	5	6	128.5	①	-	75F-3	-
D	N	100	5	1	164	①	Appendix D	VK16	-
D	S	100	5	1[e]	129	①	Appendix D	VK12	-
D	S	100	5	2	156	①	Appendix D	VK17	-
D	S	100	5	3	116.2	①	-	N4a	-
D	S	100	5	4	116.8	①	-	N4b	-
D	F	100	5	1[e]	151	②	Appendix D	VK15	-
D	F	100	5	2[e]	173	②	Appendix D	VK18	-
D	F	100	5	3	137.7	①	-	N3a	-
D	F	100	5	4	138.4	①	-	N3a	-

[a] N:No chamfering, S: slight chamfering, F: full chamfering.
[b] ①: Outer fleece fiber tear failure of the **inner** flat profile, ②: Outer fleece fiber tear failure of the **outer** flat profile.
[c] The alias is the denomination used during the experimental handling.

Table 11.2.: Listing of all *chamfered* specimen with an adhesive layer thickness of 1 mm

Geometry[a]	Chamfering[b]	$\frac{Overlap}{t_{adh.}}$	$\frac{t_o}{t_i}$	#	F_u in kN	Failure[c]	Picture(s)	Alias	Remark(s)
D	N	$\frac{50}{3}$	$\frac{5}{10}$	1	86	①	Appendix D	VK1	-
D	N	$\frac{75}{3}$	$\frac{5}{10}$	1	152	①	-	VK4	
D	S	$\frac{75}{3}$	$\frac{5}{10}$	1	124	①	Appendix D	VK5	-
D	N	$\frac{100}{3}$	$\frac{5}{10}$	1	146	①	Appendix D	VK7	-
D	S	$\frac{100}{3}$	$\frac{5}{10}$	1[e]	153	①	Appendix D	VK3	-
D	S	$\frac{100}{3}$	$\frac{5}{10}$	2	153	①	-	VK8	-
D	F	$\frac{100}{3}$	$\frac{5}{10}$	1[e]	147	①	-	VK6	-
D	F	$\frac{100}{3}$	$\frac{5}{10}$	2[e]	151	①	-	VK9	-

[a] D: Double lap joint, S: single lap joint.
[b] N:No chamfering, S: slight chamfering, F: full chamfering.
[c] ①: Outer fleece fiber tear failure of the **inner** flat profile, ②: Outer fleece fiber tear failure of the **outer** flat profile.

Table 11.3.: Listing of all *chamfered* specimen with an adhesive layer thickness of 3 mm

As it can be seen in Figs. 11.5 — pictures of the adhesively bonded splices of the inner 10 mm thick flat profiles, it is always the interface between the veil and the mats that fails. In (c) we can identify the typical woven structure of the mat.

A listing of chosen failure mode pictures is given in Appendix D.

The failure depth of approximatively 0.5 mm has been measured on several specimen. Some detail pictures (not only related to the specimen investigated in this Chapter) are displayed in Appendix D.3.

The weakest link in the whole joint seems to be the interface between the veil and the outer mats. Fig. 11.4 shows that the location of the failure lies at around 0.5 mm inside the FRP material.

Of course,due to the material architecture, this value cannot be considered as having a mathematical accuracy. The value of approximatively 0.5 mm has to be understood as a way to provide further FEA with a geometric location.

Deeper interpretations of this topic will follow in part VI.

11.3.4. STRAIN ALONG THE SPLICE

From all the investigated specimen, 6 were fully instrumented, they were denoted by an *e* in Tabs. 11.2 and 11.3.

These instrumented specimen allowed a close look at the inner load transfer inside the joint by revealing the axial strain development on the interface between the adhesive and the outer flat profile. This is the only easy-to-measure mechanical value.

The axial strain development along the splice is represented in Figs. 11.6 to 11.9 for different levels of chamfering.
Due to the geometrical symmetry of the bonded splices in the specimen, it was chosen to overlay the gathered strains of all 4 splices on just on diagram. Care had to be taken to investigate the issue of possible eccentricity.

The values correspond to a purely arbitrary reference force of 50 kN so that the influence of the geometry on the axial strain development is easier to distinguish, independent of the joint strength.
Because of the purely linear behaviour of all the mechanical components making the joints, strain profiles for other load steps can be linearly deduced.

The experimental results are compared to those obtained by FEA. The FE results are related to the analysis carried out in Chapter V.

As it can be seen, the experimental and numerical results show a good agreement. Both show that the axial strains are built up on the extremities of the overlap.

Figure 11.4.: Failure location

11.4. Conclusions

Experimental investigations on adhesively bonded double lap joints have been carried out. Ultimate loads for different levels of chamfering were investigated. For selected geometries, fully instrumented specimen allowed the determination of the strain development along the bonded joint.

The following first conclusions can be made:

- **The experiments showed that there is no significant increase on the ultimate load of adhesively bonded joints when the ends of the flat profiles are chamfered;**
- **The strain development along the splice was investigated and found to correlate well with FEA results;**
- **At higher chamfering levels, the axial strain development is not longer strictly monotonic decreasing towards the chamfered end but showing a slight increase;**
- **No visible influence of the adhesive layer thickness on the axial strain distribution can be identified within the range of investigated specimen;**
- **Failure is always triggered by the flat profile failure. The failure is initiated inside the material at a depth of approximatively 0.5 mm.**

Deeper interpretations will follow in part VI.

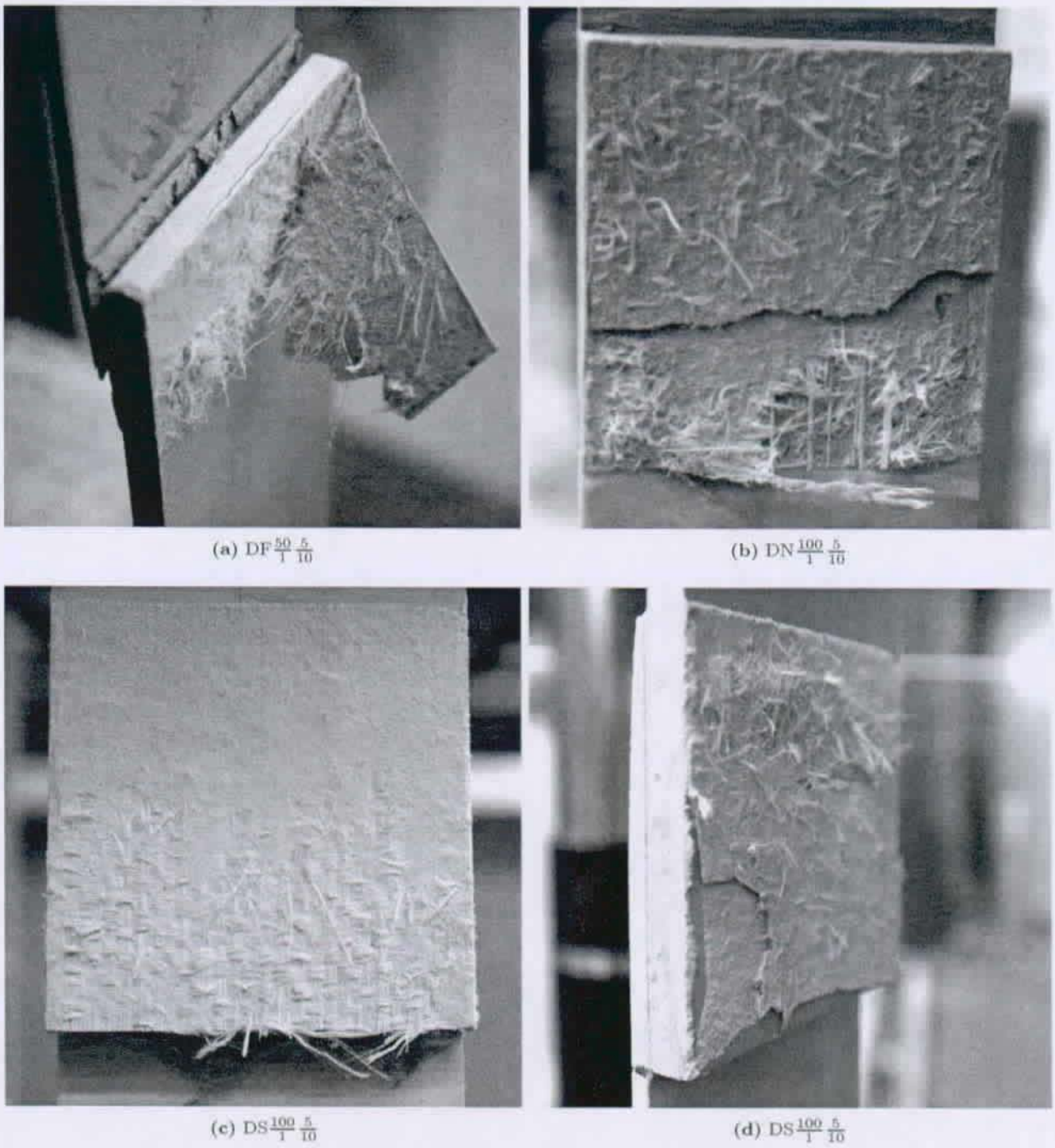

(a) DF $\frac{50}{1}\frac{5}{10}$ (b) DN $\frac{100}{1}\frac{5}{10}$

(c) DS $\frac{100}{1}\frac{5}{10}$ (d) DS $\frac{100}{1}\frac{5}{10}$

Figure 11.5.: Typical failure mode observed during the series

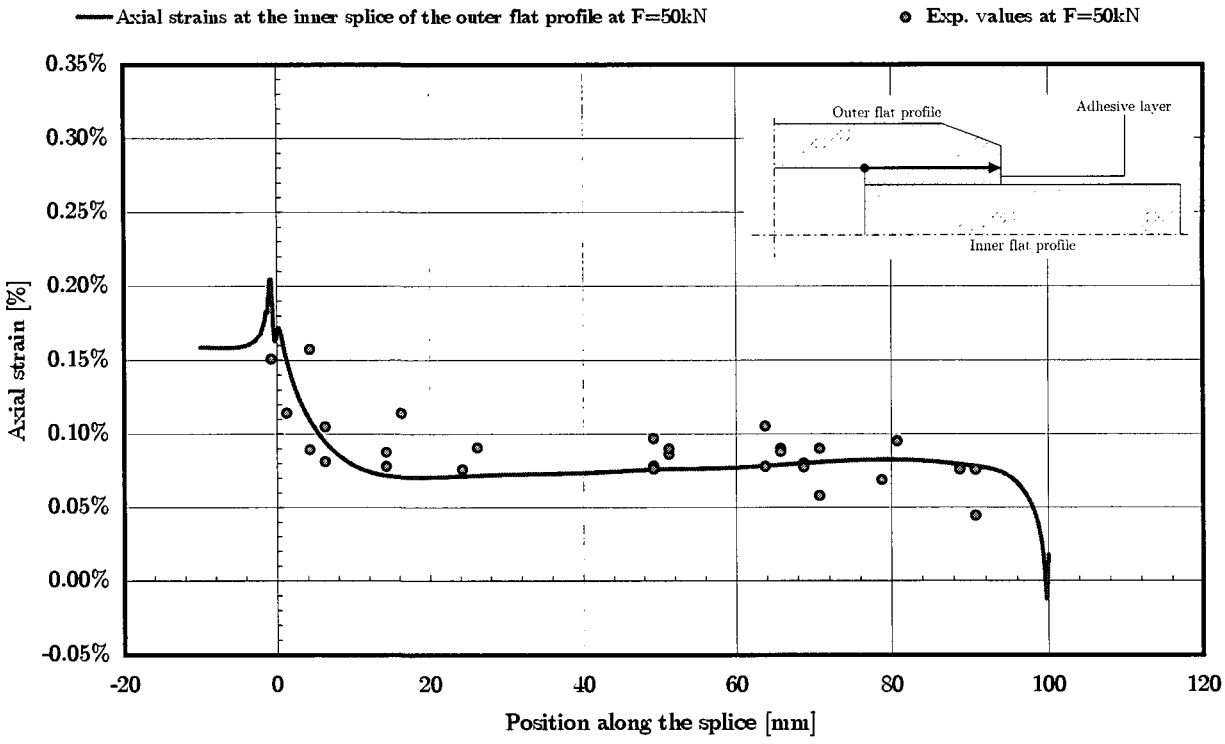

Figure 11.6.: Strain distribution for DS$\frac{100}{1}\frac{5}{10}1^e$

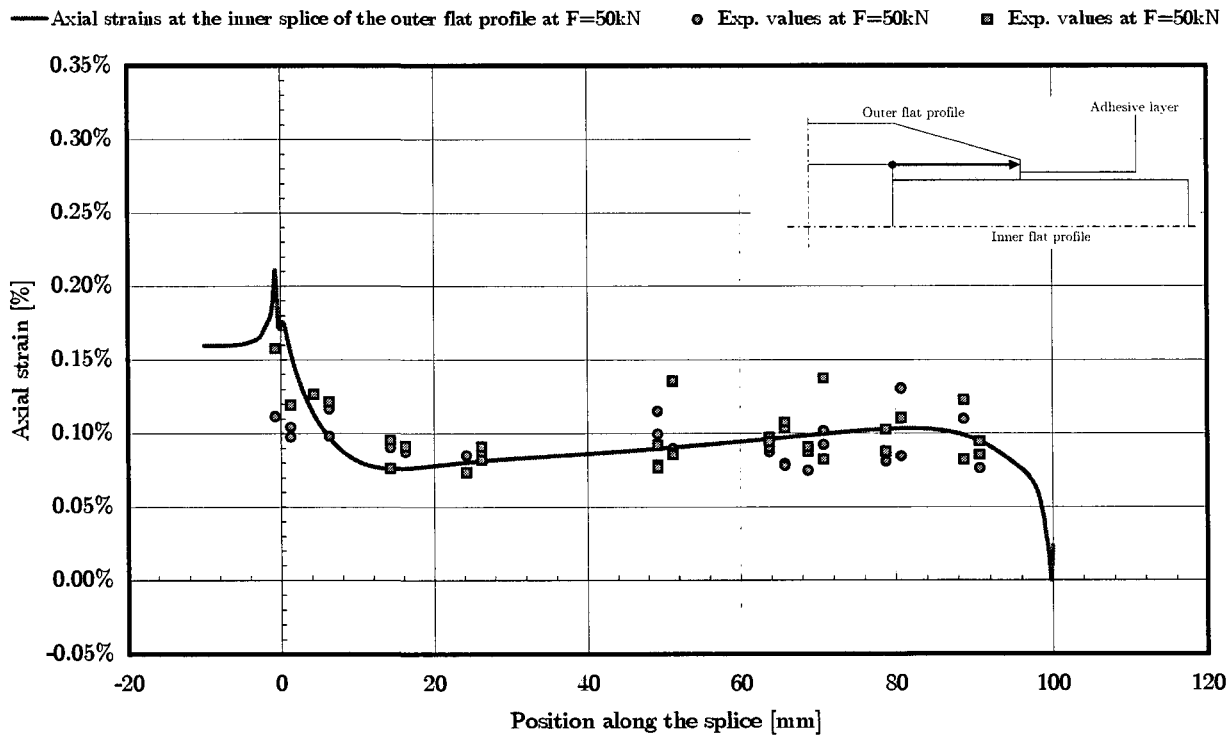

Figure 11.7.: Strain distribution for DF$\frac{100}{1}\frac{5}{10}1^e$: ○ and DF$\frac{100}{1}\frac{5}{10}2^e$: □

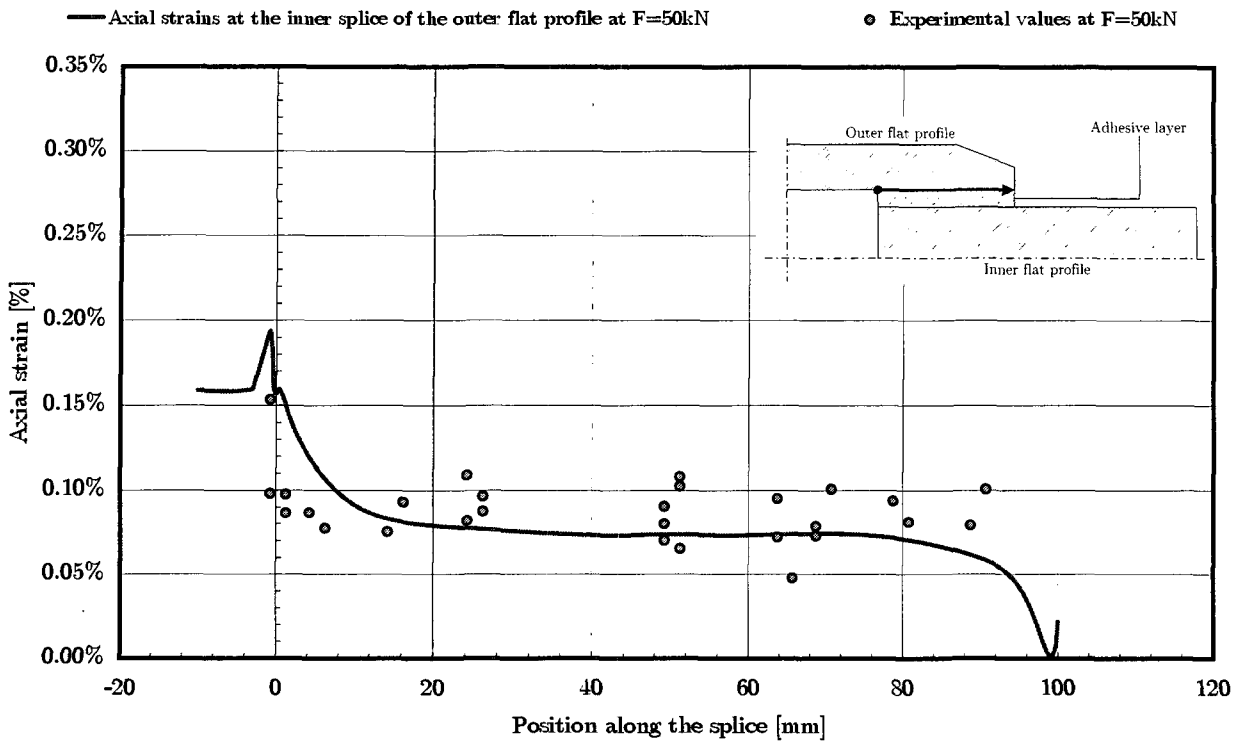

Figure 11.8.: Strain distribution for DS$\frac{100}{3}\frac{5}{10}1^e$

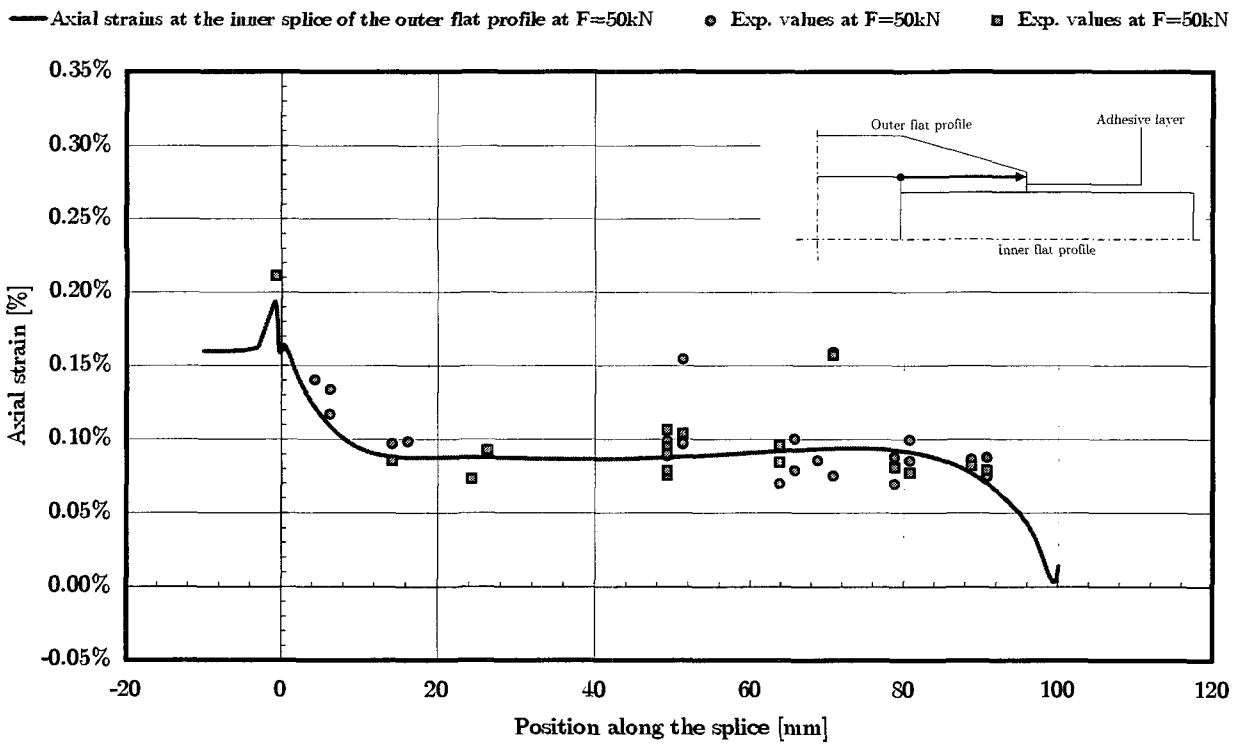

Figure 11.9.: Strain distribution for DF$\frac{100}{3}\frac{5}{10}1^e$: ○ and DF$\frac{100}{3}\frac{5}{10}2^e$: □

12. Experimental investigations involving a High Speed camera

12.1. Objectives

The experimental investigation presented in this Chapter is intended to better understand the mechanisms leading to the joint failure.

For this, typical joint configurations were filmed using a digital camera (see Fig. 12.1) able to gather up to 2000 frames per second.

The two objectives of this experimental series are:

1. **Filming the failure process of typical single and double lap joints using a high speed camera;**
2. **Locating the crack initiation in the bonded joints;**
3. **Gathering ultimate strengths of these joint configurations.**

Figure 12.1.: The high speed camera used for this experimental series

12.2. Experimental setup

12.2.1. Description

Geometrical specifications

Two different joint configurations were experimentally investigated:

① Unchamfered single lap joints

② Unchamfered double lap joints

Like in the experimental series described in Chapters 10 and 11, the specimens were manufactured using a set of four 100 mm × 500 mm flat profiles.

The following series consisting of 3 individual specimens each were manufactured:

① $\mathrm{SN}\frac{100}{2}\frac{5}{5}$
Single lap joints of **5 mm** thick flat profiles bonded together with a **2 mm** thick epoxy layer overlapping **100 mm**.

② $\mathrm{SN}\frac{100}{3}\frac{10}{10}$
Single lap joints of **10 mm** thick flat profiles bonded together with a **3 mm** thick epoxy layer overlapping **100 mm**.

③ $\mathrm{DN}\frac{100}{2}\frac{5}{10}$
Double lap joints of **5 mm** thick outer and **10 mm** thick inner flat profiles bond together with a **2 mm** thick epoxy layer overlapping **100 mm**.

Table 12.1 lists all specimen investigated.

All specimen were manufactured with an adhesive fillet showing a radius of $r_f = 1$ mm.

12.2.2. Surface treatment

See Chapters 10 and 11 for information related to the applied surface treatment.

12.2.3. Mechanical properties

All materials (FRP and adhesive) are equivalent to those used for the experimental investigation described in Chapter 11.

12.2.4. Experimental setup

The experiments were carried out using the same devices and under the same conditions as described in Chapter 11. The loading rate was also selected to match the previous experiments: 0.5 $\frac{mm}{min}$.

Geometry[a]	Chamfering[b]	$\frac{Overlap}{t_{adh.}}$	$\frac{t_2}{t_1}$	#	F_u in kN	Failure[c]	Picture(s)	Alias	Remark(s)
S	N	$\frac{100}{2}$	$\frac{5}{5}$	1	31	①	Figs. 12.5	SLJ1	-
S	N	$\frac{100}{2}$	$\frac{5}{5}$	2	30	①	Figs. 12.6	SLJ2	-
S	N	$\frac{100}{2}$	$\frac{5}{5}$	3	30	①	Figs. 12.7	SLJ3	-
S	N	$\frac{100}{2}$	$\frac{10}{10}$	1	40	①	Figs. 12.8	SLJ4	-
S	N	$\frac{100}{2}$	$\frac{10}{10}$	2	44	①	Figs. 12.9	SLJ5	-
S	N	$\frac{100}{2}$	$\frac{10}{10}$	3	42	①	Figs. 12.10	SLJ6	-
D	N	$\frac{100}{2}$	$\frac{5}{10}$	1	154	①	Figs. 12.11	DLJ1	-
D	N	$\frac{100}{2}$	$\frac{5}{10}$	2	172	①	Figs. 12.12	DLJ2	-
D	N	$\frac{100}{2}$	$\frac{5}{10}$	3	172	①	Figs. 12.13	DLJ3	-

[a]D: Double lap joint, S: single lap joint.
[b]N:No chamfering, S: slight chamfering, F: full chamfering.
[c]①: Outer fleece fiber tear failure of the **inner** flat profile, ②: Outer fleece fiber tear failure of the **outer** flat profile.

Table 12.1.: *Listing of all specimens involved in the high-speed camera experimental series*

12.3. EXPERIMENTAL RESULTS

12.3.1. ULTIMATE LOADS

Table 12.1 lists the ultimate loads reached during the experimental investigations.

12.3.2. HIGH SPEED PICTURES

All individual specimens were filmed at a rate of 2 000 fps[1], the result is displayed in Figs. 12.5 to 12.13. As it can be seen, even this high rate does not allow a very clear view of the processes leading to failure. This is due to the very high failure speed. As a matter of comparison, the crack growth speed can be approximated, according to [83], by the following equation:

$$V \approx 0.3 \ldots 0.4 \sqrt{\frac{E_x}{\rho}} \tag{12.1}$$

with E_x (axial E-Modulus) and ρ (density of the FRP material). Putting the values of the FRP material, the crack propagation speed is:

$$V \approx 0.3 \ldots 0.4 \sqrt{\frac{30000 \times 10^6}{2550}} \approx 1200 \frac{m}{sec} \tag{12.2}$$

This means that the crack grows approximatively by $\frac{1}{2000} \times 1200 = 0.6\,m$ between two shots. This makes it quite impossible to locate the beginning of a cracking process by eye[2].

Figs. 12.2-a and -b show that the crack grows in the FRP material, and not inside the adhesive.

12.3.3. SINGLE LAP JOINTS

Some comments on the sequences taken for the single lap joints are given below.

FIG. 12.5

The veil of the bottom[3] flat profile is clearly sticked on the adhesive layer, proving that the failure is initiated inside the bottom adherend;

FIG. 12.6

The failure is triggered at the left end of the adhesive layer inside the lower flat profile. The same remark as stated above can be made: the failure happens inside the lower adherend.

FIG. 12.7

The same situation as for Fig. 12.6, though the location has changed: it is the left side of the adhesive layer and the upper adherend.

FIG. 12.8

The same situation as for Fig. 12.6.

FIG. 12.9

Failure occurred at both ends, but also inside the material.

[1]Frames per second.
[2]Assuming that a normal eye is able to distinguish 20 fps, only crack increments of $\frac{1}{20} \times 1200 = 60\,m$ should be distinguishable.
[3]All locations are related to the position in the pictures.

Fig. 12.10

The images do not really allow a look at the failure process. The only information given is the fact that failure is initiated at the right end inside the upper flat profile.

12.3.4. Double lap joints

Some comments on the sequences taken for the double lap joints are given below.

Fig. 12.11

The sequence shows how fast the failure happens. On the second picture of the sequence, it is clearly identifiable that the failure is triggered at the end of the overlap at the left end.

Fig. 12.12

Basically the same remarks as for Fig. 12.11 are valid here: the failure starts at the left end of the overlap.

Fig. 12.13

The same remarks as before are valid.

12.4. Interpretation

Fig. 12.4 represents the failure sequence observed during the experimental investigations[4].

12.4.1. Single lap joints

It is relatively easy to conclude from the pictures taken the following failure sequence — for the single lap joint:

① Just below the adhesive fillet at the very end of the bonded overlap, both the out-of-plane tensile stresses σ_z and shear stresses τ_{xz} reach their maximum — as shown in Fig. 12.3 and 20.2 to 20.4;

② When reaching the ultimate load, the tensile out-of-plane stresses introduced by the outer flat profile at the end of the overlap into the inner flat profile lead in conjunction with the shear stresses to a **fiber-tear failure**[5] of one of the flat profiles.

[4] And documented in Figs. 12.5 to 12.10 for the single lap joints and Fig. 12.11 to 12.13 for the double lap joints.

[5] Using the nomenclature stated in the Standard Practice for Classifying Failure Modes in Fiber-Reinforced-Plastics (FRP)
ASTM D-5573-99 represented in Fig. 4.2.

The interfaces between the surface veil and the mat and between the mat and the rovings might be potentially weak links that could initiate failure. The reasons for that could lie — amongst other reasons — in the fact that the fibre crossings lead to stress peaks and that the manufacturing process cannot totally avoid little air bubbles at that interface. Additional weakening effects can result from the axial stresses in the axial rovings.

This kind of failure was already described before. Among those who published about this topic[6] K. Liechti, W. S. Johnson & D. A. Dillard in [71] described similar failure patterns, see also Section 4.2.4.

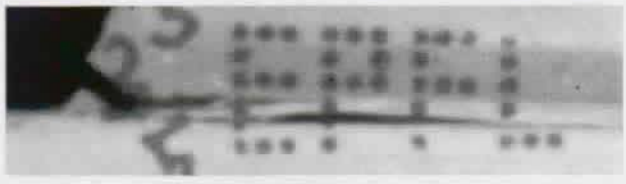

(a) SN $\frac{100}{2}\frac{5}{5}2$

(b) SN $\frac{100}{2}\frac{5}{5}3$

Figure 12.2.: Zooms of cracks

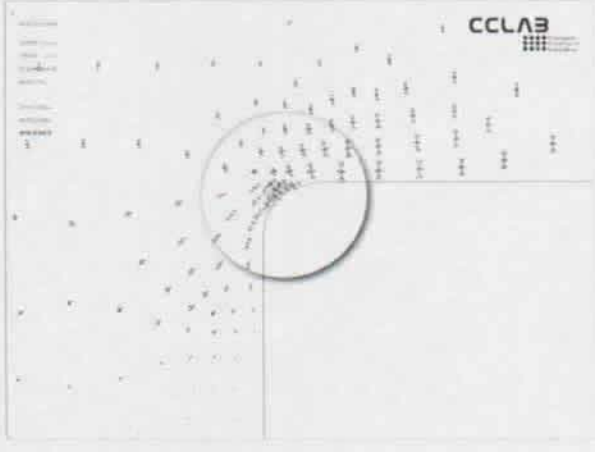

Figure 12.3.: Strains in the vicinity of the radius fillet for single lap joints

[6] But not related to pultruded material.

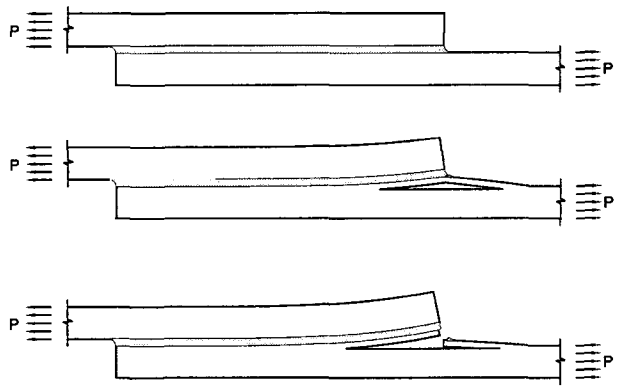

(a) Single lap joints: observed

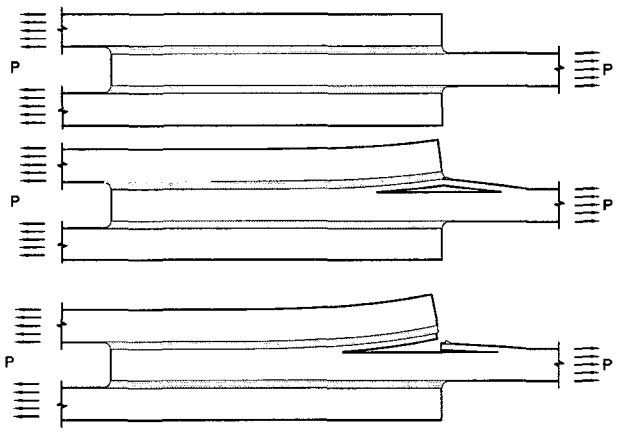

(b) Double lap joints: assumed

Figure 12.4.: Rupture sequence

12.4.2. DOUBLE LAP JOINTS

For double lap joints, this failure sequence is not identifiable with this ease because of the speed of the process.
Fig. 12.11 may allow the conclusion that the upper 5 mm flat profiles first fails at the left side of the overlap.
Assuming that the failure must have similar reasons as for the single lap joints, the following failure sequence is suggested:

① Both the out-of-plane stresses σ_z and the shear stresses τ_{xz} grow with the axial load and have their maximum just under the fillets at both ends of the overlap. But while the out-of-plane stresses at the left end of the overlaps (related to the orientation given by Figs. 12.11 to 12.13) are tensile, the σ_{xz} stresses at the right end are compressive (see for this the FEA carried out in Part V).

② When reaching the ultimate load, the σ_z-τ_{xz}-stress combination under the fillet at the left end of the overlap,(with the tensile σ_z-stresses) lead to the same failure mechanism as described for the single lap joints just a few lines above. The fact that the $\sigma - z$ stresses at the other end of the overlap are compressive means that failure is not triggered at this point.

③ Because the failure process occurs so suddenly, it is not easy to reconstruct the process just by studying the post failure specimen. This is due to the fact that a lot of secondary damage occurs by dynamic effects (as it can be seen in Figs. 12.11 to 12.13).

The suggested failure process is represented in Fig. 12.4.

12.5. CONCLUSIONS

Experiments on adhesively bonded joints were carried out. High-Speed films of the joint failure were made.

The following first conclusion can be made:

- **As described in Chapter 11, failure seems to be initiated by fiber-tear failure. This can also be seen in the pictures shown in the body of this Chapter;**
- **A failure sequence has been identified and described.**

Figure 12.5.: High speed image failure SN$\frac{100}{2}\frac{5}{5}1$, shutter of $\frac{1}{2000}$ sec.

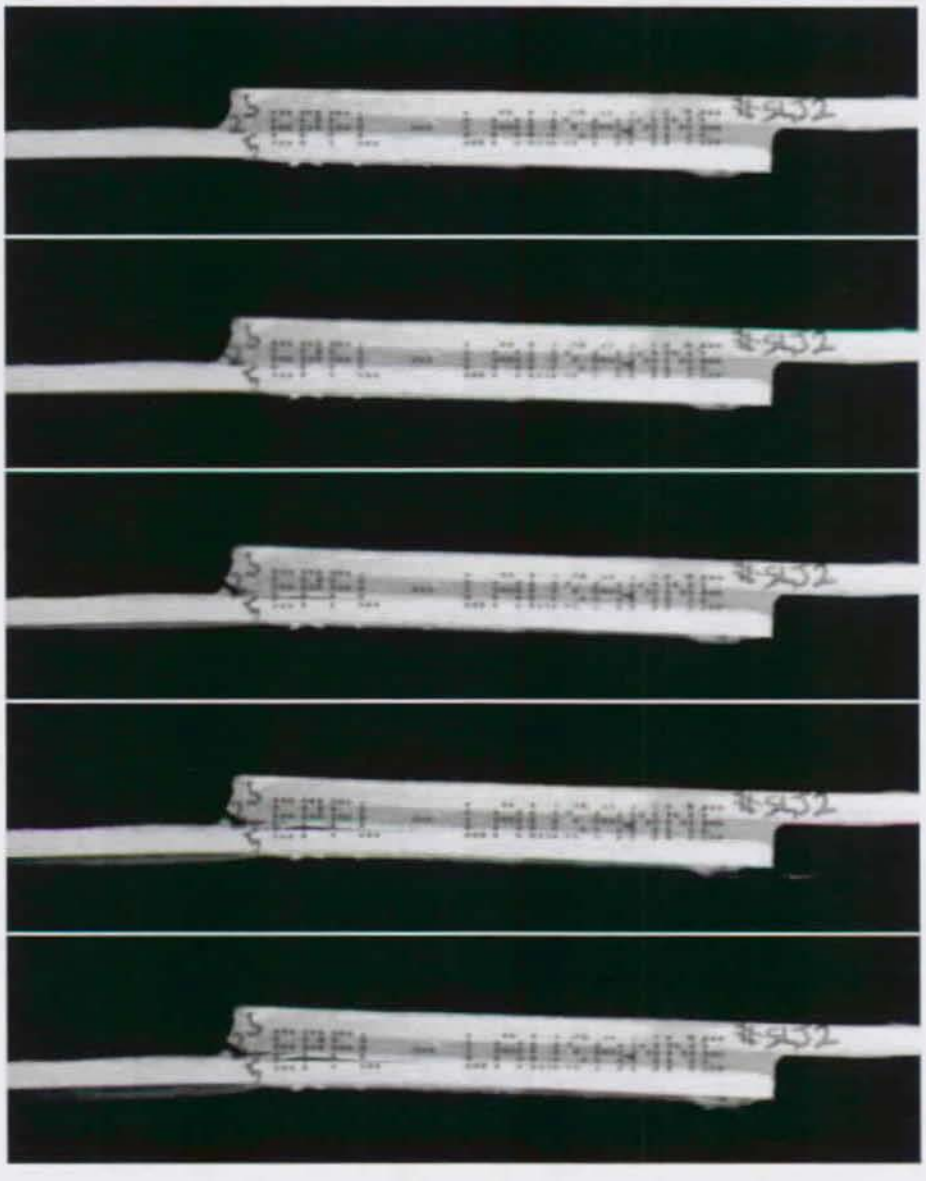

Figure 12.6.: High speed sequence SN$\frac{100}{2}\frac{5}{5}2$ at an interval of $\frac{1}{2000}$ sec.

Figure 12.7.: High speed sequence SN$\frac{100}{2}\frac{5}{5}$3 at an interval of $\frac{1}{2000}$ sec.

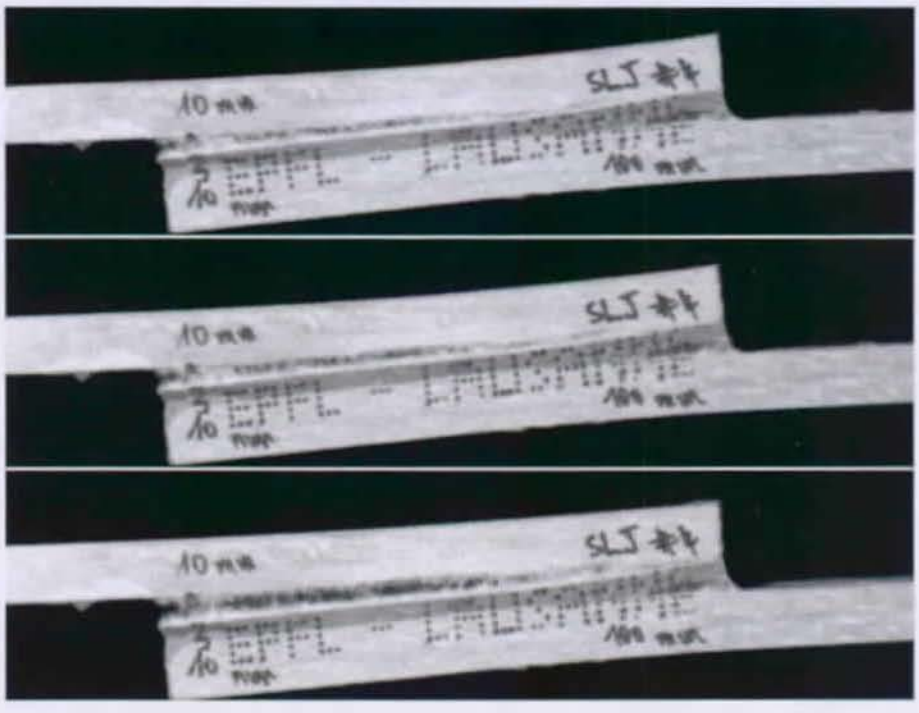

Figure 12.8.: High speed sequence SN$\frac{100}{3}\frac{10}{10}$1 at an interval of $\frac{1}{2000}$ sec.

Figure 12.9.: High speed image failure SN$\frac{100}{3}\frac{10}{10}$2, shutter of $\frac{1}{2000}$ sec.

Figure 12.10.: High speed sequence SN$\frac{100}{3}\frac{10}{10}$3 at an interval of $\frac{1}{2000}$ sec.

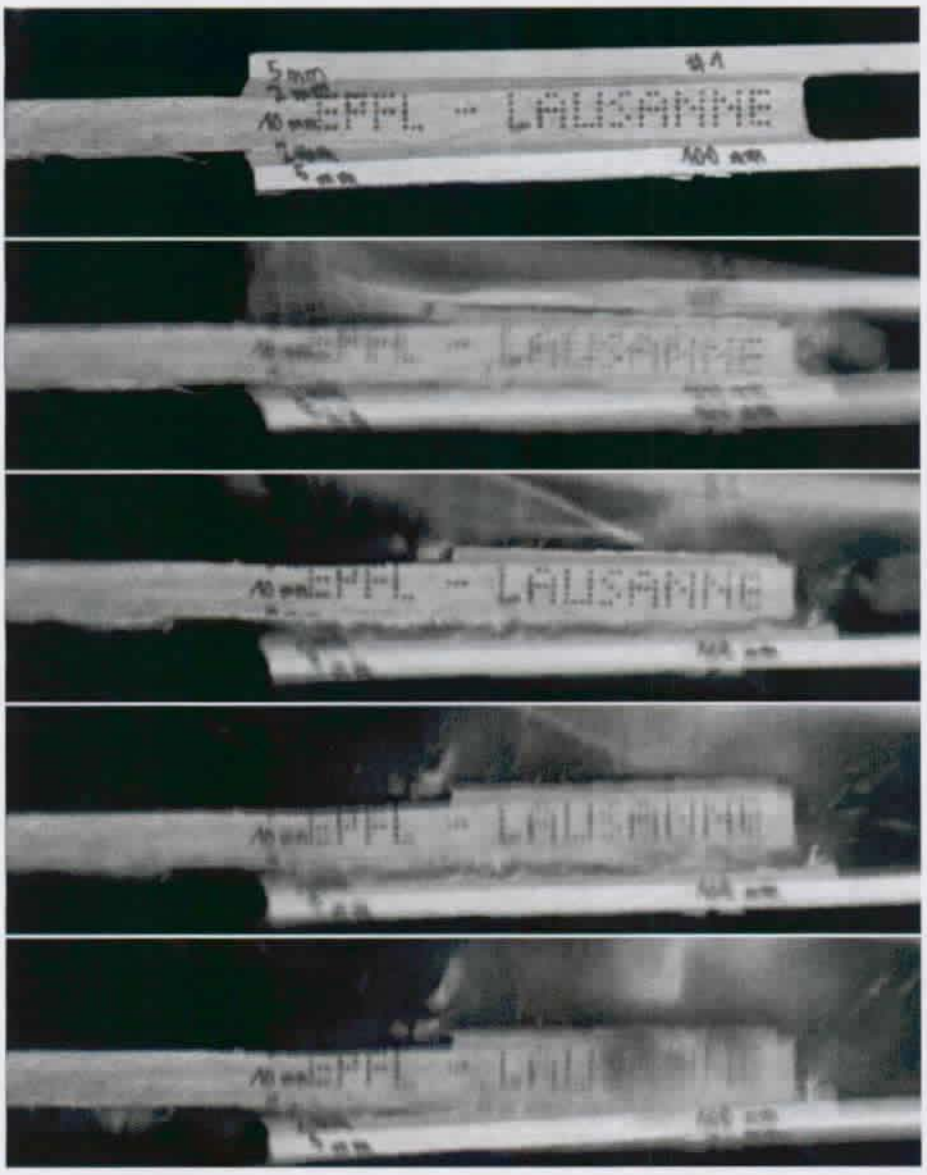

Figure 12.11.: High speed sequence DN$\frac{100}{2}\frac{5}{10}$1 at an interval of $\frac{1}{2000}$ sec.

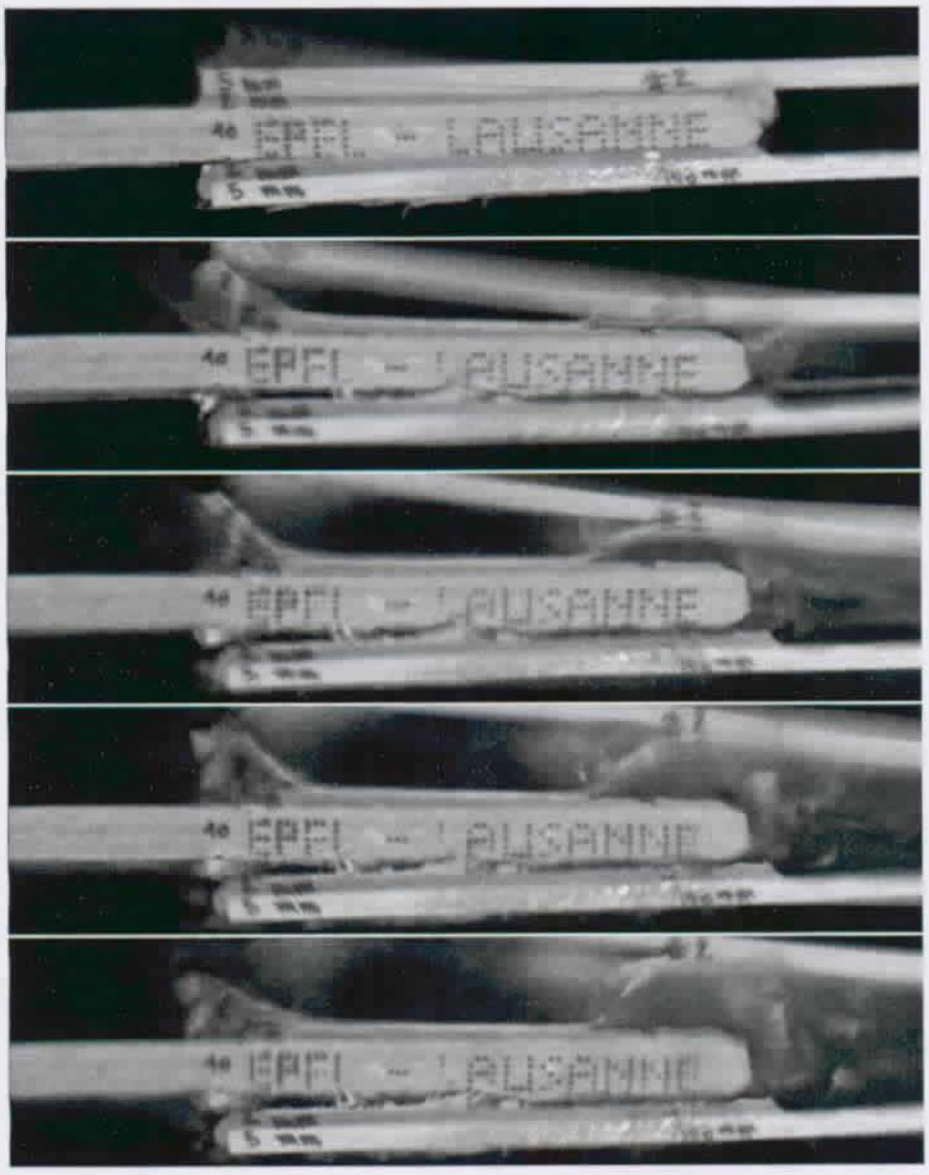

Figure 12.12.: High speed sequence DN$\frac{100}{2}\frac{5}{10}$2 at an interval of $\frac{1}{2000}$ sec.

Figure 12.13.: High speed sequence DN$\frac{100}{2}\frac{5}{10}$3 at an interval of $\frac{1}{2000}$ sec.

13. Experimental investigation on bolted and bonded joints

13.1. Objectives

To demonstrate the superiority — in terms of transmitted forces — **of adhesively bonded connections over traditionally bolted connections, an experimental series was initiated to compare the performance of:**

1. **Adhesively bonded connections;**
2. **Simply bolted connections;**
3. **Connections with torqued bolts[1];**
4. **Connections combining bolts and adhesives;**
5. **Connections combining torqued bolts and adhesives.**

The experimental series described in this Chapter has a strictly comparative character[2]. It can nevertheless give some precious indications concerning the performance of different means of connection.

It is not the topic of this Thesis to discuss the different methods of stress analysis and strength prediction of mechanically fastened joints in FRP. P. P. Camanho & F. L. Mattews have — amongst others — published a review on this topic [84].

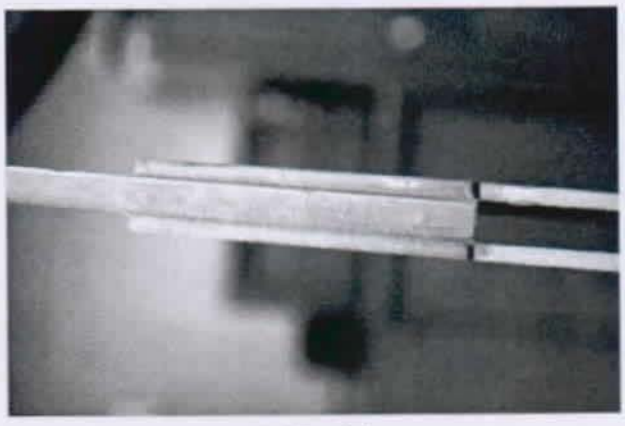

(a) Bonded

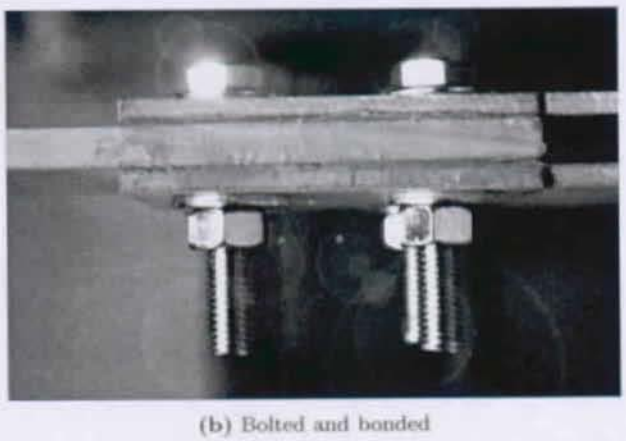

(b) Bolted and bonded

Figure 13.1.: Typical investigated specimen

13.2. Experimental setup

13.2.1. Description

Geometric specifications

The specimens were manufactured from a batch of 500 mm × 100 mm flat profiles.
The outer flat profiles were always 5 mm thick while the inner ones were 10 mm thick, so that the cumulative cross-section was kept constant.
All specimens were manufactured with an adhesive fillet showing a radius of $r_f = 1$ mm.
The overlap was kept constant throughout the experimental series to 100 mm. Figs. 13.1-a and -b give an idea about the general layout of these connections.

[1] The term *torqued bolts* is used in the meaning of bolts that have been tightened using a calibrated torque wrench.

[2] Because no variation in geometry or mechanical parameters were performed, it is formally not possible to generalize the results of this investigation, but the general trend remains certainly true.

FRP-MATERIAL USED

Own tension experiments were carried out at the CCLAB. The gathered values are given by Tab. 11.1, see also Appendix B..

ADHESIVE

The adhesive used was the SIKADUR 330 supplied by our partner SIKA; the material was experimentally investigated for previous series. See Tab. C.2 for further details.

The adhesive had approximatively 2 months to cure at room temperature. The temperature in the experimental laboratory lied around 22 ± 2 °C.

BOLTS

The bolts were 4 × M12-8.8. The associated washers had a diameter of 30 mm and a thickness of 3 mm. Fig. 13.2 gives an idea of the selected bolt layout:

① The 4 bolts were placed in a square arrangement with $\frac{e}{d} = 2.5$;

② The planned hole tolerance was less than 0,1 mm;

③ The torqued bolts were tightened with a moment of 50 N×m.

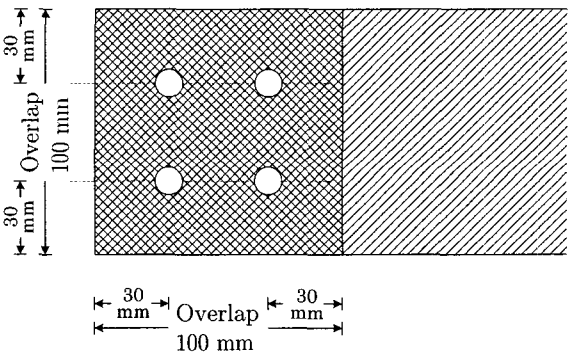

Figure 13.2.: The bolt layout

The mechanical properties of the bolts according to EUROCODE3 [85] are the following:

Ultimate Tensile Strength $F_{t,Rd}$=48,56 kN and

Ultimate Shear Strength[3] $F_{t,Rd}$=43,43 kN.

The edges of the washers have been rounded to minimize a *punching shear failure* of the adherents. All torque-moments were applied within one hour of the experiment so that long-term effects of creeping in the FRP and adhesive could be neglected.

[3]For the shaft.

13.2.2. SURFACE PREPARATION

See Chapter 10 for the regulations concerning the surface preparation.
The specimens of the experimental series Bt — featuring the simply bolted connection with torqued bolts — had the contact surface additionally roughened to increase the friction factor.

13.2.3. EXPERIMENTAL SERIES

The following 5 different experimental specimen types were experimentally investigated:

① Adhesively bonded connections
↪ Series A

② Simply bolted connections
↪ Series B

③ Connections with torqued bolts
↪ Series Bt

④ Connections combining bolts and adhesives
↪ Series C

⑤ Connections combining torqued bolts and adhesives
↪ Series Ct

Every type was experimentally investigated 3 times. The following individual specimen designation was selected: **A1** to **Ct3** .

13.2.4. EXPERIMENTAL PROCEDURE

The experimental device was an SCHENCK HYDROPULS-ZYLINDER TYP PL.
The experiments documented here were **displacement controlled** with data gathering of displacement and the corresponding force.
The applied loading rate was kept constant for all specimen to 0.5 $\frac{mm}{min}$.

13.3. EXPERIMENTAL RESULTS

13.3.1. UP TO FAILURE

As mentioned before, only load-displacement-curves were gathered during the experimental investigations. The diagrams, displayed in Figs. 13.4-a to -e, represent the *relative displacement* $\Delta_{Rel.}$ *vs. applied load* F. The relative displacement $\Delta_{Rel.}$ was defined as being the displacement of the tips of the specimen Δ_{Global} — where the load was applied — minus the elastic elongation of the free length[4] L_{free} of the flat

[4]Defined as the global specimen length minus the overlap and the section comprised in the jaws.

Geometry[a]	Chamfering[b]	$\frac{Overlap}{t_{adh.}}$	$\frac{t_s}{t_i}$	#	F_u in kN	Alias	Remark(s)
A	N	$\frac{100}{2}$	$\frac{5}{10}$	1	150	A1	-
A	N	$\frac{100}{2}$	$\frac{5}{10}$	2	116	A2	Bad bond
A	N	$\frac{100}{2}$	$\frac{5}{10}$	3	142	A3	-
B	N	$\frac{100}{2}$	$\frac{5}{10}$	1	57	B1	-
B	N	$\frac{100}{2}$	$\frac{5}{10}$	2	65	B2	-
B	N	$\frac{100}{2}$	$\frac{5}{10}$	3	65	B3	-
Bt	N	$\frac{100}{2}$	$\frac{5}{10}$	1	90	Bt1	-
Bt	N	$\frac{100}{2}$	$\frac{5}{10}$	2	79	Bt2	-
Bt	N	$\frac{100}{2}$	$\frac{5}{10}$	3	79	Bt3	-
C	N	$\frac{100}{2}$	$\frac{5}{10}$	1	130	C1	-
C	N	$\frac{100}{2}$	$\frac{5}{10}$	2	159	C2	-
C	N	$\frac{100}{2}$	$\frac{5}{10}$	3	150	C3	-
Ct	N	$\frac{100}{2}$	$\frac{5}{10}$	1	204	Ct1	-
Ct	N	$\frac{100}{2}$	$\frac{5}{10}$	2	234	Ct2	-
Ct	N	$\frac{100}{2}$	$\frac{5}{10}$	3	168	Ct3	-

[a]A: adhesively bonded, B: simply bolted, Bt: torqued bolts, C: combination of adhesive and bolts, Ct: combination of torqued bolts and bonded.
[b]N:No chamfering, S: slight chamfering, F: full chamfering.

Table 13.1.: Listing of all specimen involved in the bolted/bonded experimental investigation

profiles. Eq. 13.1 gives the corresponding mathematical formulation.

$$\Delta_{Rel.} = \Delta_{Global} - \frac{F \times L_{free}}{E \times A} \qquad (13.1)$$

with E_x the Elastic Modulus and A the cross section of the involved flat profiles.

A-SERIES

① The load-displacement behaviour can be characterized as being almost linear up to the brittle failure;

② The failure occurred without warning sings[5];

③ There is some scattering $\frac{\sigma}{m}$ =13 % in the results for the ultimate loads obtained.

B-SERIES

① The stiffness is activated after some slip. This is due to the fact that the holes were manufactured with a tolerance of 0.1 mm. This value can be found in the load-displacement diagram;

② The failure occurred without clear warning sings. After the crack initiated at the levels of the bolts, the carried load dropped down to a third of its value before and remained constant over a large portion of the displacement;

③ The scattering in the results is relatively small: $\frac{\sigma}{m}$ = 8 %.

BT-SERIES

① In a first portion (up to ≈ 32 kN), the joint is very stiff. This is certainly due to the friction load transfer initiated by the prestressed torqued bolts through the roughened surfaces;

② After a displacement of 0.1 mm (≈ hole tolerance), the behaviour of the Bt-series looks like the one observed in the B-series;

③ The scattering in the results is relatively small: $\frac{\sigma}{m}$ = 7 %.

C-SERIES

① The behaviour is, in all points similar, to the A-series up to failure. Differences appear only in the post-failure behaviour of the joint at deformations far above those corresponding to failure[6]. The scattering in the results is $\frac{\sigma}{m}$ = 10 %.

CT-SERIES

① The ultimate loads reached are the highest obtained throughout all experimental series. The force-displacement diagram loses its quasi linear character. The failure is very sudden;

② The scattering of the results is noticeable: $\frac{\sigma}{m}$ = 16 %.

13.3.2. FAILURE

Two major descriptors denote the failure:

① The ultimate load.

② The failure pattern.

ULTIMATE LOADS

The ultimate loads reached during the experimental investigations are given by Tab. 13.1.

[5]Exception made of audible cracks at approximatively $\frac{2}{3}$ of the failure load F_u.

[6]Gathering these values is of course only possible in displacement controlled experiments.

FAILURE MODES

Figs. 13.3-a to -e show how failure occurred.

For the specimens of the A series, the failure is identical to the one observed in the previous experimental series of bonded joints: tearing of the fleece by delamination.

The specimens of the B and Bt series failed by shearing the bolts through the outer 5 mm flat profiles. The only difference between the B and Bt series is that in the second case, the friction stresses induced by the torqued bolts delay this failure mode leading to an higher ultimate load.

Series C and Ct fail in a more complex way: the final result is the same like in the B and Bt series, with the difference that the outer fleece of the inner 10 mm flat profile was sheared off by the adhesive. The typical failure observed in the A series is prevented by the fact that the out-of-plane is prevented by the very high out-of-plane prestressing induced by the prestressed bolts in the Ct series.

13.4. CONCLUSIONS

Experimental investigations on bolted and bonded (and combinations of both) were carried out with the aim to compare the performance of different techniques of connection.

The following first conclusion can be drawn:

- **The experimental series described showed that adhesively bonded double-lap joints have potentially higher ultimate loads[7].**
- **Combining adhesive bonding with untorqued bolts does not lead to any significant increase in bearing loads or stiffness. Because of the higher bearing loads obtained through the adhesive bonding, no redundancy is obtained.**
- **Combining adhesive bonding with torqued bolts does lead to a significant increase in bearing loads (≈ 25 %). This is due to the fact that the torqued bolts apply a prestress at the ends of the splice so that the tensile out-of-plane stresses are at least reduced, if not totally over-compressed.**

FURTHER SUGGESTIONS

It would be interesting to extend the comparison of adhesively bonded versus bolted joint bearing capacity to different joint configurations.
Especially the increase in the bearing load for the combination of adhesive bonding **and** torqued seems interesting. In conjunction with this, it would also be interesting to study the creep behaviour of torqued/prestressed bolts on pultruded FRP's.

COMPARATIVE STUDY

As a matter of comparison, C. COOPER & G. J. TURVEY have investigated the effect of bolt torque on the structural performance of single bolt tension joints in pultruded FRP in [86].
Concerning the results, the following might be of interest:

① Concerning the load-displacement curves:
After an initial bolt movement, the plots are linear up to failure.

② The failure loads[8] could be increased by 45% for slight torque and 80% for full torque[9].

[7] This was proven for a specific combination of material, geometry and bolt arrangement, but is probably true for many configurations.

[8] Called ultimate bearing loads by C. COOPER & G. J. TURVEY in [86].

[9] In the actual experimental investigation the increase was around 34%.

(a) A-series

(b) B-series

(c) Bt-series

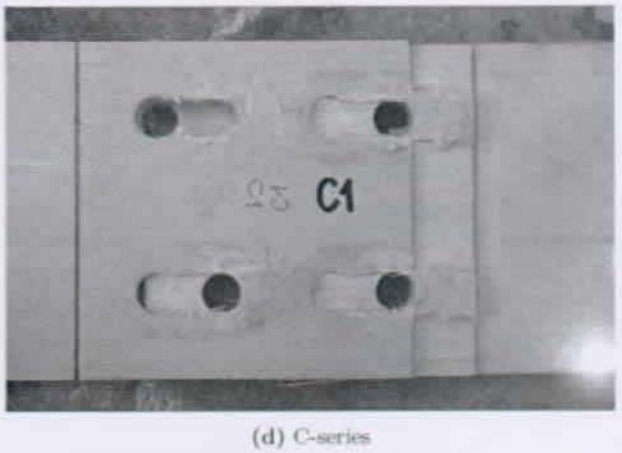

(d) C-series

(e) Ct-series

Figure 13.3.: Typical failure for specimen

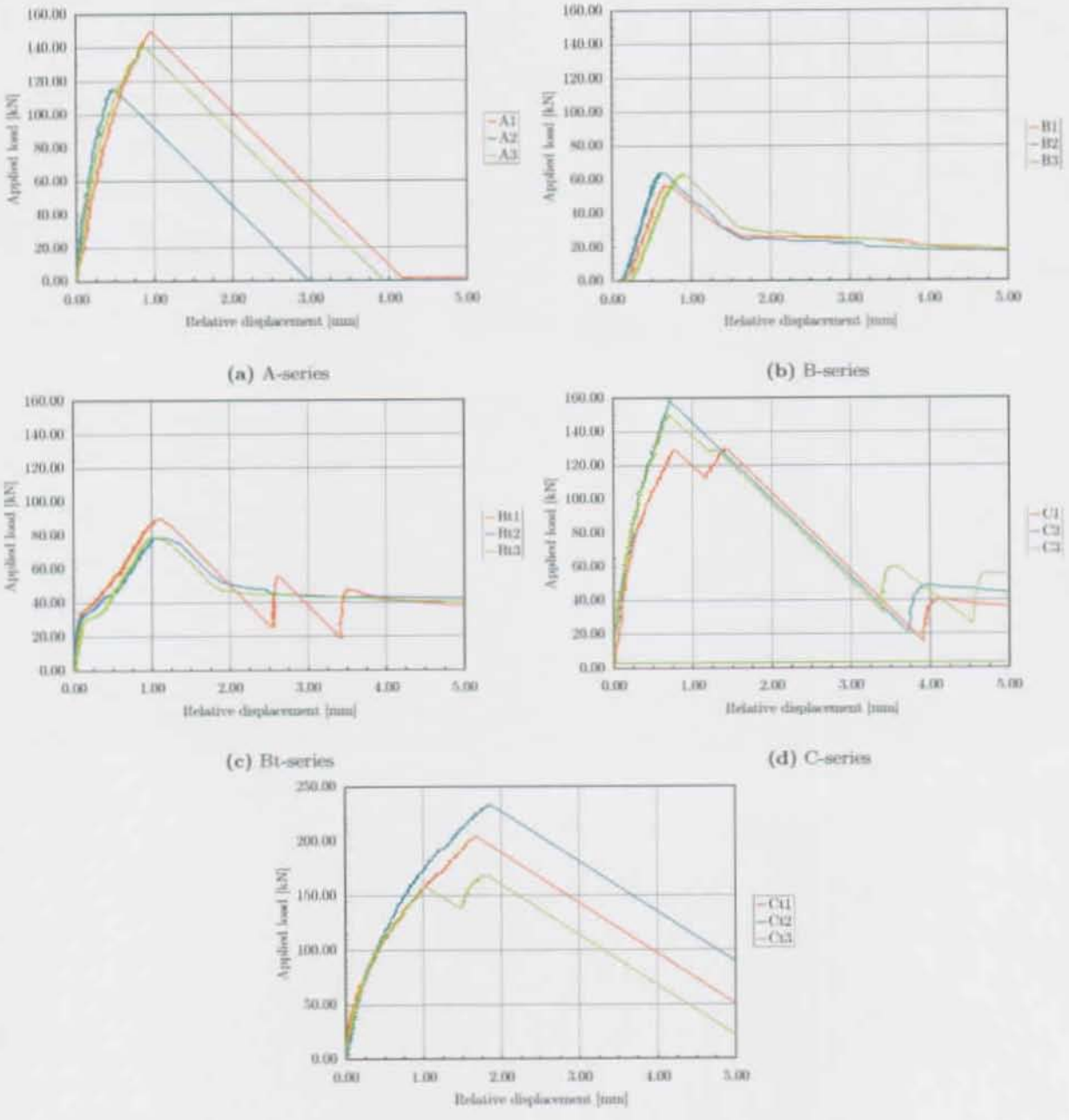

(a) A-series

(b) B-series

(c) Bt-series

(d) C-series

(e) Ct-series

Figure 13.4.: Load-displacement diagrams

14. Listing

14.1. Listing of the specimen investigated

Table 14.1 summarizes some results of the previously described experimental investigations.

For this purpose, the following indications are given:

① Geometrical description according to the convention stated in Appendix A.2;

② The number of identical geometrical configurations investigated;

③ The failure, loads F_u reached and the associated scattering expressed by the standard deviation, σ_{F_u}.

14.2. Other miscellaneous experimental investigations reported

besides the specimens described in the prvious chapters of this part, J. DeCastro reported in [31] ultimate strength values for a series of three identical epoxy bonded double lap joints with an overlap of 200 mm that have been identified as DN$\frac{200}{2}\frac{5}{10}$ according to the nomenclature selected in this Thesis. The ultimate strength reached in this series was reported to be $\mathbf{F_u = 182 \pm 15\,kN}$.

T. Tirelli reports (not published report [63]) of a series of 8 identical epoxy bonded double lap joints identifiable by DN$\frac{100}{2}\frac{5}{10}$. The ultimate strength reached in this series was reported to be $\mathbf{F_u = 141.5 \pm 12.6\,kN}$.

Y. Zhang reports in her Master's Thesis [88] on single lap joint experiments carried out under the same conditions and using the same materials as those presented in Chapter 12. The ultimate loads gathered for two geometrical configurations investigated are the following:

① SN$\frac{100}{2}\frac{5}{5}$ $F_u = 40.91 \pm 2.31\,kN$

② SN$\frac{100}{3}\frac{10}{10}$ $F_u = 39.74 \pm 2.14\,kN$

Geometry[a]	Chamfering[b]	$\frac{Overlap}{t_{adh.}}$	$\frac{t_2}{t_1}$	#	F_u in kN	$\pm\sigma_{F_u}$ [c]
D	N	$\frac{50}{1}$	$\frac{5}{10}$	IIII	101.0	5.5
D	S	$\frac{50}{1}$	$\frac{5}{10}$	IIII	93.9	7.0
D	F	$\frac{50}{1}$	$\frac{5}{10}$	###	108.3	11.5
D	N	$\frac{75}{1}$	$\frac{5}{10}$	IIII	130.2	15.5
D	S	$\frac{75}{1}$	$\frac{5}{10}$	IIII	131.3	12.2
D	F	$\frac{75}{1}$	$\frac{5}{10}$	###	142.0	9.6
D	N	$\frac{100}{1}$	$\frac{5}{10}$	I	164	※[d]
D	S	$\frac{100}{1}$	$\frac{5}{10}$	II	142.5	19.1
D	F	$\frac{100}{1}$	$\frac{5}{10}$	IIII	150.0	16.5
D	N	$\frac{50}{3}$	$\frac{5}{10}$	I	86.0	※
D	S	$\frac{75}{3}$	$\frac{5}{10}$	I	124	※
D	N	$\frac{100}{3}$	$\frac{5}{10}$	IIII	161.5	13.7
D	S	$\frac{100}{3}$	$\frac{5}{10}$	II	153	0.0
D	F	$\frac{100}{3}$	$\frac{5}{10}$	II	149	2.8
A	N	$\frac{100}{2}$	$\frac{5}{10}$	III	137.0	18
C	N	$\frac{100}{2}$	$\frac{5}{10}$	III	146	15
Ct	N	$\frac{100}{2}$	$\frac{5}{10}$	III	202	33
S	N	$\frac{100}{2}$	$\frac{5}{5}$	III	30.3	0.6
S	N	$\frac{100}{3}$	$\frac{5}{5}$	III	42.0	2.0

[a] D: Double lap joint, S: single lap joint, A & C & Ct: Double lap joints (refers to Chapter 13)
[b] N:No chamfering, S: slight chamfering, F: full chamfering.
[c] Standard deviation.
[d] No standard deviation available, because only one specimen investigated.

Table 14.1.: Summary of all tested lap joints that will be investigated in greater depth

Part IV.

The CCLab Tensile-Shear Device

Non omnia possumus omnes...

15. CCLab Tensile-Shear Device

15.1. Motivation

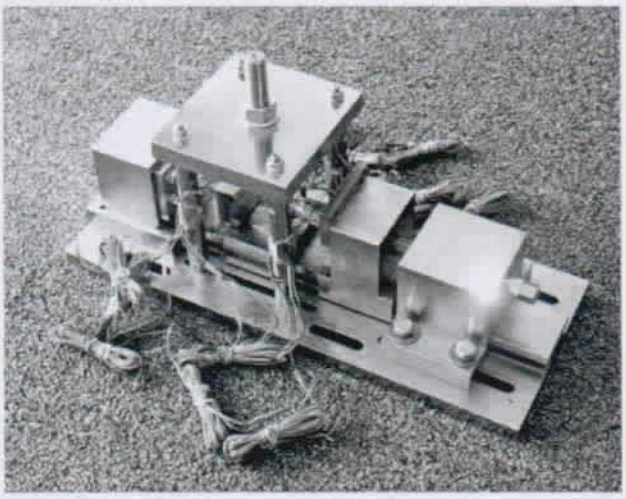

Figure 15.1.: CCLab Tensile-Shear Device

Previous experimental investigations carried out on adhesively bonded double lap joints (Chapters 10 to 12) have shown that the determination of the stress-state through FEA is sufficiently accurate.

The experimental investigations also showed also that failure is triggered by a material strength property of the FRP laminates involved and not in the adhesive layer.

The next step is therefore the determination of the ultimate strength of the FRP-material related to the two obviously important stress components:

① Out-of-plane stresses, σ_z induced by the peeling stresses in the adhesive layer;

② Shear stresses, τ_{xz}.

Inside the joint, both stresses σ_z and τ_{xz} appear simultaneously, so that there is a need for a device able to measure the failure criterion of the FRP-material under any given combination of both[1].

15.1.1. Design criteria

The Author designed an experimental device: the The CCLab Tensile-Shear Device.

To guide the design process, some design criteria were defined:

① The device should be able to independently measure and at any combination of both the ultimate tensile strength $\sigma_{z,u}$ and the ultimate shear strength $\tau_{xz,u}$;

② The device should be as independent as possible from other experimental facilities.

15.2. Literature

A survey of codes. standards and relevant literature showed that there is no device able to determine the needed values for ultimate strengths $\sigma_{z,u}$ and $\tau_{xz,u}$. Only one publication [32] gave some indications on how to proceed (see Section 4.3.1).

15.3. General description

Fig. 15.1 shows a picture of the device.

The CCLab Tensile-Shear Device is described by the drawing displayed in Fig. 15.3.

The device was manufactured in steel. The dimensions were kept as small as possible, to make it very mobile and totally independent of larger experimental facilities; the only external device needed is a data gathering unit[2]. The to test FRP sample is sticked on steel supports, see Fig. 15.4.

The device is built on a rectangular steel plate with a guiding rail ①[3].

[1] Gathering this material strength for different combinations of τ_{xz} and σ_z is equivalent to formulate a failure criterion.

[2] In this case a Spider 8, a multi-channel electronic PC measurement unit for parallel dynamic measurement data acquisition using a computer.

[3] The numerotation is related to the technical scheme given by Figure 15.3.

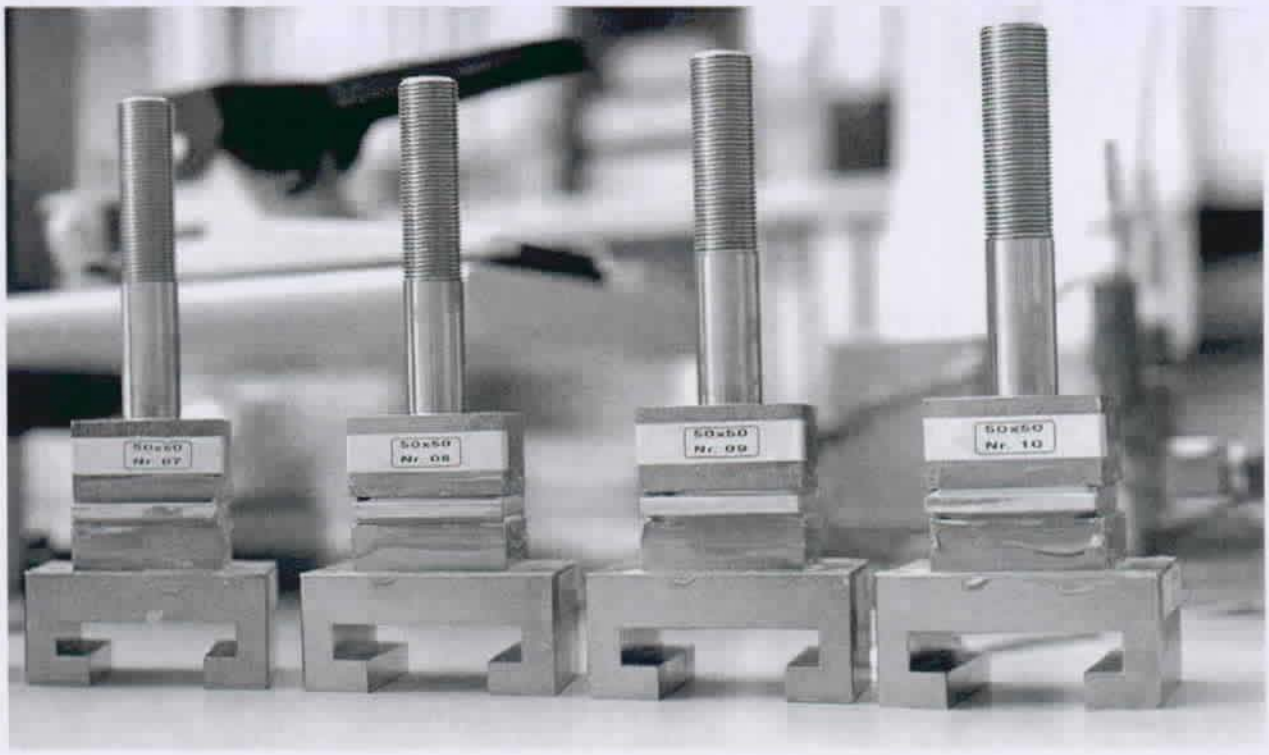

Figure 15.2.: CCLab Tensile-Shear Device: the steel supports

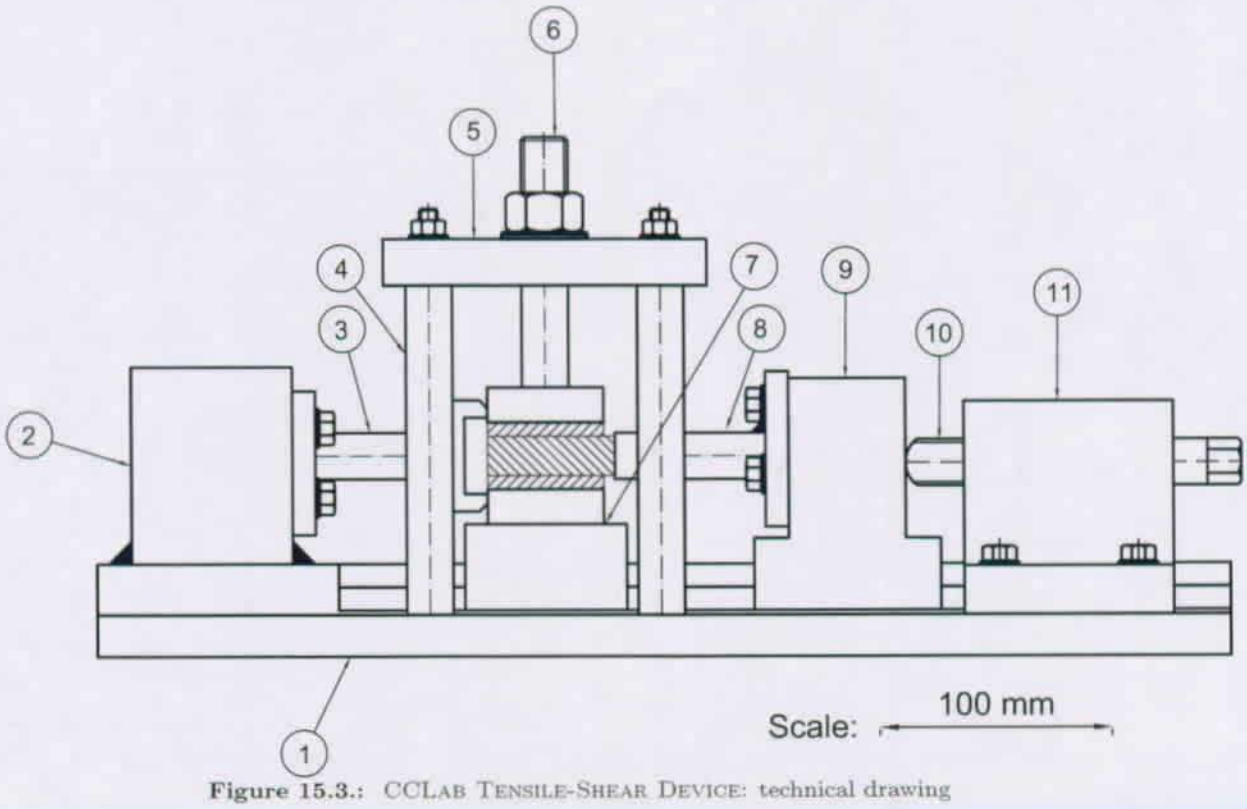

Figure 15.3.: CCLab Tensile-Shear Device: technical drawing

Two main load mechanisms coexist:

❶ The tensile loading mechanism consisting of 4 columns ④ supporting a steel plate ⑤. The load is introduced through a bolt ⑥, this bolt has a pitch of bolt of 1.5 mm;

❷ The shear loading mechanism consist of a horizontal bolt pushing the FRP (elements ⑧ to ⑩[4]) to induce shear.

Both mechanisms can be easily understood looking at the descriptive schemes:

① The tensile or out-of-plane stresses are applied by acting on the bolt ontop the upper steel support: Pos. ⑥ in Fig. 15.3.
The load is applied by turning the bolt using an appropriate wrench. The suggested loading rate can only be defined by an angular speed: experience showed that a full twist per 20...30 seconds is a good choice. This corresponds to a displacement controlled loading rate of around $4.5...3.0\,\frac{mm}{min}$.
Refer to Appendix F for more details.

② The shear stresses are applied by acting on the bolt at the right of Fig. 15.3: Pos. ⑩.
The load is applied by turning the bolt using an appropriate wrench. The suggested loading rate can only be defined by an angular speed: experience showed that a full twist per 20...30 seconds is a good choice. This corresponds to a displacement controlled loading rate of around $4.5...3.0\,\frac{mm}{min}$.
Refer to Appendix F for more details.

Both can be run simultaneously.

All experiments are carried out on rectangular FRP-samples. To investigate scale effects, two different sizes of samples were experimentally investigated: $40 \times 40\ mm^2$ and $50 \times 50\ mm^2$.
The samples are bonded to supports made of steel (see Figs. 15.2 and 15.4.).

The instrumentation consists of four strain gauges adherend in the mid-height of the round bars ③, ④ and ⑧, two of them in the axis of the bar, two at 90° to it. This combination of strain gauges gives a full WHEATSTONE-Bridge[5] that can be considered as being very precise.

The whole system was calibrated, the Calibration-Report is available at the CCLab [82].

[4]HAving also a pitch of bolt of 1.5 mm.
[5]Immune against influences of temperature.

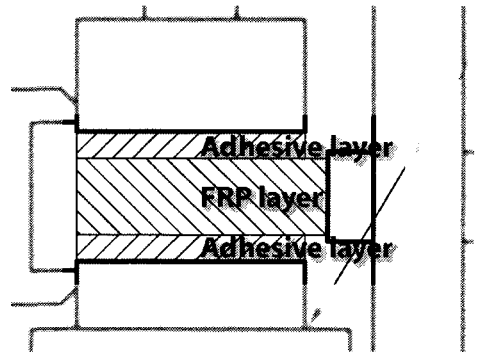

Figure 15.4.: CCLAB TENSILE-SHEAR DEVICE: FRP/steel supports detail

15.4. EXPECTED PERFORMANCE

The CCLAB TENSILE-SHEAR DEVICE measures the forces applied to the specimen[6]. The corresponding tensile and shear stresses have to be deduced from appropriate models.

To evaluate the to be expected performance using the CCLAB TENSILE-SHEAR DEVICE, FE calculations were performed before the final design.
The device was modeled using 2d elements[7]. All the materials were modeled using their given or measured mechanical properties.
The aim of these calculations was to estimate the shape of the obtained out-of-plane and shear curve over the length of the splice when the corresponding force was applied for two different adhesive types: the SIKADUR 330 and SIKAFORCE 7851.

The properties of the materials involved can be found in previous Chapters:

① For steel:
E = 210 000 MPa;

② For the SIKADUR 330 :
see Appendix C;

③ For the SIKAFORCE 7851 :
see Appendix C;

④ For the FRP:
see Appendix B and Section 16.3.2.

[6]Forces are measured because the steel bars ③, ④ and ⑧ have been calibrated and act as force dynamometers.
[7]A 3d calculation showed that a simpler 2d analysis delivers sufficiently accurate results.

It must be highlighted at this point that the following calculations were performed to judge only the quality of the out-of-plane and shear stress fields obtained by the corresponding loadings for two different adhesives.
The real load level as well as the real level of the resulting stresses do not have any importance at this point.

15.4.1. Epoxy bonded

Because of the purely linear behaviour of all involved materials (steel, epoxy and FRP) a linear calculation was performed.

Tensile loading

When applying an uplift on the specimen, a more or less uniform tensile stress distribution is obtained. This can be seen in Figure 15.5.
This means that the stress field generated by uplifting the top of the FRP-sample can be considered as being very well shaped.

Shear loading

When applying a horizontal displacement on the specimen, the out-of-plane stress distribution diaplayed in Figure 15.6 is obtained. This distribution is far away from being constant. There is also the fact that the shear loading is always associated with a corresponding non negligible out-of-plane stress state.
All this means that the shear stress field generated by pushing the FRP-sample cannot be considered as being well shaped.

15.4.2. Polyurethane bonded

Tensile loading

When applying an uplift on the specimen, a more or less uniform tensile stress distribution is obtained. This can be seen in Figure 15.7.
This means that the stress field generated by uplifting the top of the FRP-sample can be considered as being very well shaped.

Shear loading

When applying a horizontal displacement on the specimen, a close-to-uniform out-of-plane stress distribution is obtained. This can be seen in Figure 15.8.

This means that the shear stress field generated by pushing the FRP-sample can be considered as being well shaped. As a result, experimental investigations made using the much softer Polyurethane will be easier to interpretate.

For the Polyurethane bonded specimens, the two stress states (out-of-plane and shear) are totally separated so that the further interpretation will be much easier.

15.5. Conclusions

- **The Author designed a device to experimentally gather important mechanical parameters of the basic FRP material. The device is easy to use and independent of any other device;**
- **No similar device was found by the Author in the available Literature;**
- **Best results are expected to be obtained when the FRP samples are sticked using SikaForce 7851.**

(a) Deformations

(b) Stresses

Figure 15.5.: FEA for epoxy bonded specimen with a given out-of-plane displacement of 1 mm

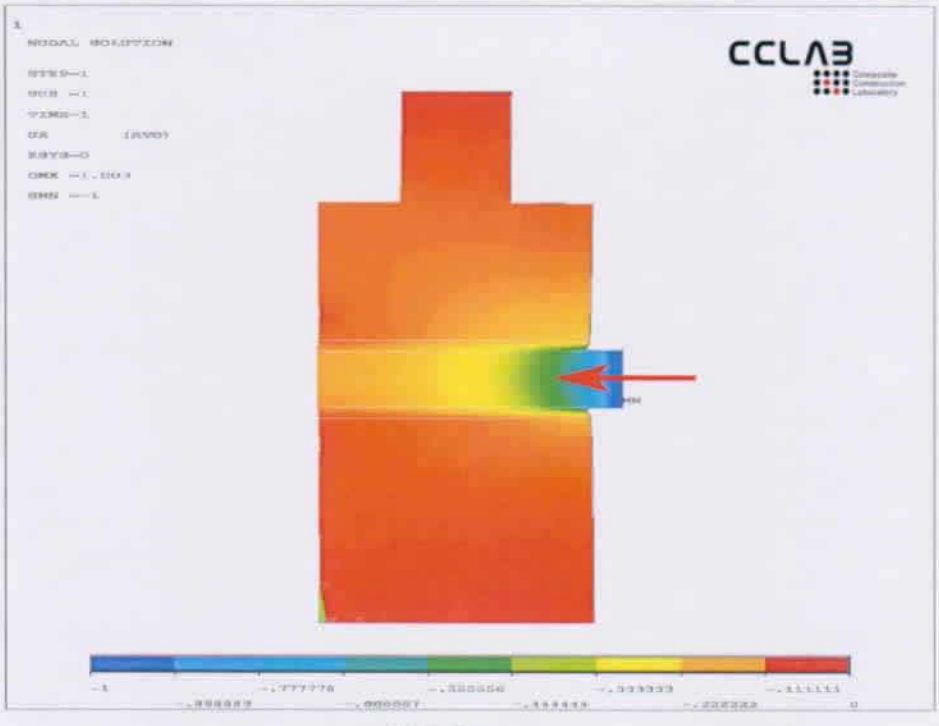

(a) Deformations

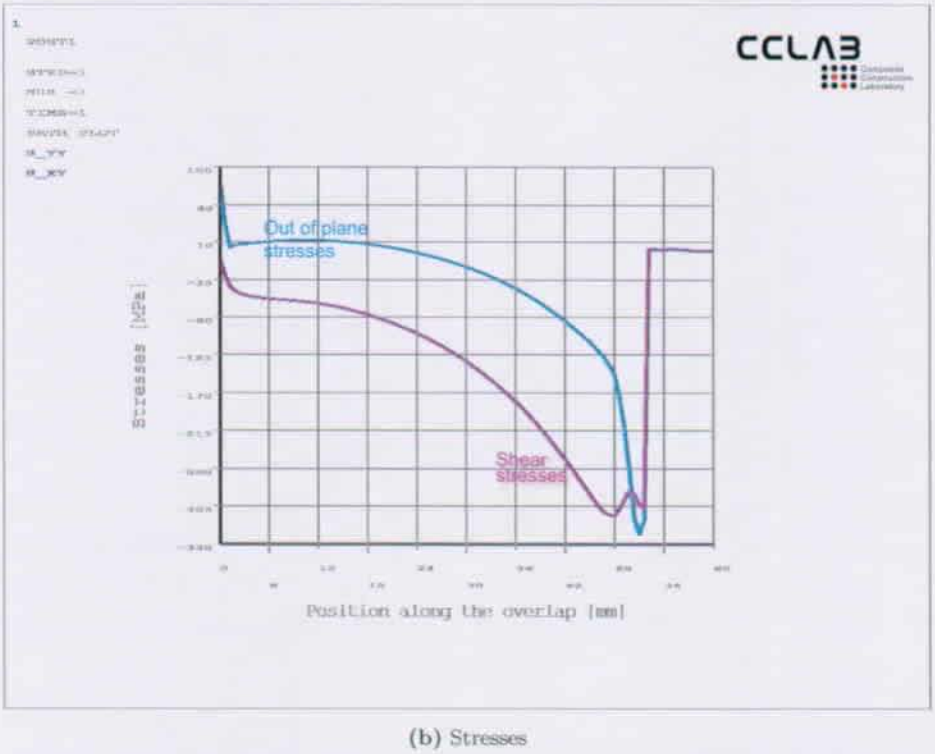

(b) Stresses

Figure 15.6.: FEA for epoxy bonded specimen with a given shear displacement of 1 mm

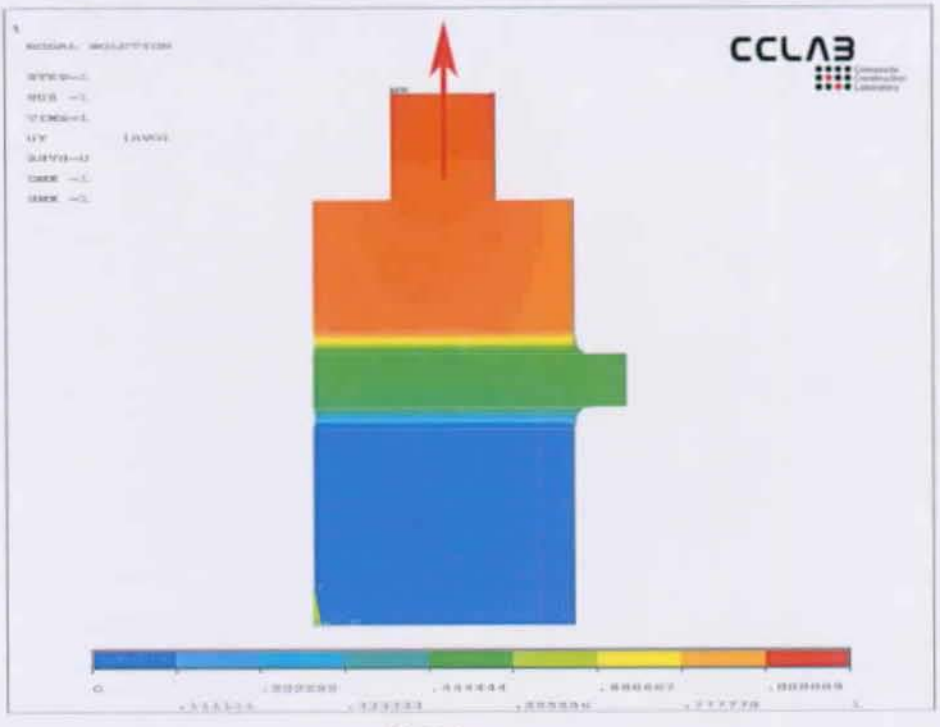

(a) Deformations

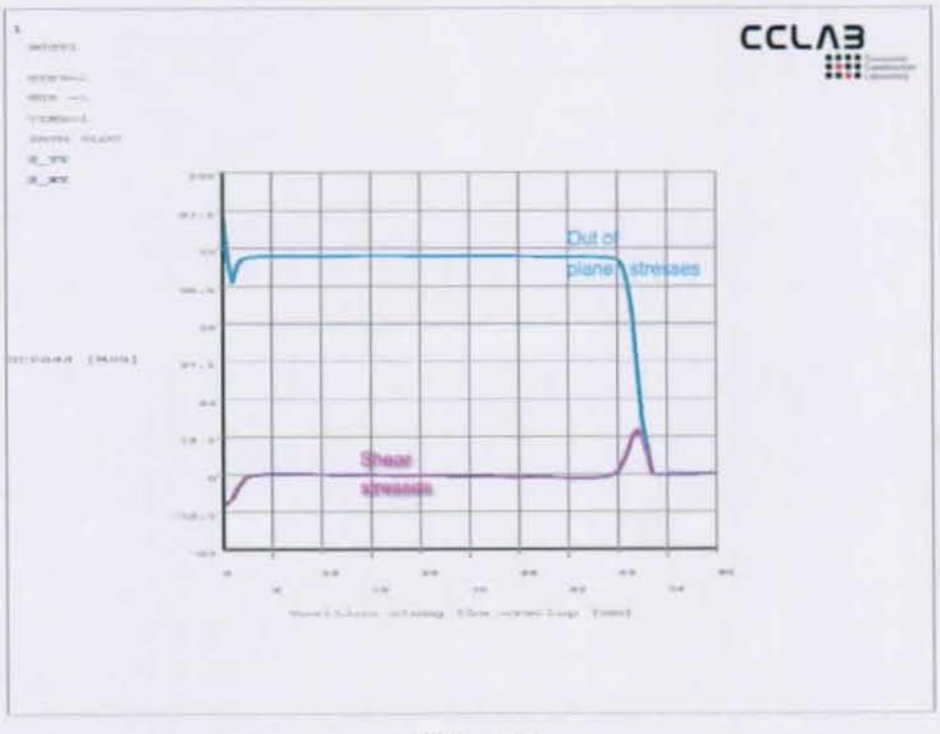

(b) Stresses

Figure 15.7.: FEA for polyurethane bonded specimen with a given out-of-plane displacement of 1 mm

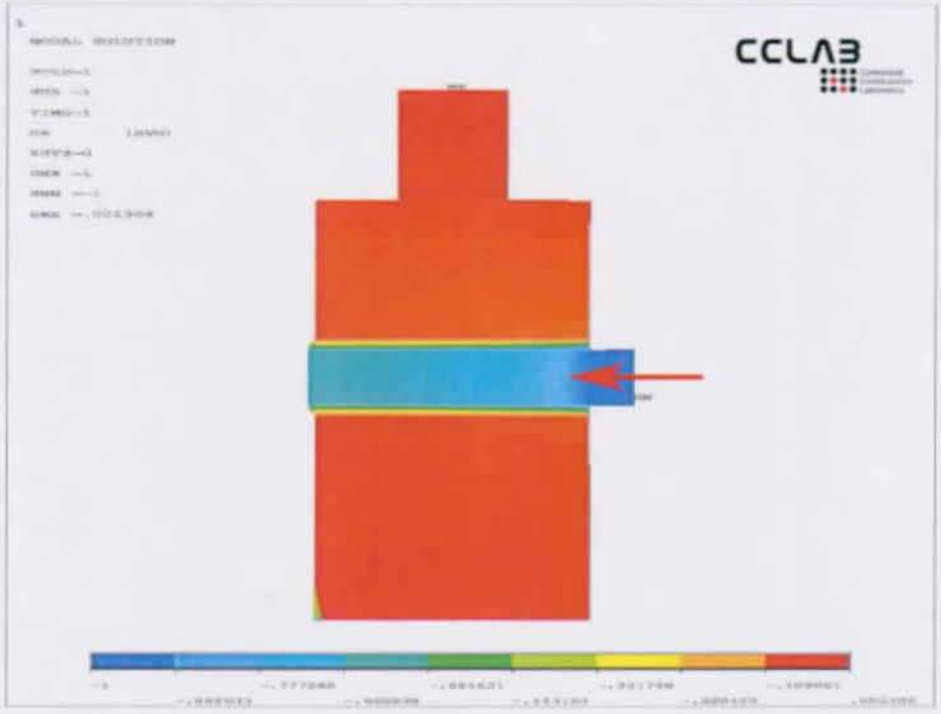

(a) Deformations

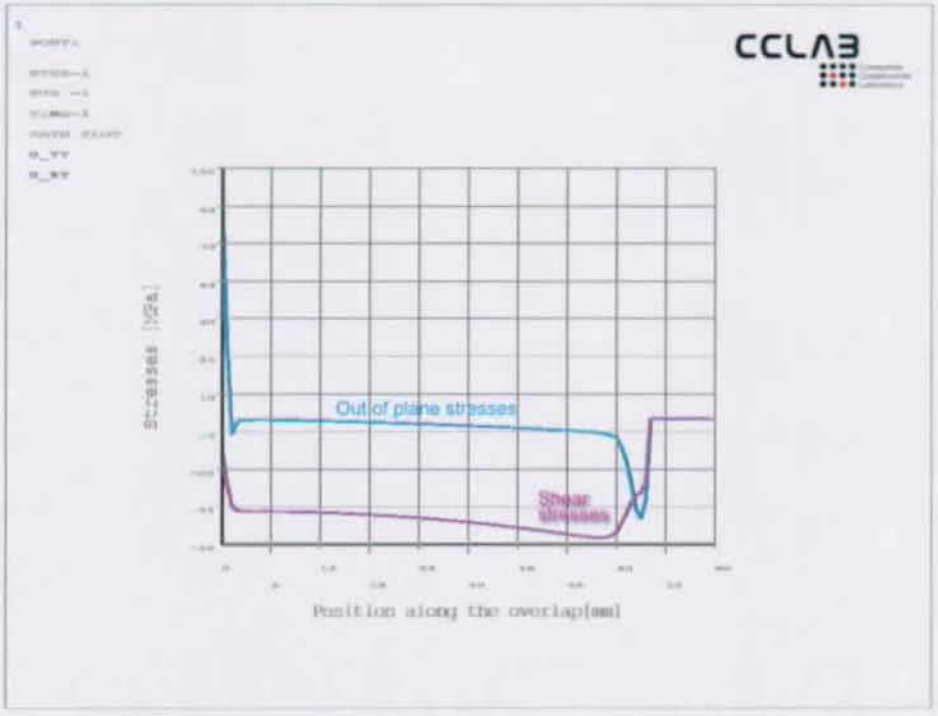

(b) Stresses

Figure 15.8.: FEA for polyurethane bonded specimen with a given shear displacement of 1 mm

16. Experimental investigations to determine E_z of the FRP and to benchmark the Device

16.1. Objectives

Among the parameters needed for the numerical model, the out-of-plane Modulus of elasticity had to be determined.

While the determination of the axial Modulus of elasticity is a relatively easy process partly ruled by codes, standards or recommendations, **gathering the out-of-plane E-Modulus** required the design of an unique experimental setup described in this Chapter.

Besides this main motivation, a second one was to compare two experimental setups to benchmark the first one.

① Using the CCLab Tensile-Shear Device, see Fig. 15.1 and Chapter 15

② Using a second method — to have a reference in terms of benchmarking — based on existent experimental hardware: a W+B 200 kN machine, see Fig. 16.1.

Both experimental setups will be described in this Chapter.

Figure 16.1.: The W+B device

16.1.1. Alternatives

A totally different approach than that selected in the frame of this research — the direct mechanical way — was selected by A. A. El Damatty & M. Abushagur in [60]. The whole test-setup described in the paper is more focused on gathering information on the in-plane and out-of-plane stresses and deformations. Both could, of course, be quickly connected together to formulate stiffnesses like the out-of-plane Modulus of elasticity. But because the whole method is based on supplemental assumptions — like an analytical description of the relatively complex system — restricting the analysis and prohibiting to take into account effects like the interaction between shear and out-of-plane stresses the Author considers this approach to be *inferior* to a direct method.

Figure 16.2.: The steel supports where the FRP squares are sticked to

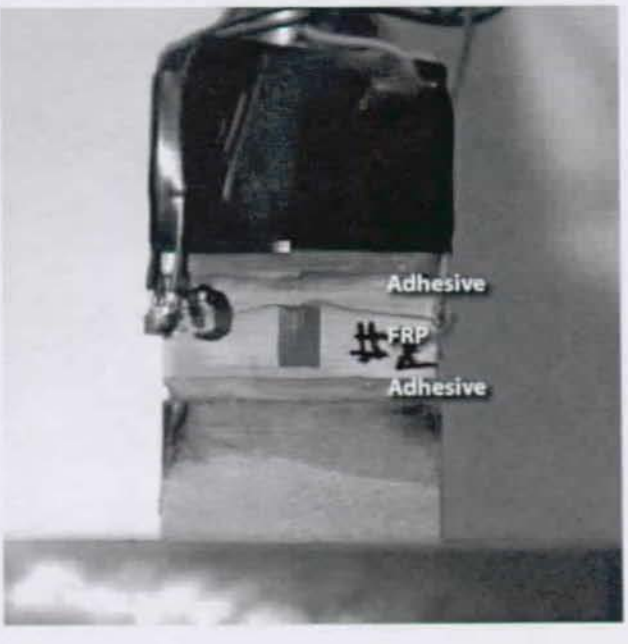

Figure 16.3.: The steel supports where the FRP squares are sticked to (zoomed on the sticked strain gauge)

16.2. Experimental setup

16.2.1. Specimen

The experimental setup is fully described by Fig. 16.2 and Fig. 16.3 in combination with Chapter 15.

The out-of-plane Modulus of elasticity was determined on 30 mm×30 mm square 10 mm thick FRP specimens. The specimen were cut out in the CCLab experimental facilities from larger 500 mm ×100 mm flat profiles already described in Chapter 11 and supplied by Fiberline.

The cut FRP squares were sticked on steel support. To measure the axial extensions in the FRP, strain gauges were sticked on all four sides (see Fig. 16.3) so that effects of load eccentricity are completely compensated. *1,5/120LY18* strain gauges manufactured by HBM[1] were used.

The FRP squares where sticked to the supports using the SikaDur 330 epoxy adhesive supplied by Sika and described in Appendix C. The SikaDur 330 was selected because it has been shown in Chapter 15 that for pure out-of-plane loading the epoxy produces an almost constant stress field.

Prior to bonding, the surfaces of the steel support were degreased and sanded (*sanding grade* $SA2\frac{1}{2}$) to enhance the adhesion between the FRP and the adhesive while those of the FRP were abraded as described in Section 10.2.2.
The adhesive had 5 days to fully cure.

16.2.2. Load mechanism

As stated before, two different systems were used:

① The CCLab Tensile-Shear Device described in Fig. 15.1;

② The W+B 200 kN machine, described in Fig. 16.1.
The device had to be slightly modified to fix the steel supports described in Fig. 16.2.

[1] Hottinger Baldwin Messtechnik GmbH

16.3. Experimental results

16.3.1. CCLab Tensile-Shear Experimental Device

Experimental program

The device is run manually, the following was measured:

① The total load acting on the FRP sample;

② The extension as given by the 4 strain gauges sticked on the FRP sample.

The displacement could not be measured.

The loading rate cannot be selected but is a function of the possibilities given by the apparatus[2], it was selected around one twist per 20...30 seconds.

Five individual tension experiments were carried out. For two of the five specimens, compression experiments were also carried out before the experiments in tension.
Table 16.1 gives an overview over the experiments carried out with the CCLab Tensile-Shear Device.

Spec.	01	02	03	04	05
Tension	T1	T2	T3	T4	T5
Compr.	C1	C2	-	-	-
$\sigma_{z,u}$ **MPa**	5.2	1.7	6.3	10.1	9.4

Table 16.1.: Overview over the experiments carried out with the CCLab Tensile-Shear Experimental Device

The Author is aware that the scattering in the results is relatively high. Expressed in terms of variance[3] it is of around 52 %. This scattering is reduced to 31 % when not considering T2.
Considering that the specimen T1 and T2, which have been compressed before being tested under tension may have been damaged, and taking only the specimen T3, T4 and T5, a scattering of *only* 24 % is obtained.

Results

The failure always occurred inside the FRP and never at the steel-adhesive or adhesive-FRP interface (see Fig. 16.4). The ultimate stresses obtained are given in Table 16.1. Because the objective of this experimental program was not the gathering of ultimate stresses, no further interpretation will be made on this topic.

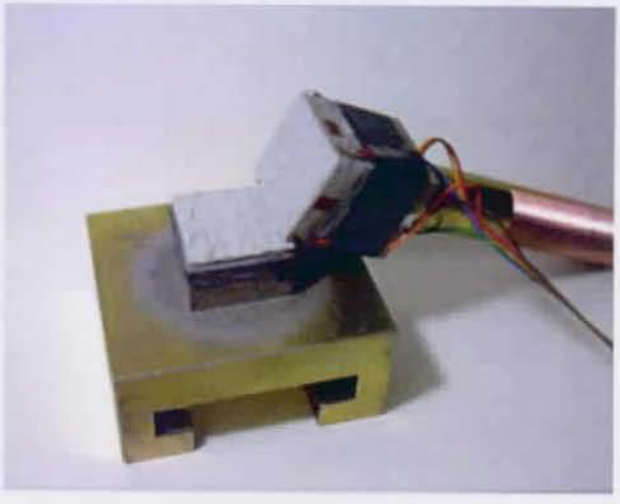

Figure 16.4.: Failure never occurred on the adhesive-steel or adhesive-FRP layer

The experimentally gathered out-of-plane extensions ε_z in tension or compression are plotted against the corresponding out-of-plane stress σ_z in Fig. 16.5.

It was selected to calculate the secant modulo according to:

$$E_i = \frac{\sigma_{z,i}}{\varepsilon_{z,i}} \tag{16.1}$$

With i indicating if it is **t**ension or **c**ompression.

The out-of-plane modulus of elasticity calculated in tension $E_{z,t}$ or compression $E_{z,c}$ are plotted against the out-of-plane stress σ_z in Fig. 16.7 [4]

Main results

① The measured out-of-plane secant modulus of elasticity in tension $E_{z,t}$ tends to 3 500 MPa;

② The out-of-plane secant modulus of elasticity in tension $E_{z,t}$ tends to decay at higher tensile stresses σ_z;

③ The measured out-of-plane secant Modulus of elasticity in compression $E_{z,c}$ is higher than $E_{z,t}$ and ranges around a value of 5 000 MPa;

④ The experimentally gathered ultimate out-of-plane stresses $\sigma_{z,u}$ averaged at 6.5 ± 3.4 MPa;

⑤ The sample size of 30 mm × 30 mm used might be too small to avoid problems with specimen tilting or other disturbing effects so that the scattering in the result is very high.

[2] Refer to Appendix F for more details concerning this topic.
[3] Standard deviation related to the mean.
[4] The corresponding load-extension curve is plotted in Fig. 16.5.

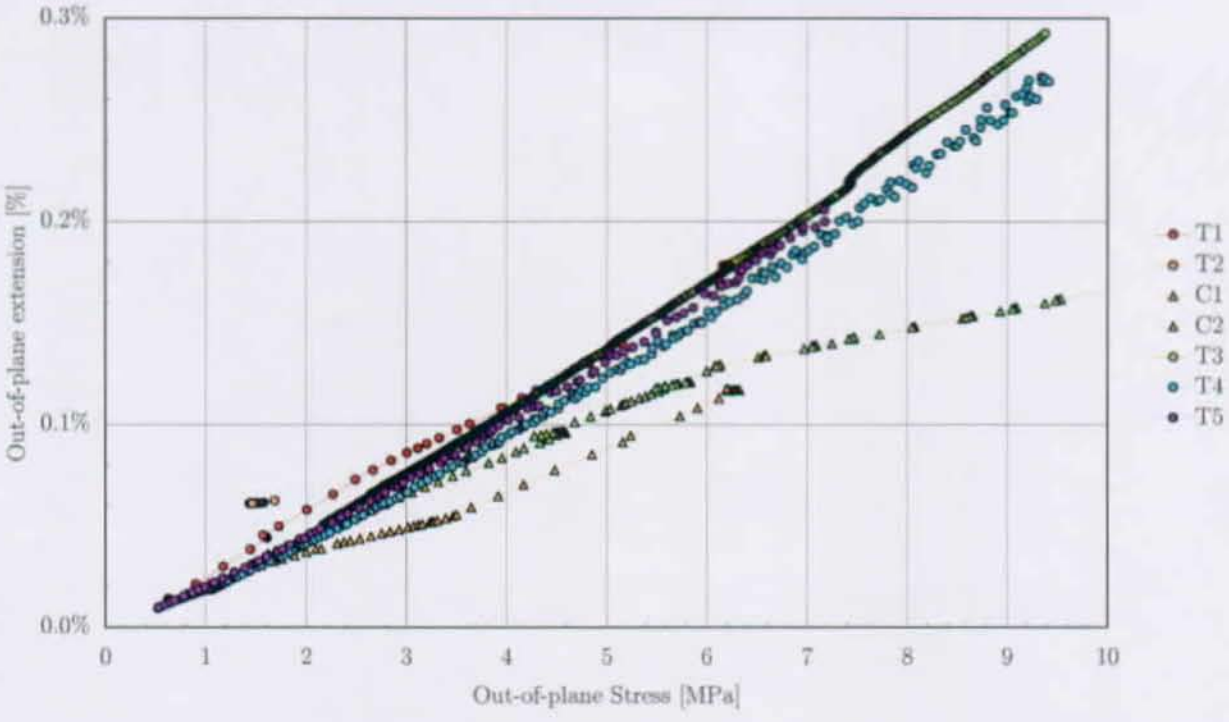

Figure 16.5.: ε_z vs. σ_z as gathered using the CCLab Tensile-Shear Experimental Device

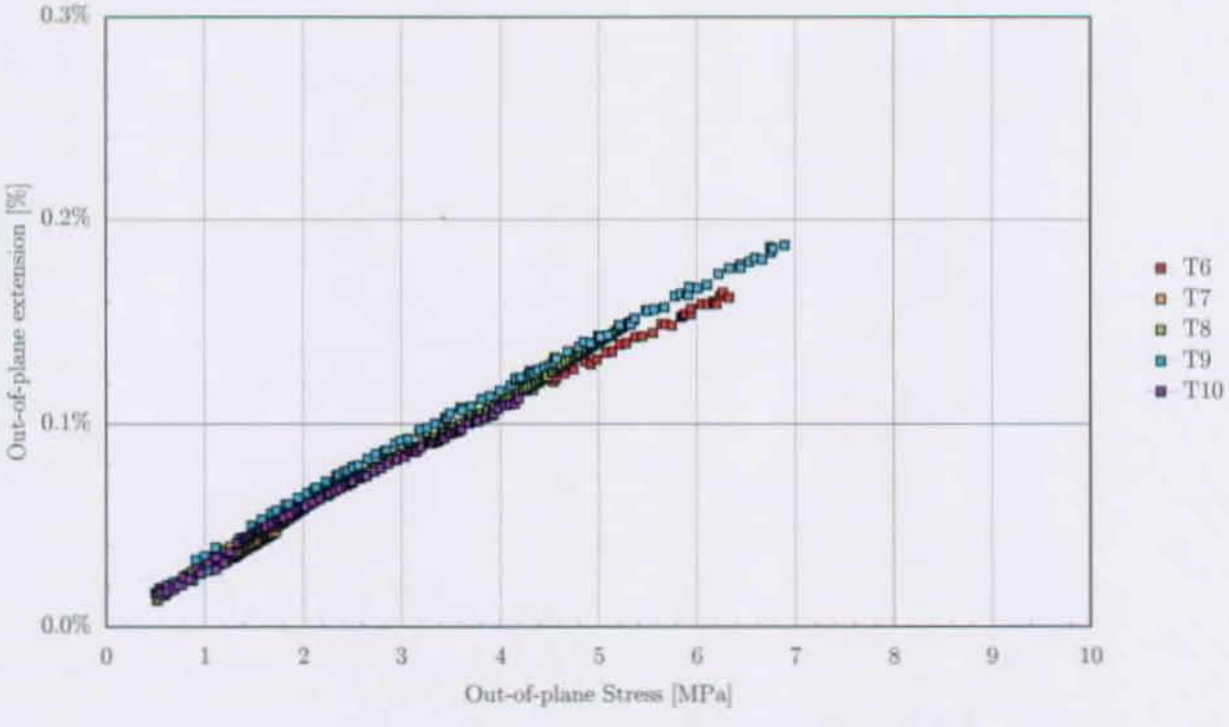

Figure 16.6.: ε_z vs. σ_z as gathered using the W+B device

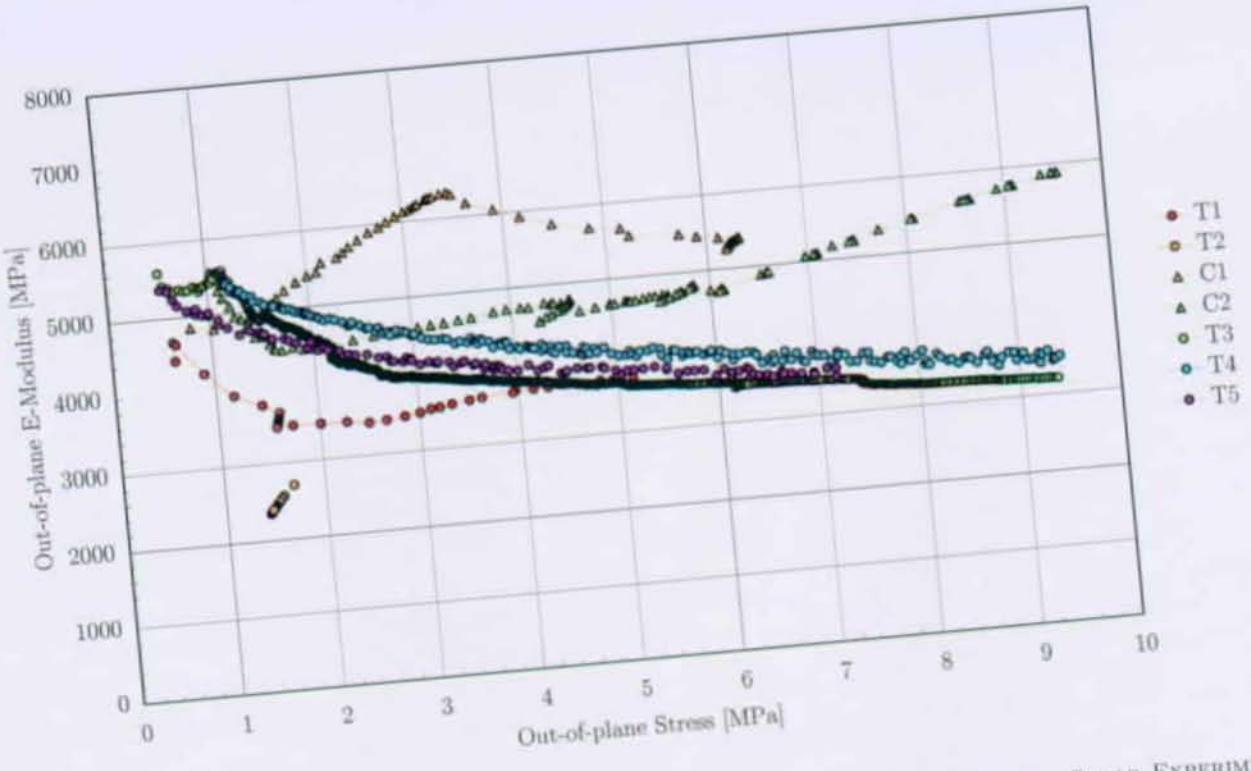

Figure 16.7.: E_z vs. σ_z as calculated using the values gathered by the CCLab Tensile-Shear Experimental Device

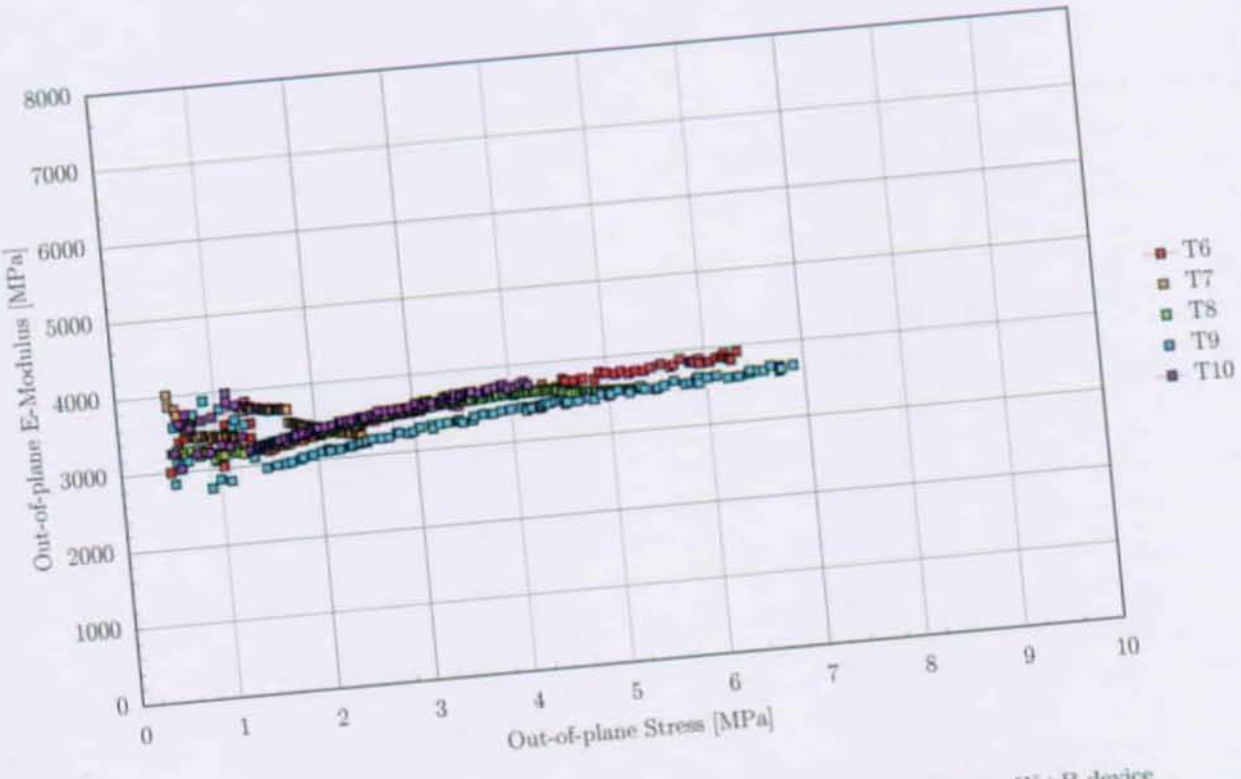

Figure 16.8.: E_z vs. σ_z as calculated using the values gathered by the W+B device

16.3.2. W+B DEVICE

EXPERIMENTAL PROGRAM

The following was measured:

① The total force acting on the FRP sample.

② The extension as given by the 4 strain gauges sticked on the FRP sample.

The machine was run by displacement control. The loading rate was selected to match closely the loading rate with the CCLAB TENSILE-SHEAR EXPERIMENTAL DEVICE[5]: $3\,\frac{mm}{min}$ was selected.

Table 16.2 gives an overview over the experiments carried out with the W+B device. The setup did not allow compression-tests.

Spec.	06	07	08	09	10
Tract.	T6	T7	T8	T9	T10
$\sigma_{z,u}$ **MPa**	6.3	2.5	5.4	6.91	4.2

Table 16.2.: Overview over the experiments carried out with the W+B device

The Author is aware that the scattering in the results is relatively high. Expressed in terms of variance[6], it is of around 35 %.

The measured out-of-plane tangential Modulus of elasticity in tension E_z are plotted against the out-of-plane stress σ_z in Fig. 16.8 [7]

MAIN RESULTS

① The measured out-of-plane secant Modulus of elasticity in tension $E_{z,t}$ tends to a value of 3 500 MPa;

② The measured out-of-plane secant Modulus of elasticity in tension $E_{z,t}$ tends to increase slightly at higher loads;

③ The measured out-of-plane secant Modulus of elasticity in tension $E_{z,t}$ as measured by the W+B device tend to the same value that the one measured by the CCLAB TENSILE-SHEAR EXPERIMENTAL DEVICE;

④ The experimental gathered ultimate out-of-plane stresses $\sigma_{z,u}$ averaged at 5.1 ± 1.8 MPa.

16.4. CONCLUSIONS

- **Both experimental devices deliver a measured out-of-plane secant Modulus of elasticity in tension of $\mathbf{E_{z,t} \approx 3\,500}$ MPa for higher tensile stresses σ_z;**
- **The experimentally gathered ultimate out-of-plane stresses $\sigma_{z,u}$ are basically comparable in their magnitude;**
- **The agreement in the experimentally gathered out-of-plane elastic modules in tension $E_{z,t}$ and the ultimate out-of-plane stresses $\sigma_{z,u}$ allow the assertion that the CCLab Tensile-Shear Device has been benchmarked;**
- **The measured out-of-plane secant Modulus of elasticity in compression is $\mathbf{E_{z,c} \approx 5\,000}$ MPa.**

[5] Refer to Appendix F for more details concerning this topic.
[6] Standard deviation related to the mean.
[7] The corresponding load-extension curve is plotted in Fig. 16.6.

17. Experimental determination of the FRP failure criterion

17.1. Objectives

Because former investigations showed that the joint failure is triggered by the failure of the involved FRP flat profiles (see Part III), it is necessary to get reliable data to describe the material strength.

The objective of the experimental investigations presented here is the

- **determination of the FRP failure criterion under any given combination of both the out-of-plane stress, σ_z and the shear stress, τ_{zt}.**

17.2. Experimental setup

All the experimental investigations described in this Chapter have been carried out using the CCLab Tensile-Shear Experimental Device described in Chapter 15.

At this point, only those elements of the device having a direct relation with the topic of this chapter will be eventually described again.

17.2.1. Geometric specifications

The experimental investigations were carried out on FRP-samples cut out of the same basic pultruded material used for manufacturing the specimens described in Chapters 11, 12 and 13.

Three different specimen sizes were specified:

① **Medium** $40 \times 40\ mm^2$;

② **Large** $50 \times 50\ mm^2$.

The investigations were carried out on the two material types defined by their thickness used in the experimental investigations described in the Chapters 11, 12 and 13:

① 5 mm

② 10 mm

Indications on the associated fiber architecture are given in Section 9.2.2.

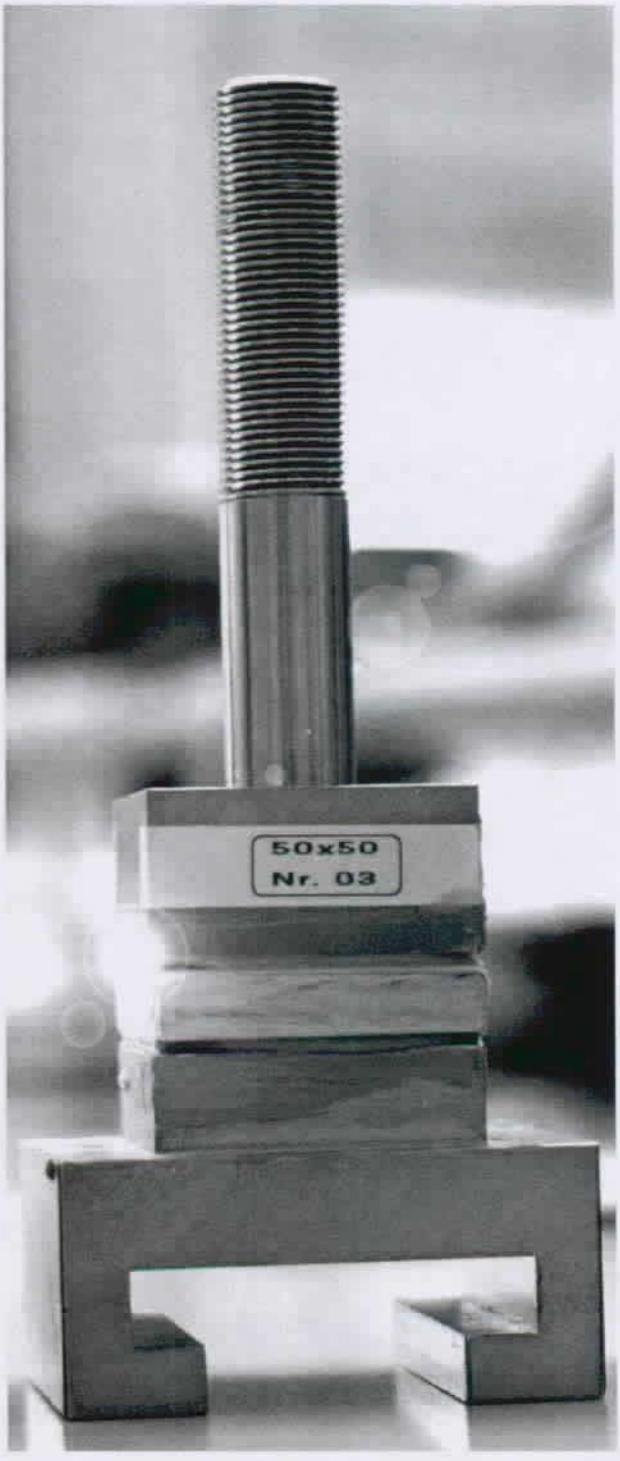

Figure 17.1.: A $50 \times 50\ mm^2$ sample ready to be tested

17.2.2. Surface preparation

The experimental investigations showed that failure was always triggered by the delamination of the pultruded elements and never by the failure of the adhesive.

Care had to be taken that the connection between the adhesive and the steel supports (see Fig. 17.1) was as well as possible — at least as well as the connection between the adhesive and the FRP elements. The desired effect was to get a failure inside the pultruded material as shown in Figs. 17.2, 17.3 and 17.7. To ensure that, the following was done:

① Sanding according to $SA2\frac{1}{2}$ the surfaces of the steel supports intended to be bonded;

② Applying the same surface treatment to the square FRP samples as the one applied to the FRP flat profiles in all the lap joint experiments (see Section 10.2.2).

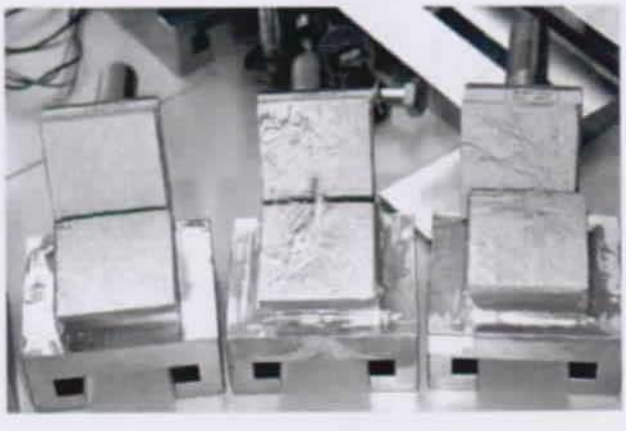

Figure 17.2.: $50 \times 50\ mm^2$ epoxy bonded specimens after failure: pure out-of-plane tests

Figure 17.3.: A $40 \times 40\ mm^2$ epoxy bonded specimens after failure: pure out-of-plane tests

Figure 17.4.: Grooves driven in the supports to increase the friction between adhesive and steel

17.2.3. FRP material

The specimens previously defined before were cut out in the CCLab experimental facilities from the larger 500 mm × 100 mm flat profiles already described in Chapter 11.

The FRP squares were sticked on the steel supports so that the fibers were oriented in the axis of the shear mechanism. This was done to reflect the conditions inside the adhesively bonded joints.

17.2.4. Adhesives

As stated in Chapter 15, two different adhesives where investigated:

① The SikaDur 330 epoxy;

② The SikaForce 7851 polyurethane.

The adhesive layer thickness was chosen to be 2 mm and was ensured by placing the same glass beads as described in section 10.2.2.

The mechanical properties of the adhesives are described in Appendix C.

EPOXY BONDED SPECIMENS

As shown in Section 15.4, the stress fields corresponding to the epoxy bonded specimens are *well shaped* for the tensile loaded specimens (see Section 15.4.2), but **not at all** well shaped for those subjected to the shear loading.
As a result, only tests involving solely out-of-plane stresses were carried out using the epoxy (see Fig. 17.2 and 17.3).
The shear loading induces such poorly shaped stress fields in the FRP samples (with stress concentrations at the beginning leading to premature failure like shown in Fig. 17.5), that further FEA has to be carried out to extract valid results from these experiments.
The fact that the shear stress field induces also a significant out-of-plane stress field reduces considerably the value of experimental results obtained by epoxy bonded specimens.

POLYURETHANE BONDED SPECIMENS

Because epoxy bonding results in a poorly shaped shear stress field in shear loaded specimens and polyurethane not, it was decided to **carry out the investigations involving shear with only the SikaForce 7851 adhesive.**

Because polyurethane does not stick as well as epoxy on steel surfaces, additional friction had to by creating concentric circular grooves on the surfaces of the steel supports[1], see Fig. 17.4.

17.2.5. EXPERIMENTAL PROCEDURE

The main advantage of the CCLAB TENSILE-SHEAR EXPERIMENTAL DEVICE is the ability to measure both of the tensile strength, $\sigma_{z,u}$ and the shear strength, $\tau_{xz,u}$ under any given combination.

To gather the material strength $\sigma_{z,u}$-$\tau_{xz,u}$-Interaction Diagram, experimental investigations involving both the tensile and the shear loading had to be carried out.
The mechanical description of how tensile and shear loading induced in the specimens is described in Chapter 15.

While the pure tensile — generating the out-of-plane stresses — loading and the pure shear loading mechanisms are obvious[2], the load mechanism for a given combination of shear force $S = S_0$ and a to determine tensile force $H = H_u$ is described by the following procedure:

① Imposing the shear force S_0 by acting on the shear load mechanism (elements ⑧ to ⑩);

② Acting on the tensile mechanism (⑥) by increasing the corresponding force H **while** verifying that the primarily imposed shear load S_0 has not changed. If the shear force drops or increases outside a self-defined range, it should be readjusted;

③ The tensile force H has to be raised up to the failure value H_u.

The CCLAB TENSILE-SHEAR DEVICE allows one to gather the tensile Force H_i and shear force S_j associated to the individual specimen failure.

Because of the well shaped stress fields for both tensile and shear (see Section 15.4.2), the formulæ to calculate the stresses from the forces are the following:

$$\sigma_{z,u} = \frac{H_i}{A} \tag{17.1}$$

$$\tau_{xz,u} = \frac{S_j}{2A} \tag{17.2}$$

with $A = a^2$ and a the dimension of the specimens — 40 mm and 50 mm.

Each time this procedure was run successfully, one point of the $\sigma - \tau$-Interaction diagram has been drawn.

LOAD RATE

The loading rate of the experimental investigations carried out with the CCLAB TENSILE-SHEAR DEVICE is mainly dictated by the possibilities given by the apparatus.
This loading rate lied for both the tensile and shear mechanism around a full twist each 20...30 seconds[3] corresponding to a to a displacement controlled loading rate of around 4.5...3.0 $\frac{mm}{min}$.

[1] Despite the fact that these grooves were driven for the purpose of enhancing the polyurethane bonded specimens, some experiments were also carried out with epoxy: Fig 17.5.

[2] The term pure tensile and pure shear loading are used in the meaning of *only* H, and *only* S respectively, and **not** in combination of both.

[3] More indications are given in Appendix F.

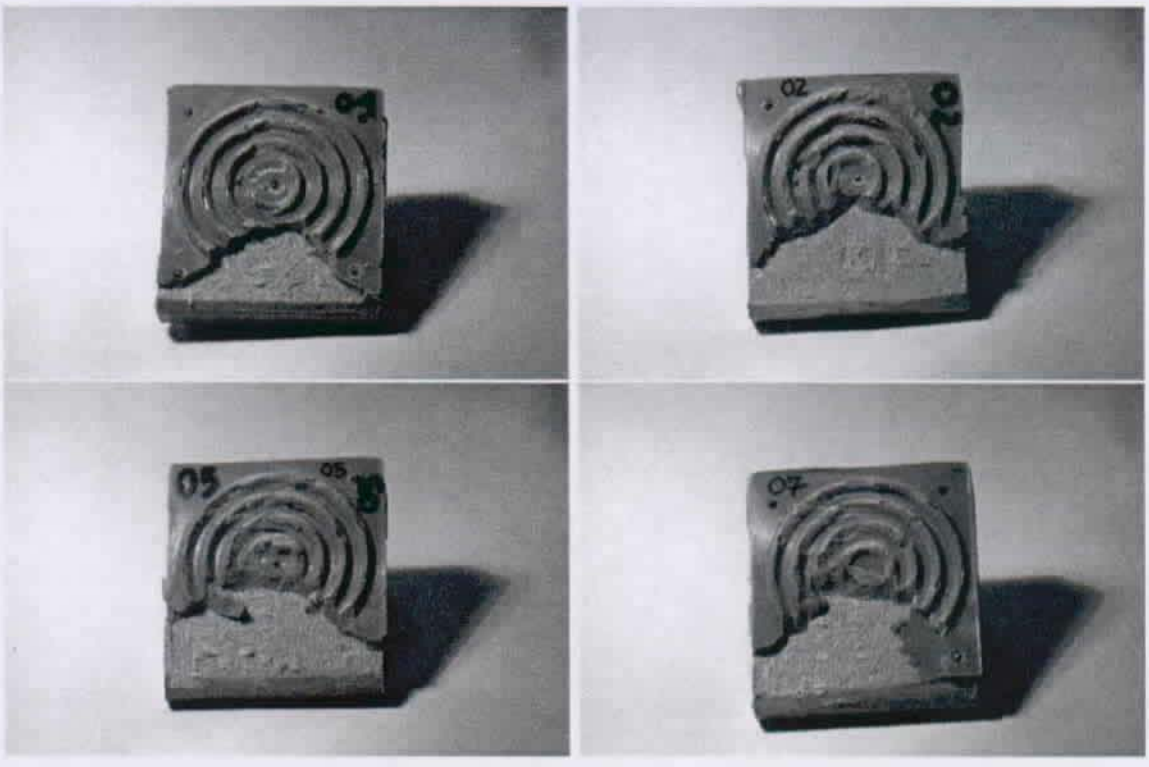

Figure 17.5.: Failure of shear loaded 50 × 50 mm^2 samples bonded with epoxy

17.3. Experimental results

Tables 17.1 to 17.4 list all the specimens tested. For each full series, 55 to 60 single experiments were carried out, which is (by far) more than the 30 recommended for basic FRP material property determination recommened in by A. Zureick & R. Bennet in [72].

17.3.1. Interaction diagrams

The experimental investigations were made on both the 5 mm and the 10 mm FRP material.
The numerical results are shown in both the Tables 17.1 to 17.4 and curves 17.9 to 17.12.

17.3.2. Failure modes

A first important result is the failure mode of the specimens: failure occurs inside the material.

As shown in Fig. 17.7 failure occurs — as in the adhesively bonded joints — at a distance of approximatively 0.5 mm inside the specimens.
Figs. 17.8(a) to (d) also show this for different combinations of out-of-plane and shear stresses.

Selected experimentally investigated specimens were more closely investigated by burning-off the resin to reveal their fiber architecture with the aim to *see* what happened after failure. Fig. 17.6 shows the result of such a burn-off test: above, a FRP square **not tested** with an intact fiber architecture, down the same for a **tested** FRP sample. The difference between the intact and the loaded sample is that the failed one has lost parts of the CSM[4], revealing by that the woven mats and that failure occurs in the layer between the veil and the woven mats.

No substantial differences in the failure pattern were observed for both the 5 mm and 10 mm material.

17.4. Conclusions

Using the self-designed CCLab Tensile-Shear Experimental Device described in Chapter 15, it was possible to quantify the basic FRP material resistance in form of interaction diagrams for shear stresses, $\tau_{xz,u}$ and out-of-plane stresses, $\sigma_{z,u}$ for different material architecture.

Failure occurs — as in the adhesively bonded joints — at a distance of approximatively 0.5 mm inside the specimens.

[4] Refer to Section 9.2.2 for further details concerning the fiber architecture.

Series	Stress	1	2	3	4	5	6	7	8	9	10
A	τ_u [MPa]	18.67	19.96	20.99	19.22	17.10	20.99	17.39	20.22	17.10	20.45
A	σ_u [MPa]	0.00	0.00	0.00	0.00	0.00	0.00	0.00	0.00	0.00	0.00
B	τ_u [MPa]	0.00	0.00	0.00	0.00	0.00	0.00	0.00	0.00	0.00	0.00
B	σ_u [MPa]	9.76	7.55	9.48	8.95	9.38	10.01	7.48	8.33	9.44	9.27
C	τ_u [MPa]	9.65	10.46	9.94	10.33	10.30	10.36	9.92	10.33	10.33	10.32
C	σ_u [MPa]	8.08	5.98	8.73	6.66	8.63	7.87	6.34	7.55	8.44	8.13
D	τ_u [MPa]	14.58	14.76	15.34	15.17	14.71	-	-	-	-	-
D	σ_u [MPa]	6.29	4.98	4.92	5.52	6.05	-	-	-	-	-
E	τ_u [MPa]	11.91	11.93	11.48	11.69	12.49	-	-	-	-	-
E	σ_u [MPa]	6.12	7.30	7.22	7.24	6.42	-	-	-	-	-
F	τ_u [MPa]	4.76	5.23	4.89	5.04	5.06	-	-	-	-	-
F	σ_u [MPa]	8.44	9.04	9.29	7.92	8.24	-	-	-	-	-
G	τ_u [MPa]	18.41	18.84	17.72	17.17	18.30	17.24	18.66	18.55	18.02	18.31
G	σ_u [MPa]	2.59	2.73	4.68	4.85	3.56	4.51	3.70	3.42	3.18	3.34

Table 17.1.: Listing of all 40×40-5 mm tested specimens

Series	Stress	1	2	3	4	5	6	7	8	9	10
A	τ_u [MPa]	17.14	21.71	22.05	20.83	19.89	20.27	21.59	21.62	18.75	20.20
A	σ_u [MPa]	0.00	0.00	0.00	0.00	0.00	0.00	0.00	0.00	0.00	0.00
B	τ_u [MPa]	0.00	0.00	0.00	0.00	0.00	0.00	0.00	0.00	0.00	0.00
B	σ_u [MPa]	8.20	7.90	8.19	8.59	9.00	7.22	7.00	8.12	8.42	8.04
C	τ_u [MPa]	10.11	10.11	9.78	10.18	10.34	-	-	-	-	-
C	σ_u [MPa]	5.84	6.66	7.92	5.81	6.37	-	-	-	-	-
D	τ_u [MPa]	14.35	14.72	14.49	14.26	14.45	15.42	15.02	15.55	15.46	14.90
D	σ_u [MPa]	6.06	6.32	5.33	6.55	5.58	4.77	4.36	4.50	5.72	5.38
E	τ_u [MPa]	12.43	12.40	11.99	12.25	12.55	11.66	12.10	12.00	11.76	12.10
E	σ_u [MPa]	7.46	5.53	7.16	6.64	5.15	6.55	7.14	6.54	5.59	6.33
F	τ_u [MPa]	4.85	4.81	5.13	5.13	5.08	-	-	-	-	-
F	σ_u [MPa]	8.08	8.38	7.61	9.14	7.86	-	-	-	-	-
G	τ_u [MPa]	18.06	17.18	17.97	18.54	18.07	-	-	-	-	-
G	σ_u [MPa]	4.12	3.77	3.42	2.93	4.10	-	-	-	-	-

Table 17.2.: Listing of all 40×40-10 mm tested specimens

Series	Stress	1	2	3	4	5	6	7	8	9	10
A	τ_u [MPa]	23.46	19.96	22.08	22.54	23.43	21.59	22.15	19.92	22.19	21.77
A	σ_u [MPa]	0.00	0.00	0.00	0.00	0.00	0.00	0.00	0.00	0.00	0.00
B	τ_u [MPa]	0.00	0.00	0.00	0.00	0.00	0.00	0.00	0.00	0.00	0.00
B	σ_u [MPa]	10.08	7.99	9.76	9.28	8.03	10.05	8.93	7.72	10.00	8.96
C	τ_u [MPa]	7.86	8.29	8.09	7.89	8.03	7.75	7.61	7.93	8.03	7.94
C	σ_u [MPa]	8.80	9.81	7.43	8.28	7.37	9.05	10.08	9.98	7.64	8.61
D	τ_u [MPa]	11.95	12.14	11.85	12.28	11.87	12.56	11.50	12.54	12.53	12.11
D	σ_u [MPa]	9.08	6.51	7.23	8.53	8.38	8.30	9.12	6.65	9.05	8.04
E	τ_u [MPa]	14.69	15.11	14.64	14.89	15.63	15.46	15.11	14.74	14.25	14.96
E	σ_u [MPa]	7.24	7.49	7.17	5.42	6.70	7.49	8.06	7.50	6.00	7.05
F	τ_u [MPa]	5.23	5.00	4.98	4.95	4.94	-	-	-	-	-
F	σ_u [MPa]	10.00	8.24	10.05	7.29	10.17	-	-	-	-	-
G	τ_u [MPa]	18.00	18.78	17.63	17.71	18.27	-	-	-	-	-
G	σ_u [MPa]	5.60	5.09	6.65	6.51	6.06	-	-	-	-	-

Table 17.3.: Listing of all 50×50-5 mm tested specimens

Series	Stress	1	2	3	4	5	6	7	8	9	10
A	τ_u [MPa]	17.60	16.44	15.31	21.66	18.40	19.79	20.22	22.15	17.98	19.74
A	σ_u [MPa]	0.00	0.00	0.00	0.00	0.00	0.00	0.00	0.00	0.00	0.00
B	τ_u [MPa]	0.00	0.00	0.00	0.00	0.00	0.00	0.00	0.00	0.00	0.00
B	σ_u [MPa]	8.94	9.10	7.38	8.01	7.10	7.87	7.22	8.89	7.02	7.98
C	τ_u [MPa]	17.94	18.15	17.58	17.72	17.41	17.21	17.64	17.86	17.80	17.64
C	σ_u [MPa]	4.16	2.74	4.37	4.04	3.47	4.21	4.47	3.48	2.82	3.73
D	τ_u [MPa]	14.40	15.27	14.65	14.55	14.38	14.74	15.24	14.34	15.51	14.76
D	σ_u [MPa]	5.18	4.20	5.55	5.48	6.61	5.46	5.39	4.35	4.37	5.32
E	τ_u [MPa]	11.98	12.24	11.53	12.43	11.87	12.48	12.19	12.60	12.33	12.11
E	σ_u [MPa]	5.71	6.04	5.33	5.44	5.59	6.06	6.30	6.05	5.87	5.95
F	τ_u [MPa]	4.87	4.97	4.95	5.10	4.87	-	-	-	-	-
F	σ_u [MPa]	7.37	7.54	6.91	8.63	8.78	-	-	-	-	-
G	τ_u [MPa]	7.83	7.69	8.39	7.98	7.78	-	-	-	-	-
G	σ_u [MPa]	6.69	6.62	8.24	6.22	8.43	-	-	-	-	-

Table 17.4.: Listing of all 50×50-10 mm tested specimens

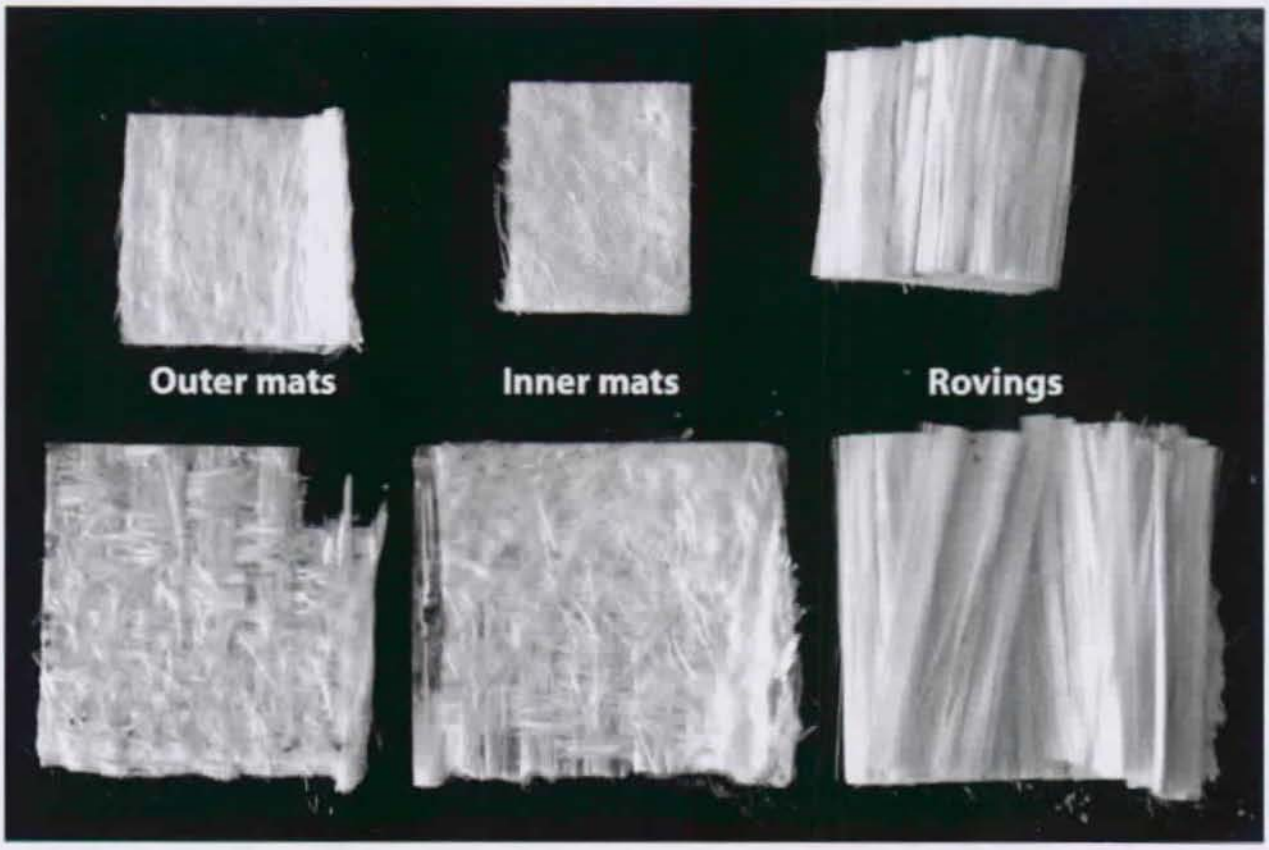

Figure 17.6.: Burn-off of not-tested and tested specimens

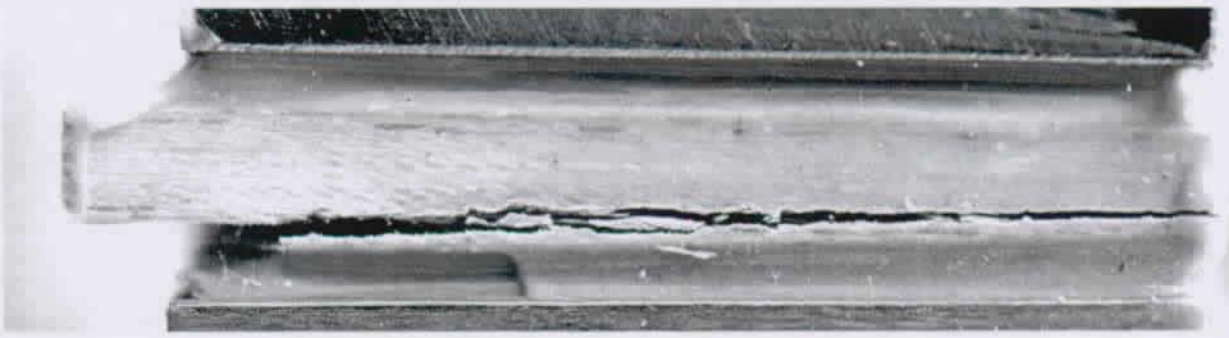

(a) B3

(b) C4

Figure 17.7.: Visible cracks in 10 mm thick 50 × 50 specimens after failure

(a) C1: Shear dominated failure ($\frac{\tau_{ik}}{\sigma_{\perp}} = \frac{17.94}{4.16}$)

(b) C3: Shear dominated failure ($\frac{\tau_{ik}}{\sigma_{\perp}} = \frac{17.58}{4.37}$)

(c) G2: Mixed out-of-plane/shear stress failure ($\frac{\tau_{ik}}{\sigma_{\perp}} = \frac{7.69}{6.62} =$

(d) G5: Mixed out-of-plane/shear stress failure ($\frac{\tau_{ik}}{\sigma_{\perp}} = \frac{7.75}{8.43}$)

Figure 17.8.: PU bonded 10 mm thick 50 × 50 after failure

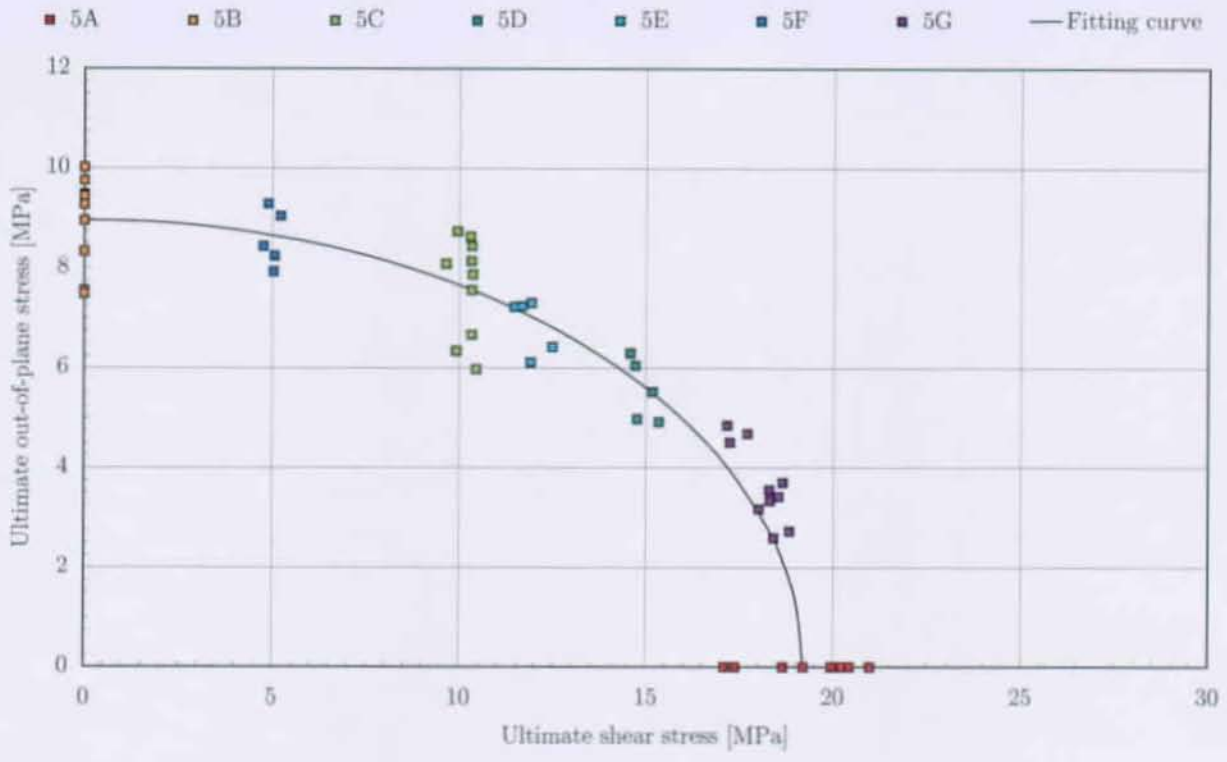

Figure 17.9.: Interaction diagram for the 5 mm thick 40 × 40 samples

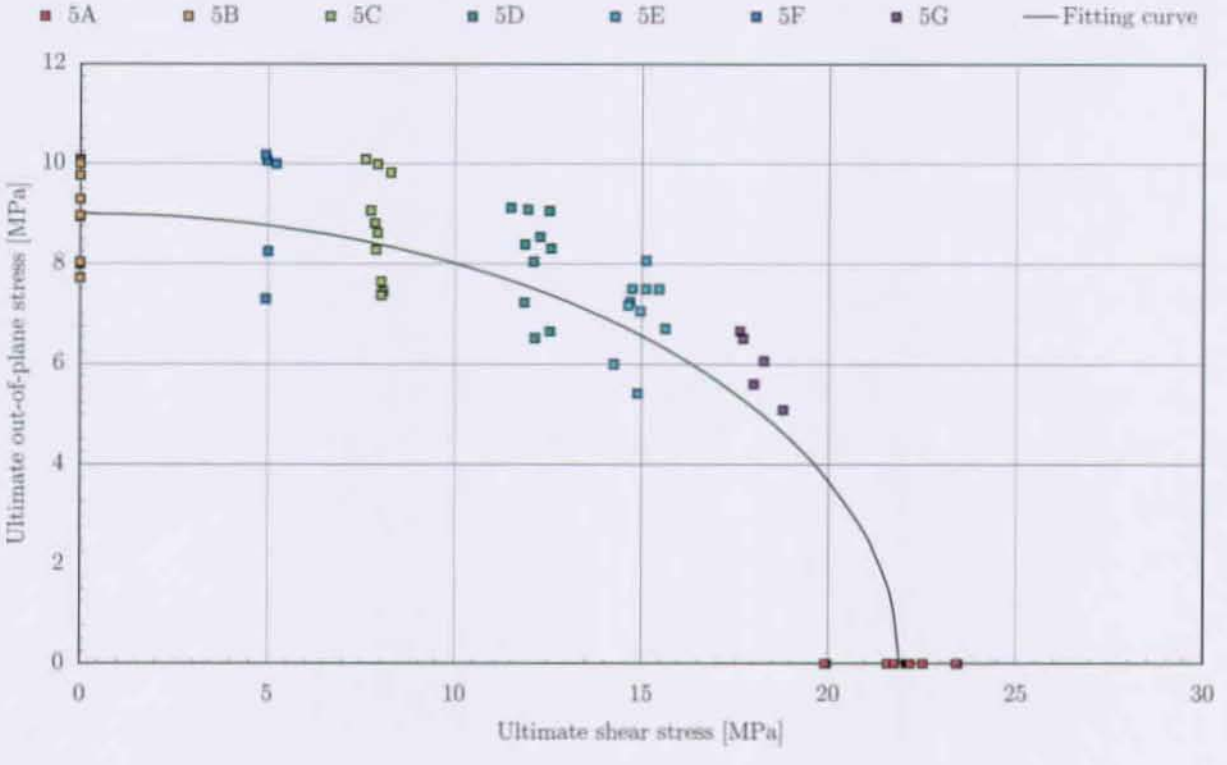

Figure 17.10.: Interaction diagram for the 5 mm thick 50 × 50 samples

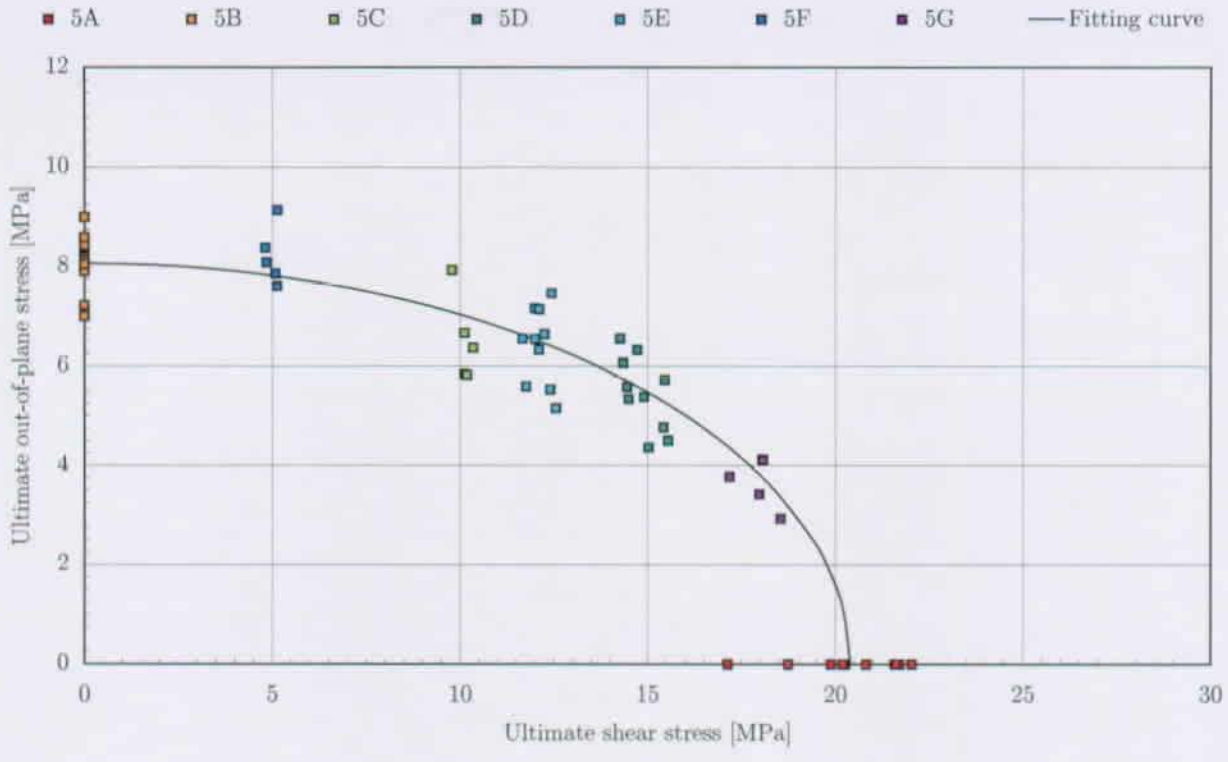

Figure 17.11.: Interaction diagram for the 10 mm thick 40 × 40 samples

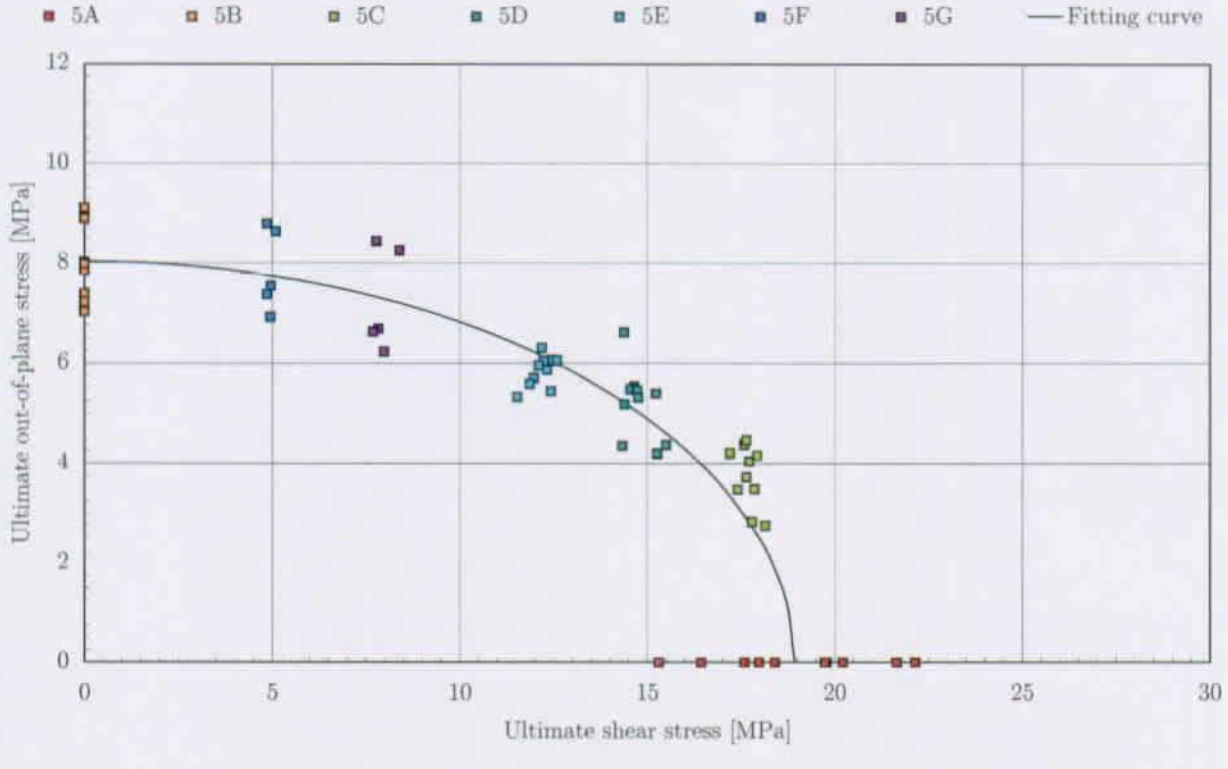

Figure 17.12.: Interaction diagram for the 10 mm thick 50 × 50 samples

18. PARTIAL SAFETY FACTOR FOR THE MATERIAL RESISTANCE

Partial safety factors are now part of every modern dimensioning method. They were first introduced in East-European Standards and codes. West-European engineers started being introduced to them in the late 1970's and begin of the 1980's ([97], [98] and [99]). Today even North-American codes use them in the form of LOAD AND RESISTANCE FACTOR DESIGN (LRFP)[1].

R. PRABHAKARAN, Z. RAZZAQ & S. DEVARA have published in [104] a Load And Resistance Factor Design (LRFD) approach for bolted joints in pultruded composites. Without entering too much in the details of the paper, one sentence might surprise: *It must be emphasized here that the ϕ_{BS} and ϕ_{NT}[2] values [in the above formulae] are proposed only on a tentative basis.* In regard to the statistical data listed in [104] and the formulæ given in [102], it would have been easy to formulate the corresponding ϕ_{BS} and ϕ_{NT}.

At the European level, [102] is an important document in the sense that it regulates the way to gather the partial safety factors based on statistical considerations. The determination of the partial safety factors — formulated according to the EUROCODES, γ_d — has been done below in Section 18.1 for the material used in the frame of this Thesis. The gathering of the partial safety factors is based on a simplified assumption: the normal distribution of the data. The Author is aware that material properties, especially strength data, cannot — from a logical point of view — be distributed according to a GAUSSian normal distribution, but is best approximated by a two- of three-parameter WEIBULL distribution.

M. ALQAM, R. M. BENNET & A.-H. ZUREICK have published in [103] a study comparing 26 mechanical property data sets of pultruded FRP. Both strength and stiffness properties were investigated. They concluded with the recommendation that the two-parameter should be used for material property characterization of pultruded material. The same recommendation is made by A. ZUREICK & R. BENNET in [72]. The reason for the use of the normal distribution has to be seen in the more convenient use of the associated partial safety formulations. For WEIBULL — or any other statistical distribution, like log-normal — distribution, no closed form derivation is possible, but iterative adaptation methods have to be used [98].

[1] For example in the Canadian Steel Code CNA/CSA-S16.1-94 [100] and the Canadian CNA/CSA-23.x-94 [101]

[2] Which are partial safety factors.

18.1. PARTIAL SAFETY FACTOR

The statistical evaluation of resistance/material experiments are described in Section D 3.2 of [102].

The following formula (D.4 in [102]) gives the design value X_d of a variable X:

$$X_d = \eta_d \, m_x \, (1 - k_n V_x) \tag{18.1}$$

where:

η_d is the design value of the conversion value

m_x is the arithmetic mean of the sample results

V_x is the coefficient of variation of X

k_n is a coefficient given in Table D.2 of [102]

The reduction factor $1 - k_n V_x$ will be reformulated and renamed γ_d using the following equation:

$$\gamma_d = \frac{1}{1 - k_n V_x} \tag{18.2}$$

The value of k_n is based on the assumption that X is normally distributed. The guiding design value for the purpose of the STRUCTURAL DESIGN METHOD FOR ADHESIVELY BONDED JOINTS OF PULTRUDED GFRP SHAPES as described in this Thesis is the material resistance as defined in Chapter 24.2.

This material resistance was defined as interaction curves for both shear, τ_{xz} and tensile, σ_z stress. The experimental results are plotted in Fig. 23.2.
The associated variance was calculated in Section G.2 of the Appendix: $V_x = 7.66\,\%$.

Because of the quadratic character of the mathematical fitting curve $\mathfrak{R}$ defined in Equation 24.1, it was selected to apply the partial safety factor as a

factor *reducing the radius* of this equation.
The data leading to the mathematical formulation in Equation 23.2 is displayed in Figs. 17.9 to 17.12 and in Fig. 23.1. The data leading to these curves included for each sample configuration[3] at least 30 samples, so that the factor k_n from Table D.2/[102] has to be taken to $k_n = 3.13$.

Taking $k_n = 3.13$ and $V_x = 7.66\,\%$, it is easy to estimate the partial safety factor, γ_d using Equation E.1 to

$$\begin{aligned} \gamma_d &= \frac{1}{1 - 3.13 \times 0.0766} \\ &= 1.32 \end{aligned} \tag{18.3}$$

[3] 5×40×40, 10×40×40, 5×50×50 and 10×50×50.

Part V.

Finite-Element Analysis

Uti, non abuti!

19. THE DOUBLE LAP JOINTS

The following Part deals with all the Finite Element Analysis in conjunction the experimental investigations carried out for the purpose of the STRUCTURAL DESIGN METHOD FOR ADHESIVELY BONDED JOINTS OF PULTRUDED GFRP SHAPES described in Part III.

All the FEA was carried out using the program ANSYS in its versions 6.1 and 7.1 on a WINDOWS/INTEL platform.

19.1. GENERALITIES ABOUT THE MODELING

19.1.1. MODELIZATION

ELEMENT

Throughout all calculations, the PLAIN82 element was selected.
Because the topic of this Thesis deals with composites, one could argue that composite elements — like SHELL91[1] — should be used. The decision to use simple orthotropic elements was not easy, but because composite elements need input data that was not available, the Author had to use those for which he had accurate mechanical input parameters.

PLAIN82 is a a two-dimensional 8-node element, each node having two degrees of freedom: translations in the nodal x and y directions (see also Fig. 19.1).

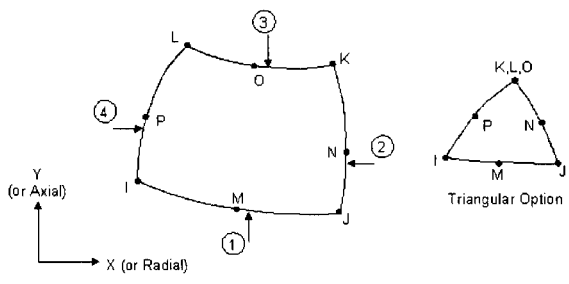

Figure 19.1.: The ANSYS PLAIN82 element used

[1] All element names are related to ANSYS elements. SHELL91 may be used for layered applications of a structural shell model or for modeling thick sandwich structures.

MODELING

Rather than restricting the model to only the sole joint area, the whole tested specimen was modeled (Fig. 19.2).
Despite the fact that this led to a much higher number of needed elements, the Author judged that this would avoid the ambiguity of choosing the right boundary conditions, as other authors have had to do to restrain their models, see for example [87].

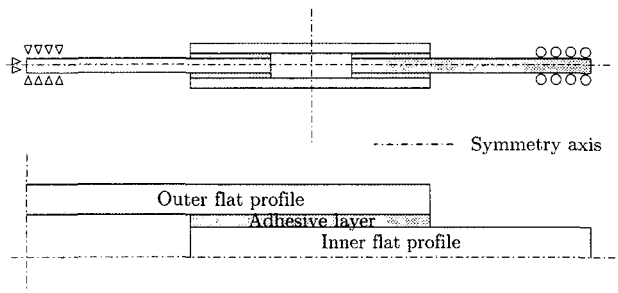

Figure 19.2.: Restraints at the modeled joint (not to scale)

SYMMETRY

Symmetries were used if the systems investigated where appropriated.

FILLETS AND ROUNDINGS

Because fillets and roundings (as defined in Fig. 19.3) have a major influence of both the stress distribution and the ultimate loads, the exact conditions were modeled as planned and verified on the manufactured specimens.

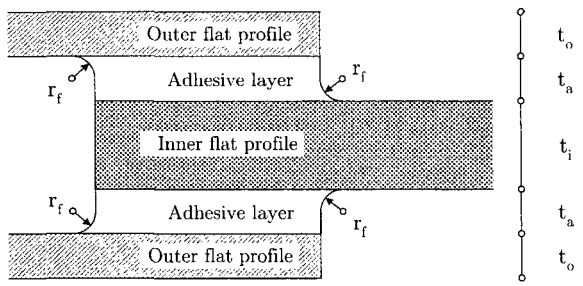

Figure 19.3.: Nomenclature related to the radius fillet

Material	E_x [MPa]	E_z [MPa]	G_{xz} [MPa]	ν_x [-]	ν_z [-]
5 mm FRP	34 348	3 500	3 500	0.26	0.26
10 mm FRP	32 525	3 500	3 500	0.26	0.26
SIKADUR 330	4 550	4 550	1 750	0.3	0.3

Table 19.1.: Material properties used for the FEA

Figs. 19.4-a and -b show how that rounding has been modeled.

ADHESIVE LAYER

All adhesive layers were modeled stacking at least three layers of adhesive. A net refinement was performed at the ends of the overlap where the stresses increase asymptotically, see Figs. 19.4-a and -b.

19.1.2. MATERIAL PROPERTIES

All material properties were modeled using the values gathered during the associated experimental investigations and listed in Table 19.1.

The pultruded FRP were modeled as being orthotropic linear material with the stiffness obtained by the experimental investigations described in each related chapter.
The adhesives were assumed to be linear and isotropic.

19.2. RESULTS

It is not possible to reproduce all the FEA results. This Section shows some selected results with the aim addressing some generalities concerning the investigated lap joints.

All results are related to 4 paths defined by Fig. 19.5 below:

(1) 0.5 mm inside the outer flat profile;

(2) At the interface of the outer flat profile and the adhesive layer[2];

(3) At the interface of the inner flat profile and the adhesive layer;

(4) 0.5 mm inside the inner flat profile.

19.2.1. AXIAL STRAINS

The FE results for a load of load F = 50 kN are plotted in Section 10.3.3.

[2]Where the strain gauges of the previous experimental series were sticked.

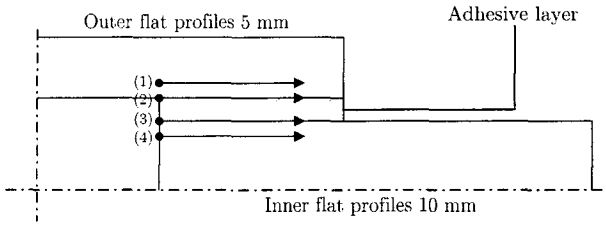

Figure 19.5.: The investigated paths

19.2.2. SHEAR AND OUT-OF-PLANE STRESSES

Shear and out-of-plane stresses for a load of F=100 kN: see Figs. 19.7 to 19.10.

19.2.3. DEFORMATION

As Fig. 19.6 shows, the deformations in the z-direction are relatively small.
The biggest of these deformations occur towards the middle of the unsupported outer flat profile.
The z-deformations of the inner flat profile and the joint area are comparatively lower.

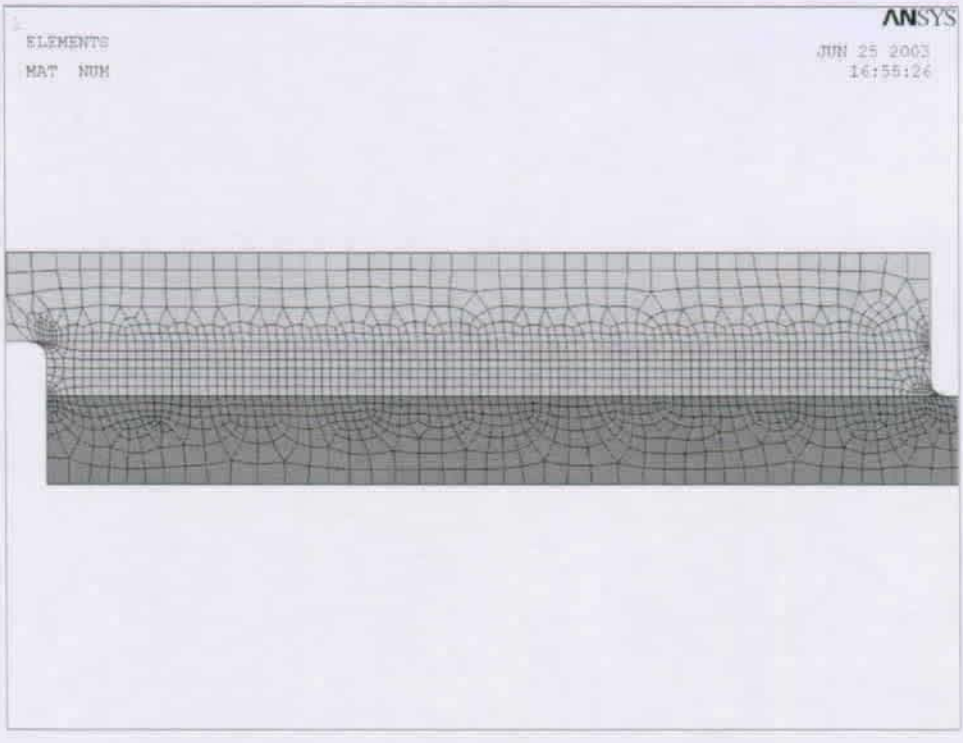

(a) Unchamfered

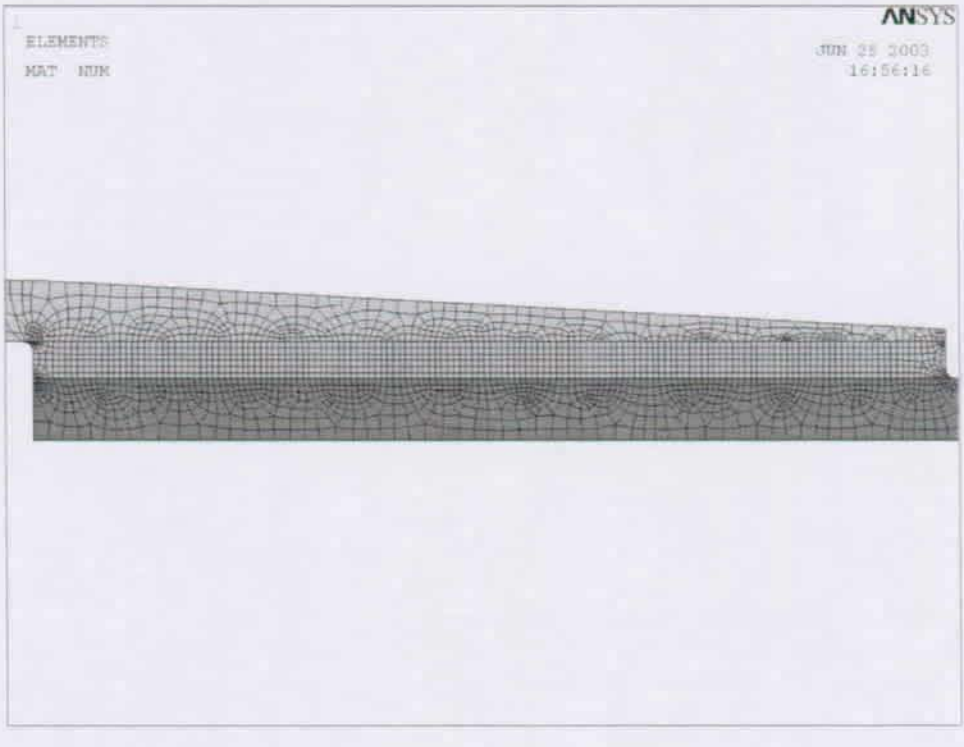

(b) Chamfered

Figure 19.4.: A typical meshing with modeled fillets and net refinement at the overlap ends

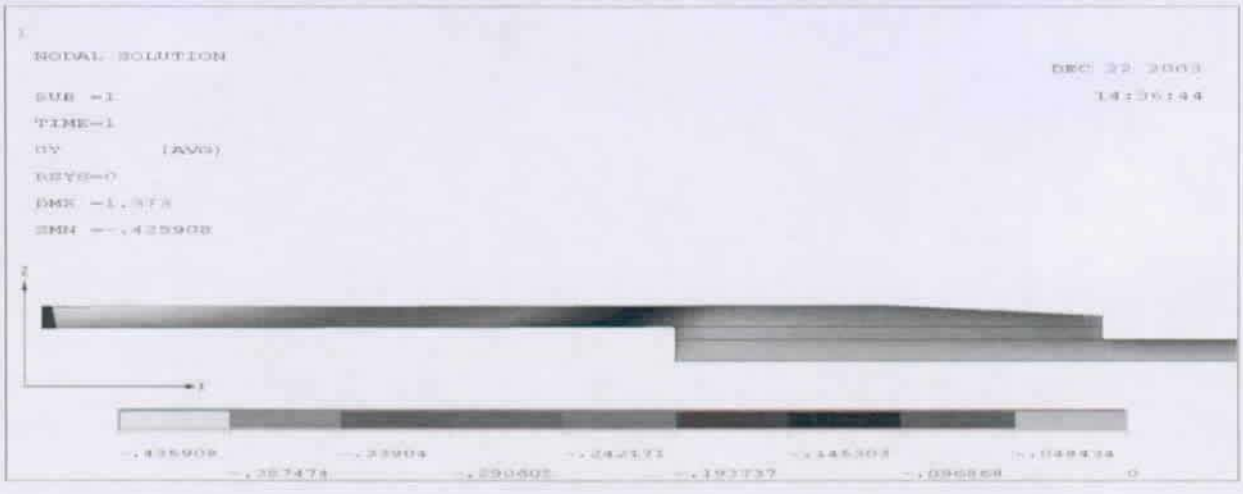

Figure 19.6.: z-Deformation plot for DS$\frac{100}{3}\frac{5}{10}$ at F=100 kN (deformation at scale relatively to the geometry)

19.3. Discussion

An extended discussion of the FEA results would go beyond the scope of this Thesis, only the following salient points will be highlighted:

① As it has already been stated in Part III, the experimentally gathered elastic axial strains and the ones gathered by FEA show a good agreement;

② With longer overlap lengths, the gradients of the shear stresses, τ_{xz} tend to be more asymptotical towards the ends, this effect is not well pronounced for the corresponding out-of-plane stresses, σ_z:
↪ Fig. 19.7;

③ The chamfers at the end of the overlaps tend to reduce both the shear stresses, τ_{xz} and the out-of-plane stresses, σ_z. The out-of-plane stresses are increased towards the unchamfered end with increasing chamfer levels.
↪ Fig. 19.8;

④ Both the shear stresses, τ_{xz} and the out-of-plane stresses, σ_z are lower at the *depth* of 0.5 mm *inside* the FRP material:
↪ Figs. 19.7 to 19.10;

⑤ The adhesive layer thickness has a relatively limited influence on the distribution of both the shear stresses τ_{xz} and the out-of-plane stresses σ_z:
↪ Figs. 19.9 and 19.10.

⑥ The displacements in z-direction are relatively small as it can be seen in Fig. 19.6:
↪ The maximum lies around $\frac{0.4\,mm}{100\,kN}$ for the geometrical configuration investigated.

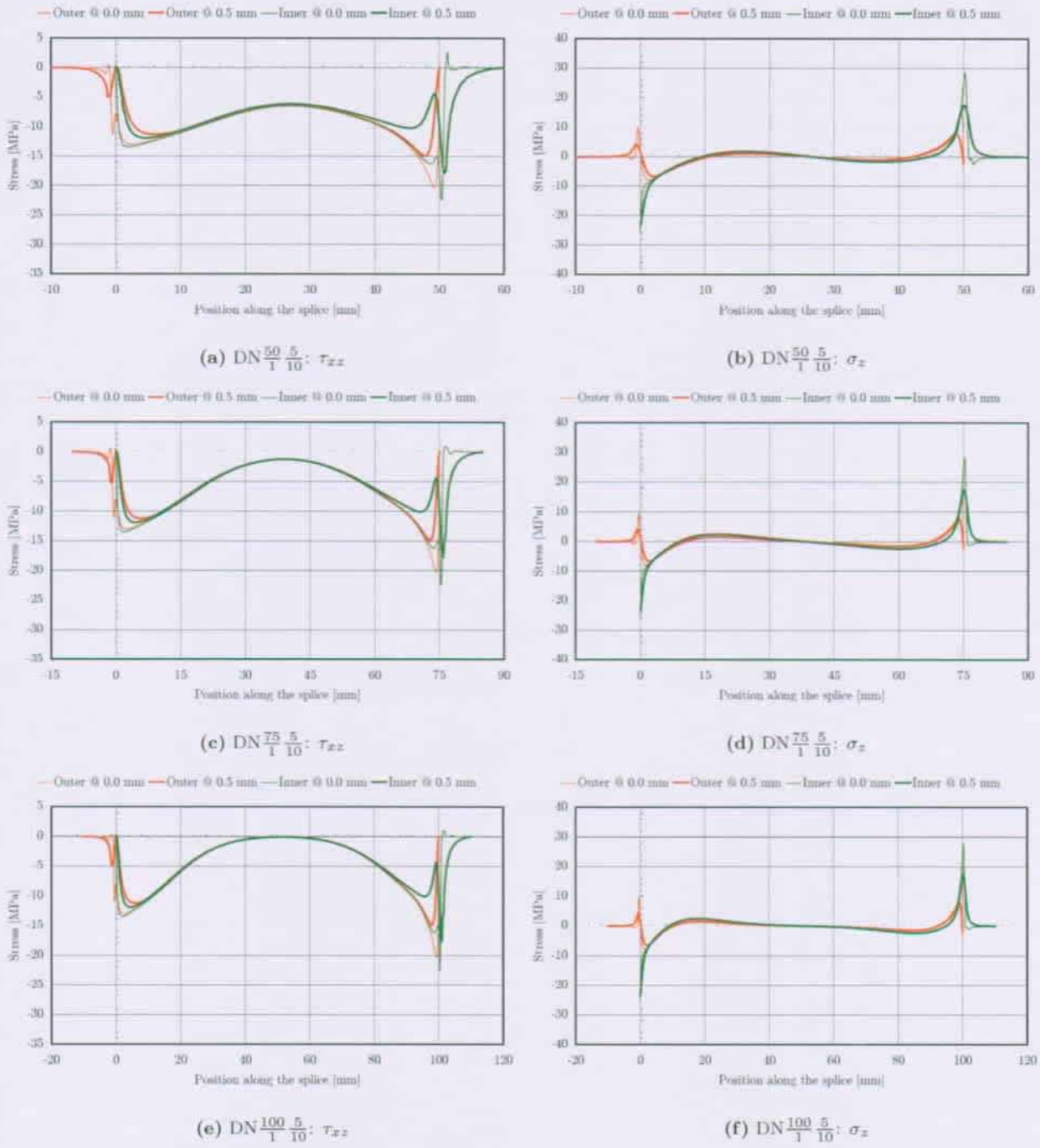

(a) DN$\frac{50}{1}\frac{5}{10}$: τ_{xz}

(b) DN$\frac{50}{1}\frac{5}{10}$: σ_z

(c) DN$\frac{75}{1}\frac{5}{10}$: τ_{xz}

(d) DN$\frac{75}{1}\frac{5}{10}$: σ_z

(e) DN$\frac{100}{1}\frac{5}{10}$: τ_{xz}

(f) DN$\frac{100}{1}\frac{5}{10}$: σ_z

Figure 19.7.: Influence of the overlap length on the shear and out-of-plane stress distribution - F=100 kN

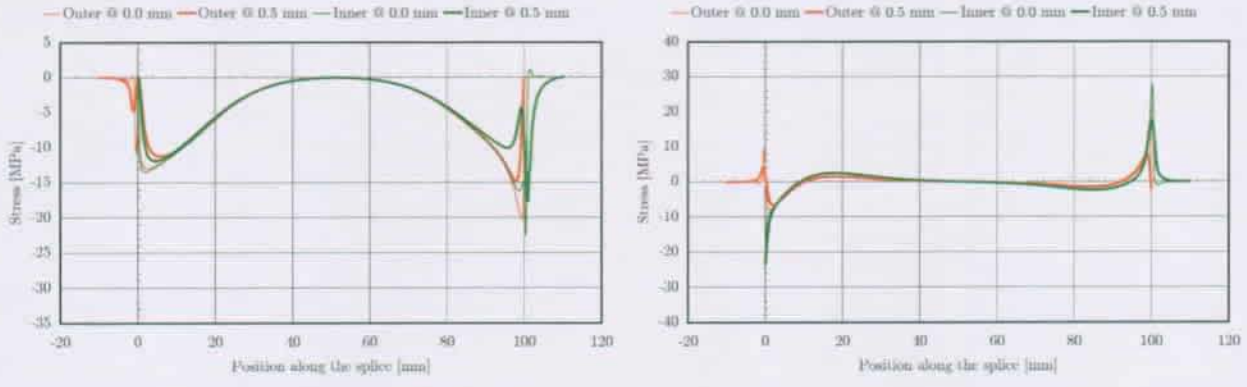

(a) DN $\frac{100}{1}\frac{5}{10}$: τ_{xz} (b) DN $\frac{100}{1}\frac{5}{10}$: σ_z

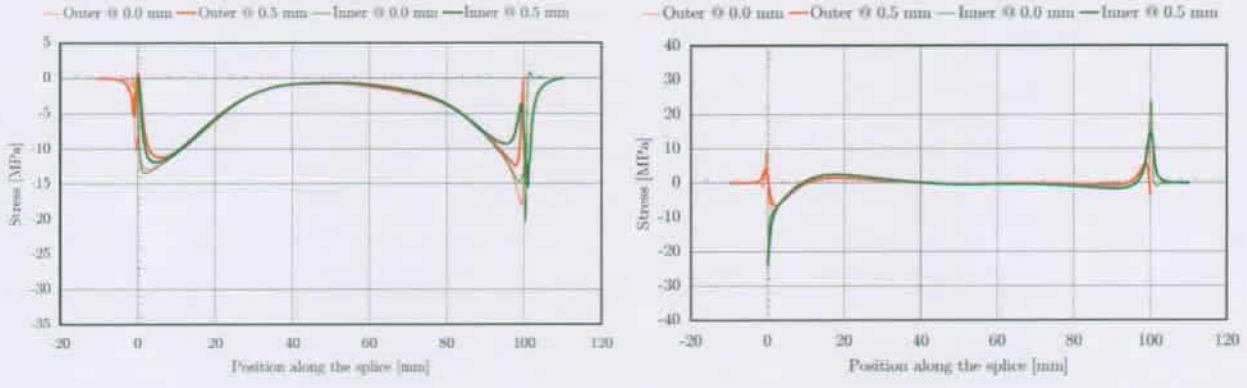

(c) DS $\frac{100}{1}\frac{5}{10}$: τ_{xz} (d) DS $\frac{100}{1}\frac{5}{10}$: σ_z

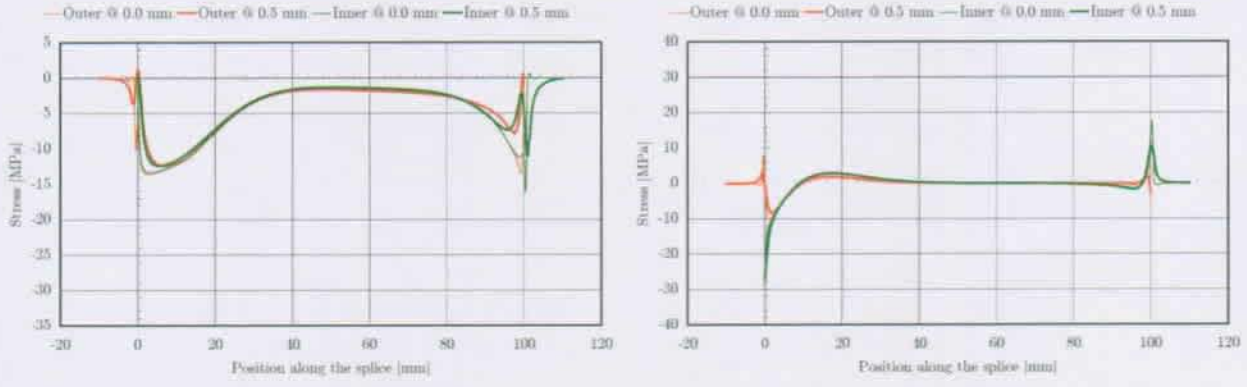

(e) DF $\frac{100}{1}\frac{5}{10}$: τ_{xz} (f) DF $\frac{100}{1}\frac{5}{10}$: σ_z

Figure 19.8.: Influence of the chamfering on the shear and out-of-plane stress distribution - F=100 kN

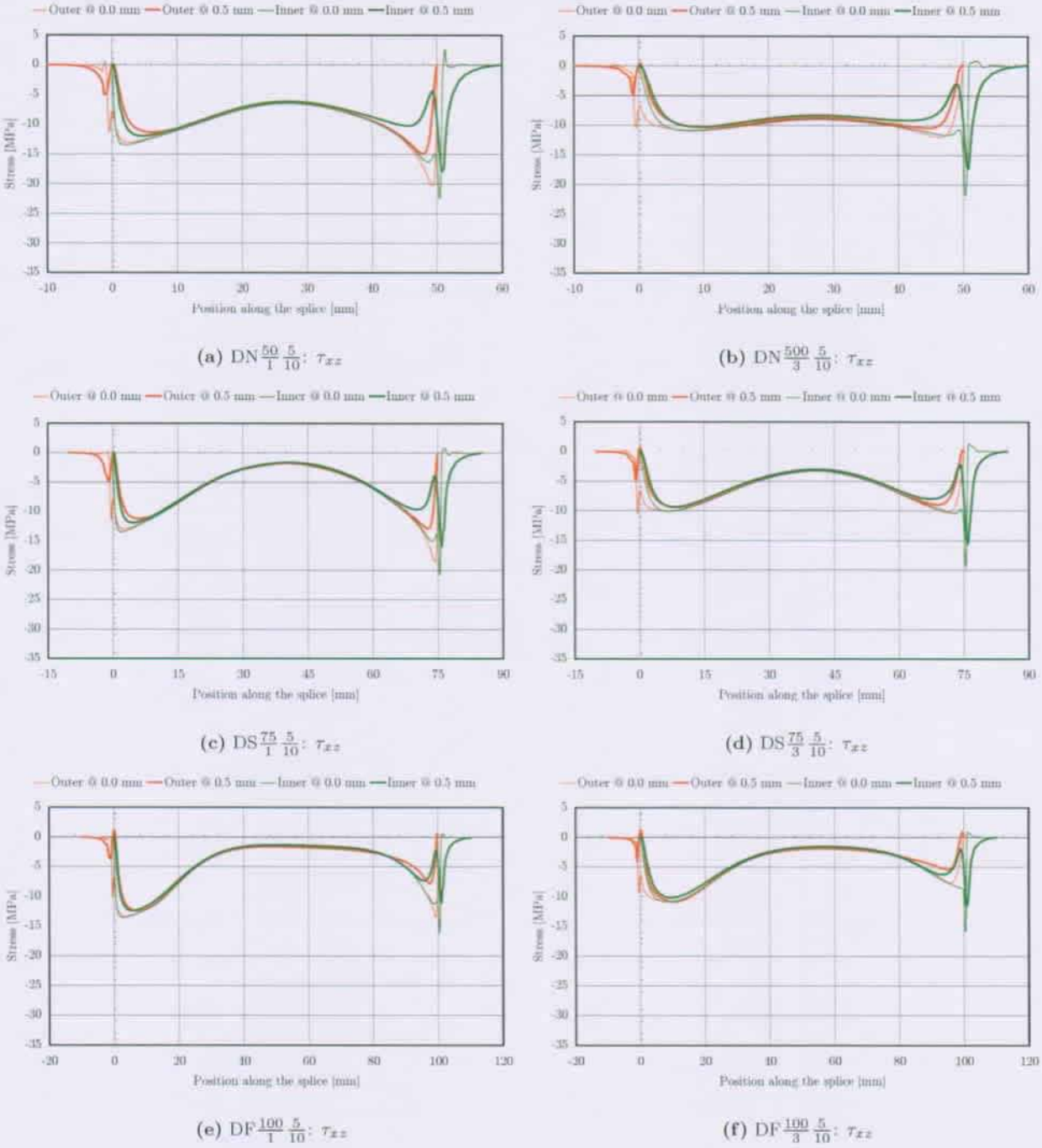

(a) DN$\frac{50}{1}\frac{5}{10}$: τ_{xz}

(b) DN$\frac{500}{3}\frac{5}{10}$: τ_{xz}

(c) DS$\frac{75}{1}\frac{5}{10}$: τ_{xz}

(d) DS$\frac{75}{3}\frac{5}{10}$: τ_{xz}

(e) DF$\frac{100}{1}\frac{5}{10}$: τ_{xz}

(f) DF$\frac{100}{3}\frac{5}{10}$: τ_{xz}

Figure 19.9.: Influence of the adhesive thickness on the shear stress distribution - F=100 kN

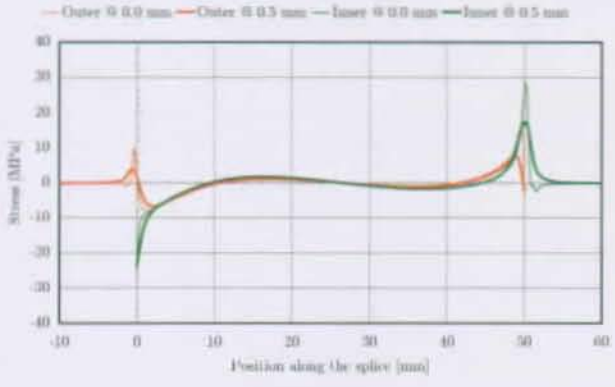

(a) DN$\frac{50}{1}\frac{5}{10}$: σ_z

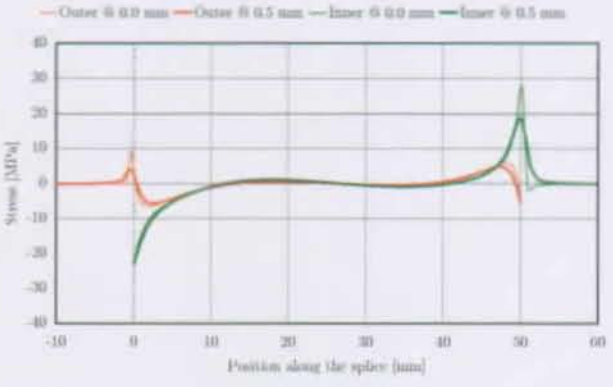

(b) DN$\frac{500}{3}\frac{5}{10}$: σ_z

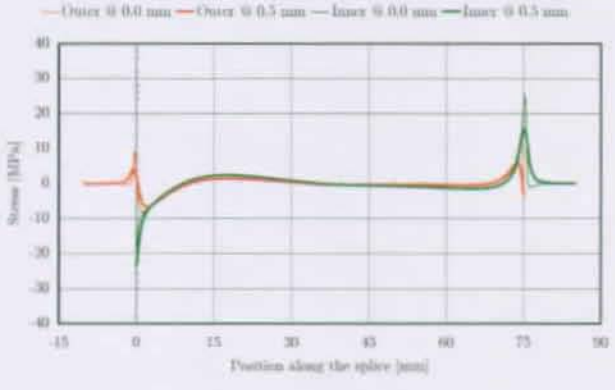

(c) DS$\frac{75}{1}\frac{5}{10}$: σ_z

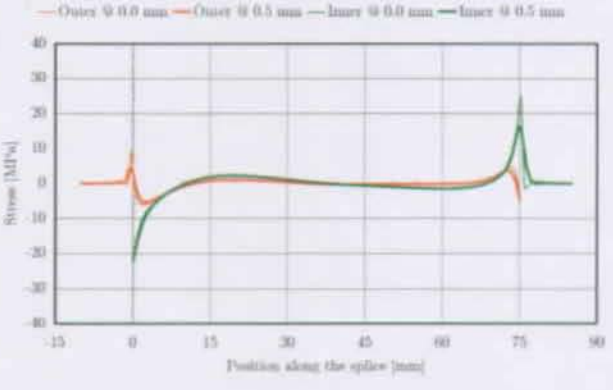

(d) DS$\frac{75}{3}\frac{5}{10}$: σ_z

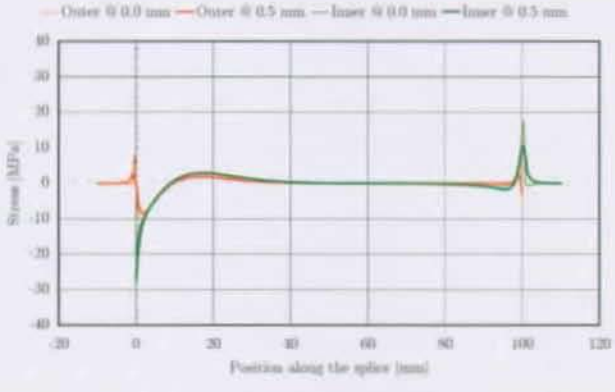

(e) DF$\frac{100}{1}\frac{5}{10}$: σ_z

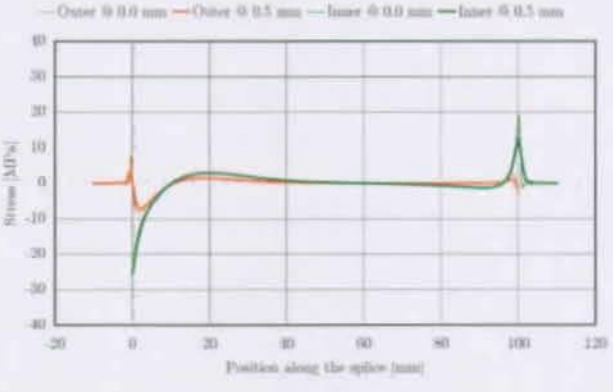

(f) DF$\frac{100}{3}\frac{5}{10}$: σ_z

Figure 19.10.: Influence of the adhesive thickness on the out-of-plane stress distribution - F=100 kN

20. Single lap joints

20.1. Modelization

Using the same principles — concerning the materials, the fillets or roundings and the modelization of the whole specimen — stated in the previous Chapter, the following investigated single lap joints were modeled: SN$\frac{100}{2}\frac{5}{5}$, SN$\frac{100}{2}\frac{10}{10}$ and SN$\frac{100}{3}\frac{10}{10}$.

20.2. Results

Deformations

Fig. 20.1 show the relatively big displacement in the z-direction for the SN$\frac{100}{3}\frac{10}{10}$1 modeled. This behavior was not observed for the double lap joints (see Fig. 20.1) and does directly lead to the fact that analytical formulations — actually only restricted to the sole joint area — cannot accurately describe the stress and strain situation inside bonded single lap joints.
More related to this specific topic can be found in Section 27.2.

Stresses

Shear and out-of-plane stresses for a load of F=100 kN are plotted in Figs. 20.2 to 20.4.

20.3. Discussion

The shear stresses are twice as high[2] for the SN$\frac{100}{2}\frac{5}{5}$ as for the SN$\frac{100}{2}\frac{10}{10}$ system, the out-of-plane stresses are around 50 % higher.
This is due to the fact that the SN$\frac{100}{2}\frac{10}{10}$ is stiffer, keeping itself *better aligned*. Thus the lower deformations does not allow the out-of-plane stresses to fully develop. This result might surprise, because the first thought would be to believe that the SN$\frac{100}{2}\frac{10}{10}$ system shows a much higher load eccentricity that could have lead to higher stresses.

The displacements in the z-direction are orders magnitudes greater than with double lap joints.

This is — in the Authors opinion — also a clear sign that analytical formulæ for bonded single lap joints cannot describe the stress-state unless they take into account the global geometry.

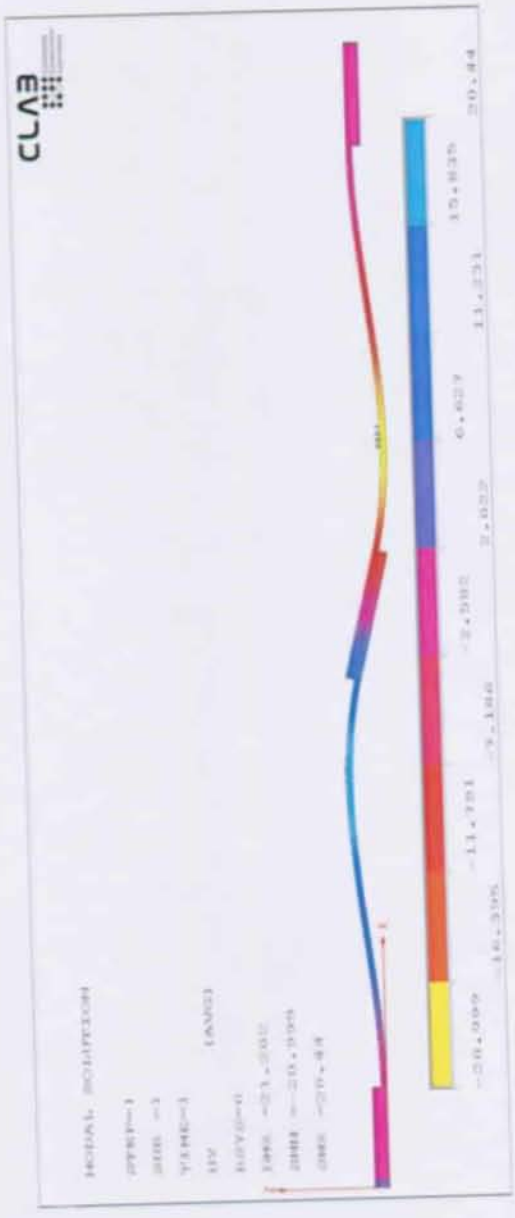

Figure 20.1.: z-Deformation plot for SN$\frac{100}{2}\frac{5}{5}$ at F=100 kN (deformation at scale relatively to the geometry)

[1] Around $\frac{21\,mm}{100\,kN}$ for the maximum displacement as shown in Fig. 20.1.

[2] When considered at the adhesive-FRP interface.

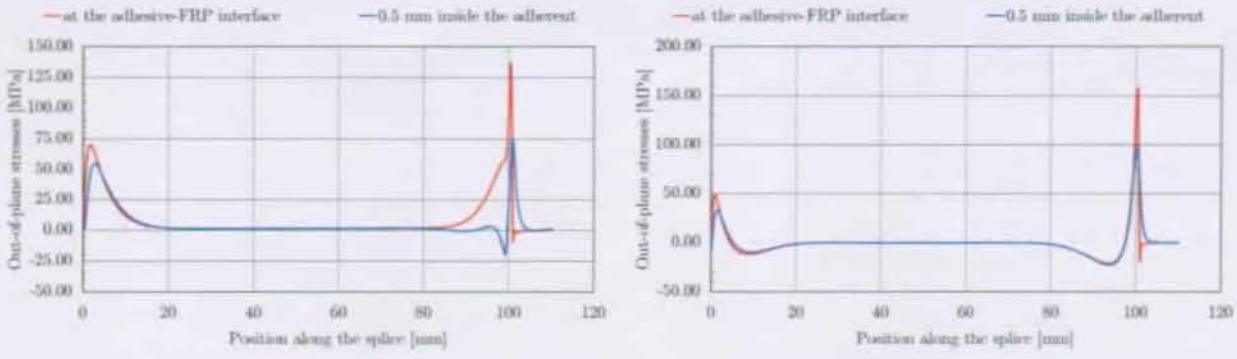

(a) τ_{xz} (b) σ_z

Figure 20.2.: SN$\frac{100}{2}\frac{5}{5}$ at F=100 kN

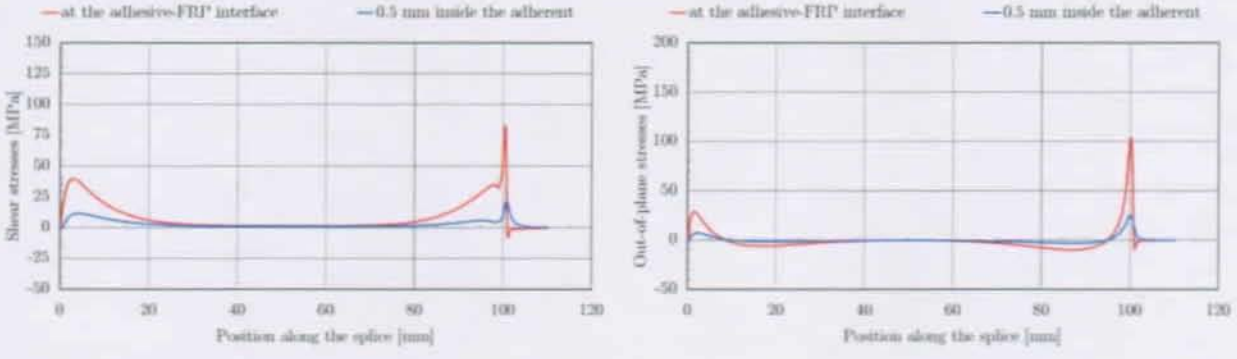

(a) τ_{xz} (b) σ_z

Figure 20.3.: SN$\frac{100}{2}\frac{10}{10}$ at F=100 kN

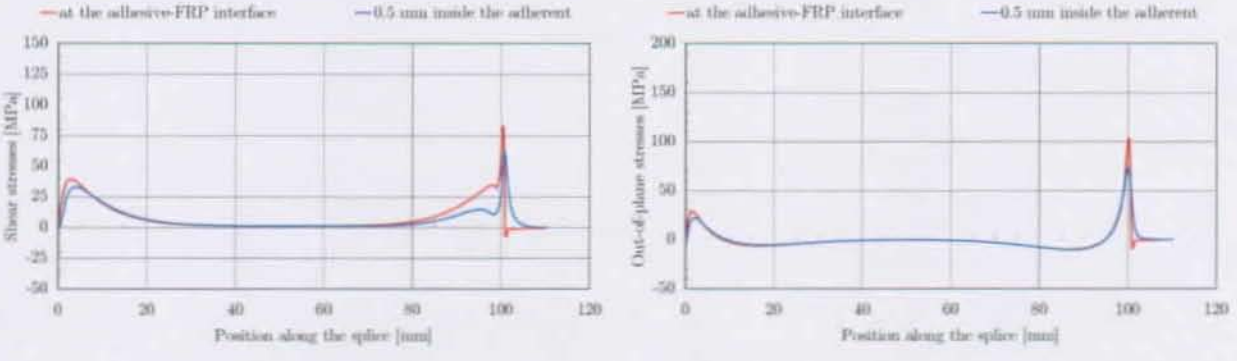

(a) τ_{xz} (b) σ_z

Figure 20.4.: SN$\frac{100}{3}\frac{10}{10}$ at F=100 kN

21. Influence of the free length of single lap joints

A series of FE calculations was performed using the material properties of the specimen described before in Chapt. 19. The joints were modeled using the 5 mm material described in the Chapters 11 to 13, a 1 mm adhesive layer thickness and a 1 mm radius fillet.

Different free lengths — as defined by Fig. 21.1 — were investigated: 125 mm 250 mm, 500 mm and 1 000 mm.

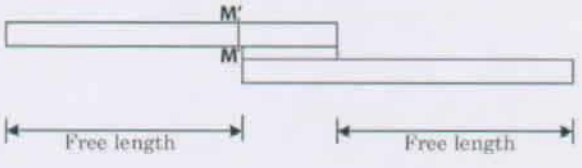

Figure 21.1.: Single lap joint

21.1. Results

The results of the investigations are displayed in Tab. 21.1 and Fig. 21.2.

Free length [mm]	1000	500	250	125
$\sigma_{FEA,max}$ [a] [MPa]	35.0	32.5	26.5	13.5
$\tau_{FEA,max}$ [b] [MPa]	30.2	27.8	22.9	11.8
$F_{FEA,u}$ [c] [kN]	32.1	34.5	41.7	77.0

[a] For a reference load of F=20kN.
[b] For a reference load of F=20kN.
[c] Refer to Chapter 24 for the method with which the prediction of the lap joint strength was performed.

Table 21.1.: Results for different balanced single lap joint for an axial load of F=20 kN

21.1.1. Stress distribution along the bonded splice

See Fig. 21.3 for the shear and out-of-plane stress distribution along the bonded overlap for different *free lengths*. As it can be seen, the longer the *free length* becomes, the steeper both the out-of-plane stresses, σ_z and the shear stresses, τ_{xz} are towards the ends of the overlaps. The maximum values of both stresses σ_z and τ_{xz} also increase with increasing *free lengths*.

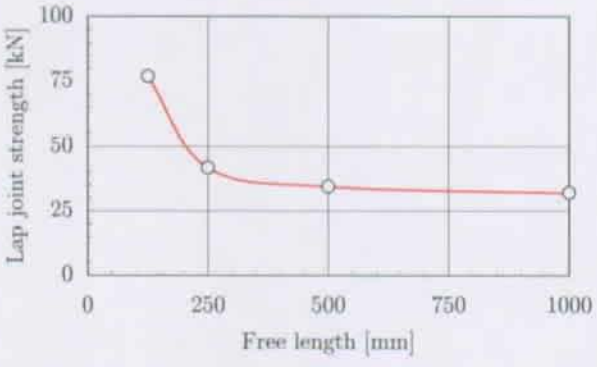

Figure 21.2.: Lap joint strength vs. free length

21.1.2. Bending moment at the end of the overlap

See Fig. 21.4 for the axial stresses just at the end of the bonded overlap (position M-M' in Fig. 21.1) for different *free lengths*.
These axial stress profiles clearly define bending moments at the end of the bonded overlap. These bending moments depend very much of the *free length* of the lap joint considered.
As it can be seen in Fig. 21.4, the shortest *free length* is associated with a normal force dominated stress state, while the longest *free length* specimen investigated is obviously much more moment dominated. In all cases the stresses are linearly distributed over the height.

21.2. Conclusions

The following conclusions might be drawn from the investigations carried out in this Chapter:

① The longer the *free length* of the connected flat profiles, the higher are the stresses inside;

② The free length of single lap joints is obviously a parameter to take into account when considering the stresses inside such joints.

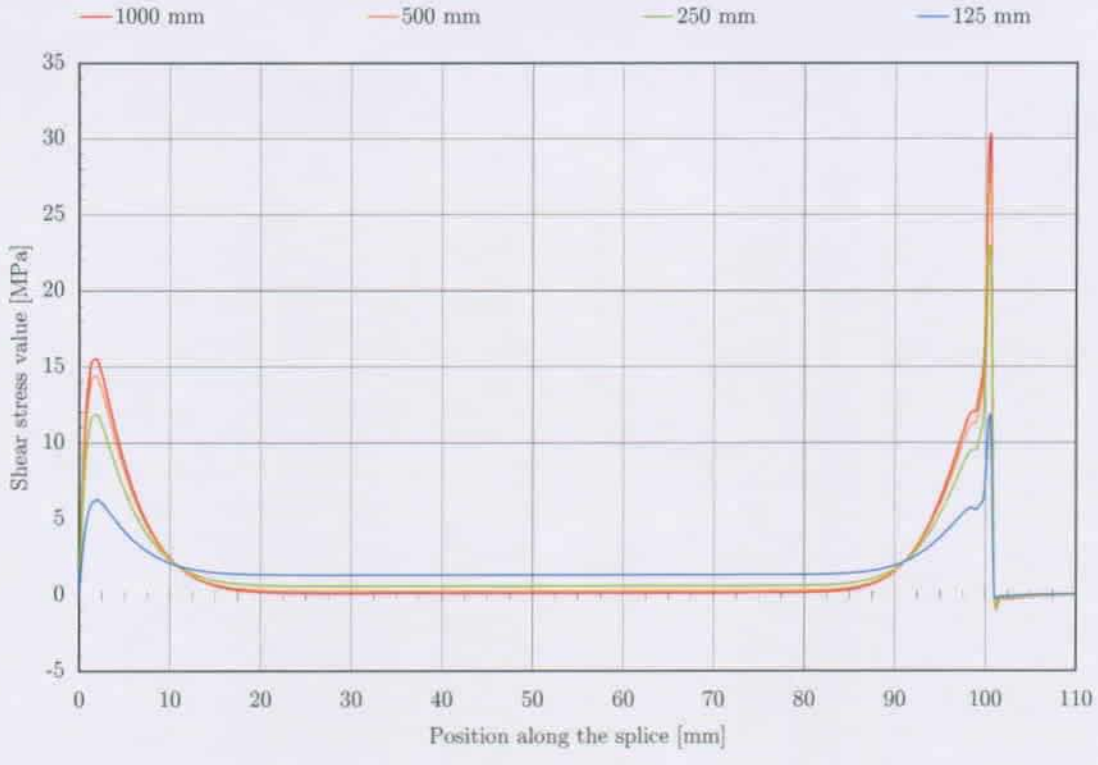

(a) σ_z

(b) τ_{xz}

Figure 21.3.: Stress distributions along the bonded splice for different *free lengths* for a given axial force of 20 kN

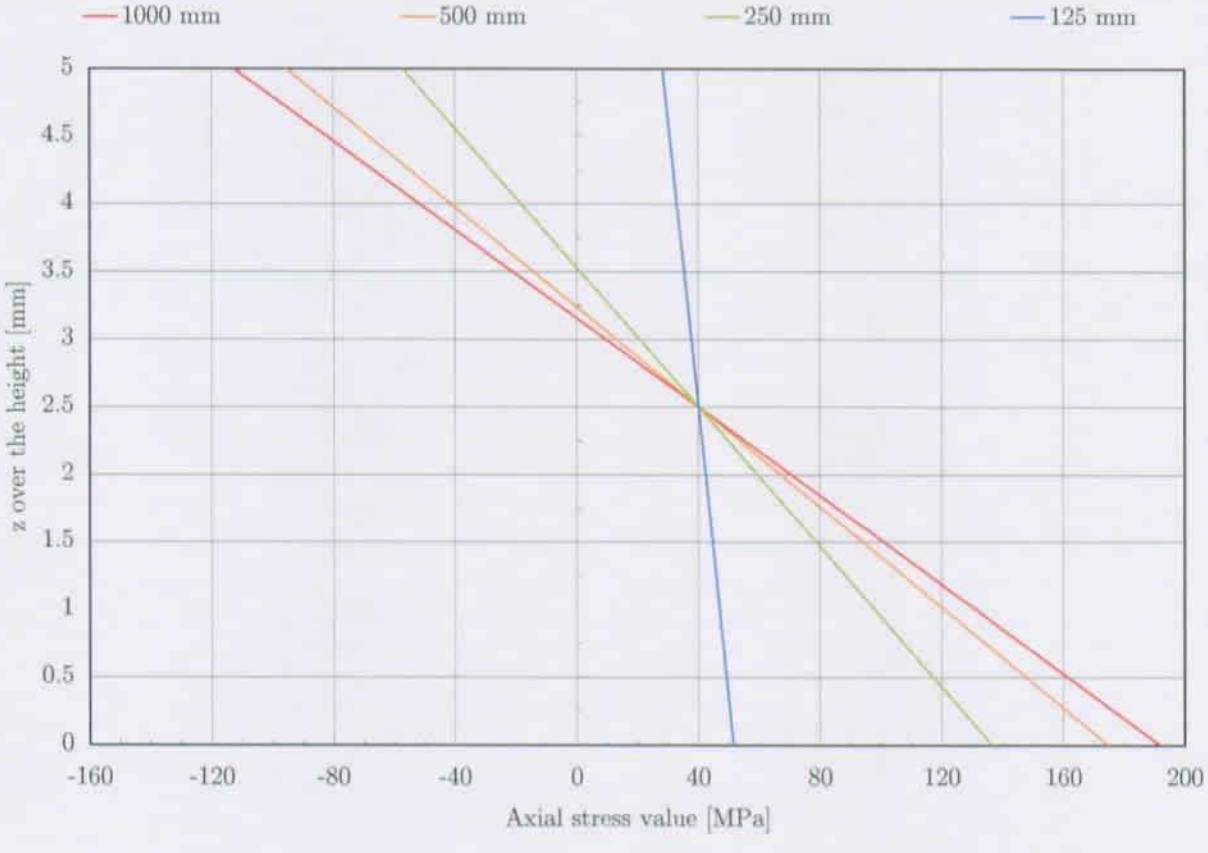

Figure 21.4.: Axial stress distribution over the height of the flat profiles at the end of the bonded splice for different *free lengths* for a given axial force of 20 kN

Part VI.

Interpretation of the investigations carried out

Felix, qui potuit rerum cognoscere causas!

22. INTRODUCTION

This Part combines the knowledge gathered in the previous Parts to express a method to predict lap joint strength.
Anticipating the conclusions to better guide the reader, the Author wants to give an important indication on how this method will look like.
Predicting the lap joint strength will be based on comparing the actual stress state inside the overlap zone to the material given resistance.
Formulated in a mathematical language, it would be written:

$$S \leq R \tag{22.1}$$

Where S denotes the stresses and R denotes the resistance.

22.1. ASSUMPTIONS AND DEFINITIONS

The left side of Eq. 22, the gathering of the stresses, is assumed to be made using either the FEA (suitable for every kind of geometric and mechanical lap joint configuration) or analytical formulæ (for restricted idealized geometrical configurations).
One important assumption is that the stresses are considered to be uniformly distributed over the *width*, the y-axis.
This assumption simplifies considerably the number of free parameters to investigate by reducing the mechanical problem to a plain-stress problem.
Another important assumption is the linearity of the mechanical behaviour of all materials involved. This assumption is almost respected by the FRP up to the ultimate loads while, the epoxy adhesive behaves in this manner within the range of expected stresses.

Basically, using FEA, it is possible, without any limitations, to investigate systems including any kind of non-linear mechanical properties, though slight changes have then to be performed[1]. The linear approach selected was not chosen for its convenience, but because it was appropriate for the involved components.

The axial direction is denoted by x, the transverse by y and the out-of-plane direction by z. The associated stresses are indexed logically according to the usual rules of indexing: σ_i for axial stresses and τ_{ij} for shear stresses[2].The full nomenclature given in Appendix A.

22.2. BASIS OF THE INTERPRETATION

To start the interpretation and processing of the gathered data, it may be useful to review the main results obtained, to explain the ideas behind them and to embed them into the larger frame of this Thesis.
This was done in graphical form and displayed in Fig. 22.1, which might be used as a roadmap for the following section.
The idea was to first gather the basic data concerning the mechanical behaviour in terms of load transfer[3] and ultimate loads[4] in function of geometrical parameters[5] and stress reduction parameters[6]. The description and raw results of these investigations form Part III.
Specific FRP-material properties relative to the dominating stress components — shear and out-of-plane stress — were gathered using the CCLAB TENSILE-SHEAR DEVICE. This device allowed the gathering of the relevant data in form of material dependent interaction diagrams displayed in Chapter 17.
To link both parts described above, Finite Element Analysis was performed. The FEA was also necessary because there is no experimentally way to accurately gather the out-of-plane stresses, σ_z — which play a role in the FRP failure mode.
Joining FEA with the formulation of the material strength leads then to the prediction of ultimate loads for any given material and geometrical configuration of adhesively bonded joints.

[1] Among them the iterative seek of the lap joint strengths.

[2] The indexes i and are j obtained through cyclic permutation over x, y and z.

[3] Done experimentally by gathering the axial extension development along the bonded splices.

[4] Done experimentally by running the experiments up to failure.

[5] Overlap, flat profile and adhesive layer thicknesses.

[6] Chamfering.

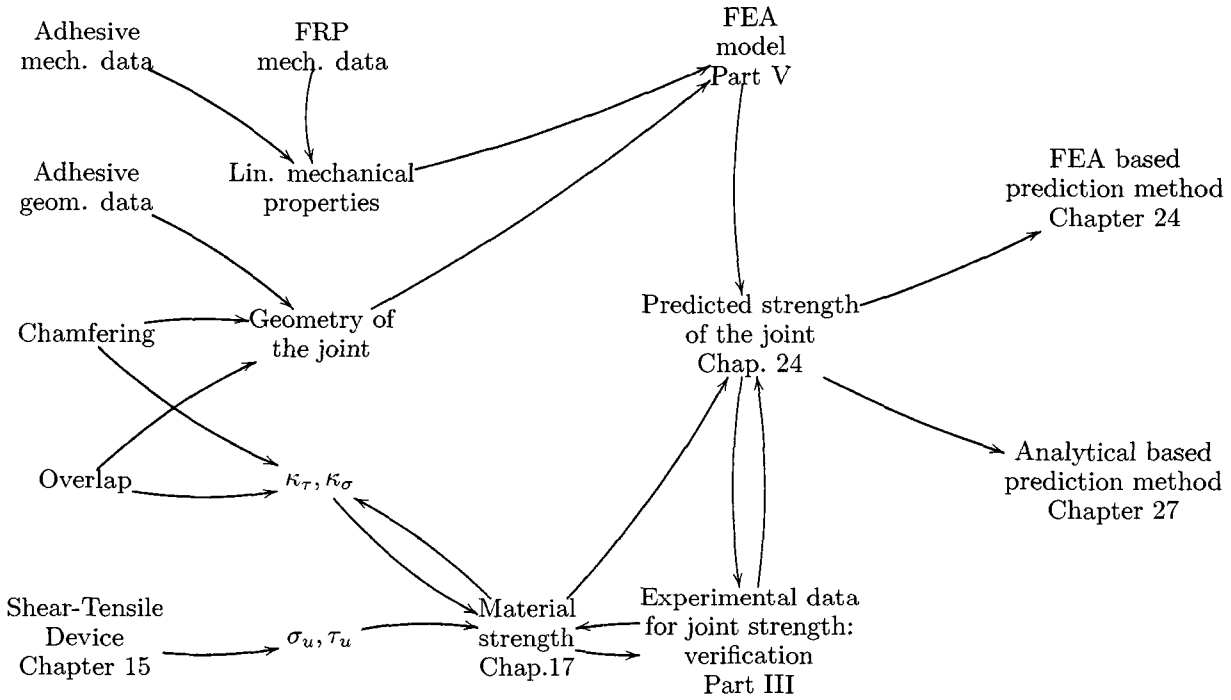

Figure 22.1.: Relations between the different parts of this research for a given joint type

23. FRP FAILURE INTERACTION CURVES

23.1. EXPERIMENTAL VALUES

The gathering of material strength data was described in Chapter 17.

Two different material thicknesses and several combinations of shear stresses τ_{xz} and out-of-plane stresses σ_z were experimentally investigated leading to 4 different **material strength interaction diagrams** plotted in Figs. 17.9 to 17.12.

The values gathered in Chapter 17, having the form of $(\hat{\tau}_{xz,i}, \hat{\sigma}_{z,j})$, are strictly speaking only valid for the geometries from which they were measured.
To distinguish the results carried out on these relatively small specimen from the one used later to describe the joint strength, they are noted using the $\hat{\alpha}$ with α the considered stress.
The same applies to the denomination of the function describing the mathematical relation between the *variables* τ_{xt}, σ_z and the *constants* $\hat{\tau}_{xz,u}$, $\hat{\sigma}_{z,u}$:

$$\hat{\mathfrak{F}} = f\left(\tau_{xz}, \sigma_z, \hat{\tau}_{xz,u}, \hat{\sigma}_{z,u}, \dots\right) \tag{23.1}$$

To analyze the shape of the interaction diagrams obtained by the experimental investigations, the data was examined to find a *simple* approximation function $\tilde{\mathfrak{F}}$.

The values corresponding to the mathematical fitting curves are denoted using the $\tilde{\alpha}$ with α the stress considered.

In regard to [32], three different types will be investigated:

① A quadratic function $\tilde{\mathfrak{F}}_1 = \left(\frac{\tau}{\tilde{\tau}_u}\right)^2 + \left(\frac{\sigma}{\tilde{\sigma}_u}\right)^2$

② A parabolic function $\tilde{\mathfrak{F}}_2 = \left(\frac{\tau}{\tilde{\tau}_u}\right)^2 + \frac{\sigma}{\tilde{\sigma}_u}$

③ A parabolic function $\tilde{\mathfrak{F}}_3 = \frac{\tau}{\tilde{\tau}_u} + \left(\frac{\sigma}{\tilde{\sigma}_u}\right)^2$

To check the suitability of these three approximation functions, all the gathered data will be used as *variables* for the functions $\tilde{\mathfrak{F}}_i$. The *constants* $\tilde{\tau}_{xz,u}$ and $\tilde{\sigma}_{z,u}$ will be, in a first step, approximated as being the average of results of the pure shear experiments and the pure tensile[1] experiments: $\tilde{\tau}_{xz,u} = \hat{\tau}_{xz,u}$ and $\tilde{\sigma}_{z,u} = \hat{\sigma}_{z,u}$.

[1] Pure state stresses are defined as being those stress states where only once of the shear (τ_{xz}) OR out-of-plane (σ_z) act.

These values can easily be calculated and are given in Tab. 23.1.

Geometry of specimen	$\hat{\tau}_{xz,u}$	$\hat{\sigma}_{z,u}$
40x40x5	19.21	8.96
40x40x10	20.40	8.07
50x50x5	21.91	9.00
50x50x10	18.93	8.03

Table 23.1.: Average pure state values as gathered

23.2. APPROXIMATION FUNCTION

Figs. 23.1-a, 23.1-b and 23.1-c represent the results for these functions, $\tilde{\mathfrak{F}}_i$.

The best correlation (represented by the least variation around the failure value[2] $\tilde{\mathfrak{F}}_i = 1$) is given by the quadratic approximation formula $\tilde{\mathfrak{F}}_1$ which is (regardless to the scattering) relatively equal[3] to $\tilde{\mathfrak{F}}_i = 1$ over all the range of experimentally investigated shear stress/tensile stress combinations.

Function	$\sigma_{\tilde{\mathfrak{F}}_1}$
$\tilde{\mathfrak{F}}_1$	7.5 %
$\tilde{\mathfrak{F}}_2$	14.7 %
$\tilde{\mathfrak{F}}_3$	71.3 %

Table 23.2.: Quality of the correlation — expressed by the standard deviation

The mathematical formulations $\tilde{\mathfrak{F}}_2$ and $\tilde{\mathfrak{F}}_3$ do lead to variations of the value at failure for different combinations of corresponding $(\tau_{xz,i}, \sigma_{z,j})$, which indicates a poorer correlation to the gathered data.

As a conclusion, Function $\tilde{\mathfrak{F}}_1$ seems to best fit the gathered data in Chapter 17.

[2] As a reminder: a fracture criteria formula $\tilde{\mathfrak{F}}_i$ has a value $\tilde{\mathfrak{F}}_i(\tau_{xz,i}, \sigma_{z,j}) \leq 1$ for stress combinations $(\tau_{xz,i}, \sigma_{z,j})$ that have not yet led to failure and the value $\tilde{\mathfrak{F}}_i = 1$ for those combinations at failure.

[3] The quality of the correlation is expressed by the standard deviation listed in Tab. 23.2.

23.3. FROM THE GATHERED DATA TO A MATHEMATICAL APPROXIMATION

The function $\tilde{\mathfrak{F}}_1$ was obtained by setting at first the values of its borders to $(\tilde{\tau}_{xz,u}, 0) = (\hat{\tau}_{xz,u}, 0)$ and $(0, \tilde{\sigma}_{z,u}) = (0, \hat{\sigma}_{z,u})$.
Using these values leads to an average *fracture* value $\tilde{\mathfrak{F}}_i(\tau_{xz,i}, \sigma_{z,j})$ different from the theoretical value 1. This average is defined by the following:

$$\tilde{\mathfrak{F}}_{1,average} = \frac{1}{n} \sum_{i=1}^{n} \tilde{\mathfrak{F}}_1 \left(\tilde{\tau}_{xz,i}, \tilde{\sigma}_{z,i}\right) \tag{23.2}$$

To correct this, the values $\tilde{\tau}_{xz,u}$ and $\tilde{\sigma}_{z,u}$ have to be *adapted* to *better fit* the *rest* of the gathered data. Such an adaptation was performed and lead to the results displayed in Tab. 23.3.

Geometry of specimen	$\tilde{\tau}_{xz,u}$	$\tilde{\sigma}_{z,u}$
40x40x5	19.40	8.96
40x40x10	20.40	8.07
50x50x5	22.56	9.36
50x50x10	19.31	8.03

Table 23.3.: Average pure state values to fit the mathematical approximation

The ultimate step to perform is to average the results of the two different specimen sizes for each to have one material strength formulation, $\mathfrak{F}$ valid for a given material architecture.
For this purpose, it is suggested to formulate a weighted average according to the following formulæ

$$\tau_{xz,u} = \frac{\sum_{i=1}^{2} \tilde{\tau}_{xz,u,i} \times A_i}{\sum_{i=1}^{2} A_i} \tag{23.3}$$

$$\sigma_{z,u} = \frac{\sum_{i=1}^{2} \tilde{\sigma}_{z,u,i} \times A_i}{\sum_{i=1}^{2} A_i} \tag{23.4}$$

with $A = a^2$ and a the dimension of the specimen (40 mm or 50 mm).

This leads to the results listed in Tab. 23.4.

Material thickness	$\tau_{xz,u}$	$\sigma_{z,u}$
5 mm	21.3	9.2
10 mm	19.7	8.0

Table 23.4.: Average pure state values to fit the mathematical approximation

The curves representing these functions for 5 mm and 10 mm are given in Fig. 23.2.

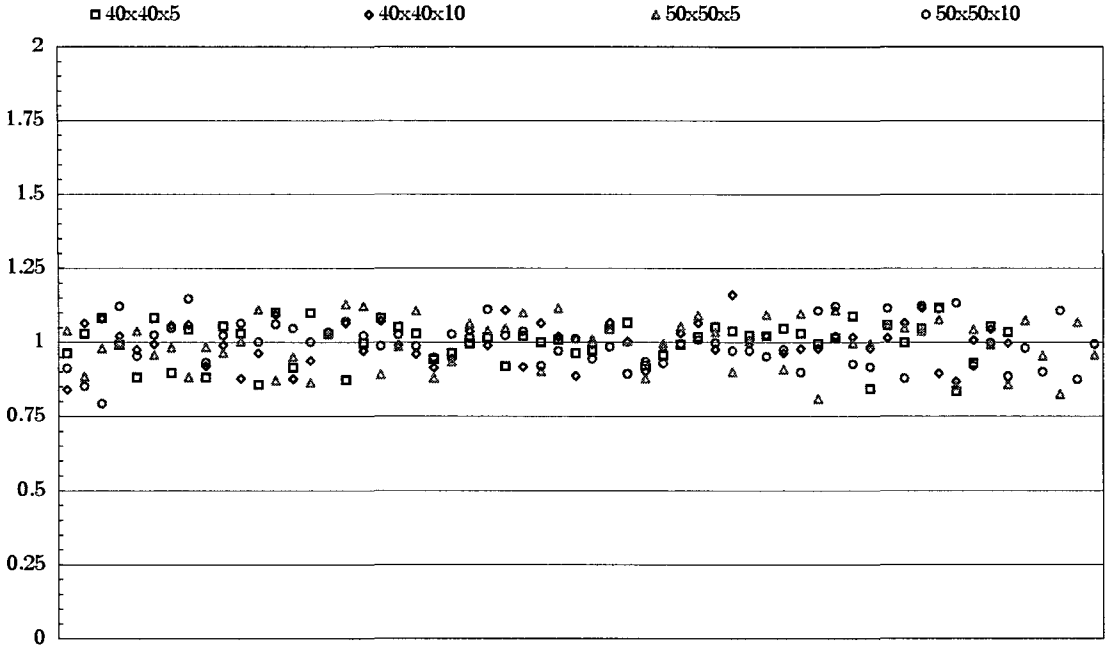

(a) Value of the quadratic failure criteria $\tilde{\mathfrak{F}}_1 = \left(\frac{\tau}{\tau_u}\right)^2 + \left(\frac{\sigma}{\sigma_u}\right)^2$

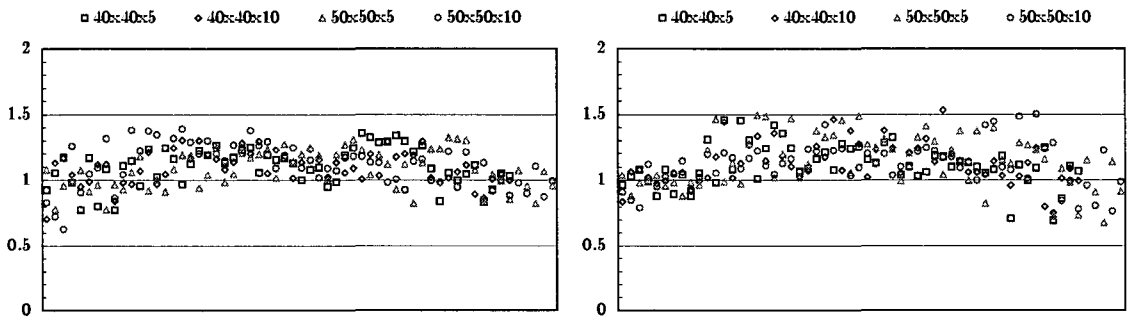

(b) Value of $\tilde{\mathfrak{F}}_2 = \left(\frac{\tau}{\tau_u}\right)^2 + \frac{\sigma}{\sigma_u}$

(c) Value of $\tilde{\mathfrak{F}}_3 = \frac{\tau}{\tau_u} + \left(\frac{\sigma}{\sigma_u}\right)^2$

Figure 23.1.: The correlation to the criteria checked

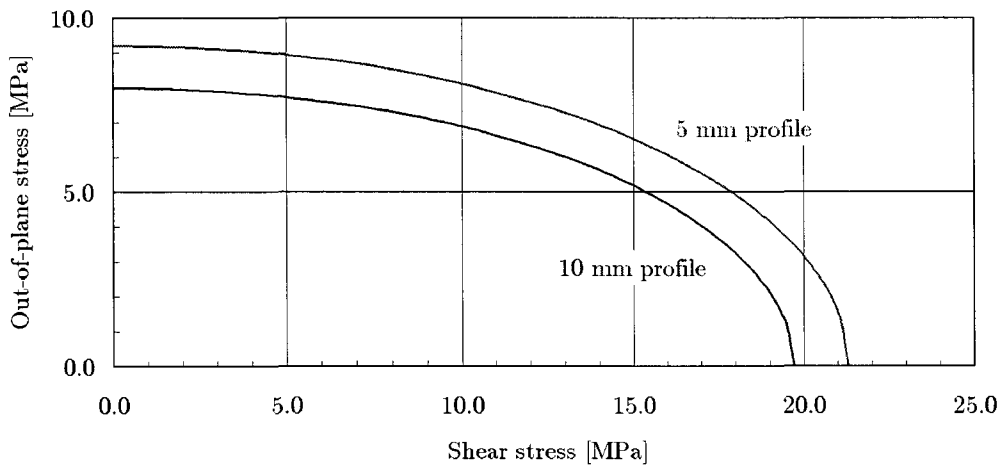

Figure 23.2.: The two mathematical strength functions — based on the averaged values

24. Combining the Failure criteria with the FEA

24.1. Introduction

Chapter 23 described how the material dependent failure criteria were gathered and formulated.
For the purpose of this Thesis, the gathered data had to be fit into two simple mathematical expressions, $\mathfrak{F}$ for the 5 mm and 10 mm material.

As stated before, the gathered data lead to functions strictly only valid for the small specimens described in Chapter 17. To transfer this data onto the mechanical conditions in the double lap joints, it is necessary to adapt this material failure criterion function, $\mathfrak{F}$ and to formulate a function, $\mathfrak{R}$.

The selected approach for this purpose was to add correction factors, κ_τ and κ_σ to the function $\mathfrak{F}$ to build up a function $\mathfrak{R}$ defined by:

$$\mathfrak{R} = \left(\frac{\tau_{xz}}{\kappa_\tau \times \tau_{xz,u}}\right)^2 + \left(\frac{\sigma_z}{\kappa_\sigma \times \sigma_{z,u}}\right)^2 \qquad (24.1)$$

The constants $\tau_{xz,u}$ and $\sigma_{z,u}$ are listed in Tab. 23.4. The values κ_τ and κ_σ are factors to adapt the material strength parameters to fit the mechanical conditions inside the joints[1].

24.2. Applying the failure criteria

The easiest way to apply a failure criteria is to simply use the stress data (τ_{xz}, σ_z) gathered experimentally or by FEA as variables for the function mathematically describing this criterion and to plot vs. a geometrical abscissa, in the present case the position x along the bonded splice.
Such plots — an example is displayed in Fig. 24.1 — indicate then for each point along the bonded splice the *distance* from the theoretical failure in terms of failure criteria or interaction diagram for a given reference load F_0.

[1] This is basically a problem related to size effects.
The size effect on nominal and average stresses of joints was widely investigated by K. Matsui in [93] to [95].

24.2.1. Applying the original $\mathfrak{F}$-criteria

The original $\mathfrak{F}$-criteria was plotted for two geometrical configurations at an arbitrary load of F = 100 kN in both Figs. 24.1 and 24.2.

As far as failure was initiated in a depth of 0.5 mm inside the material, both thicker lines for the inner and the outer flat profiles are relevant.
A numerical calculation results in, for the arbitrary load of F = 100 kN the values η representing the maximum of the $\mathfrak{F}$-function, see Tab. 24.1.

Flat-profile	DN$\frac{50}{1}\frac{5}{10}$	DN$\frac{100}{1}\frac{5}{10}$
Inner	2.27	2.25
Outer	0.76	0.76

Table 24.1.: Maximum values η of the $\mathfrak{F}$-criteria for selected configurations specimen

Because the whole system and its components behave almost linearly, it is possible to calculate the load for which these geometrical configurations reach their failure limit:

$$F_u = \frac{100\,kN}{\sqrt{\eta}} = \frac{100}{\sqrt{2.27}} = 66.37\,kN \qquad (24.2)$$

for DN$\frac{50}{1}\frac{5}{10}$ and

$$F_u = \frac{100\,kN}{\sqrt{\eta}} = \frac{100}{\sqrt{2.25}} = 66.67\,kN \qquad (24.3)$$

for DN$\frac{100}{1}\frac{5}{10}$.

For both geometrical configurations DN$\frac{50}{1}\frac{5}{10}$ and DN$\frac{100}{1}\frac{5}{10}$ the predicted strengths — according to the original $\mathfrak{F}$-function — are in contradiction with the experimental results gathered in Chapter 11.3:
101 kN for DN$\frac{50}{1}\frac{5}{10}$ and 108.3 kN for DN$\frac{100}{1}\frac{5}{10}$.

This difference is due to the fact that the material resistance as gathered does not fit the mechanical conditions inside the joints. In the experimental investigations described in Chapter 17, *both shear and out-of-plane stress fields were* constant over the cross section, while the stress gradients inside the bonded joints show a very different character with the very sharp peaks.

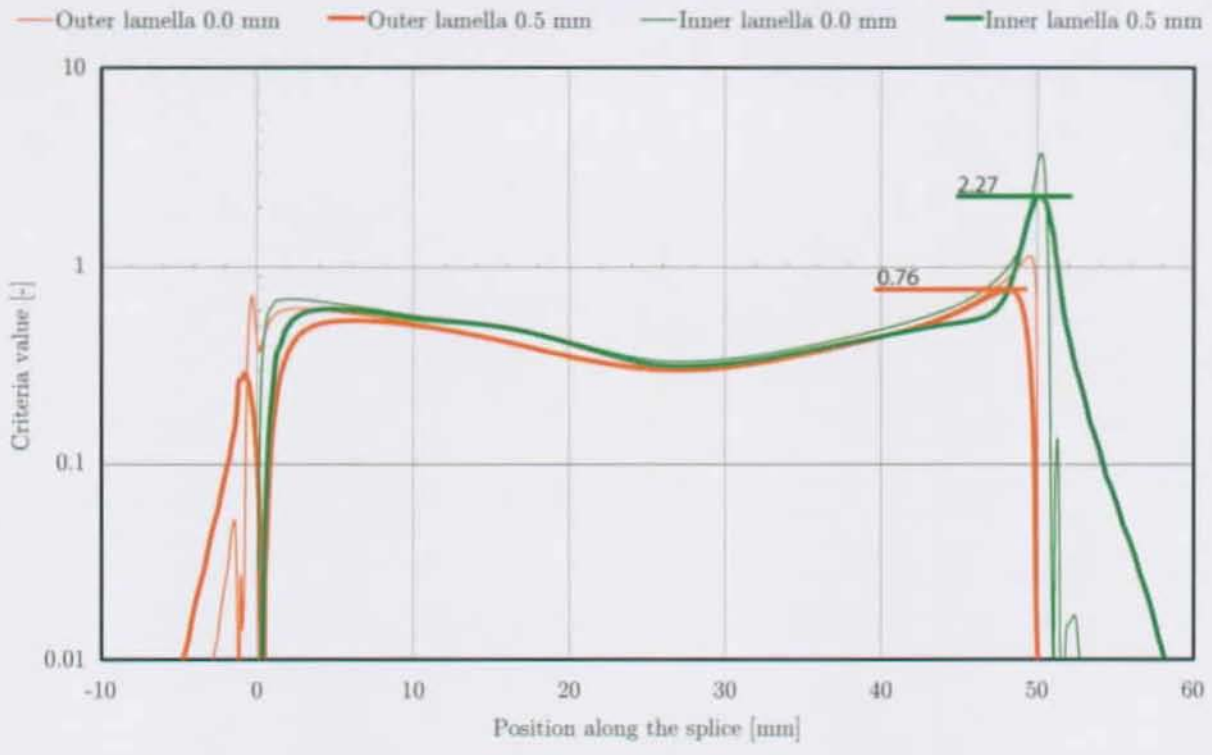

Figure 24.1.: Applying the original $\mathfrak{F}$-criteria to DN$\frac{50}{1}\frac{5}{10}$

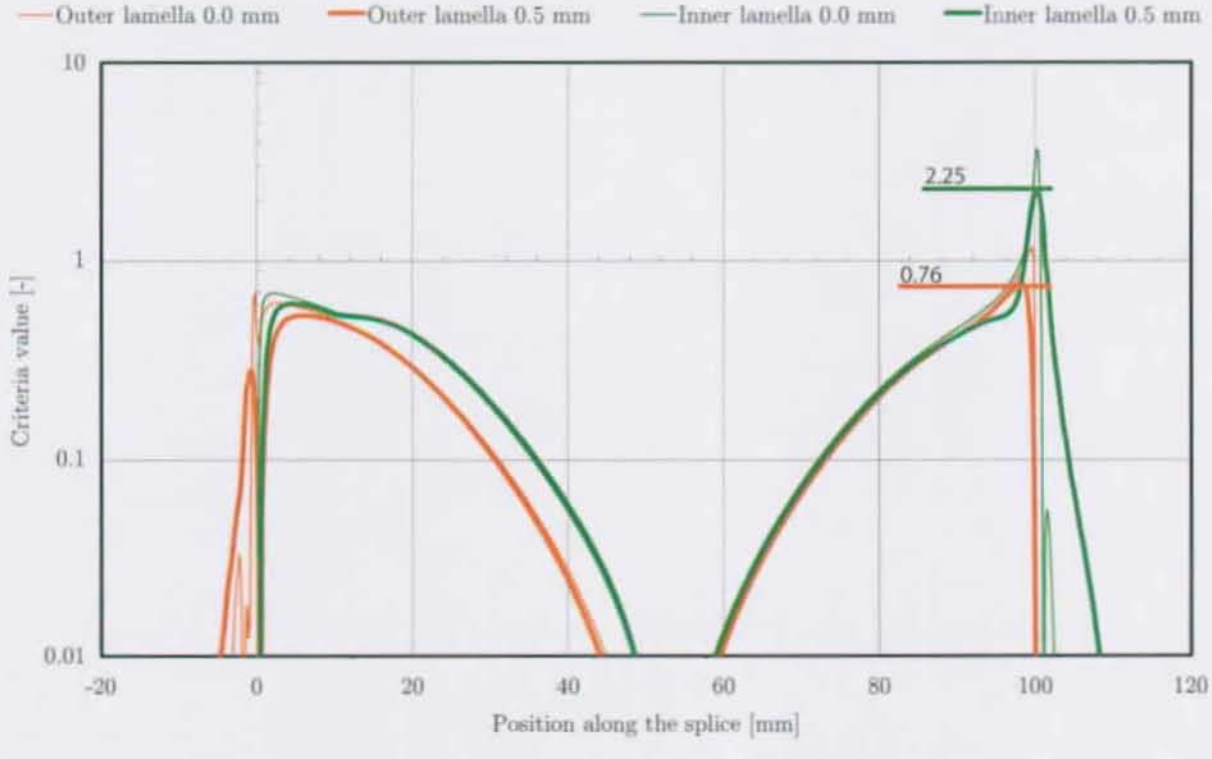

Figure 24.2.: Applying the original $\mathfrak{F}$-criteria DN$\frac{100}{1}\frac{5}{10}$

24.3. PROCEDURE TO GATHER THE κ FACTORS

Up to now, there is no theoretical way to gather the factors κ_τ and κ_σ necessary to transform the strength function $\mathfrak{F}$ (valid for the small square specimens) into the function $\mathfrak{R}$ (valid for the adhesively bonded joints).

The Author compared the experimental and numerical results using different sets of κ_τ and κ_σ. Tables 24.3 and 24.2 represent the best fitting values. This was done by the procedure described in Fig. 24.3.

It is worth noticing that each one of the parameters is only dependent of one *variable* in the mechanical sense: κ_τ depends on the overlap while κ_σ depends on the chamfering.

Overlap [mm]	50	75	100	200
κ_τ	1.0	1.5	2.0	4.0

Table 24.2.: κ_τ

Chamfering[a]	No	Slight	Full
κ_σ	4.0	3.0	2.0

[a]Refer to Fig. 11.1 for the definitions of the chamfering levels

Table 24.3.: κ_σ

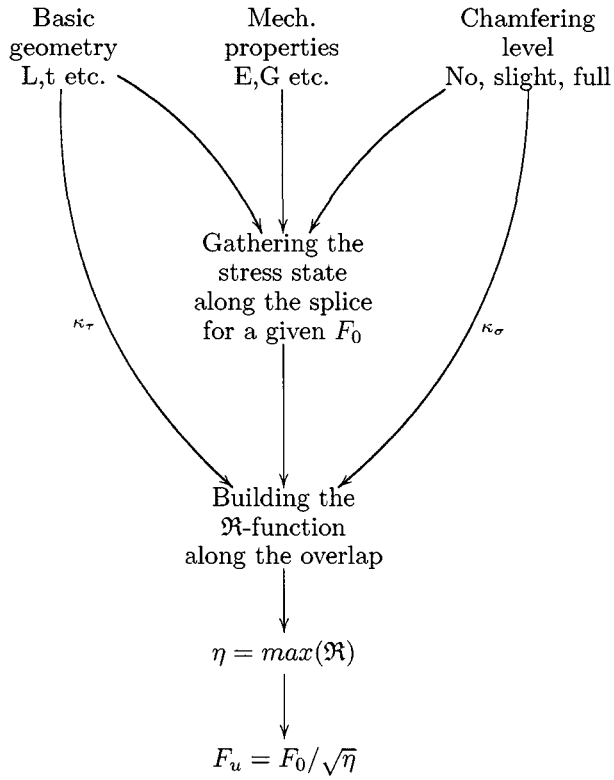

Figure 24.3.: Diagram showing the accurate prediction method

25. Influence of the adhesive thickness and the fillet radius

This Chapter investigates the influence of the adhesive thickness in conjunction with the fillet radius (as defined by Fig. 25.1) on the predicted ultimate load of adhesively bonded double lap joints.
The FEA was carried out according to Chapter V.

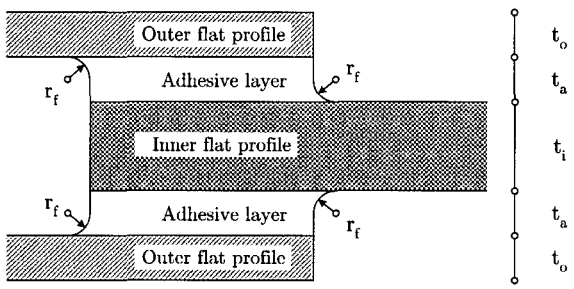

Figure 25.1.: Nomenclature related to the radius fillet

25.1. Adhesive layer thickness vs. overlap

To demonstrate that the adhesive layer thickness, t_a has a minor influence compared to the fillet radius, r_f, a series of FE calculations and ultimate load predictions were performed on the geometrical configuration DN$\frac{L}{t_a}\frac{5}{10}$ with a fillet radius, r_f =2 mm. — with, L ranging from 50 mm to 200 mm and t_a ranging from 1 mm to 5 mm.
The material properties were the same as for the experimentally investigated specimens in Chapters 11 to 13.

The results are plotted in Fig. 25.2.

As it can bee seen in Fig. 25.2, **the adhesive layer thickness, t_a has no noticeable influence on the predicted ultimate load, F_u.**

The Authors own experimental investigations have shown that for adhesive thicknesses of t_a 1 mm and 3 mm — and the same corresponding $r_f = 1$ mm — the ultimate loads did not differ significantly (see Table 26.3).

25.2. Fillet radius vs. adhesive layer thickness

A series of FE calculations was performed on the following geometrical configuration: same FRP material as for the experimentally investigated specimens in Chapters 11 to 13, inner flat profile 10 mm thick, outer flat profiles 5 mm thick and an overlap of 100 mm.

The following parameters were varied:

① The thickness t_a of the adhesive layer that was varied to 1 mm, 2 mm and 3 mm;

② The radius of the fillet r_f, varied in steps of 0.25 mm from 0 to t_a.

The results are plotted in Fig. 25.3. As it can be seen, for a given radius fillet r_f different adhesive layer thicknesses, t_a do lead to very similar predicted ultimate loads, F_u.
It is therefore obvious that **the only parameter having an influence on the ultimate load is the fillet radius, r_f of the adhesive fillet and that there is no significant influence of the adhesive layer thickness on the ultimate load.**

25.3. Considerations on the radius fillet

25.3.1. Experimental investigations on the fillet radius

The suggested ultimate load prediction routine described in Fig. 24.3 does not include a failure criteria for the adhesive fillet. This issue has been investigated in [88] by Y. Zhang.

Y. Zhang experimentally investigated adhesively bonded single lap joints where with different fillet radii, r_f and compared the results with numerical models. The aim was to model the stresses in the adhesive fillet radius and to correlate the failure with the adhesive strength (as determined on the bulk material).

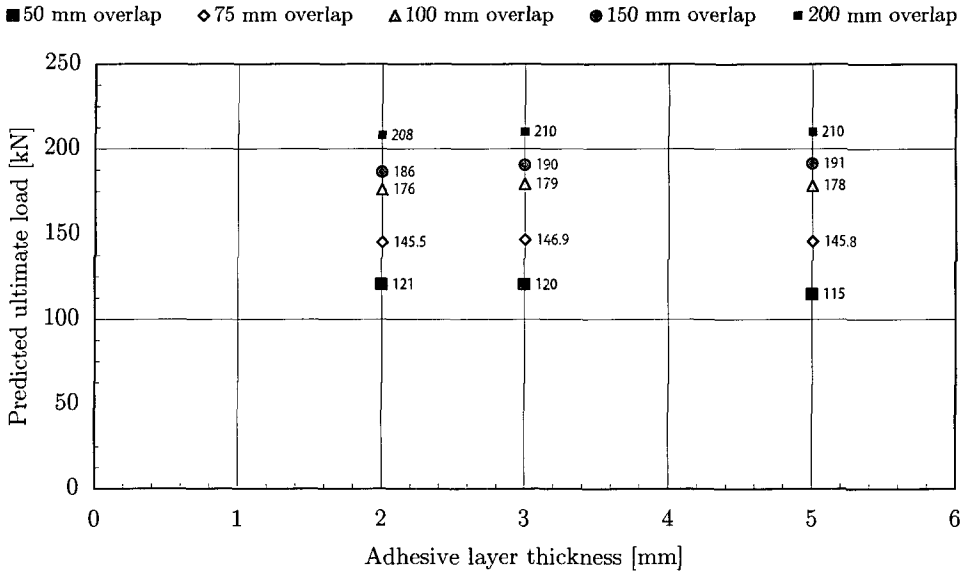

Figure 25.2.: FEA based prediction of the ultimate loads for different adhesive layer thicknesses — influence of overlap length at constant radius fillet of r_f=2 mm

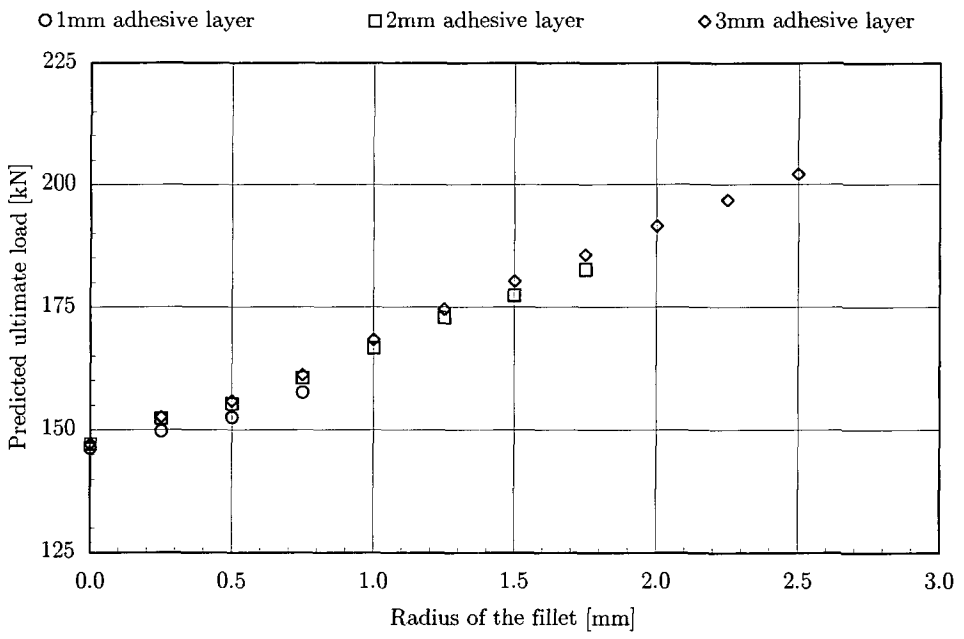

Figure 25.3.: FEA based prediction of the ultimate loads for different adhesive layer thicknesses — influence of radius fillet at constant overlap of 100 mm

25.3.2. SUGGESTION FOR TAKING THE RADIUS FILLET INTO ACCOUNT

The Authors suggestion for a STRUCTURAL DESIGN METHOD FOR ADHESIVELY BONDED JOINTS OF PULTRUDED GFRP SHAPES **taking into account the failure of the radius fillet** would be a two-stage verification: the verification of the joint according to Fig. 24.3 **and then** the verification of the radius fillet (which was discussed a few lines above in Section 25.3.1).
Both verifications are totally independent from each other.

Graphically, this might be represented by Fig. 25.4, where the prediction of the lap joint F_u according to Fig. 24.3 is the governing condition for fillet radii below a critical fillet radius,$r_{f,crit.}$, defined by a still to determine prediction method. Up to $r_{f,crit.}$[1], F_u might be increased by increasing r_f.
For values $r_f > r_{f,crit.}$ the failure is triggered by the fillet itself.

The existence of a critical fillet radius $r_{f,crit.}$, is important to know, because otherwise it would be tempting to increase r_f as much as possible to virtually obtain higher ultimate loads for the corresponding lap joint configurations.

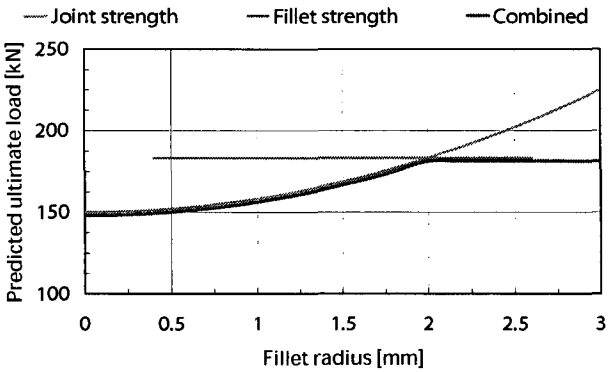

Figure 25.4.: Graphical representation of the fillet radius limiting effect — *a virtual example*

In the frame of this Thesis it was neither possible to experimentally determine the value of $r_{f,crit.}$ nor was it possible to find a correlation between experimental and numerical models.
The safest way for the STRUCTURAL DESIGN OF ADHESIVELY BONDED JOINTS OF PULTRUDED GFRP SHAPES would therefore be to make the predictions using the smallest possible value: $r_f = 0$ mm.
Experimental investigations show that $r_f = 1$ mm lies below $r_{f,crit.}$.

[1] Graphically given by the intersection of the lines corresponding to the two different prediction methods for the lap joint and the fillet strength.

26. Application

Once the values for κ_τ and κ_σ are determined, it is a relatively easy task to *predict* the ultimate loads of geometrical configurations of adhesively bonded joints. This will be the topic of this chapter.

26.1. The chamfered Double-Lap Joints

26.1.1. 1 mm thick adhesive layer

Tables 26.1 and 26.2 give the predicted ultimate loads for the double lap joints defined by the experimental series in Chapter 11.

Chamfer[a]	No	Slight	Full
50 mm	101.7 kN	101.0 kN	114.0 kN
75 mm	138.0 kN	133.2 kN	137.5 kN
100 mm	156.6 kN	146.8 kN	147.3 kN

[a]Refer to Fig. 11.1 for the definitions of the chamfering levels

Table 26.1.: Ultimate load prediction 1 mm

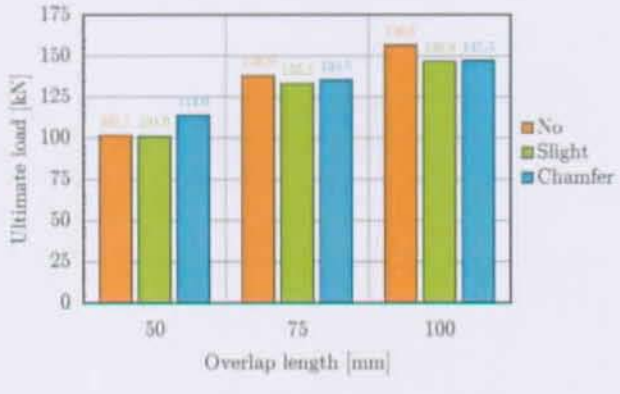

Figure 26.1.: Ultimate load prediction 1 mm

26.1.2. 3 mm thick adhesive layer

Chamfer[a]	No	Slight	Full
50 mm	104.5 kN	100.1 kN	100.1 kN
75 mm	145.5 kN	131.7 kN	118.5 kN
100 mm	165.5 kN	143.3 kN	127.1 kN

[a]Refer to Fig. 11.1 for the definitions of the chamfering levels

Table 26.2.: Ultimate load prediction 3 mm

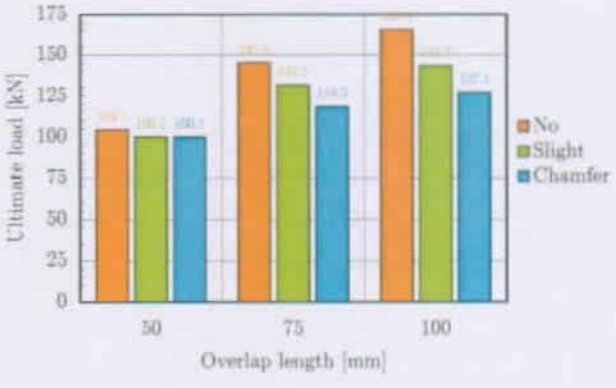

Figure 26.2.: Ultimate load prediction 3 mm

As it can be seen in Tables 26.1 and 26.2, the ultimate loads:

① Increase with growing overlap lengths;

② Generally decrease with higher chamfering levels.

While conclusion ① is not surprizing, ② is partially in contradiction with former publications and expectations.

26.1.3. The corresponding $\mathfrak{R}$-functions

The $\mathfrak{R}$-functions corresponding to the predictions made for Tables 26.1 and 26.2 are displayed in Fig. 26.3 to 26.5.
These plots are different from the corresponding $\mathfrak{F}$-functions because of the κ_σ and κ_τ factors. Because these factors have the effect of virtually raising the material resistance, they lead to lower values.

It can be noticed that:

① Thicker adhesive layers lead to a better *exploitation* of the mechanical resistance over the overlap length[1]. But as the resistance is not *enhanced* by this better distribution, no advantage can be drawn from this fact in terms of strength.

② The same *straightening* effect is obtained by the chamfering. But for the same reasons as stated in ① strength is not enhanced.

26.2. SINGLE LAP JOINTS

Both single lap joint configurations $\mathrm{SN}\frac{100}{2}\frac{5}{5}$ and $\mathrm{SN}\frac{100}{3}\frac{10}{10}$, as described and investigated in Chapter 12 were investigated with the prediction routine described in Chapter 24. This was done using $\kappa_\tau = 2$ for the overlap of 100 mm and $\kappa_\sigma = 4$ for taking into account the fact that it is an unchamfered lap joint. Applying it leads to the following results:

① $\mathrm{SN}\frac{100}{2}\frac{5}{5}$'s predicted $F_u = 35.2\,kN$

② $\mathrm{SN}\frac{100}{3}\frac{10}{10}$'s predicted $F_u = 40.7\,kN$

Taking the Author's experimental results and adding those obtained by Y. ZHANG in [88], the following experimental ultimate strengths were obtained:

① $\mathrm{SN}\frac{100}{2}\frac{5}{5}$'s experimental $F_u = 35.6 \pm 6.1\,kN$

② $\mathrm{SN}\frac{100}{3}\frac{10}{10}$'s experimental $F_u = 42.0 \pm 2.0\,kN$

The agreement between the experimental and predicted single lap joint strengths can be considered to be very good.

26.3. OTHER DOUBLE LAP JOINTS

26.3.1. $\mathrm{DN}\frac{100}{2}\frac{5}{10}$

Chapter 13 reports on the experimental investigations of a series of three $\mathrm{DN}\frac{100}{2}\frac{5}{10}$ epoxy bonded joints. The results are listed in Table 13.1.

The same geometrical configuration was investigated in Chapter 12 with the results listed in Table 12.1. If the poorly bonded specimens listed in Table 13.1 is not taken into account, combining the experimental results of both series[2] leads to an experimental ultimate strength of $F_u = 158\,kN \pm 13.5\,kN$ for $\mathrm{DN}\frac{100}{2}\frac{5}{10}$.

Investigating this configuration using the prediction method described in Chapter 24 using $\kappa_\tau = 2$ for the overlap of 100 mm and $\kappa_\sigma = 4$ for unchamfered double lap joints leads to a predicted ultimate strength of $F_u = 162.9\,kN$.

In this case the agreement between theoretically and experimentally gathered joint strengths is good.

26.3.2. THE ADHESIVELY BONDED AND TORQUED/BOLTED JOINTS

Chapter 13 also describes a series of three $\mathrm{CtN}\frac{100}{2}\frac{5}{10}$ epoxy bonded joints where torqued bolts were added. The experimental ultimate load, as gathered, was $F_u = 202\,kN \pm 33\,kN$.

Using the prediction method described in Section 24 and setting $\sigma_{z,u} = \infty$[3] leads to a predicted ultimate load of $F_u = 236.9\,kN$. Considering the raw approach, the agreement is quite good.

26.3.3. DECASTROS'S $\mathrm{DN}\frac{200}{2}\frac{5}{10}$

As stated in Section 14, J. DECASTRO determined the ultimate load of a series of three $\mathrm{DN}\frac{200}{2}\frac{5}{10}$ epoxy bonded joints leading to an ultimate strength of $F_u = 182\,kN \pm 15\,kN$.

This configuration was investigated with FEA and the prediction routine described in Chapter 24 using the following κ-factors: $\kappa_\tau = 4$ for the overlap of 200 mm and $\kappa_\sigma = 4$ taking into account the fact that it is a unchamfered double lap joint.

The predicted load is $F_u = 182.7\,kN$.

The agreement between the predicted and experimentally gathered ultimate load is very good.

26.4. COMPARISON OF PREDICTED VS. EXPERIMENTAL LOADS

Table 26.3 shows a summary of all geometrical joint configurations for which an ultimate load prediction was performed. The prediction is compared to the experimentally gathered ultimate loads.

[1] Expressed in terms of more evenly distributed $\mathfrak{R}$-values over $x \in [0; L]$ with L the overlap length.

[2] The combination of both series leads to 5 samples.

[3] Assuming that the torqued bolts and the washers prevent any tensile out-of-plane stresses to appear. The Author is aware that this very basic approach cannot be considered as more than an approach, but prediciting the ultimate strength of such joints was not the topic of this Thesis.

Specimen	$F_u, Pred.$ [a] [kN]	$F_u, Exp.$ [b] [kN]	Δ [c] [%]
DN $\frac{50}{1}\frac{5}{10}$	101.7	101.0	-0.7
DS $\frac{50}{1}\frac{5}{10}$	101.0	93.9	-7.0
DF $\frac{50}{1}\frac{5}{10}$	114.0	108.3	-5.0
DN $\frac{75}{1}\frac{5}{10}$	138.0	130.2	-5.7
DS $\frac{75}{1}\frac{5}{10}$	133.2	131.3	-1.4
DF $\frac{75}{1}\frac{5}{10}$	137.5	142.0	+3.3
DN $\frac{100}{1}\frac{5}{10}$	156.6	164.0	+4.7
DS $\frac{100}{1}\frac{5}{10}$	146.8	142.5	-2.9
DF $\frac{100}{1}\frac{5}{10}$	147.3	150.0	+1.8
DN $\frac{50}{3}\frac{5}{10}$	104.5	86.0	-17.7
DS $\frac{75}{3}\frac{5}{10}$	131.7	124.0	-5.8
DN $\frac{100}{3}\frac{5}{10}$	165.5	161.5	-2.4
DS $\frac{100}{3}\frac{5}{10}$	143.3	153.0	+6.8
DF $\frac{100}{3}\frac{5}{10}$	127.1	149.0	+17.2
SN $\frac{100}{2}\frac{5}{5}$	35.6	35.2	-1.1
SN $\frac{100}{3}\frac{10}{10}$	40.7	42.0	+3.2
CtN $\frac{200}{2}\frac{5}{10}$	236.9	202.0	-14.7

Table 26.3.: Summary of all predicted vs. experimental loads

[a] Predicted.
[b] Averaged experimental result.
[c] $\Delta = 1 - \frac{F_{pred.}}{F_{exp}}$.

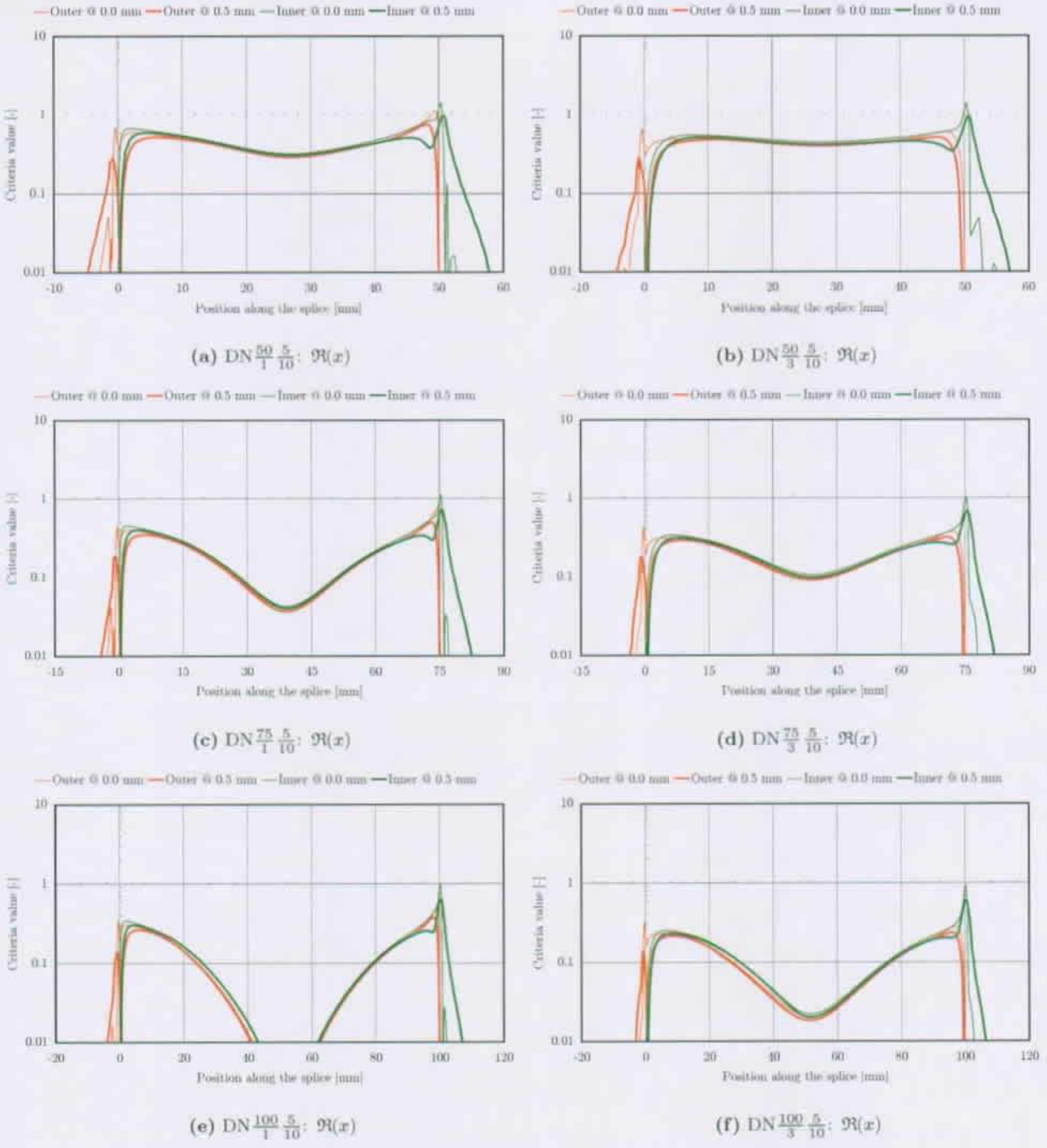

(a) DN$\frac{50}{1}\frac{5}{10}$: $\mathfrak{R}(x)$

(b) DN$\frac{50}{3}\frac{5}{10}$: $\mathfrak{R}(x)$

(c) DN$\frac{75}{1}\frac{5}{10}$: $\mathfrak{R}(x)$

(d) DN$\frac{75}{3}\frac{5}{10}$: $\mathfrak{R}(x)$

(e) DN$\frac{100}{1}\frac{5}{10}$: $\mathfrak{R}(x)$

(f) DN$\frac{100}{3}\frac{5}{10}$: $\mathfrak{R}(x)$

Figure 26.3.: The $\mathfrak{R}$-function plotted along the overlap length

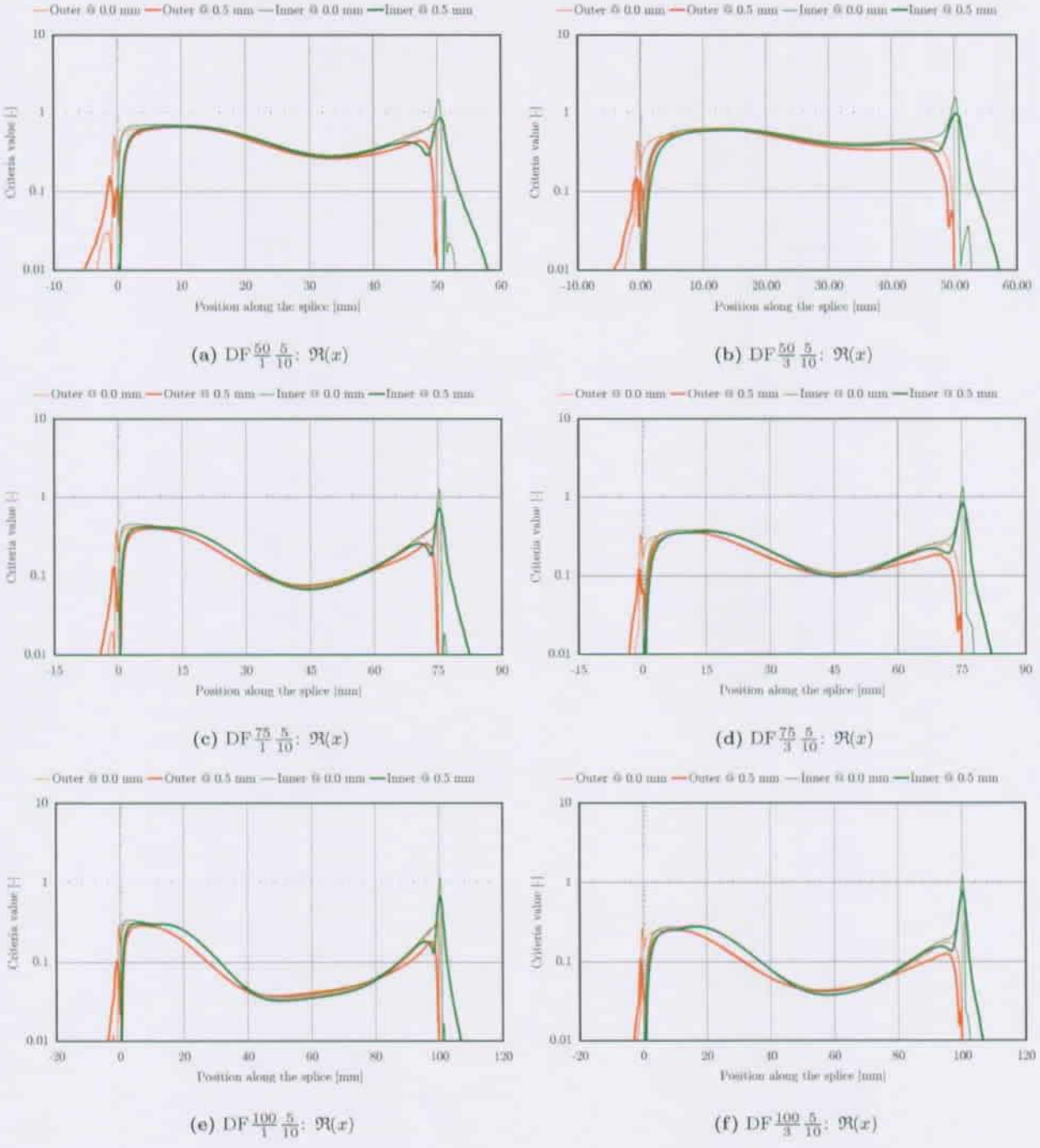

(a) DF $\frac{50}{1}\frac{5}{10}$: $\mathfrak{R}(x)$

(b) DF $\frac{50}{3}\frac{5}{10}$: $\mathfrak{R}(x)$

(c) DF $\frac{75}{1}\frac{5}{10}$: $\mathfrak{R}(x)$

(d) DF $\frac{75}{3}\frac{5}{10}$: $\mathfrak{R}(x)$

(e) DF $\frac{100}{1}\frac{5}{10}$: $\mathfrak{R}(x)$

(f) DF $\frac{100}{3}\frac{5}{10}$: $\mathfrak{R}(x)$

Figure 26.4.: The $\mathfrak{R}$-function plotted along the overlap length

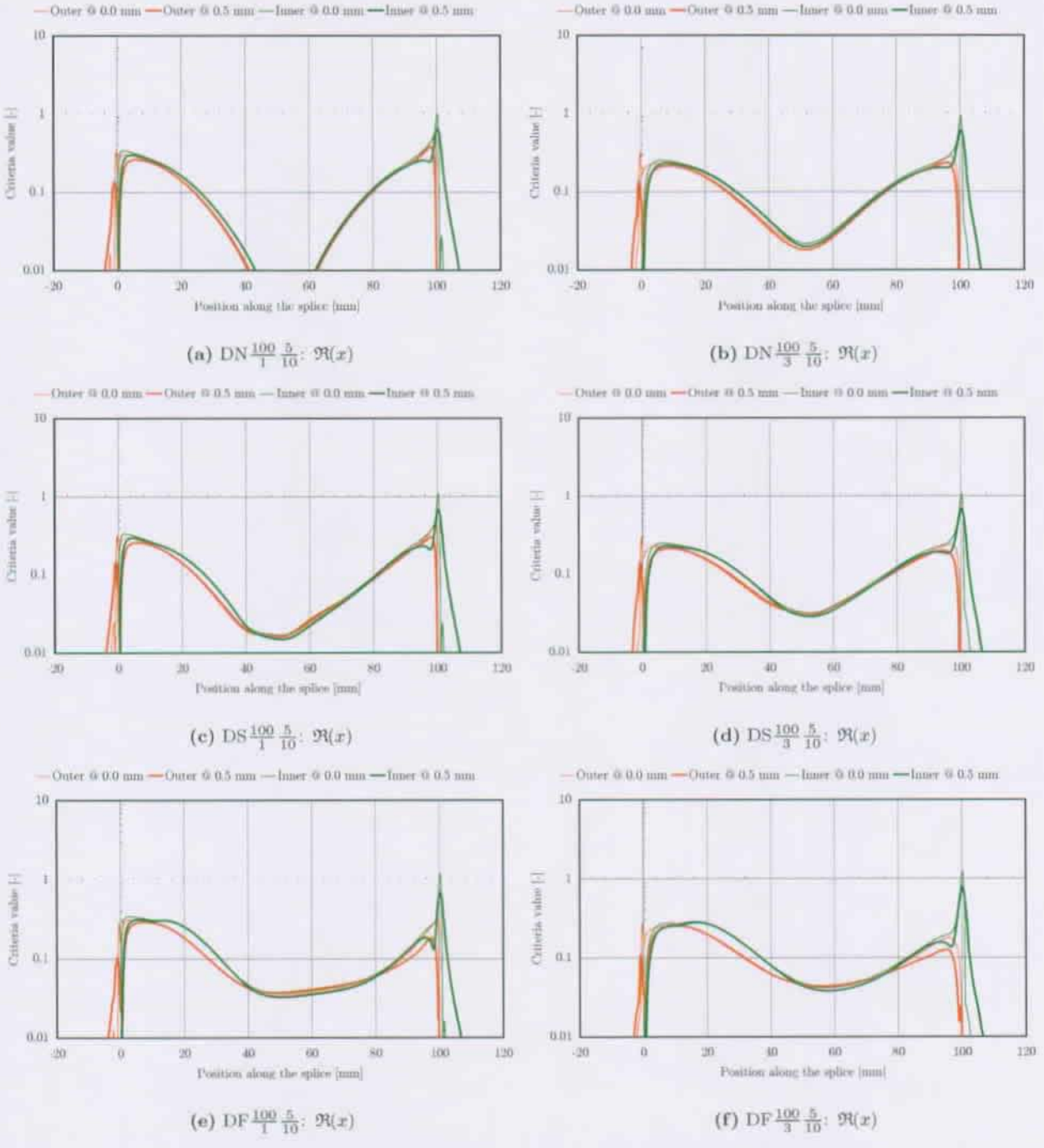

(a) DN $\frac{100}{1}\frac{5}{10}$: $\mathfrak{R}(x)$

(b) DN $\frac{100}{3}\frac{5}{10}$: $\mathfrak{R}(x)$

(c) DS $\frac{100}{1}\frac{5}{10}$: $\mathfrak{R}(x)$

(d) DS $\frac{100}{3}\frac{5}{10}$: $\mathfrak{R}(x)$

(e) DF $\frac{100}{1}\frac{5}{10}$: $\mathfrak{R}(x)$

(f) DF $\frac{100}{3}\frac{5}{10}$: $\mathfrak{R}(x)$

Figure 26.5.: The $\mathfrak{R}$-function plotted along the overlap length

26.5. Application to a non tested configuration

The following shows the application of the lap joint strength prediction to three selected virtual **but non tested** selected configurations:

① Double lap joints of both 5 mm for the inner and outer flat profiles[4];

② Double lap joints of 10 mm for the inner and 5 mm for the outer flat profiles[5];

③ Double lap joints of both 10 mm for the inner and outer flat profiles.

For these 3 series, the model was slightly changed: the gap between the two outer flat profiles was set to a constant value of 50 mm for all geometrical configurations. Fig. 26.6 shows the investigated model for an overlap of 50 mm. The overlap was varied from 25 mm to 300 mm. The restraints correspond to those applied for the formerly investigated configurations.

All lap joints were modeled using the SikaDur 330 adhesive[6], a 2 mm adhesive layer thickness and a radius fillet of 1 mm.
The overlap length was increased in steps of 25 mm from 25 mm to 300 mm.

The determination of the lap joint strength was performed using the method described in Chapter 24 and Ansys.

The results are plotted in Fig. 26.7.

① The common point in all plots is the fact that je voudrais te voir si tu as un webcam janeaimar the lap joint strength converges asymptotically with higher overlap lengths to a maximum value. Over a certain critical overlap length, there is no increase in the joint strength.

② It can also be seen that the highest lap joint strengths are obtained for the double lap joints with both 5 mm for the inner and outer flat profiles. This is due to two factors: this geometrical configuration shows the smallest eccentricity, and failure is related to the 5 mm flat profiles that are stronger in comparison to both 10 mm flat profiles[7].

③ The combination $\frac{5\,mm}{10\,mm}$ leads to higher ultimate loads than the $\frac{10\,mm}{10\,mm}$. In both cases it is the inner flat profile of 10 mm that fails, so that the differences in the strength are only due to the eccentricities.

④ The predicted lap join strength for the joint configuration DN$\frac{100}{2}\frac{5}{10}$ with:
a gap of 300 mm $\rightsquigarrow$ F_u=163.9 kN.
a gap of 50 mm $\rightsquigarrow$ F_u=186.2 kN and
showing by this that the length of the center gap has also an influence.

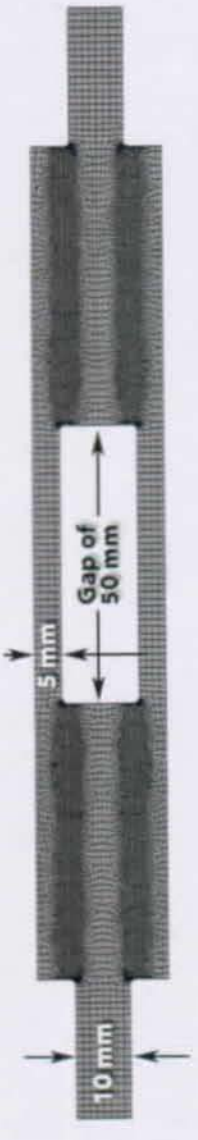

Figure 26.6.: Geometry of DN$\frac{50}{2}\frac{5}{10}$

[4]Mechanical properties of the material are as described before in Part III
[5]Mechanical properties of the material are as described before in Part III
[6]Described previously and in Appendix C.
[7]See Chapter 17 and 23.

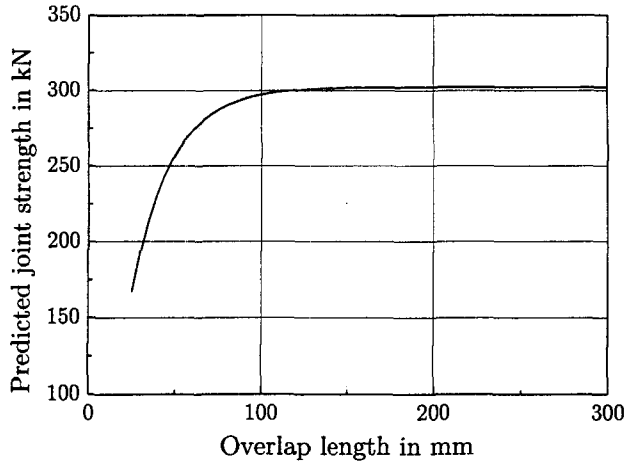

(a) DN$\frac{x}{2}\frac{5}{5}$

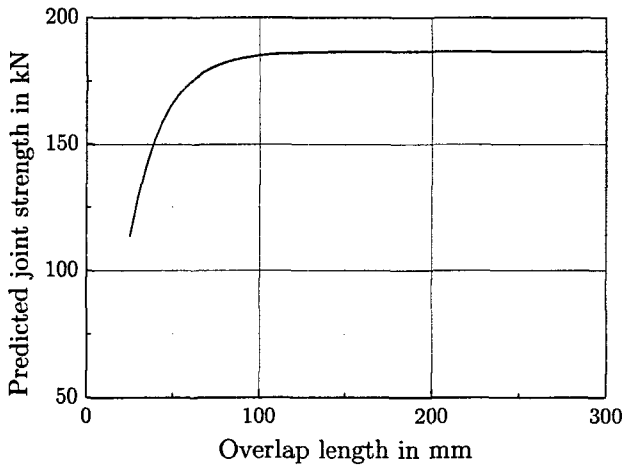

(b) DN$\frac{x}{2}\frac{5}{10}$

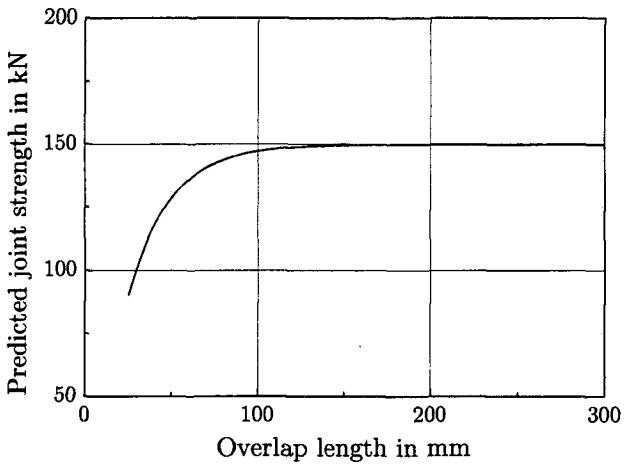

(c) DN$\frac{x}{2}\frac{10}{10}$

Figure 26.7.: Predicted strengths — $r_f = 1\,\text{mm}$ and $x \in [25; 300]$

27. Analytically based method

The prediction of the ultimate load of adhesively bonded joints as described in Chapter 24 is based on the determination of the peak of the $\mathfrak{R}$-function for all combinations of (τ_{xz}, σ_z) of the bonded overlap. This extremum lies close to the extrema of both $\tau_{xz}(x)$ and $\sigma_z(x)$.

It is tempting to try to analytically gather the extremum of at least one of the individual stress components and to formulate the other in function of the first one, in order to avoid the complicated FEA.

This Chapter suggests a simplified method to predict the strength of adhesively bonded joints based on existing analytical formulations.

It must be reminded at this point that the analytical solution does not allow the inclusion any deviation from idealized geometries (like chamfers, spews or similar).
It's use is therefore limited to special cases and is reproduced at this point simply for academic purposes, showing the agreement for such idealized boundary conditions with the method developed before on an FEA base.

One important fact not mentioned in any of the literature cited in the state-of-the-art (see Part II) is that for different adhesive layer thicknesses t_a **the only parameter having an influence on the ultimate load is the fillet radius** r_f of the adhesive fillet and that **there is no significant influence of the adhesive layer thickness** on the ultimate load.

It has been shown in the investigations described in Section 25 that **the value t_a, representing the adhesive layer thickness can be replaced by the value r_f, representing the radius of the adhesive fillet** as defined in Fig. 27.1.

27.1. Bonded double lap joints

This section gives a very condensed and adapted summary of the *Improved Theoretical Solutions for Adhesive Lap Joints* compiled[1] by M. Y. Tsai & al. in [9].

[1] All the equations presented there are based on previous works.

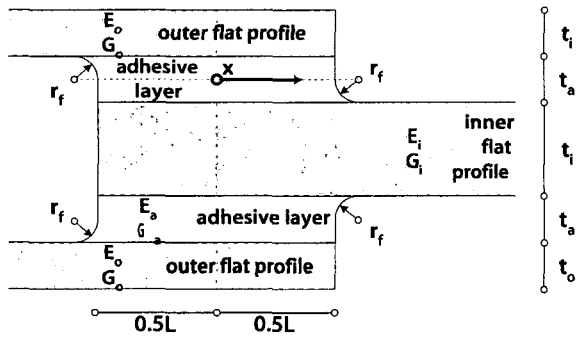

Figure 27.1.: Double lap joint

The shear stress in the adhesive layer τ_{xz}, has the following governing equation:

$$\tau_{xz}(x) = A\sinh(\beta x) + B\cosh(\beta x) \tag{27.1}$$

with

$$\beta^2 = \frac{\frac{G_a}{r_f}\left(\frac{2}{E_i t_i} + \frac{1}{E_o t_o}\right)}{\left[1 + \frac{G_a}{r_f}\left(\frac{t_i}{6G_i} + \frac{t_o}{3G_o}\right)\right]} \tag{27.2}$$

where, according to Fig. 27.1

E_i is the axial modulus of elasticity of the inner flat profile

E_o is the axial modulus of elasticity of the outer flat profile

E_a is the axial modulus of elasticity of adhesive

G_i is the shear modulus of the inner flat profile

G_o is the shear modulus of the outer flat profile

G_a is the shear modulus of the adhesive

t_i is the thickness of the inner flat profile

t_o is the thickness of the outer flat profile

t_a is the thickness of the adhesive layer

t_f is the depth of the failure layer inside the adherent

r_f is the radius of the adhesive fillet

ν is the Poisson's ratio

The values A and B can be determined by introducing $\tau_{xz,avg} = \frac{F}{2bL}$ as the average shear stress, L the length of the overlap and b the width:

$$A = \frac{\beta\frac{L}{2}\tau_{xz,avg}}{\cosh\beta\frac{L}{2}}\left[\frac{1-\frac{E_i t_i}{2E_o t_o}}{1+\frac{E_i t_i}{2E_o t_o}}\right] \qquad B = \frac{\beta\frac{L}{2}\tau_{xz,avg}}{\sinh\beta\frac{L}{2}} \tag{27.3}$$

The value $\tau_{xz}(x)$ is maximum for $x = \frac{L}{2}$ corresponding to the end of the overlap[2]: $\tau_{xz,max} = \tau_{xz}(\frac{L}{2})$.

27.1.1. BALANCED DOUBLE LAP JOINTS

For the further steps, a *balanced* double lap joint is assumed.

Balanced means:$t_i = 2t_o = t$, $E_i = E_o = E$ and $G_i = G_o = G$. The nomenclature relative to the adhesive remains unchanged.

For balanced double lap joints, TSAI gives is [9]:

$$\tau_{xz,max} = \frac{F}{2bL}\beta\frac{L}{2}\coth\beta\frac{L}{2} \tag{27.4}$$

with β

$$\beta = \sqrt{\frac{\frac{2G_a}{tEr_f}}{1+\frac{2G_a t}{3r_f G}}} \tag{27.5}$$

GATHERING THE OUT-OF-PLANE STRESS

Section 5.3 of [66] suggests, in Equation 5.17, a formulation based on previous publications (among them [13]) giving the maximum out-of-plane stress, $\sigma_{z,max}$:

$$\sigma_{z,max} = \tau_{xz,max}\sqrt[4]{3\left(1-\nu^2\right)\frac{E_a\cdot t}{E\cdot r_f}} \tag{27.6}$$

FROM THE STRESSES IN THE ADHESIVE TO THE STRESSES AT THE FAILURE LAYER

As stated in Part III, failure is not triggered at the interface of the adhesive to the FRP, but at a distance t_f inside the adherents.

It can be shown that the shear stresses do decrease following a parabolic law in the y-direction towards the center of the inner flat profile.
This is represented by Fig. 27.2 in a schematic manner.

[2]The variable $x \in [-\frac{L}{2}; +\frac{L}{2}]$ of the analytical formulations runs from the middle of the overlap. The shear stress distribution is assumed to be symmetric in regard to the middle of the overlap. Refer also to Fig. 27.1.

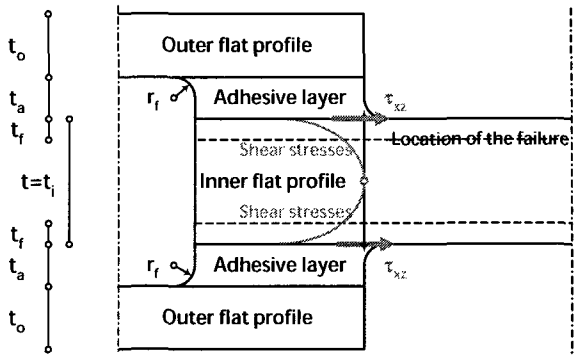

Figure 27.2.: Shear stresses vs. z

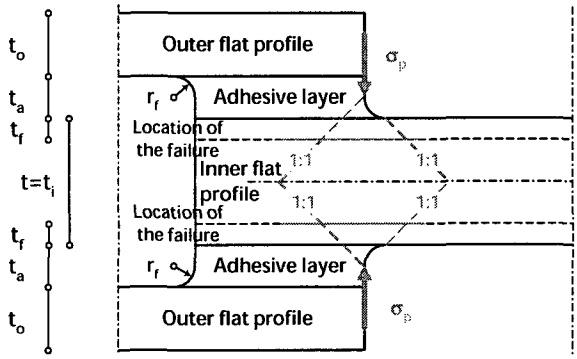

Figure 27.3.: Out-of-plane stresses vs. z

The following equations best represents the shear stresses at the depth t_f:

$$\tau_{xz,t_f} = \tau_{xz,max}\left(\frac{t-t_f}{t}\right)^2 \tag{27.7}$$

For the out-of-plane stresses, the decrease is best represented by a radiation of the stresses according to a 1:1 slope. This is represented by Fig. 27.3 in a schematic manner.
The following equations best represents the shear out-of-plane stresses at the depth t_f:

$$\sigma_{z,t_f} = \frac{\sigma_{z,max}}{2(r_f+t_f)} + \frac{\sigma_{z,max}}{2(2t-t_f+r_f)} \tag{27.8}$$

27.1.2. THE SIMPLIFIED METHOD FOR BALANCED DOUBLE LAP JOINTS

① Using Equation 27.4 it is possible get a sufficiently accurate prediction of the maximum shear stress τ_a in the adhesive layer;

② Equation 27.6 allows one to get the corresponding out-of-plane stress σ_{xz};

③ Both stresses can be used to estimate the stress level inside the inner flat profile using Equations 27.7 and 27.8;

④ The set of stresses τ_{xz,t_f} and σ_{z,t_f} has to be used as input data for Equation 24.1 on page 139.

The simplified method is therefore a cascading chain of equations described in Fig. 27.4 with the following input parameters:

① Basic joint geometry: thickness of the flat profiles and the adhesive layer and the overlap;

② Elastic material properties: axial E-moduli of the flat profiles, shear G-moduli of the flat profiles, the adhesive E-Modulus and the associated POISSON's ratio

③ Material strength data: the set of $\tau_{xz,u}$, $\sigma_{z,u}$, κ_τ and κ_σ

27.1.3. APPLICATION FOR BALANCED DOUBLE LAP JOINTS

To verify the suitability of the analytical formulæ some geometrical configurations will be checked by analytical and numerical means. The following 3 double lap joint configurations will be investigated:

① t_a=0.5 mm and r_f=0.5 mm;

② t_a=1.0 mm and r_f=1.0 mm;

③ t_a=2.0 mm and r_f=2.0 mm.

The mechanical properties of the materials involved are the following:

For the FRP:
E=33500 MPa
G=0.1 E
$t_i = 2t_o$=10 mm
FRP resistance defined in Chapter 23.2.

For the adhesive:
G=1750 MPa[3].

As is can be seen from Fig. 27.5, the results gathered though the analytical method correlate well with those obtained though the FEA based results.
The simplified analytical method delivers good results for the balanced double lap joints, at least within the range of the investigated geometrical parameters.

27.1.4. CONCLUSIONS

The simplified analytical prediction method described by Fig. 27.4 allows the determination of double lap joint strengths for idealized geometries. The method is a good tool for quickly pre-dimensioning idealized balanced double lap joint configurations. Deeper investigations should then rely on the FEA based method.

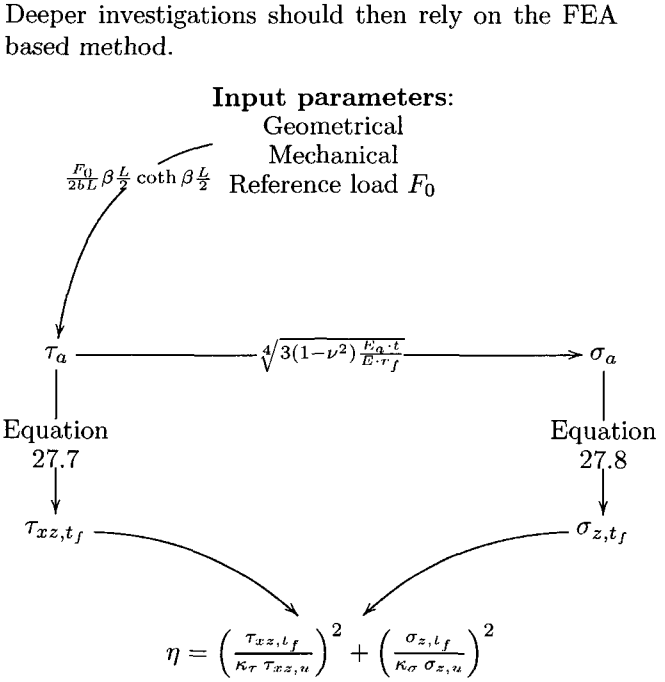

Figure 27.4.: Diagram showing the simplified prediction method

[3] Based on E=4450 MPa and ν=0.3.

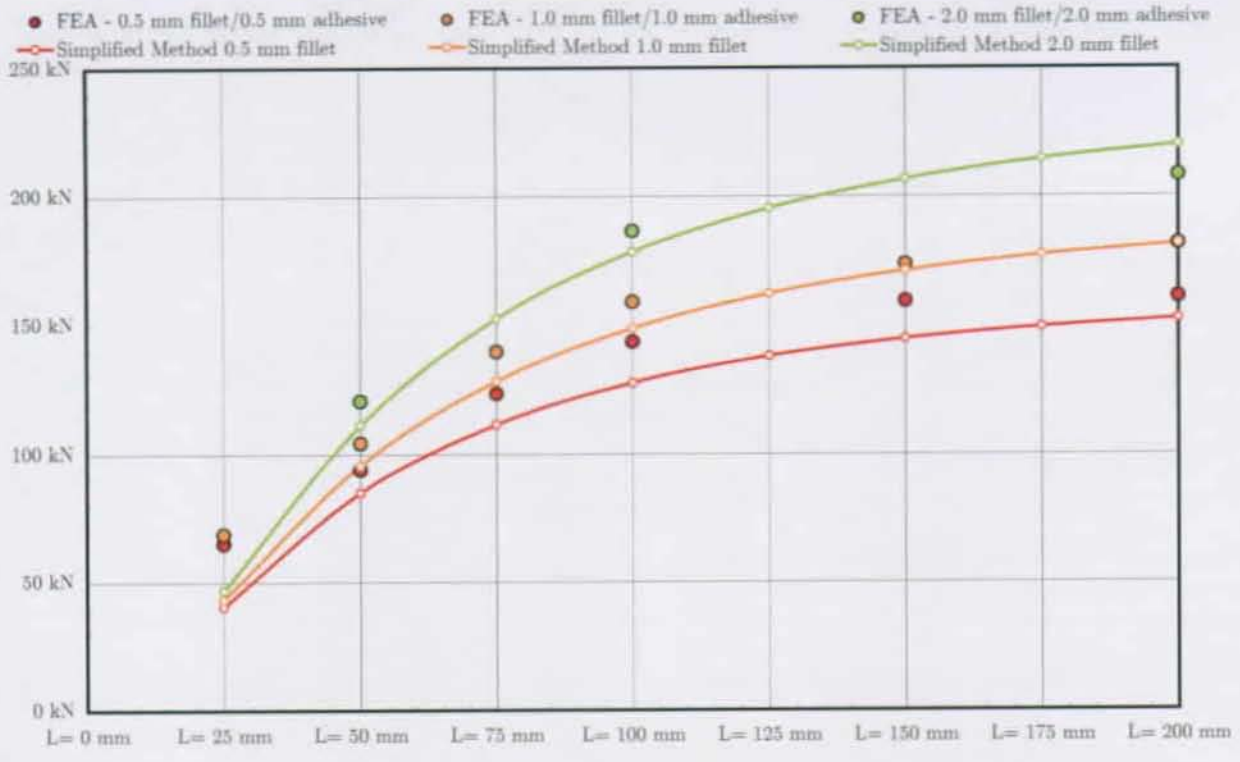

Figure 27.5.: Prediction of balanced double lap joint strengths using FEA and the simplified analytical method — refer to Section 27.1.3 for more details

27.2. Bonded single lap joints

This section gives a very condensed summary of [9].

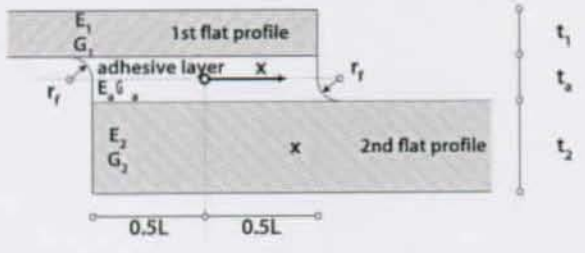

Figure 27.6.: Single lap joint

The shear stress in the adhesive layer τ_{xz} has the following governing equation[4]:

$$\tau_{xz}(x) = A\sinh(\beta x) + B\cosh(\beta x) \tag{27.9}$$

with

$$\beta^2 = \frac{\frac{G_a}{r_f}\left(\frac{1}{E_1 t_1} + \frac{1}{E_2 t_2}\right)}{\left[1 + \frac{G_a}{r_f}\left(\frac{t_1}{3G_1} + \frac{t_2}{3G_2}\right)\right]} \tag{27.10}$$

[4]The variable $x \in [-\frac{L}{2}; +\frac{L}{2}]$ of the analytical formulations runs from the middle of the overlap. The shear stress distribution is assumed to be symmetric in regard to the middle of the overlap.

where

E_1 is the modulus of elasticity of flat profile 1

E_2 is the modulus of elasticity of flat profile 2

G_1 is the shear modulus of flat profile 1

G_2 is the shear modulus of flat profile 2

G_a is the shear modulus of the adhesive

t_1 is the thickness of flat profile 1

t_2 is the thickness of flat profile 2

t_a is the thickness of the adhesive layer

r_f is the radius of the adhesive fillet

27.2.1. Balanced single lap joints

For the further steps, a *balanced* single lap joint is assumed. Balanced means that flat profile 1 and flat profile 2 are the same: $\rightsquigarrow t_1 = t_2 = t$, $E_1 = E_1 = E$ and $G_1 = G_2 = G$. The nomenclature relative to the adhesive remains unchanged.

For balanced single lap joints, the expression for β is then:

$$\beta = \sqrt{\frac{\frac{8G_a t}{E r_f}}{1 + \frac{2G_a t}{3 r_f G}}} \tag{27.11}$$

The maximum shear stress in the adhesive layer should consequently be:

$$\tau_{xz} = \frac{F}{bL}\beta\frac{L}{2}\coth\beta\frac{L}{2} \tag{27.12}$$

But instead[5], the following expression is suggested in [9]:

$$\frac{\tau_{xz,max}}{\tau_{xz,avg}} = \frac{1}{4}\left[\frac{\beta\frac{L}{2}}{t}(1+3k)\cdot\coth(\beta\frac{L}{2t})+3(1-k)\right] \tag{27.13}$$

where $k = \frac{2M_o}{Ft}$, $\tau_{xz,avg} = \frac{F}{bL}$ and F the applied axial load.

Though no indication is given on how to gather the value of the moment, M_o acting at the end of the overlap, a first logical estimation would be to set $M_o = F \cdot \frac{t+t_a}{2}$, leading to $k = \frac{t+t_a}{t}$. In Section 21 it has been shown — by the means of the FEM — that the bending moment M_o at the end of the overlap is very dependent of the free length as defined in the same section, so that it is not only dependent on t and t_a. The first approximation of $M_o = F \cdot \frac{t+t_a}{2}$ is therefore too basic to be used.

CRITICISMS

In fact, the value of M_o is strongly dependent on the *whole* geometry of the bonded element considered, including the *free length* of the connected flat profiles and their boundary conditions.

All these parameters are not explicitly part of the input values of Equations 27.11 and 27.13. They *might* be implicitly be included in a realistic estimation of M_o — which is a subparameter of Equation 27.13.

As long as no indication based on the whole joint geometry and mechanics is given, one has to consider the analytical approach described as not being useful for *engineer-adapted dimensioning* purposes.

[5]The parameter β from Equation 27.11 has no physical dimension, letting the argument $\beta\frac{L}{2}$ of the function coth having the dimension of a length, which seems illogical.
This contradiction is not observed in the expression of β for the double lap joint, where — according to Equation 27.5 — β has the dimension $\frac{1}{L}$, so that the argument $\beta\frac{L}{2}$ remains free of any dimension. This ambiguity has been avoided in Equation 27.13 by "adding" the term $\frac{}{t}$ in the argument of coth.

27.2.2. GATHERING THE OUT-OF-PLANE STRESS

Section 5.3 of [66] suggests a set of formulations expressing the maximum out-of-plane stress, $\sigma_{z,max}$ based on a factor λ defined by:

$$\lambda = \frac{L}{2t}\sqrt[4]{\frac{6E_a\cdot t}{E\cdot t_a}} \tag{27.14}$$

For $\lambda > 2.5$

$$\frac{\sigma_{z,max}}{\sigma_x} = \frac{k}{2}\sqrt{\frac{6E_a\cdot t}{E\cdot t_a}} + k'\frac{t}{\frac{L}{2}}\sqrt{\frac{6E_a\cdot t}{E\cdot t_a}} \tag{27.15}$$

where

$$k = \frac{\cosh u_2\frac{L}{2}\cdot\sinh u_1\frac{L}{2}}{\sinh u_1 L\cdot\cosh u_2\frac{L}{2}+2\sqrt{2}\cosh u_1 L\cdot\sinh u_2\frac{L}{2}}$$

$$k' = k\frac{\frac{L}{2}}{t}\sqrt{\frac{3(1-\nu^2)\sigma_x}{E}}$$

$$u_1 = 2\sqrt{2}u_2$$

$$u_2 = \frac{1}{t\sqrt{2}}\sqrt{\frac{3(1-\nu^2)\sigma_x}{E}}$$

$$\sigma_x = \frac{F}{bt}$$

ν is the POISSON's Ratio of the adherend

For $\lambda \leq 2.5$, the following expression is suggested:

$$\frac{\sigma_{z,max}}{\sigma_x} = \lambda^2\frac{k}{2}\frac{\sinh 2\lambda - \sin 2\lambda}{\sinh 2\lambda + \sin 2\lambda} - \lambda k'\frac{\cosh 2\lambda + \cos 2\lambda}{\sinh 2\lambda + \sin 2\lambda} \tag{27.16}$$

For the purpose of an *Structural Design Method for Adhesively Bonded Joints of Pultruded GFRP Shapes* with realistic geometric and mechanical specifications, only the case $\lambda > 2.5$ is considered, so that Equation 27.15 is required.

CRITICISMS

Basically the same criticisms as formulated in the paragraph related to the analytical formulation of the maximum shear stress are valid.

But beyond that, some additional critics can be made. The main one is related to the factor needed k' which includes σ:
σ is the actual axial stress in the flat profiles *outside* the joint area — which should be $\sigma_x = \frac{F}{bt}$ — depending on given load. Because σ_x appears in combination with E, the expression $\frac{\sigma}{E}$ does not lead to any dimension inconsistencies. But having the expression of an actual self defined load level, F in the algorithm for the determination of the failure load, F_u of adhesively bonded single lap joints leads necessarily to a kind of

iterative method[6].
No one can argue that iterative solutions are not suited — civil engineering has many of examples of iterative solution for specific problems, but they are then openly declared as such. In this specific case, the presented algorithm cannot avoid raising the suspicion of an *unfinished* solution.

27.2.3. CONCLUSION

As stated in the two previous criticisms, the Author considers that the analytical formulations for determining the shear stress τ_{xz} and the corresponding out-of-plane stress σ_z in the adhesive layer of single lap joints are not adapted for serious engineering applications.
The reasons for that lie in the strong dependency of these stresses from geometrical factors not taken into account by the formulæ listed before. Among these factors the more important are those leading to the correct expression of the moment, M_o at the end of the overlap.
But even an independent determination of this expression does not fix the problem, so that engineers can only rely on modeling the whole joint using FEA. It should be emphasized that correct results can only be obtained by modeling the complete joint, including the realistic boundary conditions.

APPENDIX TO THE SINGLE LAP TOPIC

Several authors have already outlined the difficulties described above concerning the accurate estimation of the edge moment M_o. One paper ([10] by M. Y. TSAI & J. MORTON) summarizes all of these issues by first comparing different approaches, showing their — obvious — limitations and suggesting the n^{th}*improvement* based on the three major theories of adhesively bonded single lap joints:

① GOLAND & REISSNER's *Stresses in Cemented Joints* [5];

② HART-SMITH's *adhesively bonded Single-Lap Joints* [12] and

③ OPLINGER's approach, the *layered beam theory for single lap joints* [96], a patchwork of equations based on several to determine parameters — *still limited to an overlap with a relatively thin and flexible adhesive*[7].

It is the Author's opinion that reproducing these equations would not lead to the Development of a *Structural Design Method for Adhesively Bonded Joints of Pultruded GFRP Shapes* because of the complexity of the procedure described.

[6] A loop of the kind *Give an F, calculate F_u, readjust F, recalculate F_u... up to self defined convergence criterion.*

[7] According to M. Y. TSAI & J. MORTON — based on comparisons between these formulæ and a carried out FEA.

28. SCOPE OF APPLICATION

28.1. ACTUAL SCOPE OF APPLICATION

28.1.1. GENERAL REQUIREMENTS

The following are the requirements for the direct application of the STRUCTURAL DESIGN METHOD FOR ADHESIVELY BONDED JOINTS OF PULTRUDED GFRP SHAPES:

① Axially loaded single and double lap joints of pultruded FRP flat profiles under short term static load;

② Almost linear mechanical properties.

The following is explicitly excluded:

① Joints subjected to non-neglectable bending moments;

② Joints subjected to extreme environmental conditions (temperature, humidity etc);

③ Joints subjected to fatigue relevant loads.

ADHERENT SPECIFICATION

The adherents are considered to be of pultruded G-FRP.
The material is considered as to be orthotropic with an almost linear mechanical behaviour in the range of the expected stresses.

The following material properties are needed and have to be gathered:

① Axial Elasticity Modulus, E_x within the range of the expected stresses;

② Out-of-plane Elasticity Modulus, E_z within the range of the expected stresses;

③ Shear Modulus G_{xz};

④ The material strength related to combinations of τ_{xz} and σ_z[1], see Section 17.

[1]The material interaction diagram.

ADHESIVE SPECIFICATION

The adhesive has to be considered as being isotropic. The adherend should behave linearly within the range of the expected range of stresses.

The following adhesive properties are needed and have to be gathered:

① Axial Elasticity Modulus, E_x within the range of the expected stresses

② Shear Modulus, G_{xz}.

28.2. EXTENDING THE SCOPE OF APPLICATION

28.2.1. CONNECTING OTHER THAN FLAT PROFILES

A special case of unbalanced double lap joints is the **connection of two axially loaded shapes** (for example I or □ shapes, see Fig. 28.1) **not subjected to bending moments in the joint area.**

Basically the same procedure as for double lap joints has to be followed.

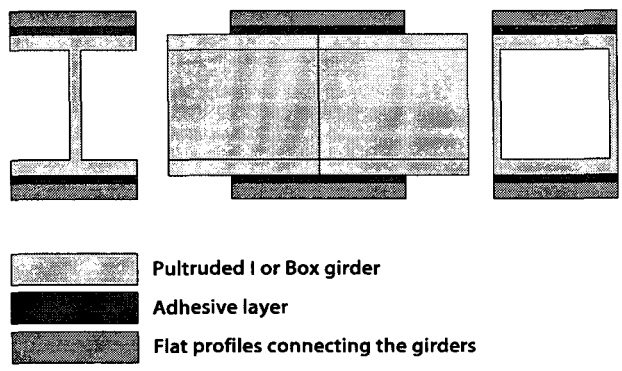

Figure 28.1.: Connecting two I or □ shapes

28.2.2. USING MECHANICAL NON-LINEAR ADHESIVES

Using mechanically non-linear adhesives, some changes are necessary to adapt the STRUCTURAL DESIGN METHOD FOR ADHESIVELY BONDED JOINTS OF PULTRUDED GFRP SHAPES.

The main change is due to the fact that loosing the linearity of the structural response of the system, solutions can no longer be obtained using the rule of proportion used with linear behavior.

EFFECT ON THE STRESS DISTRIBUTION

Both shape of the out-of-plane, $\sigma_z(x)$ and shear stresses, $\tau_{xz}(x)$ are dependent on the load level F_x. For two different loads F_i and F_j the corresponding functions, $\sigma_{z,i}(x)$ and $\sigma_{z,j}(x)$, respectively $\tau_{xz,i}(x)$ and $\tau_{xz,j}(x)$, are no longer homothetic[2] to each other.

EFFECT ON THE κ-FACTOR

The κ-factors needed to describe the material resistance inside the adhesively bonded joints in function of the interaction diagram are dependent on the shape of the corresponding σ_z- and τ_{xz}-plots.
Because the shape of these functions changes with non-linear adhesives, the κ-factors are dependent on the level of the axial load F_0.

CONSEQUENCES FOR THE SOLUTION

In general, a nonlinear equation cannot be solved without some numerical method to approximate the solution to the equation.
The solution has then to be gathered by iterative means. The easiest way would be to simply solve the problem with nested intervals.

28.2.3. EXTREME ENVIRONMENTAL CONDITIONS

In the frame of this Thesis, the material dependent interaction diagram was gathered under normal environmental conditions, allowing therefore the determination of lap joint strength at corresponding conditions.

It should be possible to gather the same interaction diagram under differently defined environmental conditions, allowing by this the prediction of lap joint strengths under these conditions.

[2] Two figures are *homothetic* if they are related by an expansion or geometric contension.

Conclusion

Oublie tes démonstrations. Je n'écoute pas ton discours, mais ta voix.

Nicolas Gomez Davila

29. Conclusion

Predicting the strength of adhesively bonded connections is an important step towards the spread of pultruded shapes in civil engineering applications.

This Thesis investigated means to dimension axially loaded **adhesively bonded** single and double **lap joints of pultruded shapes**. Such connections **have to be considered as being superior to the bolted and riveted connections** traditionally used and recommended — which was to some extent demonstrated by experimental investigations carried out by the Author.

The strength of adhesively bonded connections was experimentally investigated. The influence of major geometrical parameters has been identified. Besides this, **a closer look at the mechanisms leading to failure was made possible by using a high-speed camera.**

The load transfer inside double lap joints was investigated on well instrumented specimen: up to 40 strain gauges were used to experimentally determine the axial strain development along the bonded splice. These results were compared by FEA and a good agreement has been found. **Such direct comparisons between experimental and numerical methods were not documented before on such specimen in this quality.**

The influence of chamfering as a stress reduction method was also investigated. Such measures were previously recommended to enhance the bearing capacity of bonded joints. Due to their stress reduction action, it seemed logic to think so.
The carried out experimental investigations in the frame of this Thesis demonstrated that these measures do not have a significant effect when used in combination with pultruded FRP. This is also the first time that such a study is documented.
All previous publications did predictions at the stress level and deduced an increase in lap joint strength without ever checking their assumptions on an experimental basis.

The determination of the stress-state inside axially loaded bonded lap joints has been widely investigated since the 1930's, first on analytical and then on a numerical level. But very little experimental work to check the validity has been carried out.
This Thesis fills this gap by showing that **relatively simple numerical models are accurate enough to predict the stress-strain state inside adhesively bonded joints of pultruded FRP.**

The Thesis also shows that analytical formulations for double lap joints are accurate — if restricted to some idealized systems — to be used for predimensioning purposes, while it has been shown that this is not valid for single lap joints.

For the determination of the material dependent strength data, a new device was designed and manufactured: **the CCLab Tensile-Shear Device.**
This device is the first known device able to quantify the material's resistance for any combination of shear and out-of-plane stresses, the two stress components triggering failure.
The device was successfully used to determine this data for the FRP material used in the experimental investigations and lead to the **formulation of a material failure criteria in the form of a relatively simple mathematical formula.**

Considering the statistical aspect in parallel to gathering the material strength data lead to the formulation of material related partial safety factors, which have to be considered as an important part of any modern dimensioning concept.

By combining the knowledge about stress determination and material resistance, **it was possible to formulate a method of predicting the ultimate load of axially loaded adhesively bonded joints of pultruded shapes.**
The accuracy of this method has been verified on a large amount of individual geometrical configurations. **The prediction method is accurate enough to predict joints of pultruded flat profiles commonly produced and used in civil engineering applications under static and short term axial loads.**

The STRUCTURAL DESIGN METHOD FOR ADHESIVELY BONDED JOINTS OF PULTRUDED GFRP SHAPES was also used to investigate the effect of spews and radius fillets.
It was found that — in the range of engineer relevant geometrical configurations — **the influence of the adhesive layer is quite negligible. This is the first time that this effect was reported and experimentally and numerically verified.**

A very important parameter determining the lap joint strength is the shape and the size of spews and round fillets at the end of the adhesive overlap. **The influence of the size of radius fillets has been investigated on both experimental and numerical level, leading to an important adaptation in some formerly recognized analytical formulæ.**

30. SUGGESTIONS FOR FURTHER RESEARCH

As the research described in this Thesis applies only to adhesively bonded joints under static axial loads and under normal environmental conditions, it would be interesting to extend the investigations to long-term and fatigue loads and to extreme environmental conditions like high temperature and/or humidity.

It is known that temperature and humidity have a considerable influence on lap joint strength.
Basically the investigations carried out could relatively simply be extended to other environmental conditions. The resistance data for environmentally conditioned pultruded FRP material could be gathered using the CCLAB TENSILE-SHEAR DEVICE.

Single and double lap joints like those investigated in the frame of this Thesis are just one possibility of bonding pultruded elements together. To built-up frames, it is necessary to dimension joints including other kinds of stresses — like shear stresses from torsion. The investigation of such joints is therefore a major issue to widen the possibilities offered by adhesiv bonding.

The investigations carried around the bonded and bolted joints showed that combining adhesive bonding in combination with torqued bolts leads to an important increase in lap joint strength. But because these investigations were also carried out under short time loads, the results cannot be yet generalized. Especially the topic of the FRP creep under the torqued bolts — and the associated loss of prestress — should be investigated in a deeper study.

The long-term behaviour of adhesively bonded joints of pultruded profiles is also an under-investigated research field. In the frame of this Thesis, a couple of specimen were left — unintentionally, for technical reasons — for longer than 60 minutes in the testing machine under a load below their theoretical strength. Some failed under this lower load showing by this that the strength is already reduced after relatively short times. Because no systematic investigation was made, it cannot serve as a proof but gives some valuable indication.
Two aspects are of interest considering the long-term behaviour: the creep and the strength:

- Only epoxy was investigated as an adhesive. For epoxy bonded joints, creep is probably not a problem, but other adhesive might be more sensitive to creep. The creep behaviour of the pultruded material is also not yet clarified.
- Concerning the long term strength of all involved components, nothing can be said at this moment.

The whole issue of creep would need the planning a new series of lap joint experiments to show the tendencies.

The strength of bonded lap joints of pultruded profiles under fatigue is also an important issue, especially for bridge construction.
First investigations made by T. TIRELLI in [63] and [64] tend to the assumption that fatigue is not a very critical issue, but research has just began.

Two issues much closer to the topic of this Thesis should also be investigated deeper:

- It would be very interesting to gather by theoretical means of fracture mechanics the factors κ_τ and κ_σ necessary to adapt the material resistance as gathered by the CCLAB TENSILE-SHEAR DEVICE to the conditions of the lap joints.
- Another point is that the failure criteria investigated in the frame of this Thesis was based on pure FRP failure. The research highlighted the fact that stress reduction methods like chamfering or bigger adhesive fillets did not lead to the expected **important** increase in the ultimate load of the bonded lap joint. Especially the issue of bigger fillets or spews should theoretically lead to an increase in ultimate loads according to the STRUCTURAL DESIGN METHOD FOR ADHESIVELY BONDED JOINTS OF PULTRUDED GFRP SHAPES developed in the frame of this Thesis, indicating by this that the strength of the adhesive fillet has to be taken into account.
  This effect was described and interpretated without going deeply in the mechanics of the joint[1].

[1] Further investigations have been carried out by Y. ZHANG in [88], but it is the Author's opinion that much more work should be done in this field to be able to predict the effect of spews on the strength of bonded lap joints.

Appendix

Reports that say that something hasn't happened are always interesting to me because, as we know, there are known knowns; there are things we know we know. We also know there are known unknowns; that is to say we know there are some things we don't know.

D. Rumsfeld

Appendix A.

Nomenclature

A.1. Notations

The following nomenclature was used:

$\ldots_x$ Subscript for the axial x axis

$\ldots_y$ Subscript for the transverse y axis

$\ldots_z$ Subscript for the out-of-plane z axis

$\ldots_u$ Subscript for ultimate

$\ldots_k$ Subscript for characteristic values

$\ldots_d$ Subscript for design values

$\ldots_{max}$ Subscript for maximum

A_i Cross-sectional area

L Geometrical dimensions length

r Geometrical dimensions radius

t Geometrical dimensions thickness

b Geometrical dimensions width

E_i Modulus of elasticity in tension or compression

G_{ij} Modulus of elasticity in shear

ν Poisson's ratio

F_i Forces in i-axis

σ_i Axial Stresses

τ_{ij} Shear stresses

ε_i Axial strain

γ_{ij} Shear strain

κ_α Factors for material resistance related to the stress α

$\hat{.}$ Denotes experimental gathered FRP material resistances in the sample

$\tilde{.}$ Denotes the mathematical formulation of FRP material resistance in the sample

$\mathfrak{F}$ FRP material resistance failure criteria

$\mathfrak{R}$ Material resistance failure criteria in lap joints

γ_d Partial safety factor for material

A.2. Specimen denomination

The following section is intended to give an overview of the general nomenclature system used to describe the experimentally investigated specimen.
The following denomination system was used:

$$XY\frac{over}{adh}\frac{outer}{inner}\alpha^e \tag{A.1}$$

where:

X describes if the specimen is a single S or double D lap joint

Y describes if the outer flat profiles were not (N), slightly (S) or (F) fully chamfered;

over stands for the length of the bonded overlap;

adh stands for the thickness of the adhesive layer;

outer for the thickness of the outer flat profile;

inner stands for the thickness of the inner flat profile;

α designates the number of the individual specimens; if experimentally investigated within a series of identical specimen configurations:

^{e} if the specific specimen was instrumented with strain gauges, this symbol is used.

For example $\mathrm{DN}\frac{100}{3}\frac{3}{6}1^e$ designates a non chamfered double lap joint with an overlap of 100 mm, an adhesive thickness of 3 mm, outer flat profiles 3 mm thick and an inner flat profile 6 mm thick. Within the range of similar specimens, it was the first one experimentally investigated and this specimen was instrumented.

Because all experimental investigations where carried out using the SikaDur 330 as adhesive, no need for adding this information is necessary.

Stress designation

The drawings on the next page, Fig. A.2, define the designation and orientation of stresses in the considered systems.

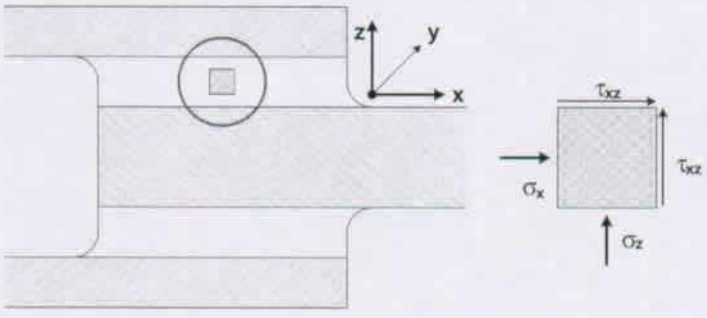

Figure A.1.: Nomenclature related to the axes and stresses

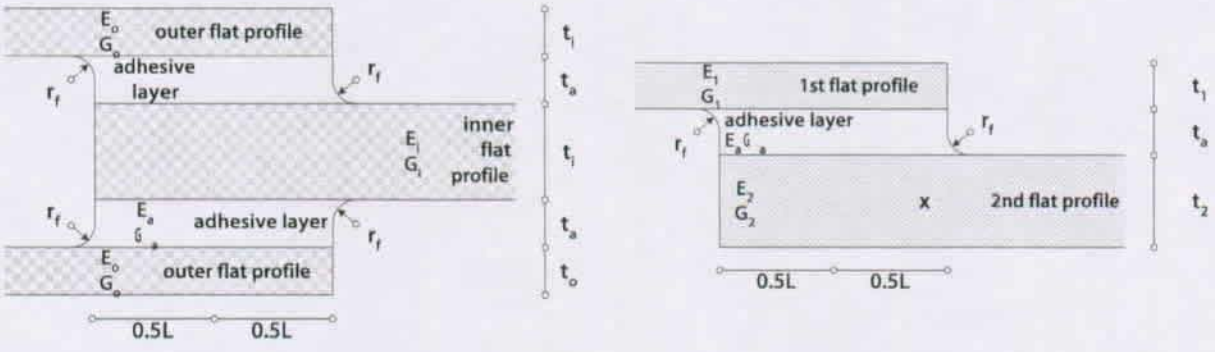

(a) Double lap joint

(b) Single lap joint

Figure A.2.: Nomenclature related to the lap joints

Appendix B.

Experimental determination of the axial E-Moudli and Strength of the used flat sheets

B.1. General experimental description

The flat profiles had the dimensions 500×100 mm (see Fig. B.3).

Reinforcing tabs[1] of the same material were glued with epoxy to the top and bottom area where the specimens were fixed to the experimental machine. Strain gauges were fixed on the specimens as illustrated in Figs. B.1 and B.3 to measure the axial extensions ε_x and ε_y. The gauges were of the same type as in the experimental series described in Part III.

As in the experiments described in Part III, the experimental device was a Schenck Hydropuls-Zylinder Typ PL.

B.1.1. Fiberline's datasheet

Fiberline's related design manual [67] gives general values that are not differentiated by material thickness, see Tab. B.1.

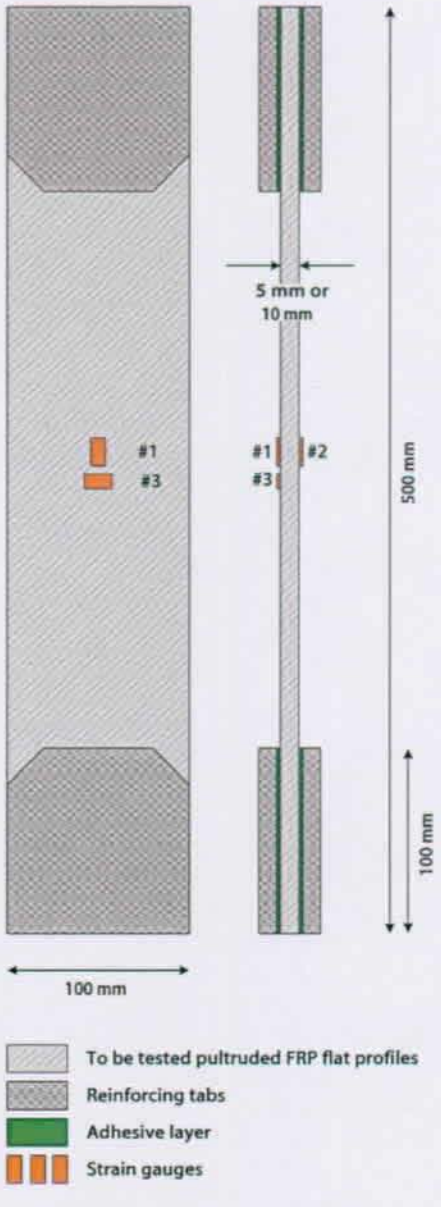

Figure B.1.: The experimental specimen

[1] The geometry of the reinforcing tabs was selected according to [89].
As it can bee seen in Fig. B.3, these tabs did not really lead to a failure outside the tabbed area: they were useless. The material's ultimate stress might therefore be higher than those measured, but the results relatively to the axial E-Moduli remain valid.

(a) Before experimentally investigating

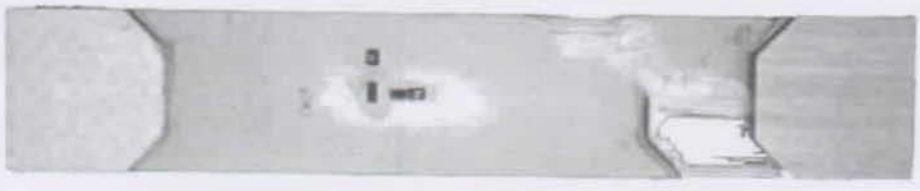

(b) After experimentally investigating

Figure B.3.: Shape of the specimen used to gather the axial E-Modulus

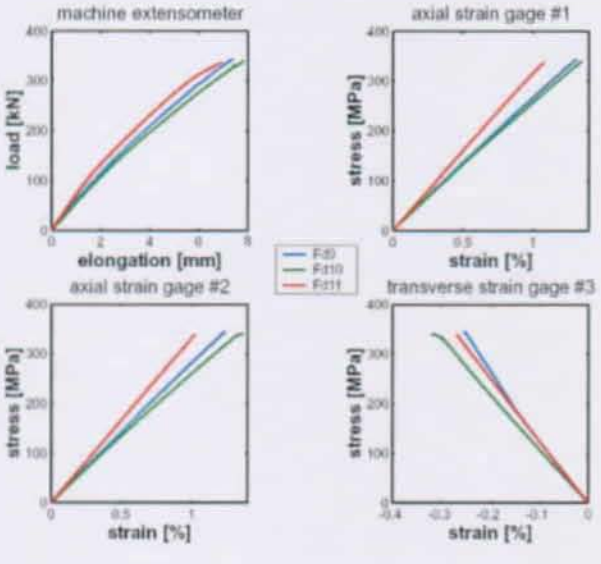

Figure B.2.: Typical plots

Flexural strength [MPa] $f_{b,0°}$	240
Flexural strength [MPa] $f_{b,90°}$	100
Tensile strength [MPa] $f_{t,0°}$	240
Tensile strength [MPa] $f_{t,90°}$	50
Compressive strength [MPa] $f_{c,0°}$	240
Compressive strength [MPa] $f_{c,90°}$	70
Modulus of elasticity [MPa] $E_{0°}$	23 000
Modulus of elasticity [MPa] $E_{90°}$	8 500
Modulus in shear [MPa] G	3 000
Poisson's ratio [MPa] $\nu_{0°90°}$	0.23
Poisson's ratio [MPa] $\nu_{90°0°}$	0.09

Table B.1.: Mechanical properties of the Fiberline-profiles according to their manufacturer's design manual [67]

The self-gathered values are quite different from the material property values given by Fiberline. The reason is that the values from Fiberline were determined by bending experiments and not by tensile experiments. Therefore the difference between the tensile Modulus and the flexural Modulus as well as the difference between the two ultimate strengths gathered by both different methods seem to be quite big.

Such experimental investigations on deep I-shaped pultruded beams have been carried out by A. Zureick, L. F. Kahn & B. J. Bandy and documented in [90].

In this experimental investigation, the authors gathered the axial elastic modulus, E_x and the shear modulus, G_{xy} by carrying out 4-point bending tests of pultruded I-beams through approximated engineering equations. Strain gauges measured the strain distribution over the height of the beam to give additional data.

The Author considers this approach as being inferior to a direct method.

B.1.2. Experimental results

The results of the investigations carried out are displayed in both Tables B.2 and B.3.

The load-deformation and load-extension diagrams as gathered — and displayed for selected specimens in Fig. B.2 — are almost linear up to failure. This complies with the results and theoretical considerations of R. Haj-Ali et al. in [19] and [20] for a force acting axially[2].

[2] With an angle of $\theta = 0°$ referring to the nomenclature used in [19].

#	F_u [kN]	$\sigma_{x,u}$ [MPa]	E_x [MPa]	ν [-]	Δ_{max} [mm]
①	163	326	28 913	0.28	6.78
②	210	420	34 032	0.29	6.95
③	228	456	33 592	0.30	7.08
④	227	454	34 392	0.28	6.73
⑤	215	430	33 929	0.24	11.85
⑥	222	444	34 549	0.30	11.92
⑦	215	430	33 947	0.27	11.58
⑧	218	436	35 551	0.29	12.37
⑨	200	400	34 788	0.28	11.00
m	217	332	**34 348**	0.28	10.00
σ	9.2	18.4	**620**	0.02	2.53

Table B.2.: Experimental results for gathering the axial Modulus of elasticity of the 5 mm flat profiles

#	F_u [kN]	$\sigma_{x,u}$ [MPa]	E_x [MPa]	ν [-]	Δ_{max} [mm]
①	332	332	34 077	0.29	5.57
②	346	346	30 586	0.28	5.72
③	359	359	32 700	0.27	5.95
④	315	315	31 147	0.23	5.13
⑤	324	324	31 147	0.27	5.03
⑥	322	322	33 184	0.26	5.18
⑦	334	334	33 956	0.27	5.58
⑧	329	329	33 191	0.26	5.16
m	332	332	**32 525**	0.27	5.41
σ	14.2	14.2	**1 330**	0.02	0.33

Table B.3.: Experimental results for gathering the axial Modulus of elasticity of the 10 mm flat profiles

Appendix C.

Experiments on Adhesives

C.1. Experimental investigations

Experimental investigations in tension and compression have been performed on small sized specimen (displayed in Fig. C.1) made of bulk of both SikaDur 330 and SikaForce 7851 adhesive in order to gather basic mechanical properties.

The following standards were applied: ISO 527[1] and ASTM D-695-96[2]

This experimental investigation is documented by J. de Castro in [92].

The results of the experimental investigations are shown as load-displacement curves in Figs. C.2 to C.5 and listed in Tabs. C.1 and C.2.

	E_x [MPa]	$\varepsilon_{x,u}$ [%]	$\sigma_{x,u}$ [MPa]
Traction	4 550	0.97	≈ 39
Compression	≈ 3000	9.65	80.7

Table C.1.: The main mechanical properties of the SikaDur 330

	E_x [MPa]	$\varepsilon_{x,u}$ [%]	$\sigma_{x,u}$ [MPa]
Traction	398	22.84	≈ 14
Compression	≈ 300	67.98	128.7

Table C.2.: The main mechanical properties of the SikaForce 7851

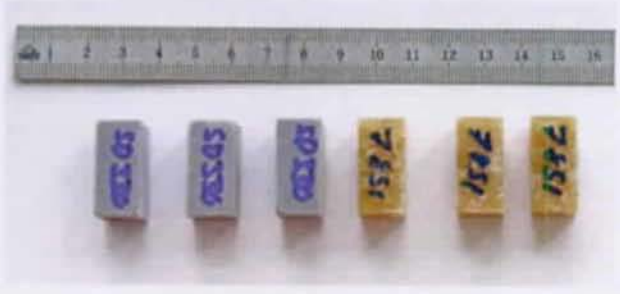

(a) Compression experiments

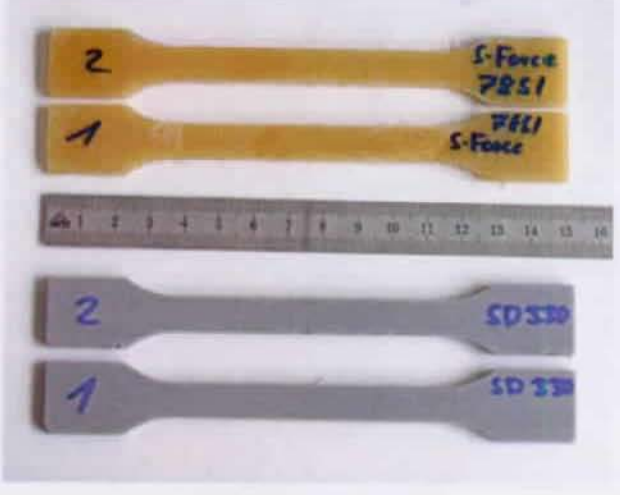

(b) Traction experiments

Figure C.1.: Adhesive specimen

[1] Axial tensile ultimate stress.
[2] Axial compressive ultimate stress.

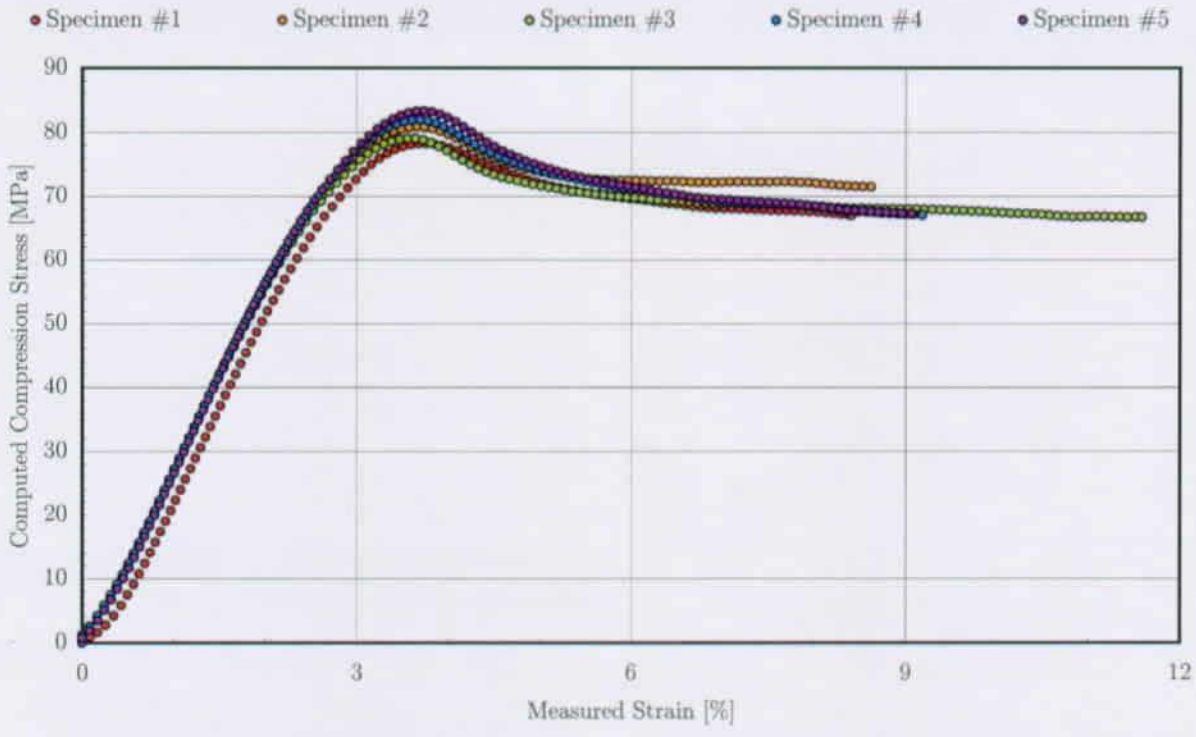

Figure C.2.: Compression experiments SikaDur330

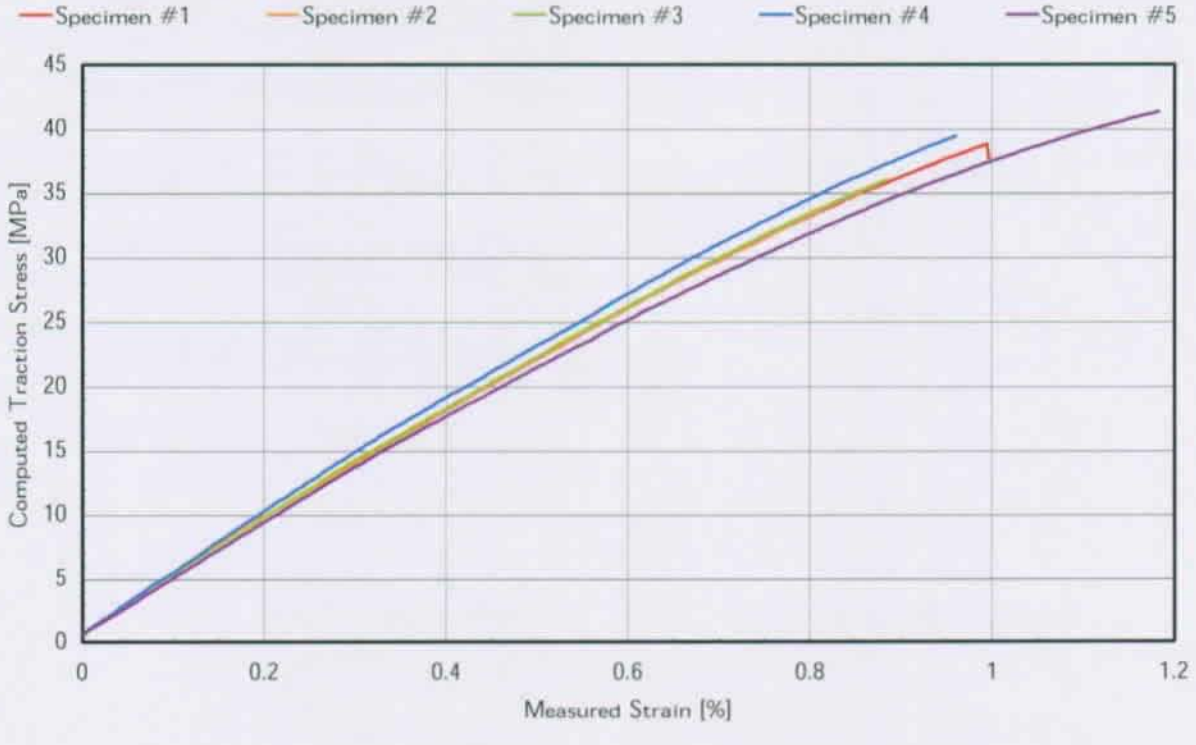

Figure C.3.: Traction experiments SikaDur330

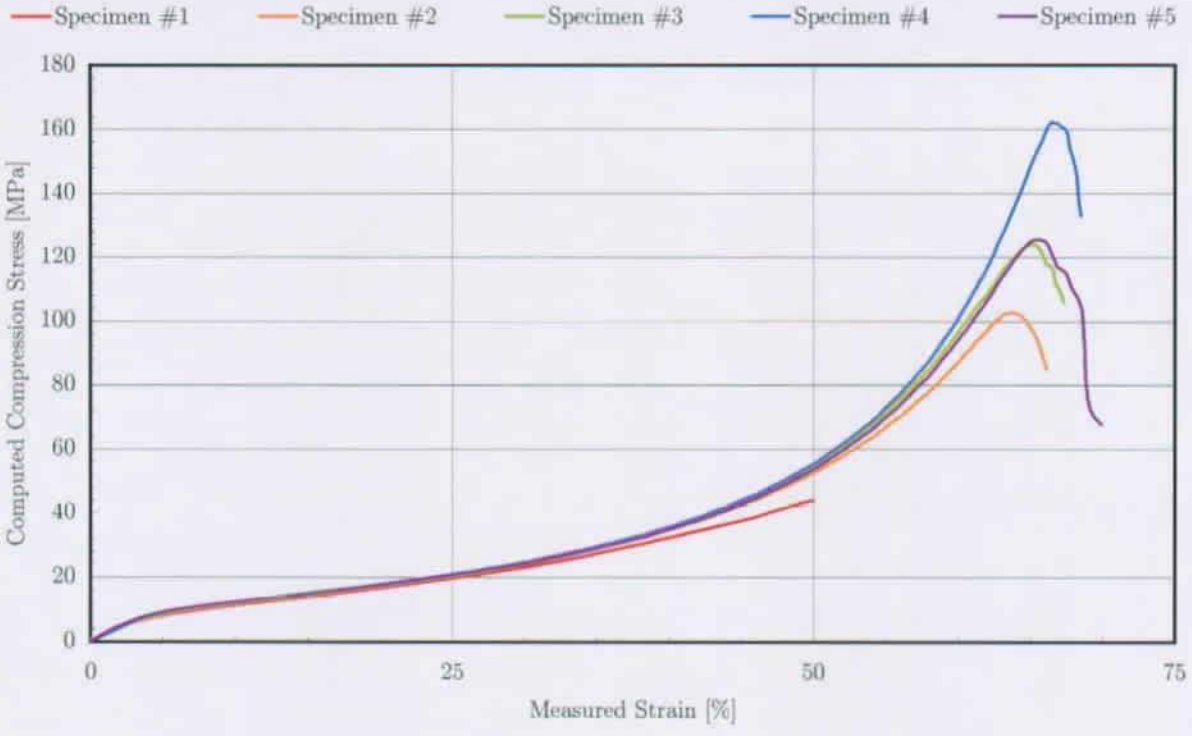

Figure C.4.: Compression experiments SikaForce 7851

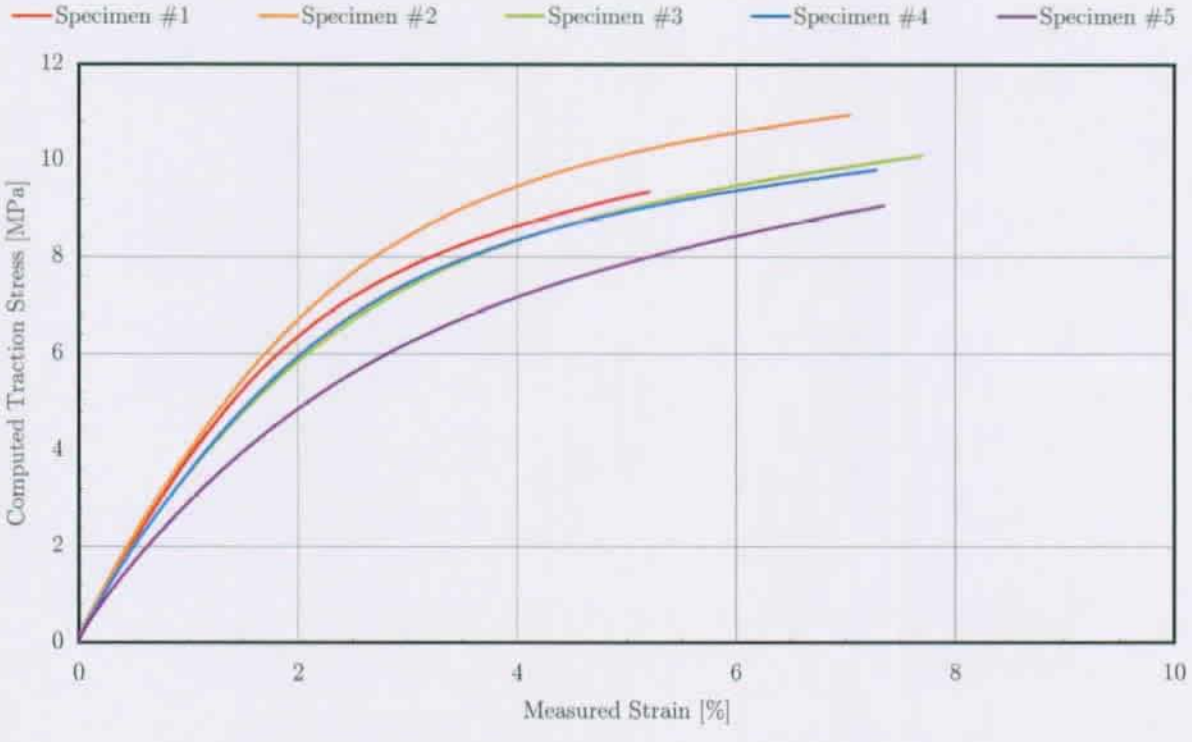

Figure C.5.: Traction experiments SikaForce 7851

Appendix D.

Pictures after failure

D.1. Specimens of the first experimental series

The pictures displayed in this section refer to the specimens experimentally investigated within the frame of Chapter 10.

Figure D.1.: Failure mode for unchamfered specimen: DN$\frac{50}{3}\frac{3}{6}1^{e}$ alias *A1*.

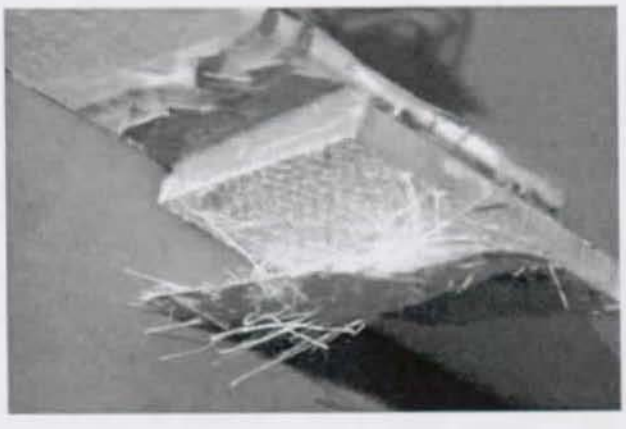

Figure D.2.: Failure mode for unchamfered specimen: DN$\frac{50}{3}\frac{4}{8}1^{e}$ alias *A2*.

Figure D.3.: Failure mode for unchamfered specimen: DN$\frac{75}{3}\frac{3}{6}1^{e}$ alias *B1*.

Figure D.4.: Failure mode for unchamfered specimen: DN$\frac{75}{3}\frac{4}{8}1^{e}$ alias *B2*.

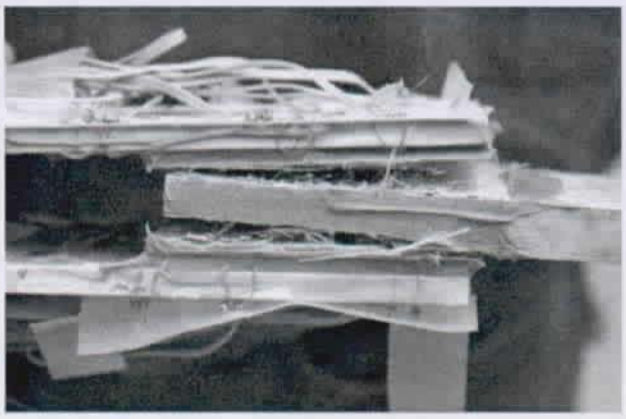

Figure D.5.: Failure mode for unchamfered specimen: DN$\frac{75}{3}\frac{6}{12}1^e$ alias *B3*.

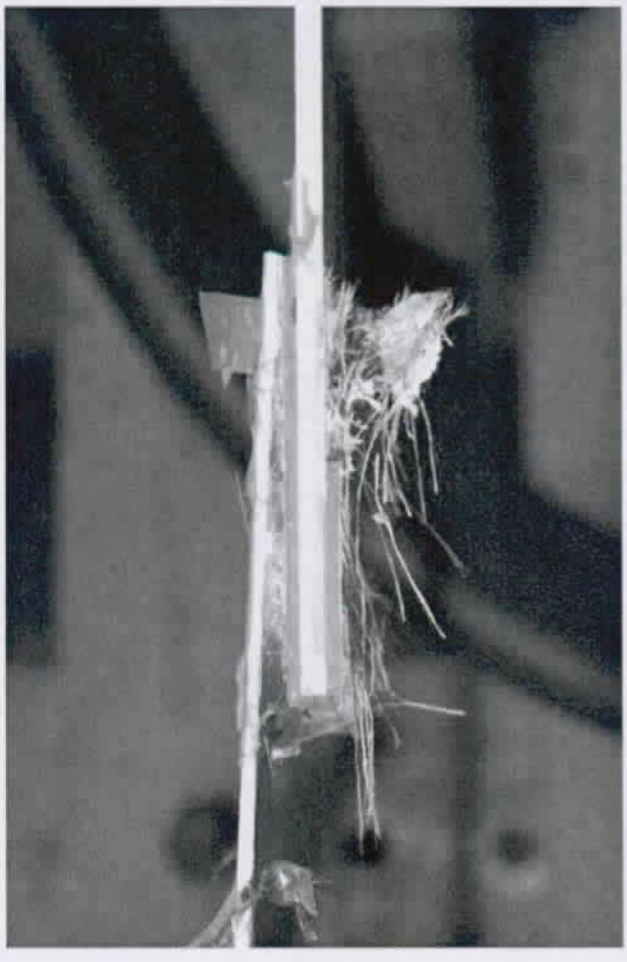

Figure D.6.: Failure mode for unchamfered specimen: DN$\frac{100}{3}\frac{3}{6}1^e$ alias *C1*.

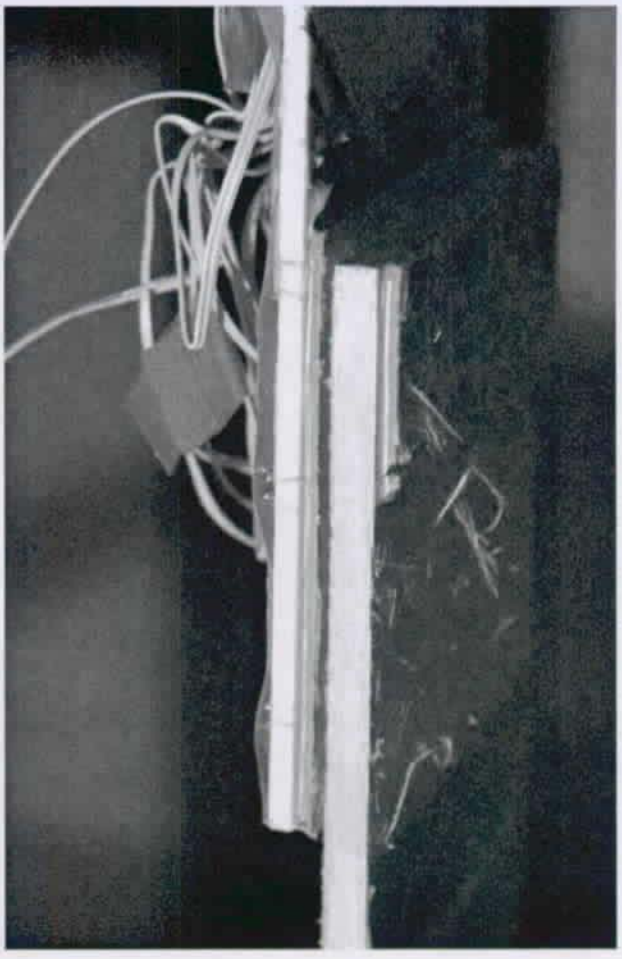

Figure D.7.: Failure mode for unchamfered specimen: DN$\frac{100}{3}\frac{4}{8}1^e$ alias *C2*.

Figure D.8.: Failure mode for unchamfered specimen: DN$\frac{100}{3}\frac{6}{12}1^e$ alias *C3*.

D.2. Specimens of the second experimental series

The pictures displayed in this section refer to the specimens experimentally investigated within the frame of Chapter 11.

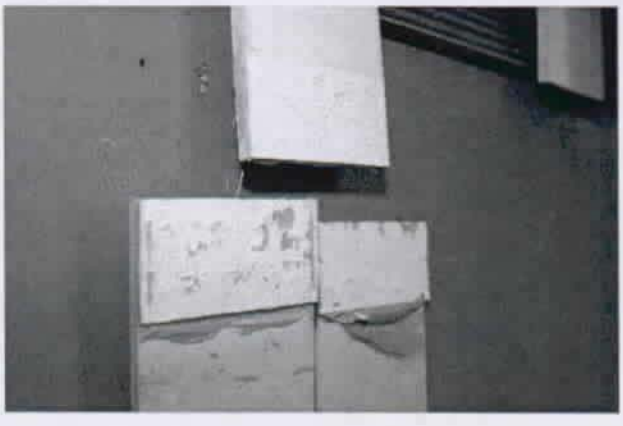

Figure D.9.: Failure mode for chamfered specimen: DN$\frac{50}{3}\frac{5}{10}$1 alias *VK1*.

Figure D.10.: Failure mode for chamfered specimen: DS$\frac{100}{3}\frac{5}{10}1^{e}$ alias *VK3*.

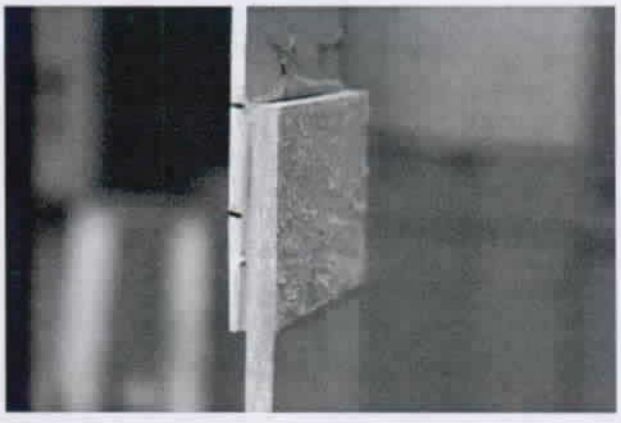

Figure D.11.: Failure mode for chamfered specimen: DS$\frac{75}{3}\frac{5}{10}$1 alias *VK5*.

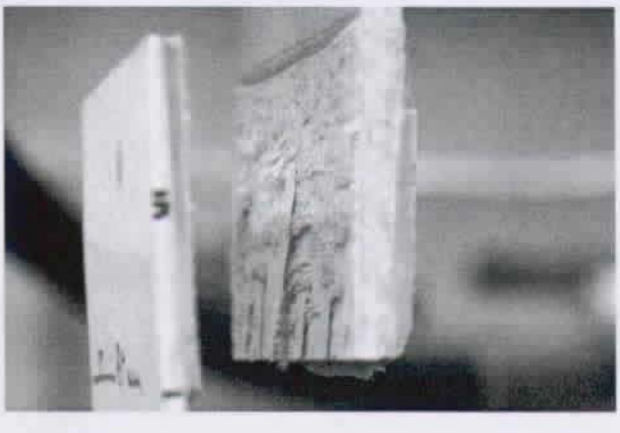

Figure D.12.: Failure mode for chamfered specimen: DS$\frac{75}{3}\frac{5}{10}$1 alias *VK5*.

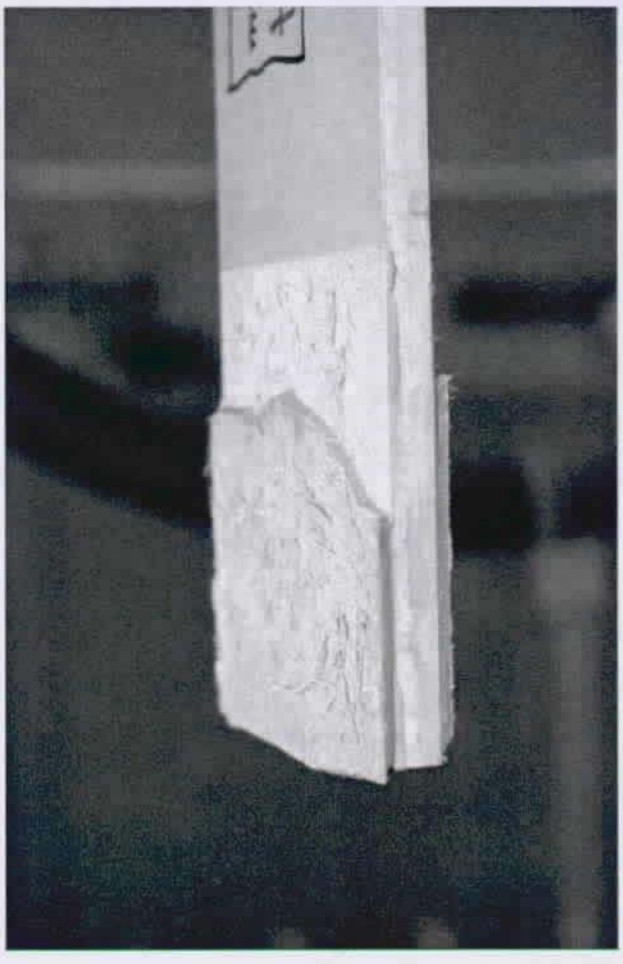

Figure D.13.: Failure mode for chamfered specimen: DN$\frac{100}{3}\frac{5}{10}$1 alias *VK7*.

Figure D.14.: Failure mode for chamfered specimen: DN$\frac{50}{1}\frac{5}{10}$1 alias *VK10*.

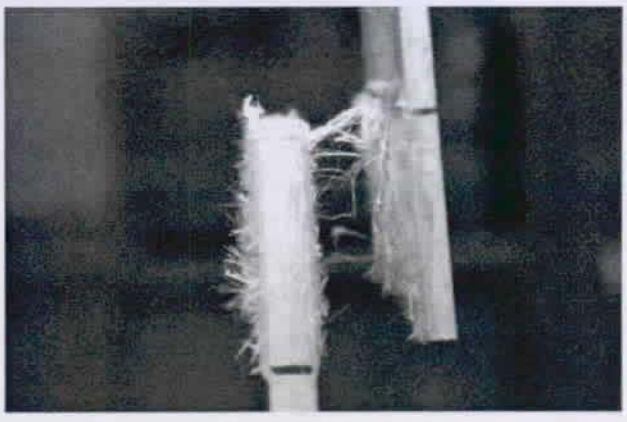

Figure D.15.: Failure mode for chamfered specimen: DN$\frac{50}{1}\frac{5}{10}$1 alias *VK10*.

Figure D.16.: Failure mode for chamfered specimen: DS$\frac{100}{1}\frac{5}{10}1^{e}$ alias *VK12*.

Figure D.17.: Failure mode for chamfered specimen: DS$\frac{100}{1}\frac{5}{10}1^{e}$ alias *VK12*.

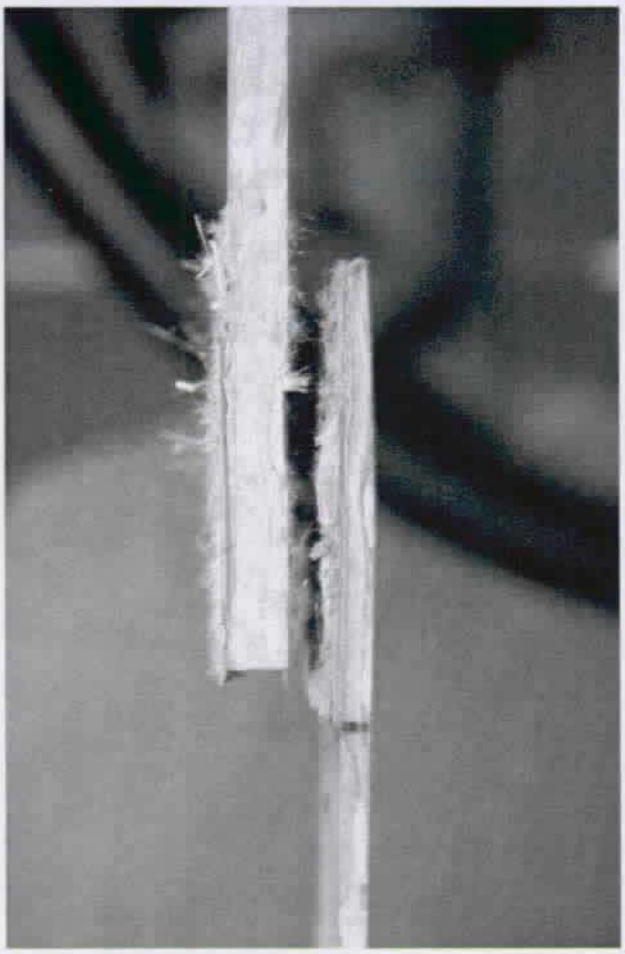

Figure D.19.: Failure mode for chamfered specimen: DS$\frac{75}{1}\frac{5}{10}1$ alias *VK14*.

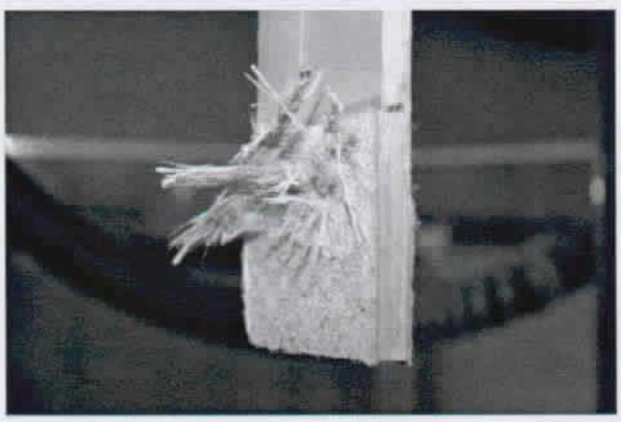

Figure D.18.: Failure mode for chamfered specimen: DN$\frac{75}{1}\frac{5}{10}1$ alias *VK13*.

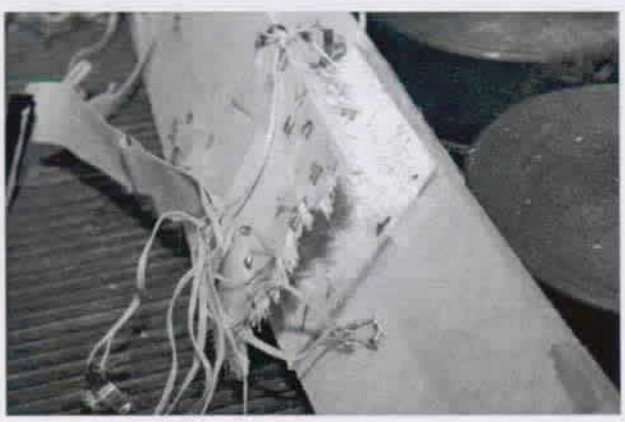

Figure D.20.: Failure mode for chamfered specimen: DF$\frac{100}{1}\frac{5}{10}1^{e}$ alias *VK15*.

Figure D.21.: Failure mode for chamfered specimen: DN$\frac{100}{1}\frac{5}{10}1$ alias *VK16*.

Figure D.22.: Failure mode for chamfered specimen: DF$\frac{100}{1}\frac{5}{10}2^{r}$ alias *VK18*.

Figure D.23.: Failure mode for chamfered specimen: DF$\frac{100}{1}\frac{5}{10}2^{r}$ alias *VK18*.

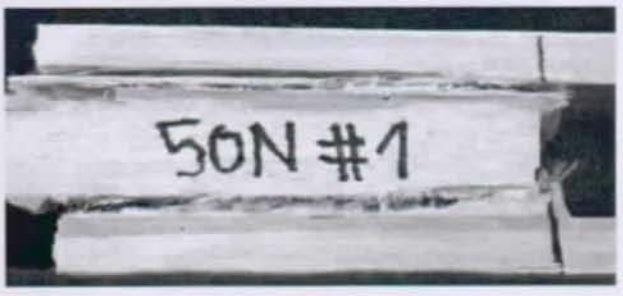

Figure D.24.: Failure mode for chamfered specimen: DN$\frac{50}{1}\frac{5}{10}2$ alias *50N-1*.

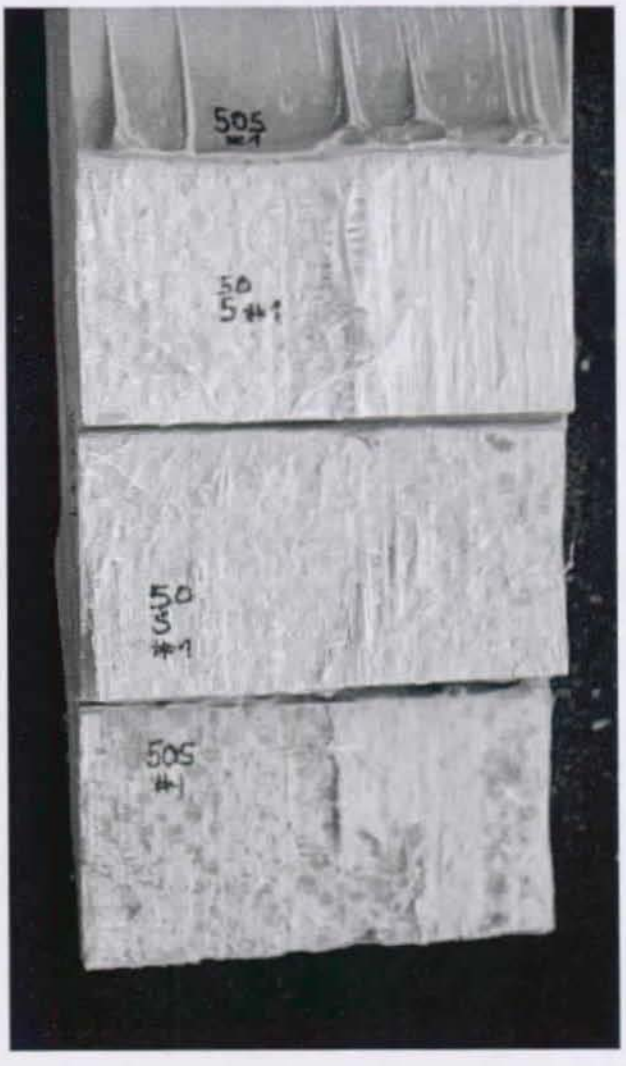

Figure D.26.: Failure mode for chamfered specimen: DS$\frac{50}{1}\frac{5}{10}2$ alias *50S-1*.

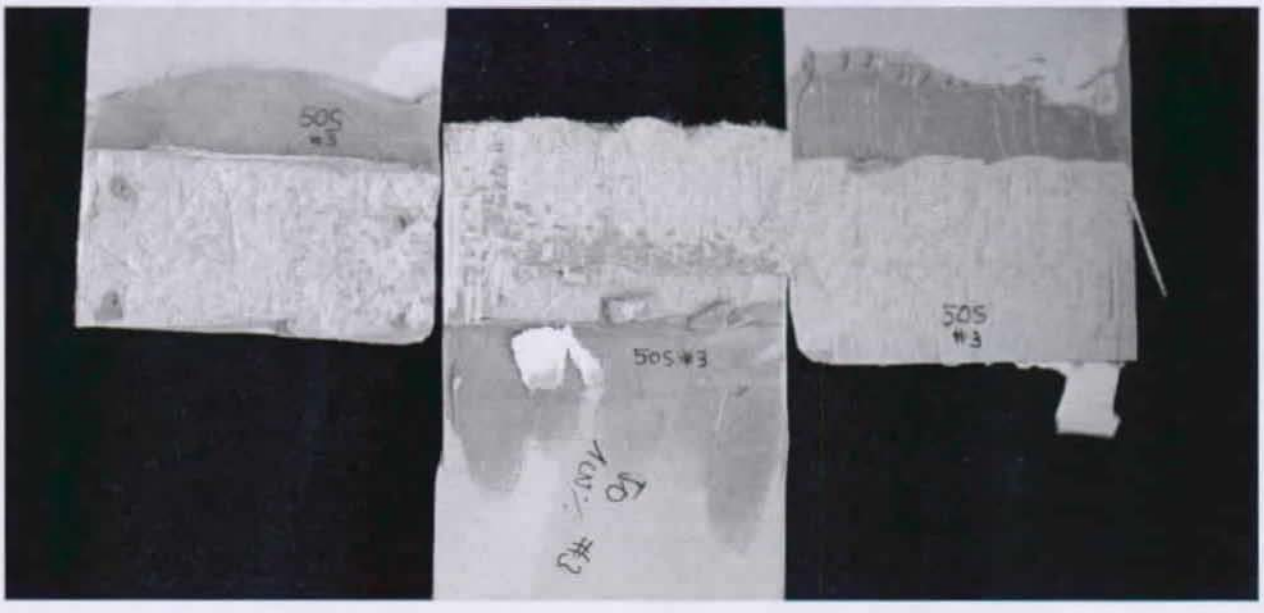

Figure D.25.: Failure mode for chamfered specimen: DS$\frac{50}{1}\frac{5}{10}$4 alias *50S-3*.

Figure D.32.: Failure mode for chamfered specimen: DS$\frac{75}{1}\frac{5}{10}$4 alias *75F-3*.

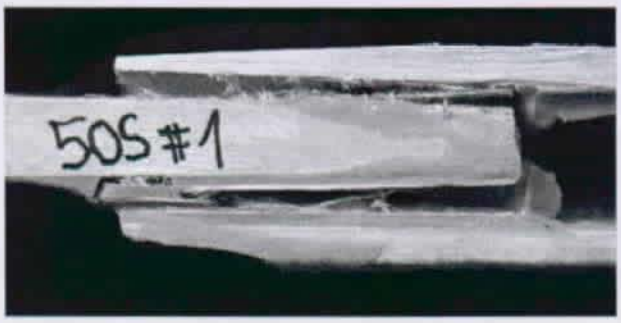

Figure D.27.: Failure mode for chamfered specimen: DS$\frac{50}{1}\frac{5}{10}$1 alias *50S-1*.

Figure D.28.: Failure mode for chamfered specimen: DN$\frac{75}{1}\frac{5}{10}$2 alias *75N-1*.

Figure D.29.: Failure mode for chamfered specimen: DS$\frac{75}{1}\frac{5}{10}$2 alias *75S-1*.

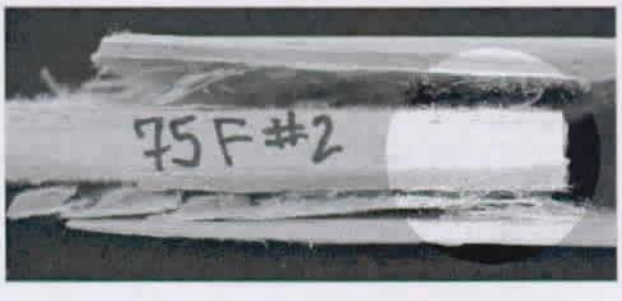

Figure D.30.: Failure mode for chamfered specimen: DS$\frac{75}{1}\frac{5}{10}$3 alias *75F-2*.

Figure D.31.: Failure for chamfered specimen: DS$\frac{75}{1}\frac{5}{10}$3 alias *75F-2*.

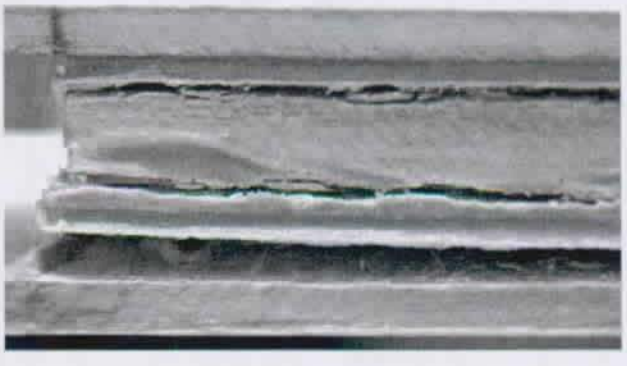

Figure D.33.: Failure mode for chamfered specimen: DN$\frac{200}{2}\frac{5}{10}$1 alias *200N-1*.

D.3. Miscellaneous pictures

The following section shows details of the failure location for selected tested specimens.
The failure location has been located at a depth of approximatively 0.5 mm inside the FRP material.

Figure D.34.: Failure of a $50 \times 50 \times 10$ square specimen showing the location of the failure layer

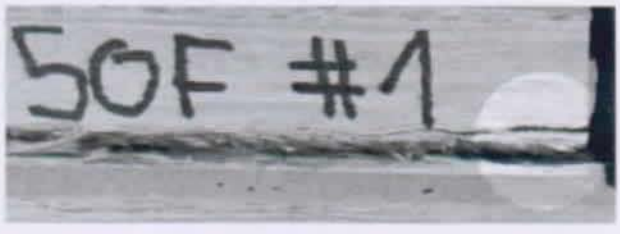

Figure D.35.: Failure of the DF$\frac{50}{1}\frac{5}{10}$3 specimen showing the location of the failure layer — Inner flat profile above

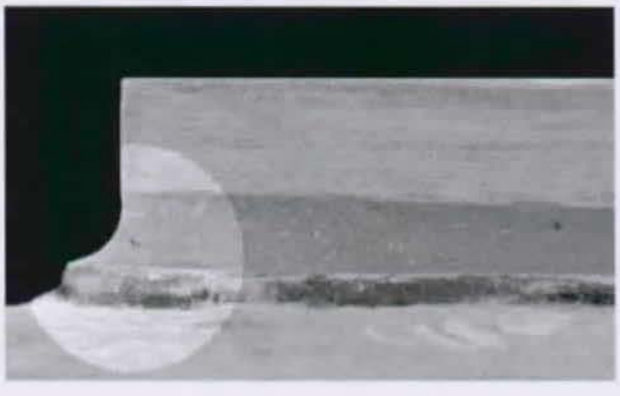

Figure D.36.: Failure of the DN$\frac{100}{3}\frac{5}{10}$3 specimen showing the location of the failure layer — Outer flat profile above

Figure D.37.: Failure of the DN$\frac{200}{2}\frac{5}{10}$1 specimen showing the location of the failure layer

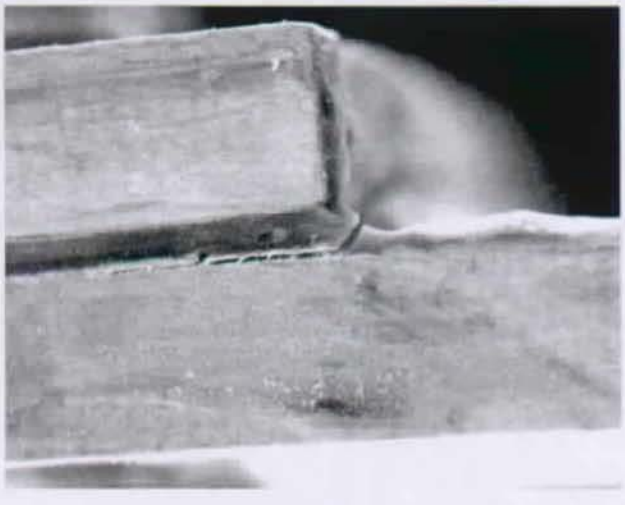

Figure D.38.: Failure of a SN$\frac{100}{1}\frac{10}{10}$ specimen showing the location of the failure layer

Appendix E.

CCLab Tensile-Shear Experimental Device: Standard Operating Procedure

E.1. Aim of the device

The CCLab Tensile-Shear Device was designed to gather material strength data of pultruded FRP-material. The strength that can be measured is related to the in-plane shear stress, τ_{xz} and the out-of-plane stress, σ_z in any given combination.
This data is necessary for dimensioning adhesively bonded joints of pultruded FRP-material.

E.2. Description

E.2.1. Device

Fig. E.2 fully describes the device. The material used to build it was steel. The device is built on a rectangular plate ①[1] with a guiding rail.

E.2.2. Steel supports

The material is experimentally investigated using the steel supports described in Fig. E.1. Each of these steel supports is made of two parts: the upper part with the bolt and the lower part with the guiding channel. Each of these parts show quadratic plane surfaces aimed to be bonded to the FRP-sample.

E.2.3. Loading mechanism

Two main load mechanism coexist:

❶ The tensile loading mechanism consisting of 4 columns ④ supporting a steel plate ⑤. The load is induced through a bolt ⑥;

❷ The shear loading mechanism consist of a horizontal bolt pushing the FRP (elements ⑧ to ⑩.)

Both mechanisms can be easily understood looking at the descriptive schemes, both can be run simultaneously.

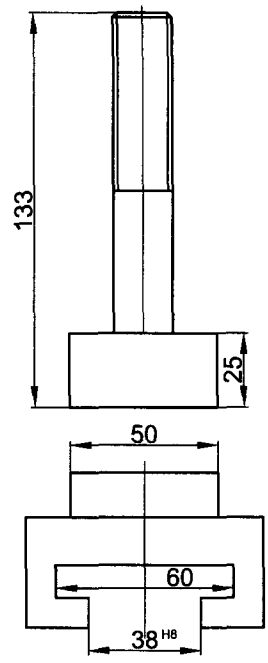

Figure E.1.: The steel support of the CCLab Tensile-Shear Experimental Device

[1] The numerotation is related to the technical scheme given by Figure E.2.

E.2.4. FRP-SAMPLES

The FRP-samples have to be cut out from the same original material for which the material strength data is needed.
Care has to be taken to not weaken the material by unappropriate cutting methods.
The surfaces of the FRP material has to be prepared. The minimum surface preparation would consist of:

① Cleaning and degreasing using acetone a first time.

② Mechanically abrading the surface veil using a handy grinding machine until the mat is revealed.

③ Re-cleaning and re-degreasing the surface using acetone a second time.

E.2.5. BONDING TO THE STEEL SUPPORTS

The FRP-samples have to be bonded onto both the surfaces of the upper and lower part of the steel support.
Appropriate measures should ensure a constant thickness to have the whole system consisting of the two steel support parts and FRP sample justified.
To ensure a relatively constant stress field under loading, the use of a not too stiff adhesive is recommended. For choosing an appropriate adhesive, FEA is helpful.

E.3. EXPRIMENTAL PROCEDURE

E.3.1. PURE TENSILE STRESSES

The tensile or out-of-plane stresses are applied by acting on the bolt ontop the upper steel support.
The load is given by turning the bolt using an appropriate wrench. The suggested load is a full twist per 20...30 seconds.

E.3.2. PURE SHEAR STRESSES

The shear stresses are applied by acting on the bolt ontop the upper steel support.
The load is given by turning the bolt using an appropriate key. The suggested load is a full twist per 20...30 seconds.

E.3.3. COMBINED LOADING

While the pure tensile loading and the pure shear loading mechanisms are obvious, the load mechanism for a given combination of shear force $S = S_0$ and a to determine tensile force $H = H_u$ is described by the following procedure:

① Imposing the shear force S_0 by acting on the tensile load mechanism.

② Acting on the tensile mechanism by increasing the corresponding force H **while** verifying that the primarily imposed shear load S_0 has not changed. If the shear force drops or increases outside a self-defined range[2], it should be readjusted.

③ The tensile force H has to be raised up to the failure value H_u.

E.4. GATHERING THE DATA

The data has to be gathered for combinations of shear stresses τ_{xz} and out-of-plane stresses σ_z.
The material strength will be defined as an interaction diagram, Fig. E.3 gives an example.

It is suggested to start the interaction diagram by first gathering the strength for the pure shear $\tau_{xz,0}$ and pure out-of-plane $\sigma_{z,0}$ stresses, the further steps should then be the application of fractions of the average $\tau_{xz,0}$ and then gathering the corresponding σ_z.

To ensure a minimum statistical quality of the gathered data, it is suggested to make at least 5 — better would be 10 — different individual experiments for each given τ_{xz}-σ_z-combination.

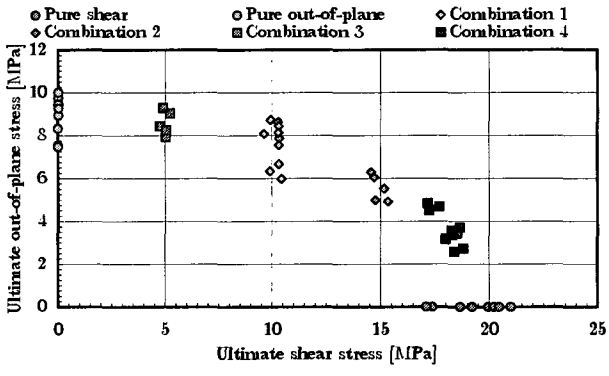

Figure E.3.: Example of an interaction diagram

[2]No indications can be given concerning this range.

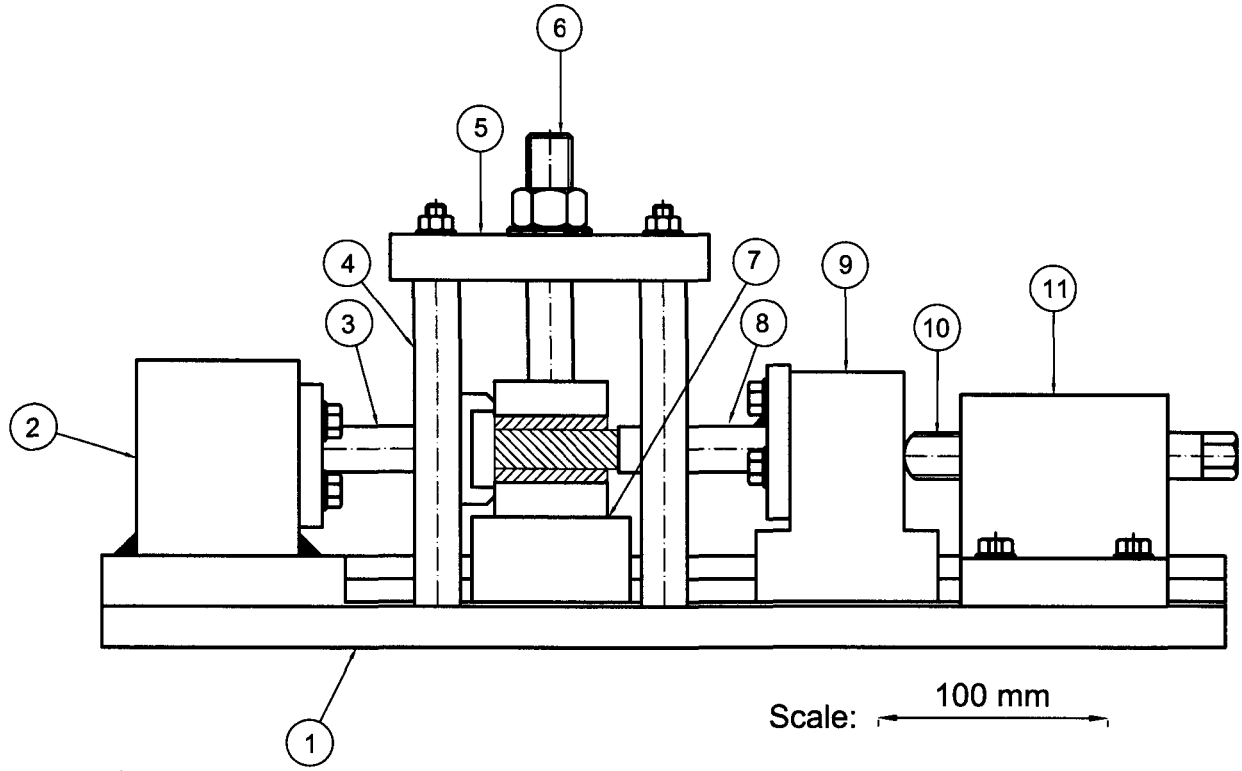

Figure E.2.: Technical drawing of the CCLAB TENSILE-SHEAR EXPERIMENTAL DEVICE

E.4.1. PARTIAL SAFETY FACTOR

The determination of the partial safety factor γ_d of the FRP strength is based on the statistical formulation of the data scattering.

γ_d is given by the following equation:

$$\gamma_d = \frac{1}{1 - k_n V_x} \tag{E.1}$$

V_x is the coefficient of variation of X

k_n is a coefficient given in Table E.1

n	1	2	3	4	5	6
k_n	4.36	3.77	3.56	3.44	3.37	3.33
n	8	10	20	30	∞	
k_n	3.27	3.23	3.16	3.13	3.08	

Table E.1.: k_n-values in function of the number of experimented individual specimen

Appendix F.

CCLab Tensile-Shear Experimental Device: Loading rate

As stated in Chapter 17 it is not possible to *chose* the loading speed for the experimental investigations with the CCLab Tensile-Shear Experimental Device. This is due to the fact that the device is run manually, so that there is a maximum loading speed imposed.
The experimental procedure was described earlier in Section 17.2.5.

F.1. Pure out-of-plane loading

It was attempted to keep the loading speed constant for all the pure out-of-plane experimental operations. The load-tension curves were measured for the pure out-of-plane loading and are shown in Figs. F.1 to F.2.

Using this data, it possible to calculate a loading-rate of approximatively

$$\begin{aligned} v &\approx \frac{4.5\,MPa}{30\,sec.} \\ &\approx 0.15\,\frac{MPa}{sec.} \\ &\approx 240\,\frac{N}{sec.} \end{aligned} \tag{F.1}$$

for the $40\times40\,mm^2$ FRP-samples and

$$\begin{aligned} v &\approx \frac{3.0\,MPa}{30\,sec.} \\ &\approx 0.10\,\frac{MPa}{sec.} \\ &\approx 250\,\frac{N}{sec.} \end{aligned} \tag{F.2}$$

for the $50\times50\,mm^2$ FRP-samples.

In both cases a loading rate of around $240\,\frac{N}{sec.}$.

F.2. Pure shear loading

It was attempted to keep the loading speed constant for all the pure shear experimental operations.
The load-tension curves were measured for the pure shear loading and are shown in Figs. F.3 and F.2.

Using this data, it possible to calculate a loading-rate of approximatively

$$\begin{aligned} v &\approx \frac{20\,MPa}{325\,sec.} \\ &\approx 200\,\frac{N}{sec.} \end{aligned} \tag{F.3}$$

for the 40×40 specimen and

$$\begin{aligned} v &\approx \frac{20\,MPa}{250\,sec.} \\ &\approx 400\,\frac{N}{sec.} \end{aligned} \tag{F.4}$$

for the 50×50 specimen.

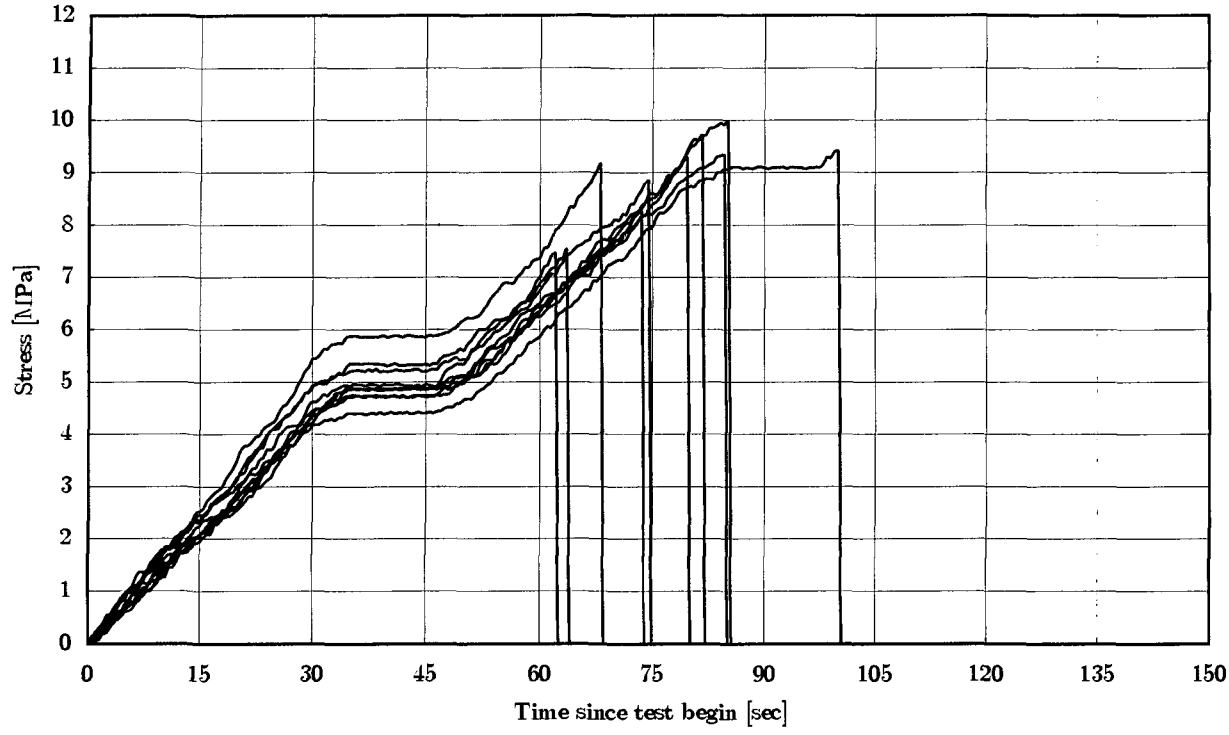

(a) 40×40×5

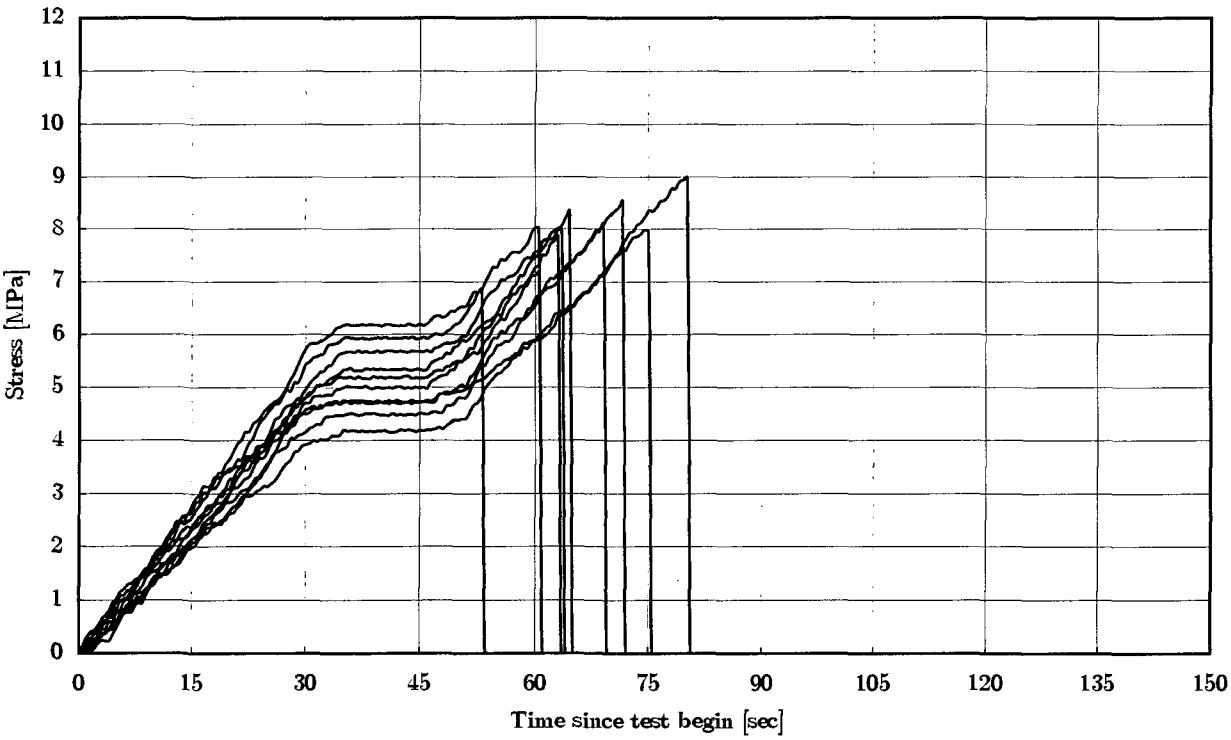

(b) 40×40×10

Figure F.1.: Time vs. out-of-plane stress curves: 40×40 specimens

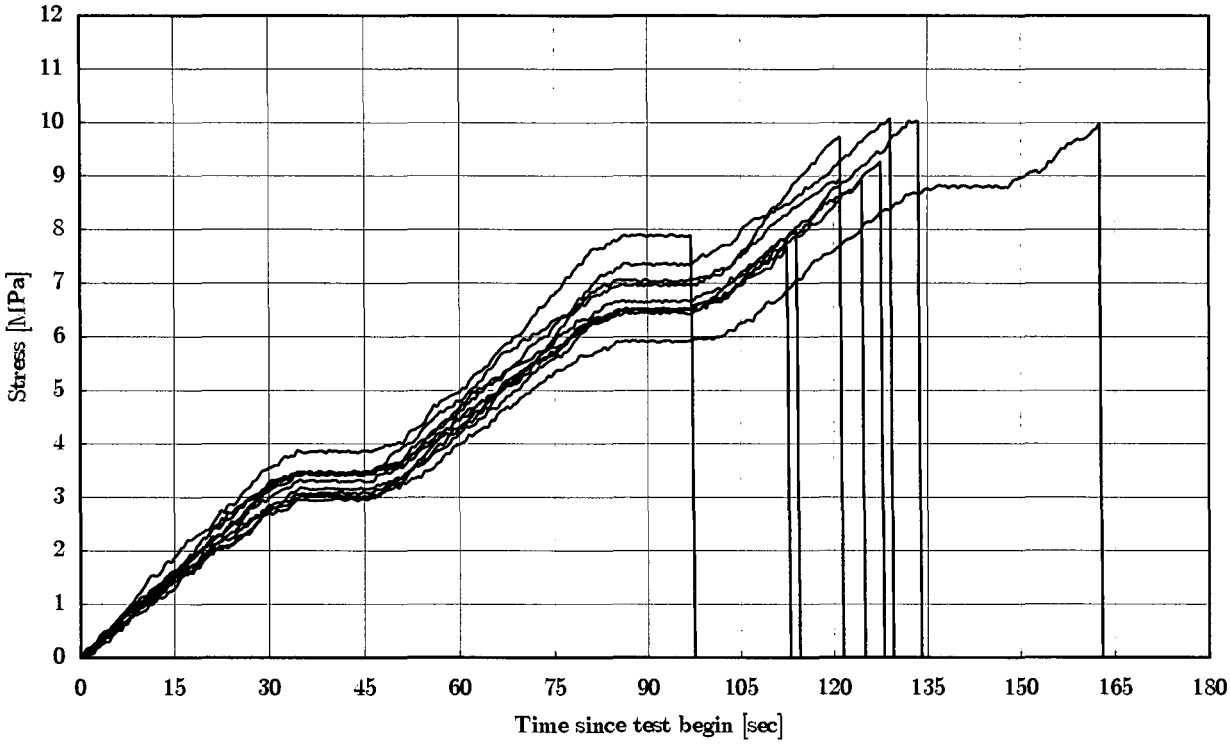

(a) 50×50×5

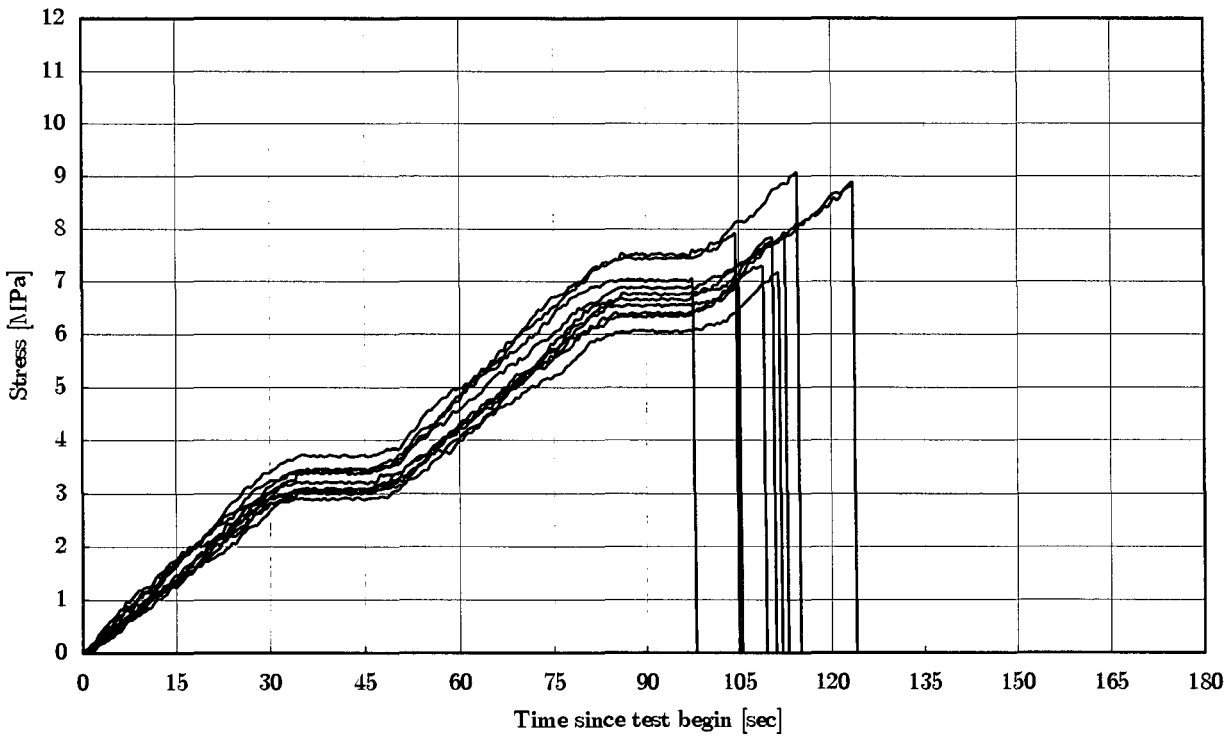

(b) 50×50×10

Figure F.2.: Time vs. out-of-plane stress curves: 50×50 specimens

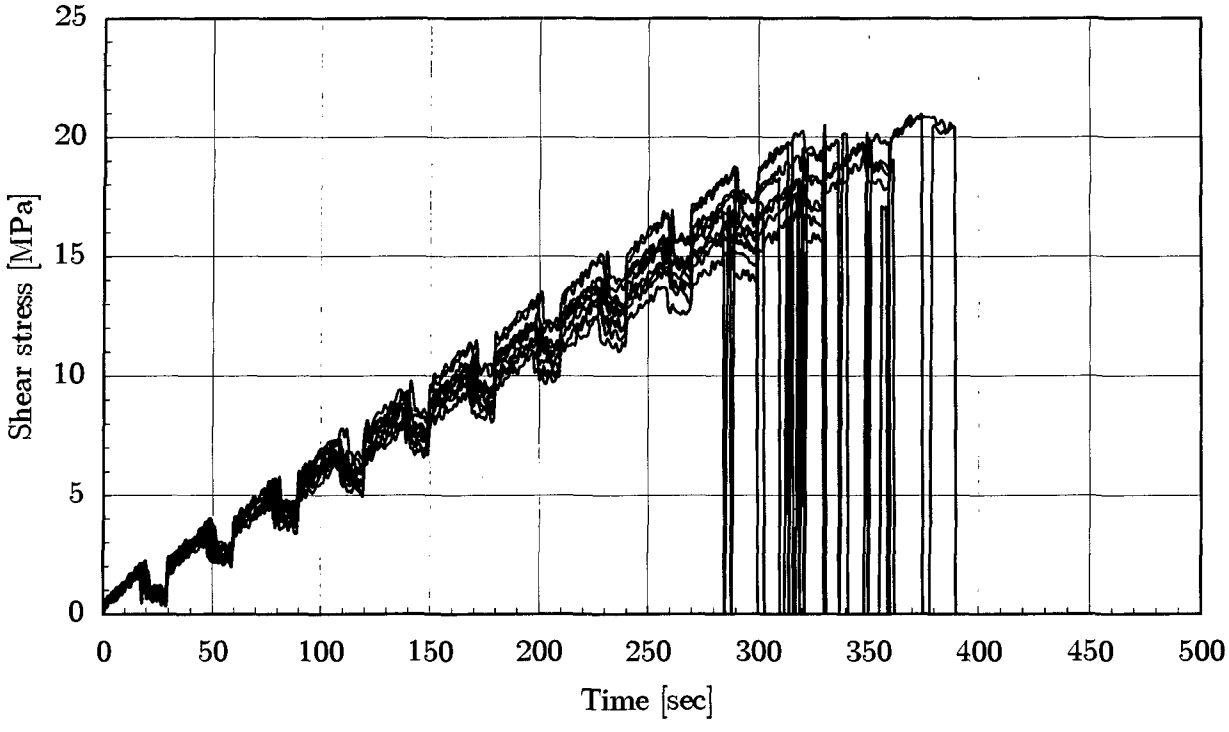

(a) 40×40×5

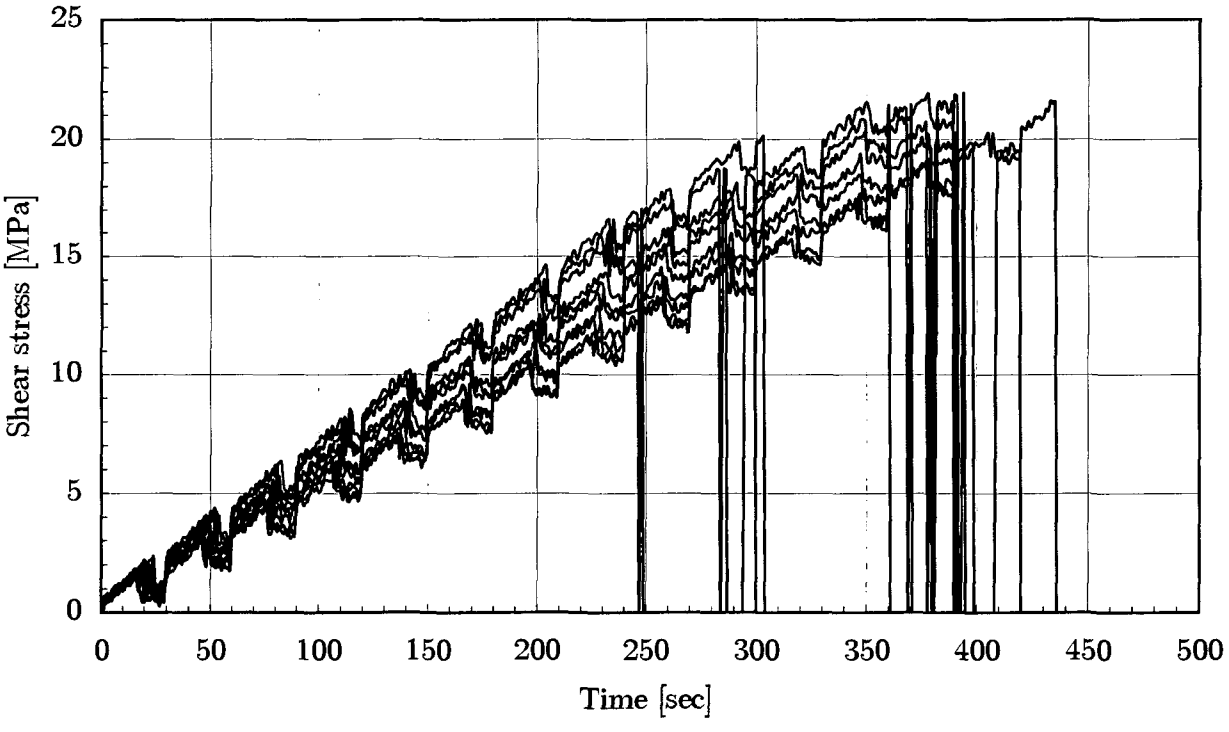

(b) 40×40×10

Figure F.3.: Time vs. shear stress curves: 40×40 specimens

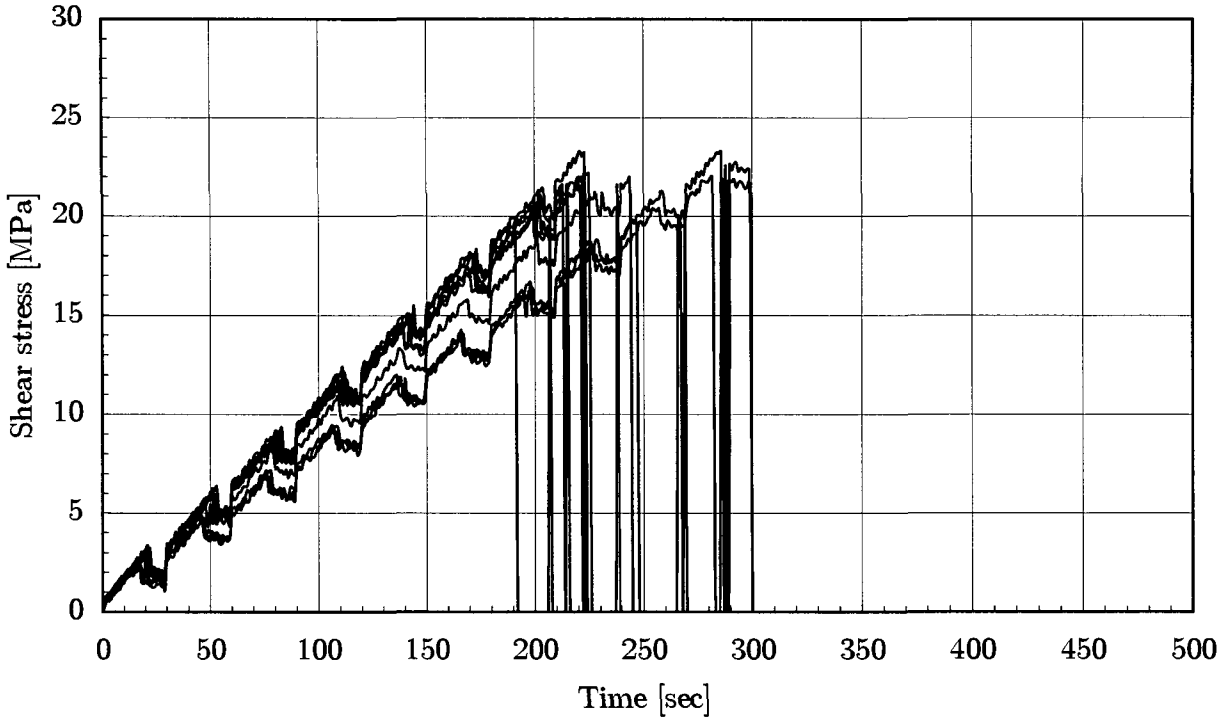

(a) 50×50×5

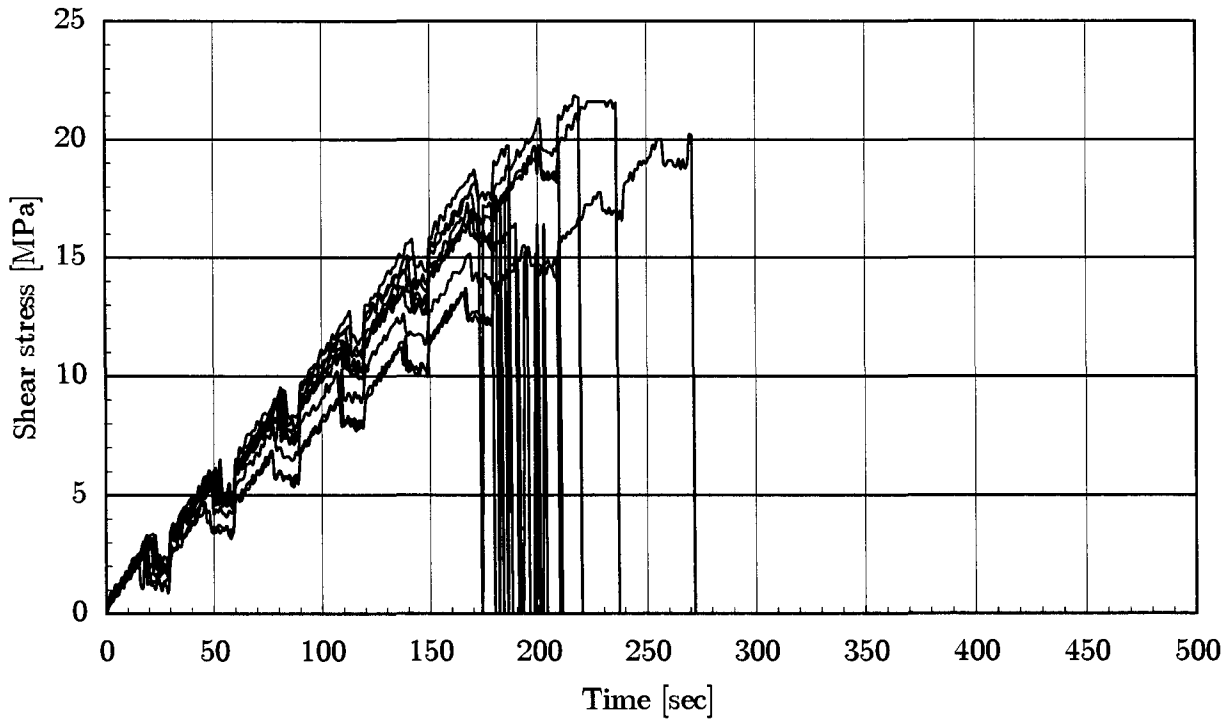

(b) 50×50×10

Figure F.4.: Time vs. shear stress curves: 50×50 specimens

Appendix G.

Statistical aspects of the investigations carried out

G.1. Experimentally gathered ultimate loads

The ultimate loads, as gathered in the experimental series described in Part III, are listed for selected geometrical joint configurations in Table 14.1. Table G.1 lists the scattering[1] obtained.

Geometrical configuration	#	$\frac{\sigma_{F_u}}{m_{F_u}}$ [%]
DN $\frac{50}{1}\frac{5}{10}$	IIII	5.4
DS $\frac{50}{1}\frac{5}{10}$	IIII	7.4
DF $\frac{50}{1}\frac{5}{10}$	IIII	10.6
DN $\frac{75}{1}\frac{5}{10}$	IIII	11.9
DS $\frac{75}{1}\frac{5}{10}$	IIII	9.3
DF $\frac{75}{1}\frac{5}{10}$	IIII	6.8
DN $\frac{100}{1}\frac{5}{10}$	I	※[a]
DS $\frac{100}{1}\frac{5}{10}$	II	13.4
DF $\frac{100}{1}\frac{5}{10}$	IIII	11.0
DN $\frac{50}{3}\frac{5}{10}$	I	※
DS $\frac{75}{3}\frac{5}{10}$	I	※
DN $\frac{100}{3}\frac{5}{10}$	IIII	8.5
DS $\frac{100}{3}\frac{5}{10}$	II	0.0
DF $\frac{100}{3}\frac{5}{10}$	II	1.9
AN $\frac{100}{2}\frac{5}{10}$	III	13.1
CN $\frac{100}{2}\frac{5}{10}$	III	10.3
CtN $\frac{100}{2}\frac{5}{10}$	III	16.3
SN $\frac{100}{2}\frac{5}{5}$	III	2.0
SN $\frac{100}{3}\frac{5}{5}$	III	4.8

[a] No standard deviation available, because only one was specimen investigated.

Table G.1.: Scattering of the experimentally gathered material strength data

[1] Scattering is expressed by the variance $v_x = \frac{\sigma_x}{m_x}$, σ_x is the standard deviation and m_x the average of the variable x.

Two methods to average the variation factor will be applied, a first one is the simple average defined by

$$v_s = \frac{1}{n}\sum_{i=1}^{n} v_i \tag{G.1}$$

with v_i, the variance of each series of identical geometrical configuration while the second one is a weighted average defined by

$$v_w = \frac{\sum_{i=1}^{n} v_i \times (m_i - 1)}{\sum_{i=1}^{n}(m_i - 1)} \tag{G.2}$$

with m_i the number of each individual samples in each series of identical specimen.

The results are listed in Table G.1.

Series	v_s [%]	v_w [%]
All configurations	**8.3**	**8.9**
Double lap joints	7.9	9.2
Single lap joints	3.4	3.4

Table G.2.: Scattering of the experimentally gathered specimen strengths

G.1.1. Additional remark

A. Zureick & R. Bennet recommended in [72] at least 6o of experimentally investigated FRP composite joints without clearly defining if these 6o specimens should be equal in geometry. Of course this recommendation has to be seen in conjunction with Zureick's work on the statistical level, especially the two and three parameter Weibull distributions. The Author of this Thesis has selected to not blindly follow this recommendation and followed a more pragmatic approach based on case-by-case judgement.

G.2. EXPERIMENTALLY GATHERED MATERIAL STRENGTH

The experimental material strength data gathered in Chapter 17 shows a scattering that will be described for the purpose of this Thesis as the scattering of the value

$$\rho = \sqrt{\tilde{\mathfrak{F}}(\tau_{xz,u,i}, \sigma_{z,u,i})} \tag{G.3}$$

with the function $\tilde{\mathfrak{F}}$ defined in Equation 23.1 and the index i identifying each sample of each experimental series 40×40×5, 40×40×10, 50×50×5 and 50×50×5.

The results of the mathematical processing is the following:

Series	σ_η [%]
40×40×5	6.95
40×40×10	6.85
50×50×5	8.36
50×50×10	7.92
Averaged according to Eq. G.4	**7.66**

Table G.3.: Scattering of the experimentally gathered material strength data

Taking a formula similar to Equation 23.4, it is possible to formulate an average indicator for the scattering of the experimentally gathered strength data:

$$v_{\tilde{\eta}} = \frac{\sum_{i=1}^{4} \eta_i \times A_i}{\sum_{i=1}^{4} A_i} \tag{G.4}$$

with $A = a^2$ and a the dimension of the specimen (40 mm and 50 mm).

BIBLIOGRAPHY

[1] J. MELLAART: *Çatal Hüyük: une des premières cités du monde* — Jardin des Arts/Tallandier - Nouveaux aspects de l'archéologie, 1971, *trad. de l'anglais par Louis Frédéric.*

[2] TH. KELLER: *Fiber reinforced polymers in building construction* — International Association for Bridge and Structural Engineering IABSE, Symposium Towards a Better Built Environment, Melbourne Australia, 2002.

[3] M. V. KARBHARI & L. ZHAO: *Use of Composites for 21st Century civil infrastructure* — Computer Methods in applied Mechanics and Engineering, 2000, pp. 433-454.

[4] O. VOLKERSEN: *Die Nietkraftverteilung in zugbeanspruchten konstanten Laschenquerschnitten* — Luftfahrtforschung 1938, Vol. 15, pp. 41-47.

[5] M. GOLAND & E. REISSNER: *The Stresses in Cemented Joints* — Journal of Applied Mechanics 1944, March, pp. A17-A27.

[6] O. VOLKERSEN: *Recherches sur la theorie des assemblages collés* — 1965, Construction Metallique, nr. 4, pp. 3-13.

[7] W. J. RENTON & J. R. VINSON: *Analysis of adhesively Bonded Joints between Panels of Composite Materials* — Trans. AMSE Journ. of applied Mechanics 1977, March, pp. 101-106.

[8] D. J. ALLMAN: *A Theory for Elastic Stresses in adhesively bonded Lap Joints* — Q. J. Mech. Appl. Math., 1977, 30(4), pp. 415-436.

[9] M. Y. TSAI & AL.: *Improved Theoretical Solutions for Adhesive Lap Joints* — 1998, Int. J. Solids Structures, Vol. 35, No. 12.

[10] M. Y. TSAI & J. MORTON: *An Evaluation of Analytical and Numerical Solutions to the Single-Lap Joint* — 1998, Int. J. Solids Structures, Vol. 31, No. 18.

[11] T. M. ROBERTS: *Shear and Normal Stresses in Adhesive Joints* — Journal of Enginnering Mechanics, 1989, Vol. 115, nr. 11, pp. 2460-2479.

[12] L. J. HART-SMITH: *adhesively bonded Single-Lap Joints — Technical Report* — NASA CR-112236 Report, January 1973.

[13] L. J. HART-SMITH: *Analysis and Design of advanced Composite Bonded Joints* — NASA CR-2218 Report, Aug. 1974.

[14] K.-J. BATHE: *Finite Element Procedures*— 1996, Prentice-Hall Int.

[15] F. RIEBEL: *Numerical analysis of fibre reinforced polymers connected by simple glued joints* — 2002, CCLAB, unpublished.

[16] D. A. BIGWOOD & A. D. CROCOMBE: *Nonlinear adhesively bonded Joints Design Analysis* — Int. Journal of Adhesion and Adhesives 1990, Vol. 10, nr. 1 January, pp. 31-41.

[17] R. D. ADAMS: *Joining fibre-reinforced plastics* - Chap. 5 — 1987, Elsevier applied science publishers.

[18] G. RICHARDSON, A. D. CROCOMBE & P. A. SMITH: *A Comparison of Two- and Three-Dimensional Finite-Element Analyses of Adhesive Joints* — Int. Journal of Adhesion and Adhesives 1993, Vol. 13, nr. 3 July, pp. 193-200.

[19] R. HAJ-ALI & H. KILIÇ: *Nonlinear behavior of pultruded FRP composites* — Composites, Part B: Engineering 2002, Vol. 33, pp. 173-191.

[20] R. HAJ-ALI & H. KILIÇ: *Nonlinear constitutive models for pultruded FRP composites* — Mechanics of Materials 2003, Vol. 35, pp. 791-801.

[21] G. WU & A. D. CROCOMBE: *Simplified finite element modelling of structural adhesive joints* — Computers and Structures 1996, Vol. 61, pp. 385-391.

[22] C. H. WANG & L. R. F. ROSE: *Determination of Triaxial Stresses in Bonded Joints* — Int. Journal of Adhesion and Adhesives 1997, Vol. 17, nr. 1, pp. 17-25.

[23] G LI & P. LEE-SULLIVAN: *Finite element and experimental studies on single-lap balanced joints in tension* — International Journal of Adhesion and Adhesives 2001, Vol. 21, pp. 211-220.

[24] G LI, P. LEE-SULLIVAN & R. W. THRING: *Nonlinear Finite element analysis of stress and strain distributions across the adhesive thickness in composite single-lap joints* — Composite Structures 1999, Vol. 46, 395-403.

[25] A. E. BOGDANOVICH & I. KIZHAKKETHARA: *Three-dimensional finite element analysis of double-lap composite adhesively bonded joint using submodeling approach* — Composites Part B 1999, Vol. 30, pp. 537-551.

[26] R. H. ANDRUET: *Special 2-D and 3-D Geometrically Nonlinear Finite Elements for Analysis of Adhesively Bonded Joints* — Dissertation 1998, Virginia Polytechnic Institute and State University.

[27] R. H. ANDRUET, D. A. DILLARD & S. M. HOLZER: *Two- and three-dimensional geometrical nonlinear Finite elements for analysis of adhesive joints* — International Journal of Adhesion and Adhesives 2001, Vol. 21, pp. 17-34.

[28] L. J. HART-SMITH: *Predictions of the original and truncated maximum-strain failure models for certain fibrous composite laminates* — Composites Science and Technology 1998, Vol. 58, pp. 1151-1178.

[29] L. J. HART-SMITH: *Expanding the capabilities of the Ten-Percent Rule for predicting the strength of fibre-polymer composites* — Composites Science and Technology 2002, Vol. 62, pp. 1515-1544.

[30] L. J. HART-SMITH: *Predictions of a generalized maximum-shear-stress failure criterion for certain fibrous composite laminates* — Composites Science and Technology 1998, Vol. 58, pp. 1179-1208.

[31] J. DE CASTRO: *Report 2000-1b-2: Experiments on bonded joints: soft adhesives* — 2003, CCLAB, unpublished.

[32] R. S. LONG: *Static Strength of Adhesively Bonded ARALL-1 Joints* — Journal of Composite Materials 1991, Vol. 25, April, pp. 391-415.

[33] J. D. CLARK & I. J. MCGREGOR: *Ultimate Tensile Stress over a Zone: A New Failure Criterion for Adhesive Joints* — Journal of Adhesion 1993, Vol. 42, pp. 227-245.

[34] G. FERNLUND & J. K. SPELT: *Failure Load Prediction of Structural Adhesive Joints* — Int. Journal of Adhesion and Adhesives 1991, Vol. 11, nr. 4 October, pp. 213-227.

[35] G. FERNLUND & AL.: *Fracture Load Predictions for Adhesive Joints* — Composite Science and Technology 1994, Vol. 51, pp. 587-600.

[36] S. W. TSAI: *A General Theory of Strength for Anisotropic Materials* — Journal of Composite Materials 1971, Vol. 5, January, pp. 58-81.

[37] F. ERDOGAN: *Fracture mechanics* — International Journal of Solids and Structures 2000, Vol. 37, pp. 171-183.

[38] A. PUCK: *Festigkeitsanalyse von Faser-Matrix-Laminaten* — Carl Hanser Verlag München - Wien, 1996 .

[39] P. DE MONTLEAU & A. RIGOLAT: *Stabilité du délaminage dans l'assemblage à double recouvrement* — Comptes rendus de l'Académie des Sciences de Paris 2000, Vol. 328, Série II, pp. 291-296.

[40] C. K. LIM, M. A. ACITELLI & W. C. HAMM: *Failure Criterion of a Typical Polyamide Cured epoxy Adhesive* — Journal of Adhesion 1974, Vol. 6, pp. 281-288.

[41] R. BREDAMO & P. A. GRADIN: *Testing of in-situ properties of adhesives* — International Journal of Adhesion and Adhesives 1986, Vol. 6, pp. 153-156.

[42] W. J. RENTON: *Analysis and Design of Adhesive Mechanical Characterization Test Specimen* — Journal of Adhesion 1979, Vol. 10, pp. 139-155.

[43] W. J. RENTON & J. R. VINSON: *The efficient design of adhesively bonded joints* — Journal of Adhesion 1975, Vol. 7, pp. 175-193.

[44] F. MORTENSEN & O. TH. THOMSEN: *Simplified lienear and non-linear analysis of stepped and scarfed adhesive-bonded lap-joints between composite laminates* — Composite Structures 1997, Vol. 38, pp. 281-294.

[45] F. MORTENSEN & O. TH. THOMSEN: *Analysis od adhesively bonded joints: a unified approach* — Composite Science and Technology 2002, Vol. 62, pp. 1011-1031.

[46] F. MORTENSEN, O. TH. THOMSEN: *Coupling effects in adhesively bonded joints* — Composite Structures 2002, Vol. 56, pp. 165-174.

[47] A. M. ALBAT & D. P. ROMILLY: *A direct linear-elastic analysis of double symmetric bonded joints and reinforcement* — Composites Science and TechnologyComposites Science and Technology 1999, Volume 59, pp. 1127-1137.

[48] M. Y. TSAI & J. MORTON: *The effect of a spew fillet on adhesive stress distributions in laminated composite single-lap joints* — Composite structures 1995, Vol. 32, pp. 123-131.

[49] T. P. LANG & P. K. MALLICK: *Effect of spew geometry on stresses single-lap joints* — International Journal of Adhesion and Adhesives 1998, Vol. 18, pp. 167-177.

[50] G. BELINGARDI, L. GOGLIO & A. TARDITI: *Investigating the effect of spew and chamfer size on the stresses in metal/plastics adhesive joints* — International Journal of Adhesion and Adhesives 2002, Vol. 22, pp. 273-282.

[51] C. H. WANG & L. R. F. ROSE: *Compact solutions for the corner singularity in bonded lap joints* — International Journal of Adhesion and Adhesives 2000, Vol. 20, pp. 145-154.

[52] S. MALL & G. RAMAMURTHY: *Effect of bond thickness on fracture and fatigue strength of adhesively bonded composite joints* — International Journal of Adhesion and Adhesives 1989, Vol. 9, pp. 33-37.

[53] R. D. ADAMS: *strength prediction for Lap joints, especially with composite adherents* — Journal of Adhesion 1989, Vol. 30, pp. 219-242.

[54] L. J. HART-SMITH: *Adhesive bonding of composite structures — Progress to date and challenges* — Journal of Composite Technology 2002, Vol. 24, pp. 133-153.

[55] TH. KELLER: *New Bidges and Buildings constructed from translucent GFRP Sandwich Panels and lued GRFP elements* — 2000, Proc. of the 3rd conference on Advanced Composite Materials in Bridges and Structures, pp. 785-792. ISBN 0-7709-0447-5.

[56] TH. KELLER: *Towards material-adapted structural Applications of advanced composite materials in bridge and building constructions* — 2001, Composites in Construction, Porto.

[57] B. FARGETTE, Y. GILIBERT & L. RIMLINGER: *Comparison between experimental and theoretical analysis of stress distribution in Adhesively bonded joints: tenon and mortise joints and single lap joints* — Journal of Adhesion 1996, Vol. 59, pp. 159-170.

[58] M. SCHOLLMAYER: *Behaviour of Girders composed of Translucent Sandwich Panels* — 2001, Diploma Thesis at the CCLAB.

[59] J. SIEBRECHT: *Shear Experiments on Bonded Double-Lap FRP-Joints* — 2001, Diploma Thesis at the CCLAB.

[60] A. A. EL DAMATTY & M. ABUSHAGUR: *Testing and modeling of shear and peel behavior of bonded steel/FRP connections* — Thin-Walled structures 2003, Vol. 41, pp. 987-1003.

[61] T. KELLER & H. GÜRTLER: *Composite action and adhesive bond between FRP bridge decks and main girders* — Journal of Composites for Construction (ASCE), Manuscript number CC/2003/022440, tentatively approved.

[62] T. KELLER & H. GÜRTLER: *In-plane compression and shear behavior of FRP bridge decks, continuation* — Journal of Composites for Construction (ASCE), Manuscript number CC/2003/022462, under review.

[63] T. TIRELLI: *Technical Report CCLab 2000.1c/2: Fatigue Behavior of Adhesively Connected Pultruded GFRP Profiles* — 2003, CCLAB, unpublished.

[64] T. KELLER & T. TIRELLI: *Fatigue behavior of adhesively connected pultruded GFRP profiles* — Composite Structures, in press.

[65] TH. KELLER & AL.: *Use of fiber reinforced polymers in bridge construction* — Structural Engineering Documents No. 7, International Association for Bridge and Structural Engineering IABSE, 2003, ISBN 3-85748-108-0.

[66] J. L. CLARKE, EDITOR: *Structural Design of Polymer Composites - EuroComp Design Code and Handbook* — 1996, E & FN Spon, London.

[67] FIBERLINE COMPOSITES: *Fiberline Design- & Konstruktionshandbuch für Konstruktionsprofile aus Verbundwerstoffen* — 1995-2001, Fiberline Composites Kolding.

[68] CREATIVE PULTRUSIONS LTD.: *The Plutrex Plutrusion Global Design Manual* — available on CD or on the Internet (*www.creativepultrusions.com*), 2001.

[69] AK TRAGENDE KUNSTSTOFFBAUTEILE: *Tragende Kunstoffbauteile im Bauwesen: Entwurf, Bemessung und Konstruction* — June 2001.

[70] AMERICAN SOCIETY FOR TESTING AND MATERIALS: *Annual book of ASTM standards* — 2000, *Section Vol 15.06.*

[71] K. LIECHTI, W. S. JOHNSON & D. A. DILLARD: *Joining fibre-reinforced plastics* - Chap. 4 — 1987, Elsevier applied science publishers.

[72] A. ZUREICK & R. BENNET: *Determination of Material Property Characteristic Values of Fiber-Reinforced Polymeric Composites* — Structural Engineering, Mechanics and Materials Research Report No. 03-2 2002, GEORGIATECH.

[73] T. F. STARR, EDITOR: *Pultrusion for Engineers* — Woodhead Publ. Ltd., 2000.

[74] J. F. DAVALOS, H. A. HALIM, P. QIAO, R. LOPEZ-ANIDO & E. J. BARBERO: *Analysis and design of pultruded FRP shapes under Bending* — Composites Part B 1996, Vol. 27B. pp. 295-305.

[75] J. F. DAVALOS, Y. KIM & E. J. BARBERO: *A layerise beam element for analysis of frames wih laminated sections and flexible joints* — Finite Elements in Analysis and Design 1995, Vol. 19. pp. 181-194.

[76] J. N. REDDY: *A generalization of two-dimensional theories of laminated composite plates* — Commun. Appl. Numer. Methods 1987, Vol. 3, pp. 173-180.

[77] S. PACIORNIK, F. M. MARTINHO, M. H. P. DE MAURICIO & J. R. M. D'ALMEIDA: *Analysis of the mechanical behaviour and characterization of pultruded glass fiber-resin matrix composites* — Composite Science and Technology 2003, Vol. 63, pp. 295-304.

[78] T. VALLÉE & J. SIEBRECHT: *Report 2001-1-1: Shear experiments on bonded FRP-Profiles under static Load. Part 1: Experiments with SikaDur330* — 2001, CCLAB, unpublished.

[79] T. VALLÉE & J. SIEBRECHT: *Report 2001-1-2: Shear experiments on bonded FRP-Profiles under static Load. Part 2: Experiments with SikaForce7851* — 2001, CCLAB, unpublished.

[80] M. DAVIS & D. BOND: *Principles and practices of adhesively bonded structural joints and repairs* — International Journal of Adhesion and Adhesives 1999, Vol. 19, pp. 91-105.

[81] T. VALLÉE & H. GÜRTLER: *Report 2002-1-2: Experiments on chamfered bonded joints* — 2002, CCLAB, unpublished.

[82] T. VALLÉE: *Report 2002-1-3: Calibration of the CCLab Flatwise Tensile Experimental Device* — 2002, CCLAB, unpublished.

[83] T. L. ANDERSON: *Fracture Mechanics*— 1994, CRC Press, Boca Raton, FL.

[84] P. P. CAMANHO & F. L. MATTEWS: *Stress analysis and strength prediction of mechanically fastened joints in FRP: a review* — Composites Bart A 1997, Vol. 28A, pp. 529-547.

[85] EUROCODE 3: *Design of steel structures* — 1992, Comité Europe´en de Normalisation (CEN), Brussels.

[86] C. COOPER & G. J. TURVEY: *Effects of joint geometry and bolt torque on the structural performance of single bolt tension in pultruded GRP sheet material* — Composite Structures 1995, Vol. 32, pp. 217-226.

[87] G. LI & P. LEE-SULLIVAN: *Finite element and experimental studies on single-lap balanced joints in tension* — 2001, Int. Journal of adhesion & adhesives 21.

[88] Y. ZHANG: *Evaluation of Stress Reduction Methods for FRP Adhesively Bonded Joints* — 2003, Master Thesis at the CCLAB, unpublished.

[89] M. FARSHAD, P. ROSSINI & P. FLÜELER: *CFK-Zugelemente vernakern* — Mechanische Werkstoffprüfung 2002, Vol. 44, pp. 179-185.

[90] A. ZUREICK, L. F. KAHN & B. J. BANDY: *Tests on Deep I-Shape pultruded beams* — 49th Annual conference, Composite Institute, The Society of the Plastic Industry 1994.

[91] B. DUNCAN & G. DEAN: *Measurements and models for design with modern adhesives* — International Journal of Adhesion and Adhesives 2003, Vol. 23, pp. 141-149.

[92] J. DE CASTRO: *Report 2000-1b-1: Experiments on adhesives* — 2003, CCLAB, unpublished.

[93] K. MATSUI: *Size effects on average ultimate shear stresses on adhesive-bonded rectangular or tubular joints under tension-shear* — International Journal of Adhesion and Adhesives 1990, Vol. 10, pp. 81-89.

[94] K. MATSUI: *Size effects on nominal ultimate tensile stresses on adhesive-bonded circular or rectangular joints under bending or peeling load* — International Journal of Adhesion and Adhesives 1990, Vol. 11, pp. 90-98.

[95] K. MATSUI: *Size effects on nominal ultimate shear stresses on adhesive-bonded circular or rectangular joints under torsion* — International Journal of Adhesion and Adhesives 1991, Vol. 11, pp. 59-64.

[96] D. W. OPLINGER: *A layered beam theory for single lap joints* — Army Material Technology Laboratory Report MTL TR91-23 1991.

[97] G. KÖNIG, K. BACHMANN & W. SCHOBBE: *Beitrag zum Bemmessungskonzept für Stahlbetonschornsteine* — Bauingenieur 1982, Vol. 56, pp. 205-214.

[98] G. KÖNIG, D. HOSSE & W. SCHOBBE: *Sicherheitsanforderungen für die Bemessung von Baulichen Anlagen nach den Empfehlungen der NABau - Eine Erläuterung* — Bauingenieur 1982, Vol. 56, pp. 69-78.

[99] G. KÖNIG & D. HOSSER: *Praktische Beispiele und Hinweise zur Festlegung von Sicherheitsanforderungen für Bauliche Anlagen nach der Empfehlung des NABau* — Bauingenieur 1982, Vol. 57, pp. 459-467.

[100] CANADIAN COMMISSION ON BUILDING AND FIRE CODES: *CSA-S16.1-94.*

[101] CANADIAN COMMISSION ON BUILDING AND FIRE CODES: *CNA/CSA-23.x-94.*

[102] EUROPEAN COMITEE FOR STANDARIZATION: *Basis of Design and Acions on Structures, ENV 1991-1* — 1991, CEN.

[103] M. ALQAM, R. M. BENNET & A.-H. ZUREICK: *Three-parameter vs. Two-parameter Weibull distribution for pultruded composite material properties* — Composite Structures 2002, Vol. 58, pp. 497-503.

[104] R. PRABHAKARAN, Z. RAZZAQ & S. DEVARA: *Load and resistance factor design (LRFD) approach for bolted joints in pultruded composites* — Composites: Part B 1996, Vol. 27B, pp. 351-360.

Curriculum vitæ

Till Vallée
Born March 11, 1969 in Wuppertal/Germany

EPFL-CCLab
Bâtiment BP
1015-Lausanne Switzerland

till.vallee@epfl.ch
www.herodote.ch

Education

- 2000-2003 — Swiss Federal Institute of Technology Lausanne - ENAC
  Doctoral thesis: Structural Design Method for Adhesively Bonded Joints of Pultruded GFRP Shapes.
- 1998-2000 — Darmstadt University of Technology (Germany).
  Part-time post-graduate program in structural steel.
- 1990-1995 — Darmstadt University of Technology (Germany)
  Civil Engineer Diploma. Special project in environmental sciences and diploma thesis in geotechnics.
- 1988-1990 — Université des Sciences et de la Technologie Houari Boumedienne (Bab- Ezzouar/Algeria)
  Tronc commun sciences éxactes.
- 1988 — Lycée de Aïn-Taya (Algeria)
  Baccalauréat de l'enseignement secondaire, série mathématiques - bilingual arabic-french.

Additional Information

- Languages — German, French and Arabic: fluent; English: very good and Spanish: good.
- Computer — Standard Office programs, Matlab, Mathematica, LaTeX, Adobe programs, Finite Element Analysis, CAD, experimental device programs, webmastering, networking etc.
- Research fields — Design and stability of steel structures, cold formed steel structures, steel-concrete composite structures, piled-raft foundations, Fibre Reinforced Polymers.
- Interests — History in general, in particular the antiquity of the mediterranean basinm, Mesopotamia and the building of modern Europe.
- Archeology: actually I'm carrying out — on a private basis — a scientific investigation in collaboration with the École Suisse d'Archéologie en Grèce.

Member of

- Hessische Ingenieurkammer, up to end 2000.
- Schweizer Ingenieure+Architekten since 2001.
- Comission informatique de l'ENAC.
- Comission pédagogique de l'ENAC, up to end of 2001.
- Comission de coordination des moyens experimentaux de l'Institut de Structure.
- Junta Directiva de ColombiaVive, asociación cultural.
- Representative of the *corps intermédiaire* de l'ENAC at the EPFL.